A UNITED STATES DEPARTMENT OF COMMERCE PUBLICATION

SECTION A

JOURNAL OF RESEARCH

of the NATIONAL BUREAU OF STANDARDS

JNBAAR 76A (2) 67-184, Mar.-Apr. 1972

Physics and Chemistry

U.S. DEPARTMENT OF COMMERCE
National Bureau of Standards

Journal of Research

of the

National Bureau of Standards

A. Physics and Chemistry

Mar.–Apr. • 1972

VOLUME • 76A

NUMBER • 2

Editor: C. W. Beckett

Associate Editor: D. D. Wagman

Publication dates:
Feb. 1, Apr. 1, June 1, Aug. 1, Oct. 1, Dec. 1, 1972

J. Res. Nat. Bur. Stand. (U.S.), A

JOURNAL OF RESEARCH

The National Bureau of Standards Journal of Research reports research and development in the fields of activity shown at right. Also included from time to time are survey articles on topics closely related to the Bureau's scientific and technical program.

The Journal is published in two separate sections as follows:

A. Physics and Chemistry

Contains papers of interest primarily to scientists working in these fields. Issued six times a year. Annual subscription: domestic, $9.50; foreign, $11.75. Single copy, varies.

B. Mathematical Sciences

Presents studies and compilations designed mainly for the mathematician and the theoretical physicist. Issued quarterly. Annual subscription: domestic, $5.00; foreign, $6.25. Single copy, $1.25.

C. Engineering and Instrumentation

Reports research and development results of interest chiefly to the engineer and the applied scientist. Issued quarterly. Annual subscription: domestic, $5.00; foreign, $6.25. Single copy, $1.25.

The National Bureau of Standards[1] was established by an act of Congress March 3, 1901. The Bureau's overall goal is to strengthen and advance the Nation's science and technology and facilitate their effective application for public benefit. To this end, the Bureau conducts research and provides: (1) a basis for the Nation's physical measurement system, (2) scientific and technological services for industry and government, (3) a technical basis for equity in trade, and (4) technical services to promote public safety. The Bureau consists of the Institute for Basic Standards, the Institute for Materials Research, the Institute for Applied Technology, the Center for Computer Sciences and Technology, and the Office for Information Programs.

THE INSTITUTE FOR BASIC STANDARDS provides the central basis within the United States of a complete and consistent system of physical measurement; coordinates that system with measurement systems of other nations; and furnishes essential services leading to accurate and uniform physical measurements throughout the Nation's scientific community, industry, and commerce. The Institute consists of a Center for Radiation Research, an Office of Measurement Services and the following divisions:

Applied Mathematics—Electricity—Heat—Mechanics—Optical Physics—Linac Radiation[2]—Nuclear Radiation[2]—Applied Radiation[2]—Quantum Electronics[3]—Electromagnetics[3]—Time and Frequency[3]—Laboratory Astrophysics[3]—Cryogenics[3].

THE INSTITUTE FOR MATERIALS RESEARCH conducts materials research leading to improved methods of measurement, standards, and data on the properties of well-characterized materials needed by industry, commerce, educational institutions, and Government; provides advisory and research services to other Government agencies; and develops, produces, and distributes standard reference materials. The Institute consists of the Office of Standard Reference Materials and the following divisions:

Analytical Chemistry—Polymers—Metallurgy—Inorganic Materials—Reactor Radiation—Physical Chemistry.

THE INSTITUTE FOR APPLIED TECHNOLOGY provides technical services to promote the use of available technology and to facilitate technological innovation in industry and Government; cooperates with public and private organizations leading to the development of technological standards (including mandatory safety standards), codes and methods of test; and provides technical advice and services to Government agencies upon request. The Institute also monitors NBS engineering standards activities and provides liaison between NBS and national and international engineering standards bodies. The Institute consists of the following divisions and offices:

Engineering Standards Services—Weights and Measures—Invention and Innovation—Product Evaluation Technology—Building Research—Electronic Technology—Technical Analysis—Measurement Engineering—Office of Fire Programs.

THE CENTER FOR COMPUTER SCIENCES AND TECHNOLOGY conducts research and provides technical services designed to aid Government agencies in improving cost effectiveness in the conduct of their programs through the selection, acquisition, and effective utilization of automatic data processing equipment; and serves as the principal focus within the executive branch for the development of Federal standards for automatic data processing equipment, techniques, and computer languages. The Center consists of the following offices and divisions:

Information Processing Standards—Computer Information—Computer Services—Systems Development—Information Processing Technology.

THE OFFICE FOR INFORMATION PROGRAMS promotes optimum dissemination and accessibility of scientific information generated within NBS and other agencies of the Federal Government; promotes the development of the National Standard Reference Data System and a system of information analysis centers dealing with the broader aspects of the National Measurement System; provides appropriate services to ensure that the NBS staff has optimum accessibility to the scientific information of the world, and directs the public information activities of the Bureau. The Office consists of the following organizational units:

Office of Standard Reference Data—Office of Technical Information and Publications—Library—Office of International Relations.

[1] Headquarters and Laboratories at Gaithersburg, Maryland, unless otherwise noted; mailing address Washington, D.C. 20234.
[2] Part of the Center for Radiation Research.
[3] Located at Boulder, Colorado 80302.

U.S. DEPARTMENT OF COMMERCE
Peter G. Peterson, Secretary
NATIONAL BUREAU OF STANDARDS
Peter G. Peterson, Acting Director

Order all publications from the Superintendent of Documents
U.S. Government Printing Office, Washington, D.C. 20402

Use of funds for printing this publication approved by the Director of the Bureau of the Budget (June 22, 1966).

JOURNAL OF RESEARCH of the National Bureau of Standards—A. Physics and Chemistry
Vol. 76A, No. 2, March–April 1972

Guidelines for the Reporting of Numerical Data and Experimental Procedures

David Garvin

Institute for Materials Research, National Bureau of Standards, Washington, D.C. 20234

(December 2, 1971)

General recommendations are made about the reporting of data and experimental procedures. These are intended as instructions to authors of papers in which quantitative physical and chemical data are reported. There is included a bibliography of standards documents and more detailed guidelines.

Key words: Chemistry; experimental procedures; numerical data; physics.

1. Introduction

Scientific journals give general guidance on the preparation of papers in editorial sections entitled "instructions to authors" and the like. Two guides of this type are presented here. They are concerned with numerical data and experimental procedures. They reflect the experience of data evaluators in decoding results reported in the primary literature. These guides indicate how numbers should be reported and what auxiliary information is needed if it is to be possible for a conscientious reader to reinterpret or repeat the measurements.

These guides are general. More specific directions have been written for particular types of experiments. A bibliography appended to this paper lists a number of these, together with some generally applicable documents that treat symbols, nomenclature and standards.

2. The Presentation of Numerical Data

Quantitative measurements of physical properties and molecular parameters have surprisingly long lives. They often survive several changes in interpretation. The author can enhance their survival value by presenting them in a form that will permit reinterpretation, permit comparison with other work and permit as assessment of both accuracy and precision.

A vital preliminary to the reporting of numerical results is an adequate description of the experimental procedures used to obtain them. What is needed is outlined in a separate section.

The suggestions below are guides to be used in planning the presentation of numerical data.

1. In the reporting of experimental measurements and of derived quantities, **use internationally approved nomenclature, symbols, units,** and **standards.** If there are over-riding reasons for using other symbols for units, identify these in terms of the internationally approved ones.

2. **Report data in a form as free from interpretation as possible.** The reader should be able to recover the measured quantities so that he may reanalyze them in terms of a different hypothesis. Often this means simply the addition of another column of data to a table. If there is a commonly accepted form for reporting the particular type of data, it should be used in addition to any form preferred by the author.

3. **Present quantitative data that still show the scatter in the measurements.** Whenever possible, publish experimental results in numerical form. If a choice must be made, plot or tabulate unsmoothed data instead of smoothed final results. Small, unexpected effects can be lost when data are smoothed or fit to a predetermined function.

4. **Put the final numerical results,** those the author wants accepted, **in a table.** Do not bury them in a discussion section—they will be lost.

5. **Report the "imprecision" of the measurements** (statistical or random uncertainty), **and define it unambiguously,** e.g. "twice the standard deviation of the mean" etc. Avoid qualitative estimates of this quantity.

6. **Estimate the "inaccuracy" of the measurements.** Quantitative data presented without an estimate of possible systematic errors deserves summary rejection. The components of this estimate include
   (a) the sensitivity or resolution possible in the measurements,

(b) the effect of assumptions made in processing the data,
(c) the effect of possible systematic trends, both those for which corrections were made and those for which this could not be done, and
(d) uncertainties in auxiliary data taken from other work.

If possible, state this estimate in the same terms as that used for imprecision. They should be comparable in meaning even though they may differ in magnitude. Experience has shown that systematic differences between two sets of data usually are more important than random errors. Attempts to estimate these possible effects usually lead to improved experimental design.

7. **Explain the method used to reduce the primary data.** This is the chain linking the measurements and the results. Often it is long and complex. Frequently, it is difficult for a reader to reconstruct it. An example is desirable. Important components of this chain are listed below. It is worthwhile to cover each point, but the detail depends upon the precision of the experiments.

(a) Mathematical expressions used to convert the data to results.
(b) Assumptions made about the experiments. Invariably some parameters are assumed to be unimportant, some are held constant and some are subject to substantial corrections. The treatment of all of these should be justified, preferably by experiment.
(c) Auxiliary data and constants taken from other sources. Both their values and imprecision should be stated.
(d) The use of standards in relating the measurements to the fundamental units of measure. The standards should be identified explicitly, particularly where changes have been made recently (as in the International Practical Temperature Scale, or atomic weights and masses).
(e) Cite the statistical procedures used.

3. The Reporting of Experimental Procedures

The quality of the information provided about how measurements were made often determines the acceptability of the results in the future. When it becomes necessary for a reader to compare the results of several studies, or to reinterpret data, he must ask, "Did the author pay attention to details that I now know to be important?" or "Could he have observed this (newly reported) effect?" If these questions cannot be answered, the work may be rejected.

The major topics that should be included in a description of the experimental procedures are listed below. Consideration of these points when planning the work will, inevitably, improve the experimental design and simplify the preparation of the final paper.

- Description of apparatus with dimensions (either directly or by reference to earlier work).
- Calibration of equipment, including a discussion of the magnitudes of possible systematic biases for which corrections were not made.
- Indication of whether and how the calibration is traceable to an established standard.
- Description of experimental procedure.
- Description of environmental conditions.
- Identification of analytical methods used (and proof of them if novel).
- Indication of the purity of materials and the evidence for it.
- Statement of sensitivity or resolution possible in the experiments and the proof thereof.
- Reporting on negative experiments.

4. Discussion

General directions for the preparation of a scientific paper serve several purposes. They set minimum standards for and promote uniformity of presentation of material. Also, they remind an author to tell his reader about what has been done as well as what has been deduced. But, in both cases such guides rely heavily upon the judgement of the author concerning what should be included.

More detailed guides are desirable when quantitative data are important *per se* as opposed to being aids in the development of concepts. These must summarize all the features of the work that should be recorded so that a step by step reanalysis can be made. Each such guide can only treat a specific type of work. Those few that have been written appear to have improved the quality of reporting of data. More are desirable.

5. Bibliography

5.1. Symbols, standards and basic quantities

SYMBOLS, UNITS, AND NOMENCLATURE

American National Standards Institute
"ISO Recommendation R1000, Feb. 1969. Rules for the use of units of the International Systems of Units and a Selection of the Decimal Multiples and Sub-multiples of the SI Units."
American National Standards Institute (New York, 1969) 1st Edition
(Basic statement on units in the SI system.)

Page, C., and Vigoreux, P.
"The International System Units (SI)"
Nat. Bur. Stand. (U.S.), Special Publ. 330, 42 pages (January 1971)
(Summary of the SI system, history of development of the system of units, discussion of practical realization of the base units. This is a translation of "Le Système International d'Unités" published by BIPM. An identical English language document was published by the British Standards Institution, London, 1970.)

International Union of Pure and Applied Physics, Commission for Symbols, Units and Nomenclature
"Symbols, Units and Nomenclature in Physics"
Document U.I.P. 11 (S.U.N. 65–3) (1965)

McGlashan, M. L.
"Manual of Symbols and Terminology for Physicochemical Quantities and Units"
Pure and Applied Chemistry (1970) **21,** 1
(Symbols etc. approved by IUPAC)

American Society for Testing and Materials
"ASTM Standard Metric Practice Guide (A Guide to the Use of SI – The International System of Units"
American Soc. for Testing and Materials (New York, 1970)
(Includes factors for conversion of customary units to SI and procedures for rounding converted values)

American Chemical Society
"Handbook for Authors of papers in the journals of the American Chemical Society"
American Chem. Soc. Publications (Washington, 1967)
(This handbook includes a bibliography (pg. 49–53) on nomenclature of chemical compounds and, to a limited extent, on terminology and symbols.)

International Union of Pure and Applied Chemistry
"Information Bulletin"
(This series includes appendices on nomenclature, symbols, units and standards for specialized fields. Many of these are about the nomenclature of compounds, but some are on reporting of data. See "Guidelines")

CODATA Newsletters
(This series regularly publishes announcements of books, handbooks, and articles that are compilations of data, or that treat nomenclature, symbols, units and standards)

ATOMIC WEIGHTS

International Union of Pure and Applied Chemistry, Inorganic Chemistry Division, Commission on Atomic Weights
"Atomic Weights of the Elements 1969"
Pure and Applied Chemistry (1970) **21,** 1
(This is the current set of atomic weights for the naturally occurring isotopic mixtures. Revisions to this atomic weight scale for the elements H, F, Na, Al, P, K, Zn, Cs, Ho and Bi were recommended to IUPAC by the Commission on Atomic Weights at their meeting in Washington, D.C. in July 1971)

ENERGY

Ginnings, D. C., editor
"Heat," vol. 6 of **"Precision Measurement and Calibration"**
Nat. Bur. Stand. (U.S.), Special Publ. 300, vol. 6, 387 pages (February 1970)
(Collection of N.B.S. papers on calorimetry (techniques, high temperature, low temperature, reaction), cryoscopic measurements and heat transfer.)

PHYSICAL CONSTANTS

Taylor, B. N., Parker, W. H., and Langenberg, D. N.
"Determination of e/h, Using Macroscopic Quantum Phase Coherence in Superconductors: Implications for Quantum Electrodynamics and the Fundamental Physical Constants"
Rev. Mod. Physics (1969) **41,** 375
(New data, included here, force a revision in the values for the physical constants now accepted (Cohen and DuMond.) A CODATA Task Group is preparing a revised set for consideration by the scientific community.)

Cohen, E. R., and DuMond, J. W. M.
"Our Knowledge of the Fundamental Constants of Physics and Chemistry in 1965"
Rev. Mod. Physics (1965) **37,** 4
(Review and selection of data and table of physical constants. The values given here are also printed in the 1965 report of the S.U.N. Commission and in Nat. Bur. Stand. Tech. News. Bull. (1963) **47,** 175. In both of these the error is given as 3 standard errors (one standard error is given in the Rev. Mod. Physics article) and the values are rounded correspondingly.

The first radiation constant, c_1, is in error in the NBS Tech. News. Bull. article. It should be 3.7415×10^{8} Wm^2 not 3.7405×10^{8} Wm^2.)

PRECISION AND ACCURACY

Ku, H. H. editor
"Statistical Concepts and Procedures," vol. 1 of **"Precision Measurement and Calibration"**
Nat. Bur. Stand. (U.S.), Special Publ. 300 (1969)
(Collective volume on the treatment of errors of measurement. Almost all papers are of interest to the experimentalist. Two of prime interest concerning the expression of precision indices and errors are: Eisenhart, C., "Expression of the Uncertainties of Final Results," paper 1.6 pg 69 (reprinted from Science (1968) **160,** 1201), and Ku, H. H., "Expression of Imprecision, Systematic Error, and Uncertainty Associated with a Reported Value" paper 1.7 pg. 73 (reprinted from Measurements and Data (July–August 1968).)

STANDARDS

National Physical Laboratory (U.K.)
"Units and Standards of Measurement Employed at the National Physical Laboratory"
(Pamphlets issued irregularly on standards and their practical realization. Topics: Length, Mass, Time; Light; Electricity; Temperature.)

TEMPERATURE

International Bureau of Weights and Measures (BIPM), Subcommitton Thermometry
"International Practical Temperature Scale of 1968"
Metrologia (1969) **5,** 35

Bedford, R. E., Durieux, M., Muijlivijk, R., and Barber, C. R.
"Relationships between the International Practical Temperature Scale of 1968 and the NBS–55, NPL–61, PRMI–54, and PSU–54 Temperature Scales in the Range from 13.81 to 90.18 K"
Metrologia (1969) **5,** 47

Douglas, T. B.
"Conversion of Existing Calorimetrically Determined Thermodynamic Properties to the Basis of the International Practical Temperature Scale of 1968"
J. Research Nat. Bur. Stand. (U.S.), (1969) **73A,** 451

Swindells, J. F., editor
"Temperature," vol 2 of **"Precision Measurement and Calibration"**
Nat. Bur. Stand. (U.S.), Special Publ. 300 vol. 2, 513 pages (August 1968)
(Collection of N.B.S. articles on temperature scales, thermometry, pyrometry and spectroscopic temperature measurement.)

5.2. Guidelines for Reporting Data in Various Fields

INFRARED SPECTRA

Coblentz Society Board of Managers
"Specifications for Evaluation of Infrared Reference Spectra"
Analytical Chemistry (1966) **38,** 27A

"Recommendations for Infrared Spectra of New Compounds"
Analytical Chemistry (1968) **40,** 2272

OPTICAL SPECTRA

Meggers, W. F., and Moore, C. E.
[Joint Commission for Spectroscopy (IAU, IUPAP)] "Report of Subcommittee e (Notation for Atomic Spectra)"
J. Optical Soc. America (1953) **43,** 422

Jenkins, F. A.
[Joint Commission for Spectroscopy (IAU, IUPAP)] **"Report of Subcommittee f (Notation for the Spectra of Diatomic Molecules)"**
J. Optical Soc. America (1953) **43,** 425

Joint Commission for Spectroscopy (IAU, IUPAP)
"Report on Notation for the Spectra of Polyatomic Molecules"
J. Chem. Phys. (1955) **23,** 1997

Triple Commission for Spectroscopy (IAU, IUPAP, IUPAC)
"Minutes of the Meeting at Tokyo 9 Sept. 1962. Appendix A. Report of Subcommittee on Units and Terminology"
J. Optical Soc. America (1963) **53,** 883
(Suggested changes in earlier recommendations)

International Union of Pure and Applied Chemistry Information Bulletin. Appendices on Tentative Nomenclature Symbols Units and Standards
No. 1 (1969) "Nomenclature, Symbols, Units and Their Usage in Spectro-Chemical Analysis—I"
No. 11 (1971) "Recommendations for the Presentation of Raman Spectra for Cataloging and Documentation in Permanent Data Collections"

"Spectrometry Nomenclature", Analytical Chemistry (1968) **40,** 2271

CHEMICAL KINETICS

(The CODATA Task Group on Data for Chemical Kinetics is preparing (1971) guidelines on the reporting of rate data. These are based on suggestions made by V. N. Kondratiev).

CRYSTALLOGRAPHY

Ibers, J. A.
"Information and Suggestions on Presentation of the Results of Crystal Structure Studies"
Inorg. Chim. Acta (Sept. 30, 1969), No. 3 (9th Prelim. page)

Kennard, O., Speakman, J. C., and Donnay, J. D. H.
"Primary Crystallographic Data"
Acta Crystallogr. (1967) **22,** 445

GAS CHROMATOGRAPHY

ASTM Committee E-19
"Proposed Recommended Practice for Gas Chromatography Terms and Relationships"
J. Gas Chromatog. (1968) **6,** 1

THERMOCHEMISTRY AND THERMODYNAMICS

McCullough, J. P., Westrum, E. F., Jr., and Evans, W. H.
"Calorimetry Group Adopts Revised Resolution on Data Publication"
Science (1960) **132,** 1658
(A revision of this recommendation was submitted by E. F. Westrum, Jr., et al. for approval of the commission on Thermodynamics and Thermochemistry at the 1971 IUPAC Conference at Washington, D.C. With approval by this and higher IUPAC committees it will be published in the Journal *"Pure and Applied Chemistry")*

THERMAL CONDUCTIVITY

Hanley, H. M. et al.
"Recommendations for Data Compilations and for the Reporting of Measurements of the Thermal Conductivity of Gases"
J. Heat Transfer (1971) **93** Series C, 479

(Paper 76A2–699)

JOURNAL OF RESEARCH of the National Bureau of Standards—A. Physics and Chemistry
Vol. 76A, No. 2, March–April 1972

A Study of Equilibrium in Argon Arcs

J. B. Shumaker and C. H. Popenoe

Institute for Basic Standards, National Bureau of Standards, Washington, D.C. 20234

(November 8, 1971)

The intensities of the 7147 Å Ar I and 4806 Å Ar II lines obtained from wall-stabilized arcs at pressures of 0.2 to 5 atm are presented in an Olsen-Richter diagram. Departures from equilibrium are evident at electron densities below 5×10^{16} cm^{-3}. The assumption of equilibrium at higher electron densities leads to transition probabilities in fair agreement with lifetime measurements.

Key words: Argon arcs; argon transition probabilities; equilibrium; LTE.

1. Introduction

For the measurement of optical transition probabilities and the Stark widths and shifts of spectral lines in plasmas no spectral source has been as fruitful as the high current atmospheric pressure stabilized arc. And of all the elements studied by this technique none has been more thoroughly worked over than argon. It is therefore a matter of considerable concern that different plasma diagnostic techniques lead to different transition probability values in argon arcs [1, 2, 3].[1] The two plasma diagnostic techniques which have been used to establish absolute scales for argon transition probabilities in arcs are various modifications of the Fowler-Milne method [4–7] and the hydrogen line shape method [2, 8, 9. 10]. The latter method leads to systematically larger transition probabilities: by about 30 percent for Ar I lines and by nearly a factor of 2 for Ar II lines. Other independent determinations of these transition probabilities such as theoretical calculations and lifetime measurements generally tend to support the higher values for Ar I and the lower values for Ar II. Since these discrepancies may be symptomatic of non-equilibrium behavior of the arcs it is important to discover whether local thermodynamic equilibrium (LTE) is a characteristic of these experiments because if not, then the large amounts of atomic data being generated by the arc technique are of doubtful value.

If we apply LTE validity criteria estimates [11, 12] to the usual experimental conditions existing in argon arcs, we find that for electron densities greater than 5×10^{16} cm^{-3} or so we may expect all neutral and singly ionized populations to be within at most 10 percent of their LTE values. Unfortunately, this LTE threshold estimation is uncertain by perhaps half an order of magnitude because of the approximate nature of the theoretical arguments and the rough estimates of collision cross sections. Experimental attempts to define the LTE threshold electron density have thus far not convincingly removed any of this uncertainty. The experimental values vary from 5×10^{14} (Bourasseau, et al.) [13] to 10^{18} cm^{-3} (Bober and Tankin) [6] with most of the measurements suggesting values in the range from 2×10^{15} to 10^{16} cm^{-3} [14–17]. A recent detailed theoretical treatment of the argon arc by Uhlenbusch, Fischer, and Hackmann [18] is in general accord with the Bober and Tankin value.

In this paper we present argon arc data which show distinct departures from LTE at electron densities below 5×10^{16} cm^{-3} and we discuss briefly the evidence that LTE prevails at higher electron densities and the relationship of this problem to hydrogen line broadening theory and to argon lifetime measurements.

2. Experimental Procedure

Our data consist of spectral intensity measurements of two well-isolated, optically thin argon lines. The measurements were performed side-on in wall-stabilized arcs. The arc chamber for most of the experiments was of the watercooled copper disk type developed by Maecker [19]. Two channel diameters were used: 4.8 mm and 3.2 mm. One experiment was performed with a 4.8 mm internal diameter fused silica tube arc chamber similar in principle to that described by Knopp and Cambel [20] in which the arc is observed within a transparent constricting tube rather than in the open gap between two copper constrictors.

We show in figure 1 our measurements of the intensities of the spectral lines 7147 Å Ar I and 4806 Å Ar II. At each of the five indicated pressures from 0.2 to

[1] Figures in brackets indicate the literature references at the end of this paper.

4.98 atm experiments were conducted at a number of arc currents. Under each operating condition the intensities of both spectral lines were recorded at a number of wavelengths encompassing the line and at generally 40 to 50 equally spaced points traversing the arc diameter. Following an Abel inversion to obtain local radial volume emission values the line intensities were computed as usual by subtracting the continuum, integrating over the line, and correcting for the distant line wings. Details of the data recording and reduction have been described previously [8]. The final result consists of corresponding pairs of intensities for the two spectral lines at a number of radial points for each arc experiment. These intensity pairs are plotted logarithmically in figure 1.

In figure 2 we show curves representing the relationship between the populations of the upper states of these two lines which would exist in complete thermodynamic equilibrium at the five pressures of our experiments. As a matter of interest we have plotted also contours of constant electron density and constant temperature. These curves were computed in accordance with Griem's treatment [11] of ionization potential lowering, partition function cut-off and pressure correction. Since the ratio of a line intensity to the upper state number density is a constant proportional to the transition probability and since on a logarithmic scale such a constant represents a simple translation it should be possible to fit the curves of figure 2 to the data of figure 1 if the arc data were obtained under LTE conditions [5]. The curves in figure 1 show such a fitting applied to the data at the three highest pressures. The fitting was performed numerically by a generalized nonlinear least squares fitting technique described by Wolberg [21]. The atomic transition probabilities obtained this way are A(7147 Ar I)= $5.57 \pm 0.02 \times 10^5$ s^{-1} and A(4806 Ar II)= $7.86 \pm 0.10 \times 10^7$ s^{-1}. The borders of figure 2 have been selected according to these transition probabilities so as to permit superposition of figures 1 and 2 and estimation of electron density and temperature in the experimental data.

Although the least squares fitting was based only on the three highest pressures it is clear that the 0.5 atm data also agree well with this choice of transition probabilities. The 0.2 atm data on the other hand are in serious disagreement with these transition probabilities and, in fact, the scatter of data clearly precludes any meaningful fitting at this pressure.

Our data include no corrections for self-absorption. Based upon experimentally measured Stark broadening parameters [7, 22] and the continuum intensities and A values measured here we estimate that the maximum error introduced by self-absorption is less than 1 percent for the 7147 Å Ar I line in our highest current, highest pressure experiment and about 1 percent for the 4806 Å Ar II line in our highest temperature atmospheric pressure experiment.

By comparing an arc with a black body in which complete LTE exists one can recognize three essential differences which may cause departures from equilibrium. First, in the arc much of the radiation escapes so that LTE will be achieved only if radiative depopulation rates are negligible compared to rates of collisional population and depopulation. Second, in the arc steep temperature and number density gradients exist which may generate diffusional fluxes of such magnitude that collisional (and radiative) processes

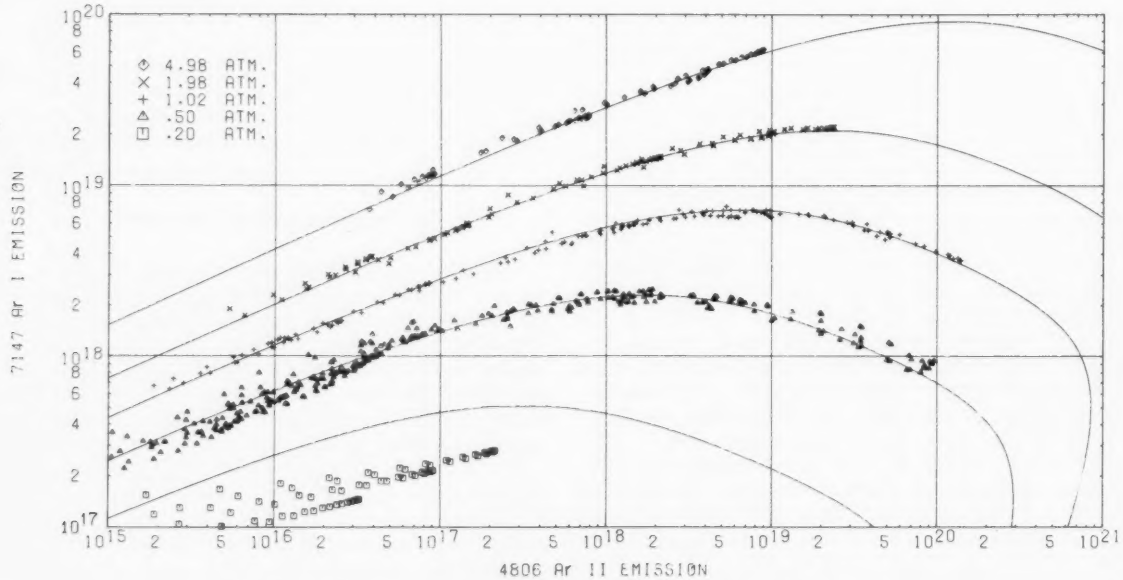

FIGURE 1. *Argon arc line intensity measurements in photons/(cm³ s).*

The curves are the family of equilibrium constant pressure contours of figure 2 least squares fitted to the 1.02, 1.98 and 4.98 atm data.

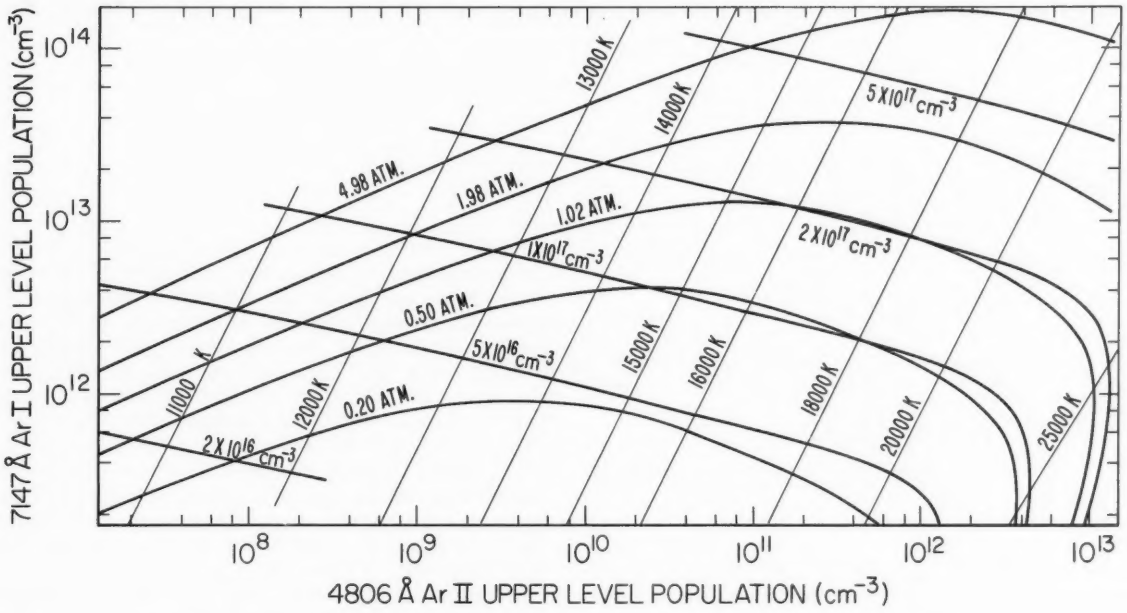

FIGURE 2. *Computed equilibrium upper level populations for conditions of experiments of figure 1.*

Also shown are constant electron density and constant temperature contours.

are unable to maintain equilibrium distributions. And third, since electrons absorb energy from an electric field much more rapidly than ions do the kinetic temperature of the electron gas will be higher than that of the heavy particle gas which obtains its energy then mainly by collisions with the electrons. Since collisional processes will be dominated by electron collisions it turns out that all of these effects should decrease rapidly in importance with increasing electron density [11, 12]. The importance of the second effect should also depend upon arc channel diameter and radial position in the arc.

The data of figure 1 span a range in electron density from 10^{16} to 5×10^{17} cm^{-3} and we see from the fitting of the LTE curves that there is a transition from a condition where no reasonable fitting is possible at low electron densities to a condition where an entirely satisfactory fit can be made at higher electron densities. This behavior is in accord with the qualitative electron density dependence arguments above and the assumption that the arc is in LTE at the higher electron densities.

At each pressure the arc currents for the successive experiments were chosen to furnish considerable overlap between the data obtained near the axis at one current and that obtained from the outer regions of the next higher current experiment. At the three higher pressures and over much of the range of the 0.5 atm data there is no significant systematic radially dependent discrepancy in these overlap regions. The data obtained from experiments with the two different channel diameters also overlap considerably. In the 1 atm data, for example the overlap in the 4806 Å Ar II intensity is two orders of magnitude with the large channel providing data from 10^{15} to 10^{19} cm^{-3} s^{-1} and the small channel from 10^{17} to 10^{20} cm^{-3} s^{-1}. The data show no evidence that the channel diameter influences the results at electron densities above 5×10^{16} cm^{-3}. At lower electron densities we have only the large channel data and cannot make the comparison. Our results, then are not inconsistent with the equilibrium hypothesis at the higher electron densities. The data in figure 1 do not include any measurements beyond a maximum radial distance which usually lay between 1.5 and 2 mm. At that distance from the arc axis the 4806 Å Ar II line intensity was generally about two orders of magnitude weaker than on axis and the remaining data were dominated by noise and scattered light.

The scatter of data in the lower left hand portion of figure 1 is caused by a dependence upon the radial point at which the measurement is made. This is shown in figure 3 where we have replotted the data from two typical experiments in this region. Data from the arc axis appear in the upper right of this figure and data from the outer regions appear at the lower left. It will be seen that the deviations from the LTE curves fitted at higher electron densities show a systematic radial behavior. At the arc center the data lie below or to the right of the curve whereas at large radii the data lie above or to the left of the curve. This behavior agrees qualitatively with that computed by Uhlenbusch [18] for a simple model in which the kinetic temperature of the heavy particles is allowed to be lower than that of the electrons, and the neutral atom ground state population is allowed to be larger

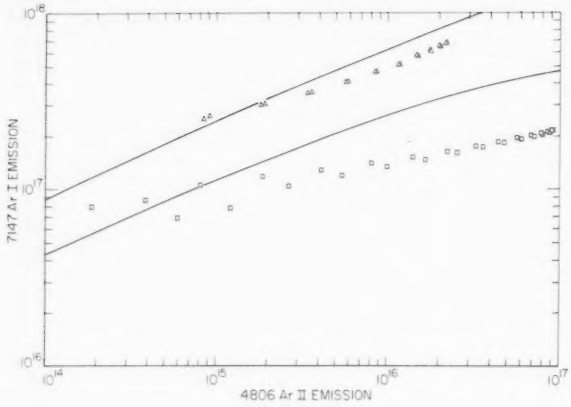

FIGURE 3. *Detail from figure 1.*

Two sub-atmospheric pressure argon arc experiments in 0.48 cm diameter channel: 0.5 atm, 47.2 amp and 0.2 atm, 62.2 amp.

than the LTE value obtained from the electron temperature and from the free electron or excited state number densities.

Using an extension of the Uhlenbusch model in which we also include ionic ground state overpopulations, we can interpret these data in terms of small departures from LTE. For this purpose we modify the usual equilibrium equations for arc diagnostics which relate pressures and temperatures to the populations of the excited states and electrons as follows:

Boltzmann distributions

$$n_0^j = \frac{n_0^0 g_0^j}{b_0 g_0^0} \exp\,(-E_0^j/kT_e) \qquad j>1 \tag{1}$$

$$n_1^j = \frac{n_1^0 g_1^j}{b_1 g_1^0} \exp\,(-E_1^j/kT_e) \qquad j>1 \tag{2}$$

Saha equation

$$\frac{n_e n_1^0}{n_0^j} = 2\left(\frac{2\pi m_e kT_e}{h^2}\right)^{3/2} \frac{g_1^0}{g_0^j} \exp\,(-(\chi_0 - E_0^j)/kT_e) \qquad j>1 \tag{3}$$

Electrical neutrality

$$n_e = \sum_{j=0} n_1^j \tag{4}$$

Dalton's Law

$$P = \left(\sum_{j=0} n_0^j + \sum_{j=0} n_1^j\right) kT_g + n_e kT_e - \Delta P$$

$$= P' - (n_0' + n_e)k(T_e - T_g) + n_0^{0'}(b_0 - 1)kT_g \tag{5}$$

where

$$n_0^{0'} = n_0^0/b_0$$

$$n_0' = n_0^{0'} + \sum_{j=1} n_0^j$$

$$P' = (n_0' + 2n_e)kT_e - \Delta P$$

In these equations the subscript 0 denotes a neutral atom; subscript 1 denotes the first ion; and higher ions have been neglected for simplicity. Superscript 0 denotes a ground state and other superscripts denote excited states. n_e, m_e, and T_e are the electron number density, mass, and kinetic temperature. χ_0 is the effective ionization energy, i.e., the ionization energy minus the lowering caused by the plasma interactions. P is the pressure and ΔP is the small pressure correction for plasma interactions. b_0 and b_1 are measures of the degree of atomic and ionic ground state overpopulation. T_g is the heavy particle kinetic temperature. We expect that $T_e \geqq T_g$, $b_0 \geqq 1$, and $b_1 \geqq 1$ with the equality sign characterizing the equilibrium condition.

In order to apply these equations to the data in figure 3 we introduce the approximation

$$n_e = n_1^0 \tag{6}$$

and equations for the line intensities

$$I_0^j = A_0^j n_0^j \text{ photons (cm}^3 \text{ sec)}^{-1} \tag{7}$$

$$I_1^j = A_1^j n_1^j \text{ photons (cm}^3 \text{ sec)}^{-1} \tag{8}$$

and for the intensity of the continuum which we measure near 4806 Å:

$$I_{\text{cont}} = 1.032 \times 10^{-11} n_e^2 \lambda^{-1} T_e^{-1/2} \xi \text{ photons (cm}^3 \text{ s)}^{-1} \tag{9}$$

where λ is the wavelength in angstroms and ξ is a slowly varying function of T_e and λ, whose value is of the order of magnitude of 1. Now we can use equations 1 to 9 and the continuum and line intensity measurements to calculate the ionic ground state overpopulation factor b_1 directly. From our measurements we cannot separate the two contributions to $P - P'$ (eq 5) but since the two effects operate in opposite directions we can obtain a lower bound to b_0 by assuming $T_g = T_e$. Actually the assumption $T_g = T_e$ probably doesn't introduce a serious error near the axis in these experiments. Kruger [23] has carried out a calculation similar to Uhlenbusch's for a 35 amp atmospheric pressure argon arc and finds $T_e - T_g = 200$ K at the arc axis where the electron density is about 10^{16}. Uhlenbusch [18] finds a similar value for 200 amperes and an electron density of 1.5×10^{17}. The evaluation of b_1 and $b_0^{\min}$ from these equations requires values for the transition probabilities and ξ (T_e, 4806). If LTE is assumed in our high pressure data these values can be calculated from these data. For this case the A values have been given

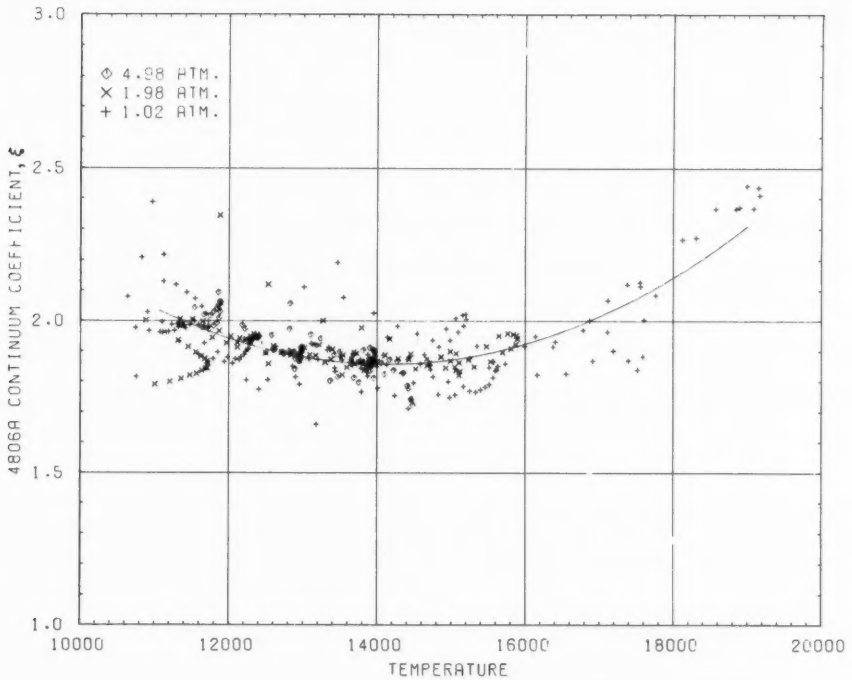

FIGURE 4. *Continuum emission correction factors at 4806 Å derived from 1.02, 1.98 and 4.98 atm experiments assuming equilibrium.*

The curve is a least squares fitted parabola.

above and values of ξ are given in figure 4. The latter are in fair agreement with Schlüter's theoretical estimate [24] of $\xi = 2.2$ at 14000 K. The results of the calculation of b_1 and b_o^{min} at the axis of the two experiments shown in figure 3 are given in table 1. The conclusion that, in the 0.5 atm. arc, for example, the neutral excited states are underpopulated by about a factor of 2 and the excited ionic states are further underpopulated by another factor of 2 is in qualitative agreement with the expected non-LTE behavior.

TABLE 1. *Departures from equilibrium at axial points of the two experiments plotted in figure 3*

P	T_e	N_e	b_0^{min}	b_1
(*atm*)	*K*	cm^{-3}		
0.5	12300	3.9×10^{16}	1.9	1.9
.2	14200	2.9×10^{16}	6.6	4.2

3. Summary and Conclusions

With respect to the question of the existence of LTE, the presentation of arc spectroscopic data in figure 1 can be interpreted to a large extent independently of any assumptions of specific transition probability values. Assuming only that the mechanisms which lead to departures from LTE become less effective as the electron density increases we can conclude that there are substantial departures from LTE in our low pressure argon arcs. Our high pressure arcs are either substantially in LTE or depart from it in a manner which consistently mimics LTE over a surprisingly wide range of conditions. Although one can never expect to obtain complete confirmation of thermodynamic equilibrium we feel that the present study strongly suggests that arcs in argon at electron densities above 5×10^{16} cm^{-3} are in LTE to within the few percent scatter of our data. This conclusion is based primarily on the apparent disappearance at this electron density of the obvious non-LTE effects of lower electron densities and the reasonable agreement of lifetime measurements with the arc-measured transition probabilities which result from the assumption of LTE. The Ar II transition probability measured here [A(4806 Ar II) $= 7.86\times10^7$] is in excellent agreement with the lifetime-based value (7.9×10^7) of Wiese's critical compilation [3]. The Ar I transition probability [A(7147 Ar I) $= 5.57\times10^5$ s^{-1}] required to fit our intensity measurements under the LTE assumption is smaller than that indicated by any other technique. A comparison of lifetimes for the upper level of this line as measured directly [25, 26] and as calculated from theory [27–29] and from this and other emission measurements [30, 31] is shown in table 2. When allowance is made for the possibility of systematic errors in the lifetime measurements and in the arc measurements—both in the absolute

intensity measurements of the present experiments and in the branching ratio determination – it is doubtful that the differences can be considered significant.

TABLE 2. *Ar I $2p_2$ lifetimes*

(nanoseconds)

Klose [25]	31 ± 2
Verolainen and Osherovich [26]	28 ± 1.4
Coates and Gaydon [30]	*26
Nodwell, Meyer and Jacobson [31]	26
Garstang and Van Blerkom [27]	29
Johnston [28]	30
Meiners [29]	26
Present experiment assuming LTE	*34

*Branching ratio taken from arc measurements of ref. [32]

Many argon transition probabilities have been extracted from experiments conducted with a trace of added hydrogen which permits the plasma diagnostics to be based on electron densities derived from H_β line shape measurements. The resulting transition probabilities, especially for Ar II lines [8, 33], are discordant with, for example, the lifetime based values of Wiese's tabulation [3]. If the arcs are in LTE then such experiments indicate that the correct electron density is about 10 percent greater than that obtained from the H_β line shape measurement and the theoretical profiles of Kepple and Griem [34]. This discrepancy is roughly equal to the estimated uncertainty of the theoretical calculations [34, 35]. On the other hand the same kind of contrived departures from LTE which would create the illusion of LTE in the data of figure 1 but with the wrong transition probabilities would also lead to an apparent constant fractional error in electron density measurements. Again this possibility cannot yet be denied. However, the fact that similar apparent errors in H_β-derived electron density measurements have been observed in many arc gases (hydrogen [36], argon [37, 38], alcohol [39]) tend to support the assumption of arc LTE.

4. References

[1] Corliss, C. H., and Shumaker, J. B., Jr., J. Res. Nat. Bur. Stand. (U.S.) 71A, (Phys. and Chem.) No. 6, 575–582, (1967).

[2] Bues, I., Haag, T., and Richter, J., Astron. and Astrophys. **2**, 249 (1969).

[3] Wiese, W. L., Smith, M. W., and Miles, B. M., NSRDS-National Bureau of Standards 22, Vol. II (U.S. Government Printing Office, Washington, D.C., 1969).

[4] Olsen, H. N., J. Quant. Spectrosc. Radiat. Transfer **3**, 305 (1963).

[5] Richter, J., Z. Astrophysik **61**, 57 (1965).

[6] Bober, L., and Tankin, R. S., J. Quant. Spectrosc. Radiat. Transfer **10**, 991 (1970).

[7] Shumaker, J. B., Jr., and Popenoe, C. H., J. Opt. Soc. Am. **59**, 980 (1969).

[8] Popenoe, C. H., and Shumaker, J. B., Jr., J. Res. Nat. Bur. Stand. (U.S.) 69A, (Phys. and Chem.) No. 6, 495–510 (1965).

[9] Wiese, W. L., Proc. VIII Int. Conf. on Ioniz. Phenom. in Gases, Vienna, 447 (1967).

[10] Wujec, T., Acta Physica Polonica **36**, 269 (1969).

[11] Griem, H. R., Plasma Spectroscopy, (McGraw-Hill, New York, 1964).

[12] Drawin, H. W., Z. Physik **228**, 99 (1969).

[13] Bourasseau, D., Cabannes, F., and Chapelle, J., Astron and Astrophys. **9**, 339 (1970).

[14] Desai, S. V., and Corcoran, W. H., J. Quant. Spectrosc. Radiat. Transfer **8**, 1721 (1968).

[15] Kolesnikov, V. N., Proc. P. N. Lebedev Phys. Inst. **30**, 53 (1966).

[16] Bott, J. F., Physics of Fluids **9**, 1540 (1966).

[17] Giannaris, R. J., and Incropera, F. P., J. Quant. Spectrosc. Radiat. Transfer **11**, 291, 1971.

[18] Uhlenbusch, J., Fischer, E., and Hackmann, J., Z. Physik **239**, 120 (1970).

[19] Maecker, H., Z. Natuforsch. **11a**, 457 (1956).

[20] Knopp, C. F., and Cambel, A. B., Rev. Sci. Instr. **37**, 332 (1966).

[21] Wolberg, J. R., Prediction Analysis, Van Nostrand, New York, 1967.

[22] Griem, H. R., Phys. Rev. Letters **17**, 509 (1966).

[23] Kruger, C. H., Physics of Fluids **13**, 1737 (1970).

[24] Schlüter, D., Z. Astrophysik **61**, 67 (1965).

[25] Klose, J. Z., J. Opt. Soc. Am., **57**, 1242 (1967).

[26] Verolainen, Ya. F., and Osherovich, A. L., Optics and Spectroscopy (U.S.S.R.) **25**, 258 (1968).

[27] Garstang, R. H., and Van Blerkom, J., J. Opt. Soc. Am. **55**, 1054 (1965).

[28] Johnston, P. D., Proc. Phys. Soc. (London) **92**, 896 (1967).

[29] Meiners, H. M., J. Quant. Spectrosc. Radiat. Transfer **9**, 1493 (1969).

[30] Coates, P. B., and Gaydon, A. G., Proc. Roy. Soc. (London) **A293**, 452 (1966).

[31] Nodwell, R. A., Meyer, J., and Jacobson, T., J. Quant. Spectrosc. Radiat. Transfer **10**, 335 (1970).

[32] Shumaker, J. B., Jr. and Popenoe, C. H., J. Opt. Soc. Am. **57**, 8 (1967).

[33] Berg, H. F., and Ervens, W., Z. Physik **206**, 184 (1967).

[34] Kepple, P., and Griem, H. R., Phys. Rev. **173**, 317 (1968).

[35] Vidal, C. R., Cooper, J., and Smith, E. W., J. Quant. Spectrosc. Radiat. Transfer **11**, 263 (1971).

[36] Wiese, W. L., Kelleher, D. C., and Paquette, D. R., submitted to Phys. Rev.

[37] Wende, B., Z. Angew, Phys. **22**, 181 (1967).

[38] Morris, J. C., and Krey, R. U., Phys. Rev. Letters **21**, 1043 (1968).

[39] Foster, E. W., J. Phys. **B3**, L145 (1970).

(Paper 76AQ–700)

JOURNAL OF RESEARCH of the National Bureau of Standards—A. Physics and Chemistry
Vol. 76A, Number 2, March–April 1972

Rates of Reaction of Atomic Oxygen III. Spiropentane, Cyclopentane, Cyclohexane, and Cycloheptane

Robert E. Huie and John T. Herron

Institute for Materials Research, National Bureau of Standards Washington, D.C. 20234

(February 9, 1971)

Rate constants have been measured from 307 to 652 K for the reactions of atomic oxygen (O^3P) with spiropentane, cyclopentane, cyclohexane, and cycloheptane. The derived Arrhenius parameters are $k(sp-C_5H_8)=10^{13.80\pm0.10}\ \exp[(-2890\pm100)/T]$, $k(cy-C_5H_{10})=10^{14.10\pm0.09}\ \exp[(-2210\pm100)/T]$, $k(cy-C_6H_{12})=10^{14.35\pm0.09}\ \exp[(-2350\pm100)/T]$, and $(cy-C_7H_{14})=10^{14.46\pm0.13}\ \exp[(-2230\pm100)/T]$ all in units of $cm^3\ mol^{-1}\ s^{-1}$.

Key words: Cycloheptane; cyclohexane; cyclopentane; oxygen; rate constants; spiropentane.

1. Introduction

In the previous papers in this series [1, 2] [1] Arrhenius parameters for the reactions of atomic oxygen (O^3P) with some alkanes and haloalkanes were reported. The results were interpreted in terms of a hydrogen atom abstraction mechanism, and the reaction rates were found to be directly related to the number and types of C–H bonds. In the present paper this work is extended to the reactions of atomic oxygen with some cycloalkanes.

2. Experimental Section

The apparatus, which has been described previously [1], consists of a discharge-flow system coupled to a mass spectrometer. Atomic oxygen was produced by passing a flow of argon containing a few percent molecular oxygen through a microwave discharge. Reactant gas was added through a movable inlet downstream from the discharge. The distance between the discharge and the reactant inlet was sufficient to allow for the quenching of any oxygen atoms in higher electronic states. The reactor was a 20 mm in diam borosilicate glass tube which could be heated by means of a four-section resistance heater or by circulating fluid through a jacket surrounding the reactor. Temperature was measured with a Pt-Pt-10 percent Rd thermocouple. The uncertainty due to thermal gradients and the measurement of emf was about 3°.

The contents of the reactor were continuously sampled through an orifice at the base of the reactor, located directly over the ionization chamber of the mass spectrometer.

In these experiments the ratio of the partial pressures of the cycloalkane at times zero and t (i.e., the time required for the gas stream to flow from the reactant inlet to the sampling orifice) was determined as the ratio of the ion currents at the appropriate mass with the discharge turned off and on. The atomic oxygen partial pressure was followed at m/e 16 at about 20 eV ionizing energy (below the appearance potential of O^+ ions from O_2), and the absolute value of its partial pressure determined by titration with nitrogen dioxide.

Rate measurements were performed with atomic oxygen in considerable excess and the extent of reaction kept small. Under these conditions the decay of the cycloalkane would be due solely to reaction with atomic oxygen. Further since at most only 10 percent of the atomic oxygen is consumed, the measured rate is not dependent on the details of atomic oxygen loss.

For the bimolecular reaction

$$O + A \rightarrow \text{Products}$$

the integrated rate expression is $k=\{\ln[A]_0/[A]_t\}/\int_0^t[O]\,dt$ where $[A]_0$ and $[A]_t$ are the concentrations of cycloalkane at times zero and t respectively, and [O] is the concentration of atomic oxygen. For the case in which the loss of atomic oxygen is small, the integral may be replaced by the average value of the oxygen atom concentration times the overall reaction time.

The assumptions underlying this rate expression have been discussed more fully previously [1]. Principally they are that the reactant A is lost only by reaction with atomic oxygen, and is not reformed in

[1] Figures in brackets indicate the literature references at the end of this paper.

subsequent reactions. These assumptions are satisfied by measuring the rate constants under conditions of excess atomic oxygen and low conversion of reactants.

However, this means that the value of the logarithm of the ratio $[A]_o/[A]_t$ is small and very sensitive to uncertainties in the measurement of ion currents. This is reflected in the scatter of the experimental data.

3. Results and Discussion

The experimental data and computed rate constants are given in tables 1–4. Velocity refers to linear flow velocity in the reactor and distance is that from the inlet to the mass spectrometer leak. Arrhenius parameters for the reactions studied were derived from plots of log k versus $1/T$ (figures 1 and 2) and are presented in table 5 along with derived rate constants at 298 and 1000 K. The reported uncertainties are standard errors based on a linear least squares treatment of the data.

In studying the reactions of atomic oxygen with the alkanes, we observed [2] that the Arrhenius plots were curved. This was interpreted as being due to the different rates of abstraction at different C–H bond sites. Consistent with this interpretation we find that the data on the cycloalkanes which have only one type of C–H bond are best fitted by a straight line.

Only a limited amount of data is available with which to compare our results. Stuckey and Heicklen [3] have studied the cyclopentane and cyclohexane reactions

TABLE 1. *Summary of rate measurements for the reaction* $O + sp-C_5H_8 \rightarrow OH + C_5H_7$

Temp. K	Total pressure Nm^{-2}[a]	Distance cm	Velocity cm s^{-1}	Reactant concentration mol cm^{-3}			10^{-10} k, cm^3 mol^{-1} s^{-1}
				$10^{11}(O)_{av}$	$10^{13}(A)_0$	$10^{13}(A)_t$	
337	282	14.4	730	10.9	11.2	9.81	0.623
339	299	14.2	750	40.8	18.1	16.7	1.01
339	299	14.2	750	45.2	18.0	16.4	1.01
339	288	14.2	740	52.2	16.3	15.1	0.792
339	304	14.0	470	46.5	18.7	15.2	0.987
339	304	14.0	470	28.9	59.8	52.3	0.614
416	318	14.3	930	50.1	10.9	8.14	3.77
417	206	13.1	1650	23.6	13.8	12.7	4.47
418	265	13.8	900	19.3	41.0	37.9	2.66
473	206	14.0	1920	9.99	10.9	9.99	11.8
480	179	14.3	1860	12.3	13.4	12.4	8.00
548	215	13.1	2235	17.9	73.8	59.8	20.3
553	272	14.7	2420	8.30	9.97	8.98	20.7
564	300	14.0	1270	4.31	11.7	10.8	16.1
647	187	15.0	3250	5.98	6.74	5.78	54.4
651	288	13.6	2850	7.26	6.97	5.76	54.8
652	182	15.0	3150	3.23	8.23	7.58	53.5

[a] 1 Torr = 133.32 Nm^{-2}.

TABLE 2. *Summary of rate measurements for the reaction* $O + cy-C_5H_{10} \rightarrow OH + C_5H_9$

Temp. K	Total pressure Nm^{-2}	Distance cm	Velocity cm s^{-1}	Reactant concentration mol cm^{-3}			10^{-10} k, cm^3 mol^{-1} s^{-1}
				$10^{11}(O)_{av}$	$10^{13}(A)_0$	$10^{13}(A)_t$	
307	182	16.0	1060	8.48	5.01	4.33	12.2
307	170	16.0	1050	10.9	5.10	4.41	9.87
331	203	13.6	1370	8.40	11.2	9.67	17.8
339	223	14.0	1440	9.29	12.4	10.7	14.9
339	410	13.9	770	4.96	12.7	11.1	15.0
415	345	13.3	940	5.70	11.4	8.96	57.0
418	198	13.6	1675	2.29	13.5	12.1	66.4
419	264	13.8	890	1.53	19.0	16.9	50.1
479	179	14.3	1860	5.06	4.82	3.13	106
493	264	14.0	2160	4.61	3.61	2.25	159
548	215	13.0	2235	2.05	10.4	7.77	240
557	205	15.0	2210	0.931	3.94	3.20	336
564	217	14.0	1680	2.22	5.16	3.47	213
631	218	13.1	3410	0.781	10.2	9.36	275
647	187	15.0	3270	0.793	4.93	4.04	541
652	182	15.0	3150	2.91	4.25	2.42	407

TABLE 3. *Summary of rate measurements for the reaction* $O + cy-C_6H_{12} \rightarrow OH + C_6H_{11}$

Temp. K	Total pressure Nm^{-2}	Distance cm	Velocity $cm\ s^{-1}$	Reactant concentration $mol\ cm^{-3}$			$10^{-10}\ k$, $cm^3\ mol^{-1}\ s^{-1}$
				$10^{11}(O)_{av}$	$10^{13}(A)_0$	$10^{13}(A)_t$	
307	210	16.0	590	20.5	5.38	2.74	14.2
307	225	16.0	610	14.0	9.55	6.11	13.7
307	170	16.0	1050	8.87	2.29	2.03	10.0
331	203	13.6	1370	7.50	9.91	8.47	21.2
339	410	13.9	770	4.54	11.0	9.59	17.1
339	223	14.0	1440	8.24	7.28	6.29	18.7
415	345	13.3	940	6.14	5.94	4.45	61.4
418	198	13.6	1675	1.90	10.4	9.25	75.3
419	264	13.8	890	1.73	7.19	6.16	57.7
474	179	14.3	1860	4.90	2.51	1.47	134
493	264	14.0	2160	4.32	3.19	1.95	174
557	205	15.0	2210	0.781	2.58	2.66	428
564	217	14.0	1680	2.07	1.52	0.83	352
631	218	13.1	3410	0.597	4.71	4.08	623
647	187	15.0	3270	0.678	3.47	2.71	774
652	182	15.0	3150	2.82	1.42	0.70	533

TABLE 4. *Summary of rate measurements for the reaction* $O + cy-C_7H_{14} \rightarrow OH + C_7H_{13}$

Temp. K	Total pressure Nm^{-2}	Distance cm	Velocity $cm\ s^{-1}$	Reactant concentration $mol\ cm^{-3}$			$10^{-10}\ k$, $cm^3\ mol^{-1}\ s^{-1}$
				$10^{11}(O)_{av}$	$10^{13}(A)_0$	$10^{13}(A)_t$	
331	203	13.6	1370	6.96	8.54	6.03	48.8
339	410	14.0	770	4.13	12.8	9.73	36.8
339	223	13.9	1440	7.78	20.7	15.3	38.3
418	198	13.6	1675	1.68	13.8	11.6	137
419	264	13.8	890	1.62	15.3	11.2	127
474	175	14.3	1860	4.70	6.85	3.52	180
493	264	14.0	2160	4.01	10.0	5.40	235
548	215	13.0	2235	1.82	7.84	4.62	486
557	205	15.0	2210	0.674	3.43	2.36	805
564	217	14.0	1680	1.90	5.95	3.11	411
631	218	13.1	3140	0.434	6.24	5.23	1010
647	187	15.0	3270	0.624	6.47	4.52	1240
652	182	15.0	3150	2.54	4.54	1.68	829

using the mercury photosensitized decomposition of nitrous oxide as their oxygen atom source. The rate constants were measured relative to that of hexafluoropropene which in turn was measured relative to 1-butene for which absolute values exist in the literature. Considering the limited precision of the data, and the amount of manipulation required to obtain the rate constants, the agreement between their rate constants and ours is reasonably good particularly near room temperature. The Arrhenius parameters differ considerably more. Because of the absolute nature of our measurements and the much greater temperature range employed we believe the results given here are to be preferred.

The only other data available is that of Avramenko et al. [4] who studied the cyclohexane reaction using a method based on the analysis of the final products of the reaction in a discharge-flow experiment and the imposition of an arbitrary and in our opinion incorrect reaction mechanism. This work is discussed more fully by Kaufman [5], and will not be considered further here.

The pre-exponential factors per C–H bond reported here for the C_5 to C_7 alkanes, i.e., $(1–2) \times 10^{13}$ $cm^3\ mol^{-1}\ s^{-1}$ are essentially the same as those found previously for the secondary C–H bonds in the normal alkanes [2]. Furthermore the activation energies for the cycloalkanes fit the same Evans-Polanyi expression

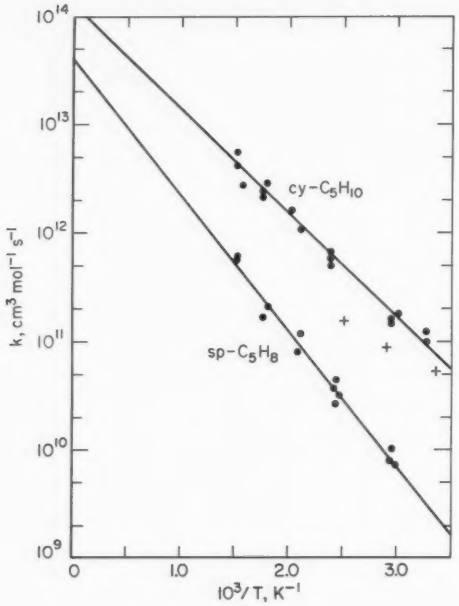

FIGURE 1. *Arrhenius plots for the reactions of atomic oxygen with spiropentane and cyclopentane.*

● This work; + Stuckey and Heicklen, Ref. [3].

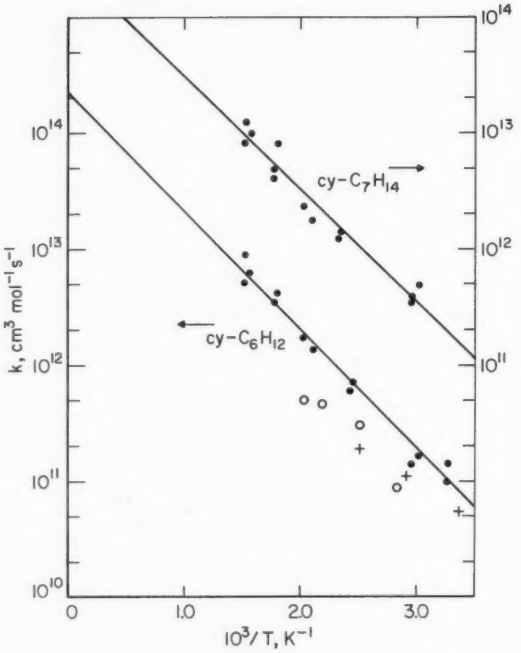

FIGURE 2. *Arrhenius plots for the reactions of atomic oxygen with cyclohexane and cycloheptane.*

● This work; + Stuckey and Heicklen, Ref. [3]; ○ Avramenko, et al., Ref. [4].

TABLE 5. *Arrhenius parameters and rate constants at 298 and 1000 K for the reactions of atomic oxygen with some cycloalkanes*[a]

Reactant	Log A	10^{-13} A (per C–H bond)	E/R	10^{-10} k(298 K)	10^{-12} k(1000 K)
Cy–C_3H_6[b]	11.49		1900		
Cy–C_4H_8[b]	12.79		2000		
Sp–C_5H_8	13.60 ± 0.10	0.50	2890 ± 100	0.25	2.2
Cy–C_5H_{10}[b]	12.68		1300		
Cy–C_5H_{10}	14.10 ± 0.09	1.25	2210 ± 100	7.5	14
Cy–C_6H_{12}[b]	12.88		1400		
Cy–C_6H_{12}[c]	13.73		2260		
Cy–C_6H_{12}	14.35 ± 0.09	1.87	2350 ± 100	8.3	21
Cy–C_7H_{14}	14.46 ± 0.13	2.06	2230 ± 140	16	31

[a] This work except as noted. Units of A and k are cm³ mol⁻¹ s⁻¹. Uncertainties are standard errors of the reported values based on a least-squares treatment.
[b] See Ref. 3.
[c] See Ref. 4.

derived earlier for the alkanes. Thus, the present results are consistent with and support the hydrogen atom abstraction mechanism proposed previously [1, 2].

This work was supported in part by the Measures for Air Quality Program of the National Bureau of Standards.

4. References

[1] Herron, J. T., and Huie, R. E., J. Phys. Chem. **73,** 1326 (1969).
[2] Herron, J. T., and Huie, R. E., J. Phys. Chem. **73,** 3327 (1969).
[3] Stuckey, W. K., and Heicklen, J., J. Chem. Phys. **46,** 4843 (1967).
[4] Avramenko, L. I., Kolesnikova, R. V., and Savinova, G. I., Izv. Akad. Nauk SSSR, Ser. Khim. **28** (1965).
[5] Kaufman, F., Progr. Reaction Kinetics, **1,** 1 (1961).

(Paper 76A2–701)

JOURNAL OF RESEARCH of the National Bureau of Standards—A. Physics and Chemistry
Vol. 76A, No. 2, March–April 1972

Densities of Compressed Liquid Methane, and the Equation of State*

Robert D. Goodwin and Rolf Prydz**

Institute for Basic Standards, National Bureau of Standards, Boulder, Colorado 80302

(September 30, 1971)

Experimental *PVT* data for liquid methane are reported at densities from 1.8 times critical up to the freezing liquid, at temperatures from 91 to 245 K and pressures to 350 bar. A nonanalytic equation of state is adjusted to these and other *PVT* data from ideal gas states to the freezing liquid, at temperatures from the triple point to 400 K.

Key words: Compressed liquid; densities; equation of state; methane; orthobaric densities.

Symbols, Units and Constants

(Subscripts c and t refer to critical and liquid triple points.)
(Subscripts g and l refer to saturated vapor and liquid.)

α, b, β, δ	constants in eq (4).
$A, B, C, D,$	density-dependent coefficients of eq (4).
$d,$	density, $d_c = 10.15$, $d_t = 28.1472$ mol/l.
l,	the liter, 1000 cm³.
mol,	16.043 grams of methane (carbon 12 scale).
$P,$	pressure, 1 bar $= 10^5$ N/m², 1 atm $=$ 1.01325 bar.
$P_t =$	0.1159 atm $=$ 0.117 4356 bar,
$P_c =$	45.9566 bar.
$R,$	the gas constant, 8.31434 J/mol-K (carbon 12 scale), R $=$ 0.0831434 bar-liter/mol K.
$\rho \equiv$	d/d_t, density reduced at the liquid triple point.
$\sigma \equiv$	d/d_c, density reduced at the critical point.
$T,$	temperature, kelvin on IPTS–1968, $T_t = 90.680$, $T_c = 190.53$.
$T_s(\rho),$	liquid.vapor coexistence temperature.
$\theta(\rho),$	a locus of temperatures.
$v \equiv$ l/$d,$	molal volume.
$\omega(\rho, T) \equiv$	$(T-\theta)/(\delta \cdot T_c)$.
$x \equiv T/T_c,$	temperature reduced at the critical point.
$Z \equiv Pv/RT,$	the "compressibility factor".

1. Introduction

This report gives experimental data and analytical formulations which are needed for the computation of tables of thermodynamic functions. Reviews of thermophysical properties [1, 2][1] show that densities available for the compressed liquid at low temperatures [3, 4] are not of the precision desired for thermal computations. Quite recently we have formulated available coexistence data [5, 6], and we have measured the melting- and vapor-pressures of methane [7].

We now report experimental *PVT* data for the compressed liquid at densities from $1.8 \cdot \rho_c$ up to the melting line, at pressures to 350 bar. We obtain densities of freezing liquid and of saturated liquid from these data by intersection with the $P(T)$ melting line and with the $P(T)$ vapor pressure line respectively. Densities of saturated vapor are obtained at intersections of the virial equation of state with the $P(T)$ vapor pressure line. The corresponding vapor-liquid saturation temperatures, $T_s(\rho)$, then are represented analytically.

Finally, we develop an equation of state for the entire $P(\rho, T)$ surface by use of *PVT* data of several authors, which data cover most of the domain at $T_t < T < 400$ K, $P \leq 350$ bar.

Temperatures are on the kelvin scale of IPTS–1968 [8]. Pressures are related to the International System by use of the bar, 1 bar $= 10^5$ Newtons per square meter (N/m^2).

*This work was carried out at the National Bureau of Standards under the sponsorship of the American Gas Association.
**Present address: Norsk Hydro, Inc., Bygdøy allé 2, Oslo 2, Norway.

[1] Figures in brackets indicate the literature references at the end of this paper.

2. Densities of the Compressed Liquid

Methane from a commercial supplier is the same lot used for $P(T)$ measurements on the two-phase boundaries [7]. It was specified to be 99.99 percent pure, the principal impurities being N_2, CO_2, and C_2H_6. Independent mass-spectral analysis yields the report of table A.

The apparatus is that developed for hydrogen [9], as modified for oxygen [10] and for fluorine [11]. We have used volumetric calibrations of the latter work [12]. For methane, the virial equation and a preliminary equation of state are used to find amounts in the gasometer and in nuisance volumes.

Uncertainty in the determination of density is at most 0.1 percent, as noted in [9]. This figure is an accumulation of errors for the total amount of sample, for the amount in capillary tube and null diaphragm, and for the temperature- and pressure-dependent volume of the pipet.

Our *PVT* data for compressed liquid methane are given in table 1 along experimental pseudo-isochores, arranged in the order of increasing densities. The first column gives our experimental sequence; the second gives density in mol/l; the third is temperature; and the fourth is observed pressure. Additional columns in this and following tables (2, 3, and 4) are discussed below. These data overlap those of Vennix [13] at $1.8 < \rho/\rho_c < 2.2$, and extend up to the melting line.

TABLE A. *Analysis of the methane sample*

Ethane	65 ppm*
Oxygen	22–60 ppm
Nitrogen	120–175 ppm
Minimum methane	99.97 percent

* Parts per million.

TABLE 1. *NBS densities for compressed liquid methane*

ID	MOL/L	T, K	P, BAR	P, CALC	P, PCT	D, PCT
1	10.150	190.530	45.957	45.957	−0.00	
2601	18.384	176.000	32.172	31.403	2.45	−0.22
2602	18.357	180.000	50.437	49.912	1.05	−0.13
2603	18.332	184.000	68.691	68.387	0.44	−0.07
2604	18.307	188.000	86.906	86.781	0.14	−0.03
2605	18.281	192.000	105.089	105.058	0.03	−0.01
2606	18.256	196.000	123.227	123.266	−0.03	0.01
2607	18.232	200.000	141.311	141.405	−0.07	0.02
2608	18.203	205.000	163.860	163.972	−0.07	0.02
2609	18.175	210.000	186.312	186.418	−0.06	0.01
2610	18.150	215.000	208.687	208.828	−0.07	0.02
2611	18.127	220.000	231.002	231.177	−0.08	0.02
2612	18.106	225.000	253.237	253.478	−0.10	0.03
2613	18.086	230.000	275.393	275.691	−0.11	0.03
2614	18.068	235.000	297.479	297.875	−0.13	0.04
2615	18.052	240.000	319.488	320.043	−0.17	0.05
2616	18.036	245.000	341.402	342.090	−0.20	0.06
2501	19.487	170.000	26.367	25.435	3.66	−0.17
2502	19.456	174.000	47.743	47.023	1.53	−0.12
2503	19.427	178.000	69.007	68.507	0.73	−0.08
2504	19.398	182.000	90.117	89.829	0.32	−0.04
2505	19.369	186.000	111.128	110.984	0.13	−0.02
2506	19.340	190.000	132.061	131.970	0.07	−0.01
2507	19.313	194.000	152.913	152.873	0.03	−0.00
2508	19.288	198.000	173.668	173.707	−0.02	0.00
2509	19.264	202.000	194.349	194.436	−0.04	0.01
2510	19.247	205.000	209.838	209.936	−0.05	0.01
2511	19.221	210.000	235.576	235.715	−0.06	0.01
2512	19.197	215.000	261.206	261.396	−0.07	0.02
2513	19.176	220.000	286.762	287.057	−0.10	0.03
2514	19.156	225.000	312.214	312.594	−0.12	0.03
2515	19.138	230.000	337.542	338.084	−0.16	0.04
2401	20.425	164.000	20.288	19.657	3.21	−0.08
2402	20.389	168.000	44.689	44.077	1.39	−0.07
2403	20.357	172.000	68.823	68.407	0.61	−0.05
2404	20.324	176.000	92.700	92.447	0.27	−0.03

TABLE 1. *NBS densities for compressed liquid methane*—Continued

ID	MOL/L	T, K	P, BAR	P, CALC	P, PCT	D, PCT
2405	20.292	180.000	116.390	116.290	0.09	−0.01
2406	20.260	184.000	139.966	139.892	0.05	−0.01
2407	20.231	188.000	163.418	163.421	−0.00	0.00
2408	20.206	192.000	186.776	186.963	−0.10	0.02
2409	20.178	196.000	210.084	210.122	−0.02	0.00
2410	20.155	200.000	233.321	233.387	−0.03	0.01
2411	20.134	204.000	256.494	256.599	−0.04	0.01
2412	20.115	208.000	279.599	279.775	−0.06	0.01
2413	20.097	212.000	302.629	302.860	−0.08	0.02
2414	20.080	216.000	325.569	325.862	−0.09	0.02
2415	20.065	220.000	348.434	348.867	−0.12	0.03
2301	21.371	158.000	19.836	19.616	1.12	−0.02
2302	21.332	162.000	47.537	47.203	0.71	−0.03
2303	21.294	166.000	74.747	74.479	0.36	−0.02
2304	21.258	170.000	101.595	101.522	0.07	−0.01
2305	21.223	174.000	128.287	128.293	−0.00	0.00
2306	21.189	178.000	154.807	154.806	0.00	−0.00
2307	21.158	182.000	181.216	181.214	0.00	−0.00
2308	21.129	186.000	207.556	207.477	0.04	−0.01
2309	21.103	190.000	233.818	233.691	0.05	−0.01
2310	21.080	194.000	260.026	259.888	0.05	−0.01
2311	21.059	198.000	286.118	286.015	0.04	−0.01
2312	21.040	202.000	312.140	312.093	0.02	−0.00
2313	21.022	206.000	338.043	338.053	−0.00	0.00
2201	22.125	152.000	14.593	15.002	−2.73	0.03
2202	22.080	156.000	45.088	45.142	−0.12	0.00
2203	22.040	160.000	74.923	75.141	−0.29	0.01
2204	22.001	164.000	104.403	104.772	−0.35	0.02
2205	21.962	168.000	133.692	133.981	−0.22	0.02
2206	21.929	172.000	162.772	163.249	−0.29	0.03
2207	21.892	176.000	191.756	191.825	−0.04	0.00
2208	21.862	180.000	220.648	220.612	0.02	−0.00
2209	21.836	184.000	249.520	249.420	0.04	−0.01
2210	21.812	188.000	278.308	278.109	0.07	−0.01
2211	21.791	192.000	307.015	306.799	0.07	−0.01
2212	21.772	196.000	335.575	335.425	0.04	−0.01
2101	22.873	146.000	13.127	14.032	−6.45	0.05
2102	22.824	150.000	46.703	46.959	−0.55	0.01
2103	22.782	154.000	79.462	79.859	−0.50	0.02
2104	22.739	158.000	111.736	112.134	−0.36	0.02
2105	22.698	162.000	143.810	144.060	−0.17	0.01
2106	22.660	166.000	175.712	175.764	−0.03	0.00
2107	22.626	170.000	207.555	207.387	0.08	−0.01
2108	22.596	174.000	239.330	238.979	0.15	−0.02
2109	22.570	178.000	271.112	270.591	0.19	−0.02
2110	22.546	182.000	302.767	302.060	0.23	−0.03
2111	22.525	186.000	334.282	333.523	0.23	−0.03
2001	23.570	140.000	12.262	13.567	−9.62	0.06
2002	23.518	144.000	48.910	49.337	−0.87	0.02
2003	23.472	148.000	84.500	84.959	−0.54	0.02
2004	23.426	152.000	119.526	119.919	−0.33	0.02
2005	23.383	156.000	154.350	154.555	−0.13	0.01
2006	23.343	160.000	189.067	188.918	0.08	−0.01
2007	23.308	164.000	223.762	223.280	0.22	−0.02
2008	23.278	168.000	258.440	257.710	0.28	−0.03
2009	23.252	172.000	293.040	292.156	0.30	−0.03
2010	23.228	176.000	327.578	326.431	0.35	−0.04
1901	24.183	134.000	6.861	8.975	−23.55	0.08
1902	24.125	138.000	46.383	47.136	−1.60	0.03

453-425 OL - 72 - 2

TABLE 1. *NBS densities for compressed liquid methane*—Continued

ID	MOL/L	T, K	P, BAR	P, CALC	P, PCT	D, PCT
1903	24.076	142.000	84.630	85.409	−0.91	0.03
1904	24.027	146.000	122.240	122.896	−0.53	0.02
1905	23.981	150.000	159.656	159.984	−0.20	0.01
1906	23.940	154.000	197.040	196.975	0.03	−0.00
1801	24.174	134.000	5.841	8.040	−27.35	0.09
1802	24.141	136.000	25.770	26.798	−3.84	0.04
1803	24.115	138.000	45.258	46.066	−1.75	0.03
1804	24.090	140.000	64.512	65.231	−1.10	0.03
1805	24.066	142.000	83.348	84.303	−1.13	0.04
1806	24.042	144.000	102.134	103.182	−1.02	0.04
1807	24.017	146.000	120.944	121.757	−0.67	0.03
1808	23.994	148.000	139.702	140.373	−0.48	0.02
1809	23.971	150.000	158.374	158.811	−0.28	0.02
1810	23.950	152.000	177.053	177.312	−0.15	0.01
1811	23.931	154.000	195.747	195.889	−0.07	0.00
1812	23.912	156.000	214.417	214.311	0.05	−0.00
1813	23.893	158.000	232.888	232.581	0.13	−0.01
1814	23.877	160.000	251.636	251.080	0.22	−0.02
1815	23.862	162.000	270.317	269.571	0.28	−0.02
1816	23.849	164.000	288.962	288.191	0.27	−0.02
1817	23.836	166.000	307.694	306.691	0.33	−0.03
1818	23.824	168.000	326.391	325.205	0.36	−0.04
1819	23.812	170.000	344.986	343.606	0.40	−0.04
1701	24.605	130.000	7.286	9.055	−19.54	0.06
1702	24.572	132.000	28.230	28.867	−2.21	0.02
1703	24.546	134.000	48.781	49.241	−0.93	0.02
1704	24.519	136.000	68.894	69.262	−0.53	0.01
1705	24.494	138.000	88.639	89.295	−0.74	0.02
1706	24.469	140.000	108.425	109.110	−0.63	0.02
1707	24.443	142.000	128.176	128.587	−0.32	0.01
1708	24.419	144.000	147.856	148.106	−0.17	0.01
1709	24.396	146.000	167.516	167.554	−0.02	0.00
1710	24.374	148.000	187.222	186.939	0.15	−0.01
1711	24.354	150.000	206.921	206.403	0.25	−0.02
1712	24.335	152.000	226.644	225.827	0.36	−0.03
1713	24.317	154.000	246.119	245.219	0.37	−0.03
1714	24.301	156.000	265.906	264.725	0.45	−0.04
1715	24.286	158.000	285.671	284.221	0.51	−0.04
1716	24.273	160.000	305.459	303.856	0.53	−0.05
1717	24.260	162.000	325.155	323.358	0.56	−0.05
1718	24.248	164.000	344.921	342.874	0.60	−0.06
1601	24.996	126.000	4.795	7.075	−32.23	0.07
1602	24.960	128.000	26.740	27.553	−2.95	0.03
1603	24.933	130.000	48.275	48.887	−1.25	0.02
1604	24.905	132.000	69.442	69.831	−0.56	0.01
1605	24.879	134.000	90.206	90.781	−0.63	0.02
1606	24.852	136.000	110.901	111.354	−0.41	0.01
1607	24.826	138.000	131.487	131.823	−0.25	0.01
1608	24.801	140.000	152.046	152.198	−0.10	0.00
1609	24.777	142.000	172.619	172.489	0.08	−0.00
1610	24.754	144.000	193.223	192.707	0.27	−0.01
1611	24.734	146.000	213.859	213.146	0.33	−0.02
1612	24.715	148.000	234.593	233.538	0.45	−0.03
1613	24.714	148.000	234.564	233.395	0.50	−0.03
1614	24.697	150.000	255.294	253.895	0.55	−0.04
1615	24.681	152.000	276.024	274.371	0.60	−0.05
1616	24.666	154.000	296.684	294.833	0.63	−0.05
1617	24.652	156.000	317.346	315.290	0.65	−0.06
1618	24.639	158.000	338.030	335.751	0.68	−0.06

TABLE 1. *NBS densities for compressed liquid methane*—Continued

ID	MOL/L	T, K	P, BAR	P, CALC	P, PCT	D, PCT
1501	25.386	122.000	3.482	6.324	−44.94	0.08
1502	25.348	124.000	26.168	27.592	−5.16	0.04
1503	25.320	126.000	48.814	49.922	−2.22	0.03
1504	25.293	128.000	70.363	72.103	−2.41	0.05
1505	25.266	130.000	92.218	94.005	−1.90	0.05
1506	25.239	132.000	114.039	115.637	−1.38	0.04
1507	25.212	134.000	135.786	137.005	−0.89	0.03
1508	25.211	134.000	135.814	136.859	−0.76	0.03
1509	25.184	136.000	157.173	157.971	−0.50	0.02
1510	25.160	138.000	178.801	179.281	−0.27	0.01
1511	25.137	140.000	200.430	200.510	−0.04	0.00
1512	25.116	142.000	222.144	221.822	0.15	−0.01
1513	25.097	144.000	243.865	243.231	0.26	−0.02
1514	25.080	146.000	265.643	264.755	0.34	−0.02
1515	25.064	148.000	287.462	286.251	0.42	−0.03
1516	25.049	150.000	309.282	307.728	0.50	−0.04
1517	25.035	152.000	330.987	329.197	0.54	−0.04
1518	25.022	154.000	352.726	350.667	0.59	−0.05
1401	25.777	118.000	4.740	7.269	−34.80	0.07
1402	25.739	120.000	28.487	29.634	−3.87	0.03
1403	25.710	122.000	51.814	53.002	−2.24	0.03
1404	25.682	124.000	74.303	76.199	−2.49	0.05
1405	25.654	126.000	97.196	99.086	−1.91	0.05
1406	25.625	128.000	120.010	121.516	−1.24	0.04
1407	25.598	130.000	142.846	143.967	−0.78	0.03
1408	25.574	132.000	165.554	166.619	−0.64	0.03
1409	25.550	134.000	188.320	189.008	−0.36	0.02
1410	25.524	136.000	211.062	210.816	0.12	−0.01
1411	25.503	138.000	233.855	233.195	0.28	−0.02
1412	25.503	138.000	233.445	233.195	0.11	−0.01
1413	25.484	140.000	256.331	255.678	0.26	−0.02
1414	25.466	142.000	279.330	278.111	0.44	−0.03
1415	25.450	144.000	302.209	300.677	0.51	−0.04
1416	25.435	146.000	325.227	323.221	0.62	−0.05
1417	25.422	148.000	348.148	345.926	0.64	−0.05
1301	26.142	114.000	4.106	5.811	−29.34	0.04
1302	26.103	116.000	28.896	29.135	−0.82	0.01
1303	26.072	118.000	52.968	53.369	−0.75	0.01
1304	26.044	120.000	76.358	77.737	−1.77	0.03
1305	26.014	122.000	100.162	101.430	−1.25	0.03
1306	25.985	124.000	123.929	124.955	−0.82	0.02
1307	25.956	126.000	147.655	148.158	−0.34	0.01
1308	25.929	128.000	171.338	171.393	−0.03	0.00
1309	25.904	130.000	195.123	194.677	0.23	−0.01
1310	25.881	132.000	218.955	218.030	0.42	−0.02
1311	25.880	132.000	218.534	217.855	0.31	−0.01
1312	25.859	134.000	242.441	241.293	0.48	−0.03
1313	25.840	136.000	266.440	264.837	0.61	−0.03
1314	25.822	138.000	290.474	288.323	0.75	−0.05
1315	25.807	140.000	314.577	312.130	0.78	−0.05
1316	25.792	142.000	338.590	335.726	0.85	−0.06
1201	26.519	110.000	5.935	7.782	−23.73	0.04
1202	26.480	112.000	31.839	32.288	−1.39	0.01
1203	26.449	114.000	56.444	57.777	−2.31	0.03
1204	26.419	116.000	81.054	83.045	−2.40	0.04
1205	26.388	118.000	105.870	107.750	−1.74	0.04
1206	26.357	120.000	130.659	132.083	−1.08	0.03
1207	26.327	122.000	155.400	156.241	−0.54	0.02
1208	26.299	124.000	180.154	180.425	−0.15	0.01

TABLE 1. *NBS densities for compressed liquid methane*—Continued

ID	MOL/L	T, K	P, BAR	P, CALC	P, PCT	D, PCT
1209	26.274	126.000	204.975	204.840	0.07	−0.00
1210	26.251	128.000	229.892	229.325	0.25	−0.01
1211	26.230	130.000	254.906	253.899	0.40	−0.02
1212	26.211	132.000	280.025	278.581	0.52	−0.03
1213	26.193	134.000	305.214	303.196	0.67	−0.04
1214	26.192	134.000	304.967	303.002	0.65	−0.04
1215	26.176	136.000	330.185	327.759	0.74	−0.05
1101	26.901	106.000	12.022	12.593	−4.54	0.01
1102	26.864	108.000	38.986	38.731	0.66	−0.00
1103	26.833	110.000	64.591	65.550	−1.46	0.02
1104	26.801	112.000	90.300	91.734	−1.56	0.03
1105	26.768	114.000	116.122	117.294	−1.00	0.02
1106	26.736	116.000	141.871	142.638	−0.54	0.01
1107	26.706	118.000	167.653	167.983	−0.20	0.01
1108	26.679	120.000	193.539	193.550	−0.01	0.00
1109	26.653	122.000	219.542	218.964	0.26	−0.01
1110	26.630	124.000	245.820	244.647	0.48	−0.02
1111	26.631	124.000	245.678	244.851	0.34	−0.02
1112	26.610	126.000	272.049	270.626	0.53	−0.03
1113	26.592	128.000	298.510	296.721	0.60	−0.03
1114	26.574	130.000	325.020	322.534	0.77	−0.04
1115	26.559	132.000	351.423	348.707	0.78	−0.05
1001	27.232	102.000	8.474	9.235	−8.24	0.01
1002	27.192	104.000	36.489	36.050	1.22	−0.01
1003	27.160	106.000	63.034	63.985	−1.49	0.02
1004	27.127	108.000	89.515	91.224	−1.87	0.03
1005	27.093	110.000	116.218	117.781	−1.33	0.03
1006	27.060	112.000	142.937	144.093	−0.80	0.02
1007	27.029	114.000	169.612	170.392	−0.46	0.01
1008	27.001	116.000	196.480	196.915	−0.22	0.01
1009	27.001	116.000	196.471	196.915	−0.23	0.01
1010	26.976	118.000	223.568	223.689	−0.05	0.00
1011	26.952	120.000	250.862	250.311	0.22	−0.01
1012	26.931	122.000	278.278	277.234	0.38	−0.02
1013	26.912	124.000	305.898	304.267	0.54	−0.03
1014	26.895	126.000	333.424	331.430	0.60	−0.03
901	27.588	98.000	12.437	12.343	0.76	−0.00
902	27.548	100.000	41.407	40.503	2.23	−0.01
903	27.516	102.000	68.696	69.861	−1.67	0.02
904	27.481	104.000	96.270	98.007	−1.77	0.03
905	27.447	106.000	124.002	125.853	−1.47	0.03
906	27.413	108.000	151.755	153.199	−0.94	0.02
907	27.382	110.000	179.649	180.747	−0.61	0.02
908	27.353	112.000	207.794	208.298	−0.24	0.01
909	27.328	114.000	236.148	236.336	−0.08	0.00
910	27.305	116.000	264.752	264.435	0.12	−0.01
911	27.305	116.000	264.894	264.435	0.17	−0.01
912	27.285	118.000	293.612	292.851	0.26	−0.01
913	27.266	120.000	322.446	321.144	0.41	−0.02
801	27.900	94.000	7.513	6.980	7.64	−0.01
802	27.858	96.000	37.517	36.064	4.03	−0.02
803	27.825	98.000	65.517	66.637	−1.68	0.02
804	27.789	100.000	94.061	95.894	−1.91	0.03
805	27.753	102.000	122.725	124.572	−1.48	0.03
806	27.719	104.000	151.383	153.178	−1.17	0.03
807	27.686	106.000	180.222	181.498	−0.70	0.02
808	27.657	108.000	209.351	210.286	−0.44	0.01
809	27.630	110.000	238.728	239.088	−0.15	0.01
810	27.607	112.000	268.394	268.423	−0.01	0.00

TABLE 1. *NBS densities for compressed liquid methane*—Continued

ID	MOL/L	T, K	P, BAR	P, CALC	P, PCT	D, PCT
811	27.586	114.000	298.261	297.832	0.14	−0.01
812	27.567	116.000	328.347	327.343	0.31	−0.01
1	28.147	90.680	0.117	0.117	0.00	0.00
601	28.209	92.000	44.123	42.754	3.20	−0.02
602	28.175	94.000	72.852	74.640	−2.40	0.02
603	28.137	96.000	102.543	104.830	−2.18	0.03
604	28.101	98.000	132.353	134.893	−1.88	0.04
605	28.066	100.000	162.180	164.607	−1.47	0.03
606	28.066	100.000	162.190	164.607	−1.47	0.03
607	28.034	102.000	192.243	194.518	−1.17	0.03
608	28.004	104.000	222.687	224.401	−0.76	0.02
609	27.978	106.000	253.551	254.808	−0.49	0.02
610	27.955	108.000	284.641	285.515	−0.31	0.01
611	27.935	110.000	316.018	316.555	−0.17	0.01
612	27.916	112.000	347.527	347.429	0.03	−0.00
701	28.391	94.000	128.133	131.785	−2.77	0.05
702	28.354	96.000	158.893	162.333	−2.12	0.04
703	28.321	98.000	189.886	193.337	−1.78	0.04
704	28.290	100.000	221.338	224.286	−1.31	0.04
705	28.264	102.000	253.222	256.041	−1.10	0.04
706	28.240	104.000	285.440	287.814	−0.82	0.03
707	28.219	106.000	318.049	319.914	−0.58	0.02
708	28.200	108.000	350.566	352.099	−0.44	0.02
514	28.552	96.500	224.938	228.216	−1.44	0.04
515	28.545	97.000	233.128	236.381	−1.38	0.04
516	28.531	98.000	249.643	252.596	−1.17	0.04
517	28.507	100.000	282.843	285.748	−1.02	0.03
518	28.507	100.000	282.935	285.748	−0.98	0.03
519	28.486	102.000	316.433	319.221	−0.87	0.03
520	28.466	104.000	350.093	352.461	−0.67	0.03

TABLE 2. *Methane densities via the virial equation of* [5]

MOL/L	T, K	P, BAR	P, CALC	P, PCT	D, PCT
0.500	140.000	5.213	5.221	−0.14	0.16
0.500	145.000	5.443	5.448	−0.09	0.10
0.500	150.000	5.670	5.673	−0.05	0.06
0.500	155.000	5.896	5.898	−0.03	0.03
0.500	160.000	6.120	6.121	−0.01	0.01
0.500	165.000	6.344	6.344	−0.00	0.00
0.500	170.000	6.566	6.566	0.00	−0.00
0.500	175.000	6.788	6.787	0.01	−0.01
0.500	180.000	7.009	7.008	0.01	−0.01
0.500	185.000	7.229	7.228	0.01	−0.01
0.500	190.000	7.448	7.448	0.01	−0.01
0.500	195.000	7.668	7.667	0.01	−0.01
0.500	200.000	7.887	7.886	0.00	−0.00
0.500	205.000	8.105	8.105	0.00	−0.00
0.500	210.000	8.323	8.323	−0.00	0.00
0.500	215.000	8.541	8.541	−0.00	0.00
0.500	220.000	8.758	8.759	−0.00	0.00
0.500	225.000	8.976	8.976	−0.01	0.01
0.500	230.000	9.193	9.193	−0.01	0.01
0.500	235.000	9.409	9.410	−0.01	0.01
0.500	240.000	9.626	9.627	−0.01	0.01
0.500	245.000	9.842	9.844	−0.01	0.01
0.500	250.000	10.059	10.060	−0.01	0.01
0.500	255.000	10.275	10.276	−0.01	0.01
0.500	260.000	10.491	10.492	−0.01	0.01
0.500	265.000	10.707	10.708	−0.01	0.01
0.500	270.000	10.923	10.924	−0.01	0.01
1.000	150.000	10.230	10.247	−0.16	0.21
1.000	155.000	10.723	10.731	−0.08	0.09
1.000	160.000	11.209	11.211	−0.02	0.02
1.000	165.000	11.689	11.687	0.02	−0.02
1.000	170.000	12.165	12.160	0.04	−0.05
1.000	175.000	12.636	12.630	0.05	−0.06
1.000	180.000	13.105	13.097	0.06	−0.07
1.000	185.000	13.570	13.563	0.06	−0.06
1.000	190.000	14.033	14.026	0.05	−0.06
1.000	195.000	14.494	14.488	0.05	−0.05
1.000	200.000	14.954	14.948	0.04	−0.04
1.000	205.000	15.411	15.406	0.03	−0.04
1.000	210.000	15.867	15.864	0.02	−0.03
1.000	215.000	16.322	16.320	0.02	−0.02
1.000	220.000	16.776	16.774	0.01	−0.01
1.000	225.000	17.229	17.228	0.00	−0.01
1.000	230.000	17.681	17.681	−0.00	0.00
1.000	235.000	18.132	18.133	−0.01	0.01
1.000	240.000	18.583	18.585	−0.01	0.01
1.000	245.000	19.032	19.035	−0.01	0.02
1.000	250.000	19.481	19.485	−0.02	0.02
1.000	255.000	19.930	19.934	−0.02	0.02
1.000	260.000	20.378	20.382	−0.02	0.03
1.000	265.000	20.825	20.830	−0.03	0.03
1.000	270.000	21.272	21.278	−0.03	0.03
1.500	160.000	15.310	15.319	−0.06	0.09
1.500	165.000	16.084	16.081	0.02	−0.03
1.500	170.000	16.847	16.834	0.08	−0.10
1.500	175.000	17.599	17.580	0.11	−0.14
1.500	180.000	18.343	18.321	0.12	−0.15
1.500	185.000	19.079	19.056	0.12	−0.15
1.500	190.000	19.809	19.787	0.11	−0.14

TABLE 2. *Methane densities via the virial equation of* [5]—Continued

MOL/L	T, K	P, BAR	P, CALC	P, PCT	D, PCT
1.500	195.000	20.535	20.514	0.10	−0.12
1.500	200.000	21.256	21.237	0.09	−0.11
1.500	205.000	21.973	21.956	0.08	−0.09
1.500	210.000	22.686	22.672	0.06	−0.07
1.500	215.000	23.397	23.386	0.05	−0.06
1.500	220.000	24.106	24.097	0.03	−0.04
1.500	225.000	24.812	24.806	0.02	−0.02
1.500	230.000	25.516	25.513	0.01	−0.01
1.500	235.000	26.218	26.218	0.00	−0.00
1.500	240.000	26.919	26.921	−0.01	0.01
1.500	245.000	27.618	27.622	−0.02	0.02
1.500	250.000	28.315	28.322	−0.02	0.03
1.500	255.000	29.012	29.021	−0.03	0.03
1.500	260.000	29.707	29.718	−0.04	0.04
1.500	265.000	30.401	30.414	−0.04	0.04
1.500	270.000	31.094	31.108	−0.04	0.05
2.000	170.000	20.664	20.639	0.12	−0.19
2.000	175.000	21.729	21.691	0.18	−0.26
2.000	180.000	22.776	22.731	0.20	−0.28
2.000	185.000	23.810	23.761	0.21	−0.28
2.000	190.000	24.831	24.782	0.20	−0.26
2.000	195.000	25.843	25.796	0.18	−0.24
2.000	200.000	26.847	26.803	0.16	−0.21
2.000	205.000	27.843	27.804	0.14	−0.18
2.000	210.000	28.833	28.800	0.12	−0.14
2.000	215.000	29.818	29.790	0.09	−0.11
2.000	220.000	30.798	30.777	0.07	−0.09
2.000	225.000	31.775	31.759	0.05	−0.06
2.000	230.000	32.747	32.737	0.03	−0.04
2.000	235.000	33.717	33.712	0.01	−0.02
2.000	240.000	34.683	34.684	−0.00	0.00
2.000	245.000	35.647	35.653	−0.02	0.02
2.000	250.000	36.609	36.619	−0.03	0.03
2.000	255.000	37.568	37.583	−0.04	0.04
2.000	260.000	38.526	38.544	−0.05	0.05
2.000	265.000	39.482	39.504	−0.06	0.06
2.000	270.000	40.436	40.461	−0.06	0.07

TABLE 3. *Methane densities of Vennix* [13]

MOL/L	T, K	P, BAR	P, CALC	P, PCT	D, PCT
2.560	172.527	24.660	24.653	0.03	−0.06
2.560	174.691	25.283	25.269	0.05	−0.09
2.559	177.203	25.994	25.976	0.07	−0.12
2.559	183.176	27.666	27.642	0.09	−0.14
2.559	190.532	29.676	29.664	0.04	−0.06
2.558	191.849	30.038	30.016	0.07	−0.10
2.556	203.084	33.048	33.036	0.04	−0.05
2.555	213.041	35.672	35.668	0.01	−0.02
2.555	217.864	36.931	36.930	0.00	−0.00
2.554	223.831	38.481	38.483	−0.00	0.00
2.553	233.546	40.990	40.989	0.00	−0.00
2.552	239.797	42.590	42.593	−0.01	0.01
2.551	252.833	45.897	45.910	−0.03	0.03
2.550	263.399	48.559	48.575	−0.03	0.04
2.548	273.380	51.058	51.074	−0.03	0.04
6.469	190.429	44.720	44.545	0.39	−2.53
6.471	190.532	44.814	44.641	0.39	−2.47
6.464	208.574	60.270	60.264	0.01	−0.02
6.459	223.234	72.346	72.419	−0.10	0.17
6.456	234.440	81.433	81.539	−0.13	0.20
6.453	243.733	88.913	89.016	−0.12	0.16
6.453	243.773	88.939	89.048	−0.12	0.17
6.451	251.376	95.018	95.119	−0.11	0.14
6.447	262.190	103.601	103.700	−0.10	0.12
6.444	272.155	111.478	111.550	−0.06	0.08
6.444	272.185	111.494	111.573	−0.07	0.08
7.235	190.052	44.989	44.798	0.43	−5.39
7.237	190.532	45.493	45.304	0.42	−4.35
7.235	190.750	45.710	45.532	0.39	−3.80
7.237	191.032	46.001	45.827	0.38	−3.40
7.234	193.325	48.336	48.192	0.30	−1.76
7.233	197.737	52.722	52.644	0.15	−0.57
7.231	202.753	57.627	57.604	0.04	−0.11
7.229	208.224	62.909	62.934	−0.04	0.10
7.228	212.165	66.689	66.736	−0.07	0.15
7.226	217.136	71.421	71.494	−0.10	0.20
7.224	222.926	76.909	76.995	−0.11	0.20
7.222	230.050	83.614	83.713	−0.12	0.19
7.219	237.336	90.432	90.536	−0.11	0.17
7.217	242.709	95.434	95.540	−0.11	0.15
7.215	248.444	100.757	100.861	−0.10	0.14
7.215	250.194	102.376	102.481	−0.10	0.13
7.214	253.445	105.378	105.483	−0.10	0.13
7.212	258.642	110.172	110.270	−0.09	0.11
7.210	263.050	114.229	114.323	−0.08	0.10
7.209	268.301	119.049	119.134	−0.07	0.09
7.207	273.171	123.504	123.581	−0.06	0.07
9.844	190.532	45.870	45.958	−0.19	12.43
9.844	191.032	46.579	46.685	−0.23	9.45
9.840	191.551	47.318	47.434	−0.25	7.18
9.840	192.938	49.282	49.431	−0.30	4.43
9.839	195.243	52.563	52.742	−0.34	2.62
9.838	197.562	55.870	56.069	−0.36	1.87
9.837	200.411	59.977	60.154	−0.29	1.13
9.835	202.829	63.417	63.620	−0.32	1.01
9.834	206.370	68.503	68.695	−0.28	0.72
9.830	213.503	78.771	78.921	−0.19	0.37
9.825	223.647	93.389	93.464	−0.08	0.12
9.819	236.398	111.767	111.738	0.03	−0.03

TABLE 3. *Methane densities of Vennix* [13]—Continued

MOL/L	T, K	P, BAR	P, CALC	P, PCT	D, PCT
9.814	248.147	128.674	128.567	0.08	−0.09
9.811	255.163	138.749	138.596	0.11	−0.12
9.802	273.167	164.504	164.289	0.13	−0.13
10.220	190.532	45.875	45.960	−0.18	16.32
10.219	191.032	46.607	46.705	−0.21	11.70
10.216	190.839	46.342	46.417	−0.16	11.88
10.216	191.040	46.618	46.717	−0.21	11.72
10.216	191.229	46.900	46.999	−0.21	9.98
10.216	191.428	47.188	47.296	−0.23	9.07
10.216	191.820	47.762	47.881	−0.25	7.34
10.216	192.076	48.131	48.264	−0.27	6.76
10.215	193.522	50.263	50.427	−0.32	4.00
10.214	195.158	52.700	52.877	−0.33	2.60
10.213	197.926	56.836	57.030	−0.34	1.64
10.212	200.575	60.814	61.011	−0.32	1.17
10.210	204.037	66.036	66.221	−0.28	0.78
10.208	207.855	71.799	71.978	−0.25	0.56
10.208	207.855	71.833	71.978	−0.20	0.46
10.206	213.044	79.691	79.814	−0.15	0.29
10.196	233.386	110.688	110.614	0.07	−0.08
10.186	252.887	140.387	140.173	0.15	−0.16
10.176	273.016	170.925	170.615	0.18	−0.17
10.176	273.058	170.987	170.679	0.18	−0.17
11.163	190.532	45.834	46.006	−0.37	30.29
11.162	191.032	46.643	46.808	−0.35	18.86
11.158	191.848	47.983	48.136	−0.32	5.62
11.158	191.873	48.009	48.177	−0.35	6.32
11.158	193.248	50.248	50.442	−0.39	3.48
11.157	195.110	53.340	53.540	−0.37	2.07
11.156	197.300	56.992	57.211	−0.38	1.50
11.155	199.216	60.228	60.441	−0.35	1.12
11.154	200.901	63.092	63.294	−0.32	0.87
11.153	203.064	66.782	66.968	−0.28	0.65
11.150	207.564	74.518	74.650	−0.18	0.33
11.147	213.197	84.266	84.322	−0.07	0.10
11.147	213.204	84.282	84.334	−0.06	0.10
11.147	213.212	84.293	84.348	−0.07	0.10
11.141	223.184	101.660	101.576	0.08	−0.10
11.136	233.161	119.122	118.904	0.18	−0.20
11.131	243.137	136.601	136.272	0.24	−0.24
11.126	253.153	154.123	153.739	0.25	−0.23
11.120	263.124	171.554	171.120	0.25	−0.22
11.115	273.092	188.977	188.493	0.26	−0.22
11.115	273.150	188.927	188.594	0.18	−0.15
11.771	190.532	45.823	46.135	−0.68	38.23
11.771	191.032	46.701	46.992	−0.62	16.17
11.767	192.498	49.295	49.551	−0.52	3.70
11.765	195.840	55.256	55.516	−0.47	1.65
11.764	198.182	59.511	59.756	−0.41	1.10
11.760	203.434	69.192	69.378	−0.27	0.50
11.755	212.034	85.308	85.352	−0.05	0.07
11.755	212.035	85.310	85.354	−0.05	0.07
11.749	222.632	105.407	105.264	0.14	−0.15
11.744	233.402	125.956	125.658	0.24	−0.23
11.744	233.403	125.973	125.660	0.25	−0.24
11.741	237.033	132.922	132.549	0.28	−0.26
11.741	237.034	132.920	132.551	0.28	−0.26
11.737	243.378	145.053	144.614	0.30	−0.27
11.737	243.381	145.050	144.620	0.30	−0.27

TABLE 3. *Methane densities of Vennix* [13]—Continued

MOL/L	T, K	P, BAR	P, CALC	P, PCT	D, PCT
11.732	253.284	163.987	163.492	0.30	−0.25
11.726	263.449	183.402	182.854	0.30	−0.24
11.724	268.300	192.683	192.101	0.30	−0.24
11.724	268.300	192.678	192.101	0.30	−0.24
11.721	272.694	201.050	200.469	0.29	−0.23
11.721	272.695	201.049	200.471	0.29	−0.22
11.721	272.698	201.046	200.476	0.28	−0.22
12.873	190.032	45.236	45.783	−1.20	11.00
12.872	191.032	47.247	47.773	−1.10	5.03
12.873	190.532	46.239	46.774	−1.15	6.77
12.868	190.703	46.599	47.111	−1.09	5.71
12.868	191.454	48.097	48.616	−1.07	4.21
12.868	192.397	49.969	50.523	−1.10	3.45
12.865	196.505	58.521	58.995	−0.80	1.47
12.861	203.573	73.642	73.948	−0.41	0.51
12.857	209.295	86.110	86.266	−0.18	0.19
12.851	218.622	106.682	106.607	0.07	−0.06
12.845	228.103	127.755	127.493	0.21	−0.17
12.839	238.550	151.093	150.664	0.28	−0.21
12.834	245.920	167.546	167.060	0.29	−0.21
12.829	252.972	183.347	182.778	0.31	−0.22
12.825	260.108	199.300	198.695	0.30	−0.21
12.821	267.312	215.373	214.767	0.28	−0.19
12.816	274.151	230.576	230.010	0.25	−0.16
13.756	188.969	43.856	44.457	−1.35	4.64
13.756	189.258	44.502	45.108	−1.34	4.05
13.756	189.767	45.639	46.262	−1.35	3.43
13.759	190.032	46.240	46.872	−1.35	3.19
13.755	190.172	46.549	47.183	−1.35	3.09
13.759	191.032	48.523	49.161	−1.30	2.50
13.755	190.447	47.177	47.812	−1.33	2.87
13.759	190.532	47.379	48.014	−1.32	2.80
13.755	190.738	47.840	48.478	−1.32	2.68
13.755	191.075	48.615	49.251	−1.29	2.48
13.753	192.892	52.817	53.453	−1.19	1.80
13.752	195.048	57.893	58.501	−1.04	1.31
13.752	195.065	57.928	58.542	−1.05	1.32
13.751	197.100	62.787	63.356	−0.90	1.00
13.749	200.010	69.812	70.306	−0.70	0.69
13.746	203.322	77.904	78.293	−0.50	0.44
13.744	207.197	87.439	87.726	−0.33	0.27
13.740	213.323	102.706	102.776	−0.07	0.05
13.733	222.792	126.432	126.292	0.11	−0.08
13.730	227.846	139.174	138.931	0.17	−0.12
13.727	233.272	152.884	152.544	0.22	−0.14
13.723	238.508	166.109	165.711	0.24	−0.15
13.720	242.985	177.429	176.987	0.25	−0.16
13.716	248.766	192.026	191.574	0.24	−0.15
13.713	253.111	203.005	202.554	0.22	−0.14
13.710	258.314	216.145	215.688	0.21	−0.13
13.707	262.932	227.811	227.350	0.20	−0.12
13.703	267.819	240.117	239.690	0.18	−0.11
13.703	267.886	240.288	239.861	0.18	−0.11
13.700	273.153	253.551	253.145	0.16	−0.09
14.976	187.649	43.274	43.891	−1.41	1.34
14.975	188.927	46.771	47.426	−1.38	1.18
14.978	190.532	51.216	51.918	−1.35	1.05
14.973	191.453	53.786	54.477	−1.27	0.94
14.971	194.804	63.256	63.941	−1.07	0.71

TABLE 3. *Methane densities of Vennix* [13]—Continued

MOL/L	T, K	P, BAR	P, CALC	P, PCT	D, PCT
14.967	199.611	77.104	77.688	−0.75	0.45
14.965	203.054	87.135	87.635	−0.57	0.33
14.961	207.627	100.574	100.948	−0.37	0.20
14.958	212.935	116.265	116.512	−0.21	0.11
14.951	221.360	141.310	141.395	−0.06	0.03
14.946	228.637	163.016	163.004	0.01	−0.00
14.940	236.599	186.801	186.739	0.03	−0.02
14.934	245.086	212.140	212.082	0.03	−0.01
14.928	253.068	235.968	235.924	0.02	−0.01
14.922	260.836	259.036	259.131	−0.04	0.02
14.917	268.824	282.716	282.976	−0.09	0.05
14.912	275.154	301.472	301.821	−0.12	0.06
16.529	183.351	38.252	38.638	−1.00	0.30
16.527	185.267	44.884	45.439	−1.22	0.38
16.524	189.259	58.970	59.716	−1.25	0.41
16.528	190.532	63.513	64.353	−1.31	0.43
16.520	194.419	77.509	78.329	−1.05	0.35
16.517	198.420	91.963	92.864	−0.97	0.33
16.514	201.044	101.638	102.427	−0.77	0.27
16.509	207.770	126.173	127.056	−0.70	0.25
16.504	213.668	147.882	148.744	−0.58	0.21
16.496	222.893	181.824	182.777	−0.52	0.20
16.488	232.812	218.350	219.431	−0.49	0.19
16.481	241.295	249.578	250.780	−0.48	0.19
16.471	254.531	298.027	299.605	−0.53	0.21
16.464	261.826	324.594	326.421	−0.56	0.23
16.459	267.883	346.584	348.640	−0.59	0.24
16.455	272.981	364.997	367.288	−0.62	0.26
17.570	179.140	33.044	32.888	0.48	−0.07
17.570	179.830	35.849	35.772	0.22	−0.03
17.568	181.008	40.651	40.700	−0.12	0.02
17.565	184.441	54.773	55.111	−0.61	0.12
17.566	190.532	80.090	80.938	−1.05	0.24
17.555	196.384	104.601	105.638	−0.98	0.25
17.551	200.537	122.244	123.296	−0.85	0.23
17.544	208.822	157.426	158.617	−0.75	0.22
17.537	217.044	192.276	193.684	−0.73	0.22
17.530	225.022	225.974	227.709	−0.76	0.24
17.522	233.079	259.963	261.996	−0.78	0.25
17.515	240.996	293.223	295.632	−0.81	0.27
17.507	250.735	333.924	336.853	−0.87	0.30
17.500	258.646	366.598	370.211	−0.98	0.35
17.493	266.750	400.092	404.263	−1.03	0.37
17.486	274.303	431.136	435.827	−1.08	0.39
18.495	182.834	65.518	66.743	−1.84	0.27
18.495	182.834	65.491	66.743	−1.87	0.28
18.502	175.629	31.376	31.857	−1.51	0.13
18.500	178.081	42.935	43.709	−1.77	0.20
18.490	188.292	91.648	93.246	−1.71	0.30
18.494	190.532	102.401	104.296	−1.82	0.34
18.485	193.630	117.303	119.193	−1.59	0.32
18.480	198.667	141.558	143.673	−1.47	0.32
18.476	203.156	163.181	165.489	−1.39	0.32
18.472	208.214	187.511	190.068	−1.35	0.33
18.467	212.424	207.694	210.472	−1.32	0.34
18.462	218.758	238.049	241.163	−1.29	0.35
18.457	223.742	261.867	265.231	−1.27	0.35
18.452	229.135	287.485	291.240	−1.29	0.37
18.448	233.395	307.683	311.741	−1.30	0.38

TABLE 3. *Methane densities of Vennix* [13]—Continued

MOL/L	T, K	P, BAR	P, CALC	P, PCT	D, PCT
18.444	237.607	327.596	331.970	−1.32	0.39
18.439	243.055	353.252	358.014	−1.33	0.40
18.434	248.039	376.587	381.812	−1.37	0.42
18.429	253.126	400.348	405.992	−1.39	0.44
18.420	263.283	447.525	454.082	−1.44	0.47
18.411	272.927	498.737	499.450	−0.14	0.05
20.003	172.566	55.009	57.430	−4.21	0.32
19.997	178.480	90.082	93.134	−3.28	0.36
19.988	186.850	139.761	143.501	−2.61	0.38
19.991	190.532	161.544	165.925	−2.64	0.42
19.979	196.089	194.310	198.830	−2.27	0.40
19.970	204.181	241.785	246.973	−2.10	0.41
19.963	211.525	284.629	290.457	−2.01	0.43
19.955	219.063	328.253	334.799	−1.95	0.44
19.946	227.105	374.341	381.848	−1.97	0.47
19.938	235.300	421.001	429.484	−1.98	0.50
19.929	244.174	470.891	480.637	−2.03	0.53
19.919	253.828	524.859	535.856	−2.05	0.56
19.913	259.343	555.441	567.200	−2.07	0.58
19.905	267.733	601.053	614.570	−2.20	0.63
19.898	274.489	638.125	652.480	−2.20	0.65
21.221	172.766	113.831	119.246	−4.54	0.42
21.216	176.889	142.805	148.646	−3.93	0.42
21.211	181.669	176.336	182.542	−3.40	0.42
21.201	189.783	232.523	239.707	−3.00	0.44
21.207	190.532	237.772	245.506	−3.15	0.47
21.193	197.315	284.387	292.377	−2.73	0.45
21.186	204.169	331.269	339.933	−2.55	0.46
21.176	212.644	388.576	398.246	−2.43	0.48
21.158	228.430	493.464	505.405	−2.36	0.52
21.150	235.778	541.550	554.696	−2.37	0.55
21.138	247.380	616.528	631.777	−2.41	0.59
21.131	252.992	652.311	668.704	−2.45	0.61
22.419	168.753	169.422	177.589	−4.60	0.42
22.405	180.116	262.685	271.707	−3.32	0.41
22.395	188.528	330.450	340.419	−2.93	0.42
22.400	190.532	346.440	357.440	−3.08	0.45
22.385	196.791	396.392	407.118	−2.63	0.42
22.376	204.366	455.919	467.593	−2.50	0.43
22.368	211.255	509.403	522.106	−2.43	0.45
22.360	218.293	563.516	577.319	−2.39	0.46
22.350	226.285	624.075	639.303	−2.38	0.49
22.340	234.420	685.032	701.878	−2.40	0.51

TABLE 4. *Methane densities of Douslin et al.* [22]

MOL/L	T, K	P, BAR	P, CALC	P, PCT	D, PCT
0.750	273.150	16.376	16.377	−0.00	0.01
0.750	298.142	18.020	18.020	0.00	0.00
0.750	303.143	18.347	18.348	−0.00	0.00
0.750	323.140	19.656	19.658	−0.01	0.01
0.750	348.143	21.292	21.292	0.00	−0.00
0.750	373.150	22.925	22.923	0.01	−0.01
0.750	398.160	24.557	24.551	0.03	−0.03
1.000	273.150	21.558	21.559	−0.01	0.01
1.000	298.142	23.786	23.787	−0.01	0.01
1.000	303.143	24.232	24.232	0.00	−0.00
1.000	323.140	26.006	26.007	−0.00	0.00
1.000	348.143	28.221	28.219	0.01	−0.01
1.000	373.150	30.431	30.425	0.02	−0.02
1.000	398.160	32.637	32.627	0.03	−0.03
1.500	273.150	31.539	31.545	−0.02	0.02
1.500	298.142	34.993	34.999	−0.02	0.02
1.500	303.143	35.685	35.688	−0.01	0.01
1.500	323.140	38.427	38.434	−0.02	0.02
1.500	348.143	41.852	41.853	−0.00	0.00
1.500	373.150	45.267	45.260	0.02	−0.02
1.500	398.160	48.676	48.656	0.04	−0.04
2.000	273.150	41.053	41.063	−0.03	0.03
2.000	298.142	45.804	45.817	−0.03	0.03
2.000	303.143	46.753	46.764	−0.02	0.03
2.000	323.140	50.530	50.538	−0.01	0.02
2.000	348.143	55.222	55.232	−0.02	0.02
2.000	373.150	59.920	59.905	0.02	−0.03
2.000	398.160	64.582	64.561	0.03	−0.03
2.500	273.150	50.139	50.158	−0.04	0.04
2.500	298.142	56.263	56.286	−0.04	0.04
2.500	303.143	57.485	57.506	−0.04	0.04
2.500	323.140	62.343	62.364	−0.03	0.04
2.500	348.143	68.390	68.403	−0.02	0.02
2.500	373.150	74.424	74.411	0.02	−0.02
2.500	398.160	80.411	80.392	0.02	−0.02
3.000	273.150	58.842	58.875	−0.06	0.06
3.000	298.142	66.415	66.451	−0.05	0.06
3.000	303.143	67.940	67.958	−0.03	0.03
3.000	323.140	73.926	73.958	−0.04	0.05
3.000	348.143	81.391	81.413	−0.03	0.03
3.000	373.150	88.835	88.825	0.01	−0.01
3.000	398.160	96.229	96.201	0.03	−0.03
3.500	273.150	67.222	67.258	−0.05	0.06
3.500	298.142	76.307	76.356	−0.06	0.07
3.500	303.143	78.146	78.166	−0.02	0.03
3.500	323.140	85.324	85.367	−0.05	0.05
3.500	348.143	94.279	94.310	−0.03	0.03
3.500	373.150	103.203	103.198	0.00	−0.00
3.500	398.160	112.073	112.039	0.03	−0.03
4.000	273.150	75.307	75.354	−0.06	0.07
4.000	298.142	85.992	86.049	−0.07	0.07
4.000	303.143	88.142	88.175	−0.04	0.04
4.000	323.140	96.585	96.638	−0.06	0.06
4.000	348.143	107.094	107.143	−0.05	0.05
4.000	373.150	117.577	117.581	−0.00	0.00
4.000	398.160	127.993	127.961	0.02	−0.02
4.500	273.150	83.156	83.208	−0.06	0.07
4.500	298.142	95.511	95.577	−0.07	0.08
4.500	303.143	98.002	98.035	−0.03	0.04

TABLE 4. *Methane densities of Douslin et al.* [22]—Continued

MOL/L	T, K	P, BAR	P, CALC	P, PCT	D, PCT
4.500	323.140	107.779	107.820	−0.04	0.04
4.500	348.143	119.920	119.965	−0.04	0.04
4.500	373.150	132.013	132.030	−0.01	0.01
4.500	398.160	144.083	144.026	0.04	−0.04
5.000	273.150	90.802	90.868	−0.07	0.09
5.000	298.142	104.911	104.986	−0.07	0.08
5.000	303.143	107.745	107.792	−0.04	0.05
5.000	323.140	118.912	118.962	−0.04	0.05
5.000	348.143	132.781	132.827	−0.03	0.04
5.000	373.150	146.583	146.600	−0.01	0.01
5.000	398.160	160.346	160.293	0.03	−0.03
5.500	273.150	98.315	98.381	−0.07	0.08
5.500	298.142	114.261	114.327	−0.06	0.06
5.500	303.143	117.449	117.498	−0.04	0.05
5.500	323.140	130.030	130.119	−0.07	0.07
5.500	348.143	145.748	145.787	−0.03	0.03
5.500	373.150	161.321	161.351	−0.02	0.02
5.500	398.160	176.887	176.827	0.03	−0.03
6.000	273.150	105.680	105.793	−0.11	0.13
6.000	298.142	123.585	123.650	−0.05	0.06
6.000	303.143	127.160	127.202	−0.03	0.04
6.000	323.140	141.261	141.342	−0.06	0.06
6.000	348.143	158.896	158.902	−0.00	0.00
6.000	373.150	176.308	176.348	−0.02	0.02
6.000	398.160	193.701	193.694	0.00	−0.00
6.500	273.150	113.057	113.153	−0.08	0.10
6.500	298.142	132.941	133.007	−0.05	0.05
6.500	303.143	136.921	136.958	−0.03	0.03
6.500	323.140	152.692	152.691	0.00	−0.00
6.500	348.143	172.195	172.234	−0.02	0.02
6.500	373.150	191.585	191.655	−0.04	0.03
6.500	398.160	211.015	210.966	0.02	−0.02
7.000	273.150	120.494	120.510	−0.01	0.02
7.000	298.142	142.411	142.453	−0.03	0.03
7.000	303.143	146.809	146.822	−0.01	0.01
7.000	323.140	164.208	164.225	−0.01	0.01
7.000	348.143	185.865	185.850	0.01	−0.01
7.000	373.150	207.347	207.346	0.00	−0.00
7.000	398.160	228.706	228.722	−0.01	0.01
7.500	273.150	127.854	127.913	−0.05	0.05
7.500	298.142	152.040	152.044	−0.00	0.00
7.500	303.143	156.783	156.851	−0.04	0.04
7.500	323.140	175.966	176.007	−0.02	0.02
7.500	348.143	199.807	199.821	−0.01	0.01
7.500	373.150	223.440	223.497	−0.03	0.02
7.500	398.160	247.053	247.045	0.00	−0.00
8.000	273.150	135.410	135.417	−0.01	0.01
8.000	298.142	161.873	161.844	0.02	−0.02
8.000	303.143	167.135	167.111	0.01	−0.01
8.000	323.140	188.142	188.109	0.02	−0.02
8.000	348.143	214.218	214.222	−0.00	0.00
8.000	373.150	240.078	240.192	−0.05	0.04
8.000	398.160	266.023	266.023	−0.00	0.00
8.500	273.150	143.090	143.080	0.01	−0.01
8.500	298.142	171.979	171.918	0.04	−0.04
8.500	303.143	177.736	177.669	0.04	−0.04
8.500	323.140	200.673	200.604	0.03	−0.03
8.500	348.143	229.193	229.139	0.02	−0.02
8.500	373.150	257.427	257.522	−0.04	0.03

TABLE 4. *Methane densities of Douslin et al.* [22]—Continued

MOL/L	T, K	P, BAR	P, CALC	P, PCT	D, PCT
8.500	398.160	285.758	285.756	0.00	−0.00
9.000	273.150	151.095	150.964	0.09	−0.09
9.000	298.142	182.470	182.341	0.07	−0.07
9.000	303.143	188.733	188.602	0.07	−0.07
9.000	323.140	213.759	213.577	0.09	−0.08
9.000	348.143	244.766	244.660	0.04	−0.04
9.000	373.150	275.434	275.585	−0.05	0.05
9.000	398.160	306.209	306.349	−0.05	0.04
9.500	273.150	159.307	159.142	0.10	−0.10
9.500	298.142	193.423	193.194	0.12	−0.11
9.500	303.143	200.116	199.993	0.06	−0.06
9.500	323.140	227.366	227.118	0.11	−0.09
9.500	348.143	261.024	260.888	0.05	−0.04
9.500	373.150	294.478	294.490	−0.00	0.00
9.500	398.160	327.865	327.918	−0.02	0.01
10.000	273.150	167.979	167.694	0.17	−0.16
10.000	298.142	204.825	204.570	0.12	−0.11
10.000	303.143	212.100	211.935	0.08	−0.07
10.000	323.140	241.534	241.329	0.09	−0.07
10.000	348.143	278.048	277.931	0.04	−0.03
10.000	373.150	314.250	314.355	−0.03	0.03
10.000	398.160	350.494	350.589	−0.03	0.02
10.500	273.150	177.002	176.711	0.16	−0.15
10.500	298.142	216.938	216.570	0.17	−0.14
10.500	303.143	224.805	224.534	0.12	−0.10
10.500	323.140	256.572	256.321	0.10	−0.08
10.500	348.143	296.014	295.912	0.03	−0.03
10.500	373.150	335.101	335.310	−0.06	0.05
10.500	398.160	374.301	374.500	−0.05	0.04
11.000	273.150	186.780	186.294	0.26	−0.22
11.000	298.142	229.688	229.307	0.17	−0.13
11.000	303.143	238.292	237.903	0.16	−0.13
11.000	323.140	272.539	272.219	0.12	−0.09
11.000	348.143	315.031	314.962	0.02	−0.02
11.000	373.150	357.297	357.495	−0.06	0.04
11.000	398.160	399.523	399.798	−0.07	0.05
11.500	273.150	197.051	196.557	0.25	−0.20
11.500	298.142	243.451	242.905	0.22	−0.17
11.500	303.143	252.507	252.170	0.13	−0.10
11.500	323.140	289.542	289.157	0.13	−0.10
11.500	348.143	335.104	335.226	−0.04	0.03
11.500	373.150	380.866	381.064	−0.05	0.04
12.000	273.150	208.211	207.621	0.28	−0.21
12.000	298.142	257.950	257.501	0.17	−0.12
12.000	303.143	267.883	267.472	0.15	−0.11
12.000	323.140	307.555	307.281	0.09	−0.06
12.000	348.143	356.651	356.860	−0.06	0.04
12.000	373.150	405.932	406.182	−0.06	0.04
12.500	273.150	220.275	219.620	0.30	−0.21
12.500	298.142	273.788	273.241	0.20	−0.13
12.500	303.143	284.252	283.960	0.10	−0.07
12.500	323.140	326.974	326.751	0.07	−0.04
12.500	348.143	379.993	380.035	−0.01	0.01

3. The Coexistence Densities

To obtain densities of freezing and of saturated liquid, we represent initial points of each experimental pseudo-isochore from table 1 by

$$P = A + B \cdot T + C/T + D/T^2, \tag{1}$$

used for extrapolation to the $P(T)$ melting- and vapor-pressure lines of [7] respectively. Adjustment is made for the negligible change of density over the range of extrapolation. On the melting line, we obtain three densities to a maximum pressure of 220 bar. On the vapor pressure line, we obtain 19 densities to a maximum temperature of 175 K. Vapor densities are obtained by use of the virial equation of [5] and vapor pressures of [7] to a maximum temperature of 175 K.

The analytical functions used to represent these densities are given in the appendix. The single-valued function $T_s(\rho)$ for coexisting vapor and liquid then was adjusted to data from the above functions. We omit details of all this tedious work because they are not essential to development of the equation of state. They will be given in later reports. For the saturated liquid, however, we give in Appendix table 1 the derived and calculated densities because these are of especial technological importance.

4. The Equation of State

On the notorious problem of the equation of state [14, 14a], we have investigated further a form which is nonanalytic at the critical point [15], rectifying one defect and making simplifications. For background, it was found with hydrogen that an excellent isochoric equation is of the form

$$(Z-1) \cdot x/\rho = A + B \cdot T + C/T + D/T^2, \tag{2}$$

provided we avoid the neighborhood of saturation and that we modify the second term on the right for consistency with high-temperature behavior of the second virial coefficient. We then modified the last term on the right to obtain $C_v \to \infty$ on approach to the critical point, as computed along the critical isotherm by means of the thermodynamic relation

$$C_v(\rho, T) = C_v^0(T) - T \cdot \int_0^\rho (\partial^2 P/\partial T^2)_\rho \, d\rho/\rho^2. \tag{3}$$

We now have developed the following isochoric equation of state for methane via many exploratory computations

$$(Z-1) \cdot x/\rho = A + B \cdot \Phi(T) + C/x + D \cdot \Psi(\rho, T). \tag{4}$$

The temperature-dependent functions are

$$\Phi(T) \equiv x \cdot [1 - \exp(-b - \beta/x)], \tag{4a}$$

$$\Psi(\rho, T) \equiv [1 - \omega \cdot \ln(1 + 1/\omega)]/x. \tag{4b}$$

The argument ω is defined

$$\omega(\rho, T) \equiv (T - \theta)/(\delta \cdot T_c) \tag{4c}$$

by use of the locus of temperatures

$$\theta(\rho) \equiv T_s(\rho) \cdot \exp[-u(\sigma)/2], \tag{4d}$$

where $u(\sigma)$ is defined

$$u(\sigma) \equiv \alpha_g \cdot [|\sigma - 1|^3 - (\sigma - 1)^3] + \alpha_l \cdot [|\sigma - 1|^3 + (\sigma - 1)^3].$$

The saturation temperatures $T_s(\rho)$ are given in the appendix.

Density-dependent coefficients of (4) are formulated as power series,

$$A(\rho) \equiv \sum_{i=0}^{3} A_i \cdot \rho^i, \qquad B(\rho) \equiv \sum_{i=0}^{2} B_i \cdot \rho^i,$$

$$C(\rho) \equiv \sum_{i=1}^{3} C_i \cdot \rho^i, \qquad D(\rho) \equiv (\sigma - 1) \cdot \sum_{i=0}^{2} D_i \cdot \rho^i.$$

An essential modification from [15] is the above formulation of $\theta(\rho)$. The quadratic $(\sigma - 1)^2$, formerly used in the exponential, gives a logarithmic infinity in $\partial^3 P/\partial \rho^3$ at the critical point.

Coefficients of (4) are found by least squares after multiplying each polynomial throughout by its temperature-dependent factor. Via the least squares program [16], we impose four constraints: the pressure shall be our assigned values at the triple- and critical-points; and we shall have $\partial P/\partial \rho = \partial^2 P/\partial \rho^2 = 0$ at the critical point.

Experimental *PVT* data from four sources cover virtually the entire domain of interest here, namely $T_t < T < 400$ K and $P \leq 350$ bar. Table 5 gives these sources and the range of their data in T, P, and d. We then give the number of data, N, selected for present work. The last two columns give the mean of relative pressure deviations $\Delta P/P$ and the rms of relative density deviations $\Delta d/d$, each from eq (4) with constants given below.

The constants of eq (4) for methane are given in the last column of table 6. Behavior of the coefficients $A(\rho) \ldots D(\rho)$ is quite similar to plots given in [15]. A calculated table of P and of $\partial P/\partial \rho$ along the critical isotherm shows that $\partial P/\partial \rho = 0$ at the critical point, and $\partial P/\partial \rho > 0$ at all adjacent densities. Higher derivatives through $\partial^4 P/\partial \rho^4$ also should be zero at the critical point according to a recent scaling-law equation of state [17], but we have not investigated these for eq (4).

Complete *PVT* data and deviations are given by tables 1 through 4 in response to readers' requests. The source of data is given by the heading for each table. Columns give the density in mol/l, the temperature, the pressure, the calculated pressure, and, in the last two columns, the relative deviations of pres-

TABLE 5. *Data used for the equation of state*

Source	Range of the data				Δ, %	
	T, K	P, bar	d, mol/l	N	P	d
Virial eq [5]	140–270	5–46	0.5–2.0	96	0.05	0.09
Vennix [13]	172–273	25–400	2.5–17.5	133	0.22	0.26
This report	94–245	20–350	18–28.5	279	0.66	0.03
Douslin [22]	273–398	16–400	0.75–12.5	171	0.05	0.06

sure and of density from eq (4), respectively, expressed in percent.

The reader should note that the derivative $(\partial P/\partial \rho)_T$ approaches zero at the critical point. Density deviations in this region (Vennix data) therefore should be ignored. This derivative becomes extremely large, on the other hand, for compressed liquid at low temperatures, and here the pressure deviations (NBS data) should be ignored.

5. Comments on the Equation of State

Equation (4) yields the perfect gas law $Z=1$ in the limit of low density. In the limit of high temperature it approximates the perfect gas, and yields $Z=1$ for the special case $b=0$. Due to its structure and relatively small number of least-squares coefficients, it tends to preserve important qualitative characteristics of the $P(\rho,T)$ surface. Among these are consistency with the known behavior of some specific heats [18]. For methane, we have examined the shape of isochores from eq (4), finding that they have monotonically negative curvature, $\partial^2 P/\partial T^2$, at $\rho < \rho_c$; a sigmoid shape in the range $1 < \rho/\rho_c < 2$; and (unlike hydrogen) negative curvature again at higher densities. The critical isochore has a very small, positive curvature at the critical point, similar to results for hydrogen [15].

The nonanalytic function $\Psi(\rho,T)$, eq (4b), is designed to give a large increase of C_v upon close approach to the critical point. It is similar to that used for hydrogen [15], through transformation of variables. Via the definition (4c) for $\omega(\rho, T)$, however, we now have the fact that $\Psi(\rho,T)$ exists in the limit $\theta \to 0$, whereas formerly it vanished. This function Ψ behaves like $1/T^2$ at high temperatures. At low temperatures, it terminates with a value of $1/x$ on the locus of temperatures $\theta(\rho)$ inside the coexistence envelope, at which point it gives infinite curvature $\partial^2 P/\partial T^2$. As density increases through the critical point, the sign of this curvature is reversed by means of the root $(\sigma-1)$ in the formula for coefficient $D(\rho)$.

Temperature dependence in eq (4) is similar to that of the well-known Beattie-Bridgeman equation,

$$(Z-1)\cdot x/\rho = \bar{A} + \bar{B}\cdot x + \bar{D}/x^2, \qquad (5)$$

in domains away from saturation. In particular, the absence of a constant term in our formula for $C(\rho)$ means that a term in $1/T^2$ is missing from description of the second virial coefficient, consistent with (5).

We have used eq (4) for extrapolation at pressures up to 700 bar (10,000 psi) along isochores at $T \leq 400$ K, finding that the pressure increases monotonically and that the derivatives $\partial P/\partial T$ and $\partial P/\partial \rho$ are well-behaved. This is noteworthy for the compressed liquid at low temperatures because few if any of the well-known equations of state can pass this test and at the same time represent PVT data over the enormous range of the entire $P(\rho, T)$ surface, from ideal gas states up to compressed liquid states near the melting line at low temperatures.

The number of temperature-dependent terms in equation (4) appears to exceed the number needed for qualitative description of isochores. The second term on the right gives weak negative curvature at high temperatures, and the last term may give curvature of either sign at low temperatures. We have, indeed, formulated an equation like eq (4) for methane, omitting the term $C(\rho)/x$ [19]. This was prior to our PVT measurements on the compressed liquid. As with hydrogen, we have found a term in $1/x$ necessary on the right of eq (4) to obtain a reasonably precise representation of PVT data when these include the compressed liquid states.

We have applied the present equation of state to hydrogen and to oxygen without any special difficulties, indicating therefore that it is not unique for

TABLE 6. *Constants of equation (4) for* H_2, O_2, *and* CH_4

Constant	Hydrogen	Oxygen	Methane
T_t, K	13.800	54.3507	90.680
T_c, K	32.962	154.52	190.53
d_t, mol/l	38.203	40.83	28.1472
d_c, mol/l	15.59	13.52	10.15
P_t, *	0.0695	0.0015	0.1174
P_c, *	12.704	49.650	45.957
α_g	0.3	0.4	0.5
α_l	.1	.4	.5
b	.8	1	.8
β	7	3	4
δ	1	1	1.2
A_0	−3.6990 3501	−4.7457 9188	−4.1545 2847
A_1	−1.5630 8113	−3.6883 8499	−4.7739 0186
A_2	5.0231 6164	−1.1695 4201	3.5199 9044
A_3	−0.7443 2571	8.2956 4587	4.2573 7412
B_0	1.2426 3871	2.0447 2804	1.7474 4656
B_1	0.6032 6565	2.5732 0035	2.5767 9569
B_2	.0692 4977	2.1530 4750	0.4653 8980
C_1	3.9354 2987	5.3321 8510	5.1033 5931
C_2	−9.9450 4679	−13.4213 9563	−12.4202 2748
C_3	5.7268 9781	7.6933 8807	6.3612 4273
D_0	1.0188 2911	1.7942 7732	1.8838 3919
D_1	−2.1414 4245	−3.1707 7491	−3.5471 3477
D_2	1.2924 7888	1.2788 3788	1.8740 8815

*For H_2 and O_2 the equation of state is in atmospheres; for CH_4, in bars.

453-425 OL - 72 - 3

methane. Densities for these other gases also ranged up to the melting line. Saturation temperatures $T_s(\rho)$ are given in [21]. In some cases the coefficients A_3 and B_2 for eq (4) show a low significance, suggesting that the corresponding terms of eq (4) might be omitted when PVT data extend to densities no higher than about $2 \cdot \rho_c$. In table 6 we see that coefficients for all three substances are similar and mostly of the same sign.

The authors are indebted to R. D. McCarty for use of the least squares program open to constraints [16], and to D. E. Diller and L. A. Weber for many discussions and important suggestions.

6. Appendix

6.1. Functions for Densities on the Coexistence Boundaries

(1) The freezing liquid densities are described by

$$d/d_t = (T/T_t)^{1/4},$$

a form developed for hydrogen [20].

(2) The saturated liquid densities are described as in [6] by

$$d_l/d_c = 1 + a \cdot z + b \cdot z^{0.36} + c \cdot \exp[-\epsilon \cdot x^2/z],$$

where $x \equiv T/T_c$, $z \equiv (1-x)$, and

$$a = 0.539\,403 \qquad c = -0.018\,387.$$
$$b = 1.896\,635 \qquad \epsilon = 0.88.$$

The triple point liquid density from this equation is $d_t = 28.1472$ mol/l. Derived and calculated values are given in Appendix table 1 below.

TABLE A1. *Derived and calculated densities of saturated liquid methane*

T, K	Mol/l	Calculated	Percent
175.053	18.390	18.392	−0.01
169.326	19.492	19.492	0.00
163.699	20.428	20.425	0.02
157.199	21.379	21.379	−0.00
151.555	22.130	22.131	−0.00
145.448	22.880	22.882	−0.01
139.352	23.578	23.581	−0.01
133.773	24.186	24.186	0.00
133.878	24.176	24.175	0.01
129.657	24.611	24.613	−0.01
125.825	24.999	24.999	0.00
121.893	25.388	25.383	0.02
117.746	25.782	25.778	0.01
113.772	26.146	26.147	−0.00
109.611	26.527	26.525	0.01
105.165	26.916	26.919	−0.01
101.434	27.243	27.243	0.00
97.173	27.605	27.606	−0.01
93.512	27.910	27.913	−0.01

(3) The saturated vapor densities are described more simply than in [6] by

$$\ln(d_g/d_c) = A_1 \cdot w + A_2 \cdot w^{1/3} + \sum_{i=3}^{5} A_i \cdot u^{i-2},$$

where

$$u \equiv (T_c - T)/(T_c - T_t), \quad w \equiv (T_c/T - 1)/(T_c/T_t - 1),$$

$$A_1 = -6.815\,239, \qquad A_4 = 0.736\,090,$$
$$A_2 = -2.012\,860, \qquad A_5 = 0.416\,449.$$
$$A_3 = 1.203\,942,$$

(4) The saturation temperature $T_s(\rho)$ for coexisting vapor and liquid are described here by a function which is constrained to the triple point, in contrast with our earlier form [21]. Define the variables.

$$Y(T_s) \equiv (T_c/T_s - 1)/(T_c/T_t - 1),$$
$$U(\rho) \equiv (\sigma - 1)/(\sigma_t - 1),$$
$$F(\rho) \equiv \sum_{i=2}^{8} A_i \cdot \rho^{i-2},$$

where σ_t is the constant, d_t/d_c. The function now is

$$Y(T_s) = U^{8/3} \cdot [1 + A_1 \cdot \ln(\rho) + (\rho - 1) \cdot F(\rho)],$$

$$A_1 = -0.814\,6680, \qquad A_5 = -142.308\,6536,$$
$$A_2 = 2.482\,4192, \qquad A_6 = 240.076\,9868,$$
$$A_3 = -6.872\,7440, \qquad A_7 = -195.876\,1459,$$
$$A_4 = 43.037\,4662, \qquad A_8 = 63.300\,1385.$$

7. References

[1] Tester, H. E., Methane, in Thermodynamic Functions of Gases, Vol. 3, F. Din, Editor (Butterworths, London, 1961).
[2] Zagoruchenko, V. A., and Zhuravlev, A. M., Thermophysical Properties of Gaseous and Liquid Methane, (Moscow, 1969). National Technical Information Service, Springfield, Va. 22151.
[3] van Itterbeek, A., Verbeke, O., and Staes, K., Measurements on the equation of state of liquid argon and methane up to 300 kg/cm² at low temperatures, Physica **29**, 742 (1963).
[4] Dobrovol'skii, O. A., Belyaeve, T. N., and Golubev, I. F., Gazovaya Promyshlennost' **11**:47 (1964).
[5] Goodwin, R. D., Thermophysical properties of methane: virial coefficients, vapor and melting pressures, J. Res. Nat. Bur. Stand. (U.S.), **74A** (Phys. and Chem.), No. 5, 655 (Sept.–Oct. 1970).
[6] Goodwin, R. D., Thermophysical properties of methane: orthobaric densities and some thermal properties, J. Res. Nat. Bur. Stand. (U.S.) **75A** (Phys. and Chem.), No. 1, 15 (Jan.–Feb. 1971).
[7] Prydz, R., and Goodwin, R. D., Experimental melting and vapor pressures of methane, submitted to J. Chem. Thermodynamics, 1971.
[8] The international practical temperature scale of 1968, Metrologia **5** (2), 35–49 (1969).
[9] Goodwin, R. D., Apparatus for determination of PVT relations and specihc heats of hydrogen to 350 atm at temperatures above 14 K, J. Res. Nat. Bur. Stand. (U.S.) **65C** (Phys. and Chem.), No. 4, 231 (July–Aug. 1961).

[10] Weber, L. A., P-V-T, thermodynamic and related properties of oxygen from the triple point to 300 K at pressures to 33 MN/m², J. Res. Nat. Bur. Stand. (U.S.) **74A** (Phys. and Chem.), No. 1, 93 (Jan.–Feb. 1970).
[11] Straty, G. C., and Prydz, R., Fluorine-compatible apparatus for accurate PVT measurements, Rev. Sci. Instruments **41** (8), 1223 (1970).
[12] Prydz, R., and Straty, G. C., The thermodynamic properties of compressed gaseous and liquid fluorine, Nat. Bur. Stand. (U.S.), Tech. Note 392, 182 pages (Oct. 1970).
[13] Vennix, A. J., Low temperature volumetric properties and development of an equation of state for methane, Thesis, Dept. of Chem. Engineering, Rice Univ., Houston, Texas, April 1965.
[14] Tsonopoulos, C., and Prausnitz, J. M., Equations of state: a review for engineering applications, Cryogenics **9** (5), 315 (Oct. 1969).
[14a] Macdonald, J. R., Review of some experimental and analytical equations of state, Rev. Mod. Phys. **41**, 316–349 (1969).
[15] Goodwin, R. D., Formulation of a nonanalytic equation of state for parahydrogen, J. Res. Nat. Bur. Stand. (U.S.), **73A** (Phys. and Chem.), No. 6, 585 (Nov.–Dec. 1969).
[16] Hust, J. G., and McCarty, R. D., Curve-fitting techniques and applications to thermodynamics, Cryogenics **7** (4), 200 (Aug. 1967).
[17] Jansoone, V., Gielen, H., de Boelpaep, J., and Verbeke, O. B., The pressure-temperature-volume relationship of methane near the critical point, Physica **46**, 213 (1970).
[18] Diller, D. E., The specific heats C_v of dense simple fluids, Cryogenics **11** (3), 186 (June 1971).
[19] Private communication 9781 (methane), this laboratory, Feb. 1, (1971).
[20] Goodwin, R. D., Density-temperature formulae for coexisting liquid and vapor and for freezing liquid parahydrogen, J Res. Nat. Bur. Stand. (U.S.), **70A** (Phys. and Chem.), No. 6, 541 (Nov.–Dec. 1966).
[21] Goodwin, R. D., Estimation of critical constants, T_c, ρ_c from the $\rho(T)$ and $T(\rho)$ relations at coexistence, J. Res. Nat. Bur. Stand. (U.S.), **74A** (Phys. and Chems), No. 2, 221 (Mar.–April 1970).
[22] Douslin, R. D., Harrison, R. H., Moore, R. T., and McCullough, J. P., P–V–T relations for methane, J. Chem. and Eng. Data **9** (3) 358 (1964).

(Paper 76A2–702)

JOURNAL OF RESEARCH of the National Bureau of Standards—A. Physics and Chemistry
Vol. 76A, No. 2, March–April 1972

Spin-Relaxation Effects on the EPR Spectrum of Gaseous Hydrogen Atoms

Robert L. Brown

Institute for Materials Research, National Bureau of Standards, Washington, D.C. 20234

(November 19, 1971)

A theoretical analysis is presented of the relaxation processes which lead to the magnetization of gaseous hydrogen atoms in a strong magnetic field. Experiments are described which demonstrate that the spin-lattice relaxation time in a pure H_2 carrier can be of the order of 10 ms. From the effects of traces of O_2 on the hydrogen atom EPR spectrum, a H-O_2 spin-exchange collision cross section of $(8.0 \pm 2.5) \times 10^{-16}$ cm^2 was derived.

Key words: Electron spin resonance; hydrogen atoms: spin-exchange; spin-relaxation.

1. Introduction

It has been demonstrated that gaseous nitrogen atoms can have a spin-lattice relaxation time T_1 of the order of several milliseconds [1].[1] In high speed discharge-flow systems with EPR atom detection, this T_1 can be longer than the transit time of the atoms between the discharge and the EPR microwave cavity. Anomalously small EPR absorption intensities will arise in this situation because the atoms entering the cavity will not be completely magnetized. Decreasing the gas flow rate or decreasing T_1 by adding a paramagnetic impurity like O_2 will increase the magnetization at the cavity. The EPR signal will thus increase even if the atom concentration in the cavity remains constant. To measure atom concentrations quantitatively by EPR under such conditions one must know how far the magnetization lies from equilibrium or else produce an equilibrium condition by adding sufficient paramagnetic impurity.

In general, large values of T_1 are to be expected for S-state atoms because of the weak coupling of the electron spin to the rest of the atom and hence, through collisions, to the lattice [2]. During the N atom studies described in reference [1], H atoms were examined briefly [3]. Under some circumstances they were also found to be incompletely magnetized. EPR signal enhancements of the order 1.3 were observed on addition of trace amounts of O_2. Recently, this enhancing effect on the H atom spectrum has been reported by Breen and Glass [4] for trace additions of NO_2. Westenberg and De Haas [5] have also reported an enhancement of H atom signals by O_2, but the effect was very small and noticeable only at very high carrier flow rates. Using power saturation methods, they measured T_1 for H and found values of the order of 100 μs. These are much shorter relaxation times than those observed in reference [1] for N atoms. Because their observed T_1 values were independent of carrier flow velocity and increased with increasing carrier pressure, they concluded that the predominant relaxation process occurred on the flow tube walls.

The work of Westenberg and De Haas prompted the writer to make a more detailed study of spin-relaxation effects on the H atom spectrum than that reported earlier. Both experimental and theoretical aspects of the problem were examined. For the experiments, H atoms were generated by thermal dissociation [6] of pure H_2 thereby avoiding the need for impurities (such as O_2, N_2, or H_2O) [7] normally required for efficient dissociation by a discharge. In this system traces of O_2 added *downstream* from the dissociation point produced significant enhancements of the H atom EPR signal. Furthermore, the amount of microwave power required to produce a given degree of saturation increased with increasing H_2 flow rate. These two observations demonstrated that in the absence of added O_2, T_1 for this system was of the order of 10 ms, far larger than that observed in the system of Westenberg and De Haas. A simplified analysis of the H-H spin-exchange process showed that spin-exchange collisions alone can lead to partial magnetization of the atoms in the absence of any added paramagnetic impurity. In a typical EPR experiment, the maximum H atom signal enhancement to be expected on addition of O_2 is only a factor of two, in contrast to the case of N atoms where much larger enhancements are possible. The effects of atom diffusion on the apparent relaxation time measured by power saturation were also examined theoretically.

[1] Figures in brackets indicate the literature references at the end of this paper.

Because of the difficulty in applying corrections for diffusion and the additional problems caused by inhomogeneously broadened lines and the uncertainties in estimating the microwave magnetic field strength inside the flow tube, no attempt was made to measure absolute relaxation times by power saturation methods.

2. Theory

Hydrogen atoms in their ground electronic state possess four magnetic hyperfine levels. In this section a general expression will be derived for the time rate of change of the concentrations c_i of these levels in a cylindrical flow tube.

A number of processes produce changes in the c_i. The most important ones are, (a) spin-exchange collisions between the H atoms themselves, (b) spin-exchange collisions with gas phase paramagnetic impurities, (c) collisions with the walls, (d) interactions with rf radiation, (e) mass flow, and (f) diffusion. The effects of each of these mechanisms will be evaluated separately and the results added to give the total rate of change in the c_i. The general equation contains nonlinear terms arising from the H-H spin-exchange process. It will be linearized by considering only small departures from equilibrium. To solve the linearized equation, further simplifications are necessary. Steady state solutions will be obtained by neglecting diffusion and assuming a uniform velocity profile for the carrier. The effects of axial diffusion will be examined by solving a rate equation for a two level model, again assuming a uniform carrier velocity.

2.1. Spin-Exchange Interaction Between H Atoms

Consider a collision between two H atoms, the first in state Ψ_i and the second in state Ψ_j. We want to calculate the probability of the first atom being in state Ψ_k and the second in state Ψ_l after the collision. In terms of strong field spin eigenfunctions, the wave functions Ψ_i, $i=1\rightarrow 4$, for any value of the dc EPR magnetic field, are

$$\begin{aligned}\Psi_1&=\alpha a\\ \Psi_2&=(1-\epsilon)^{1/2}\alpha b+\epsilon^{1/2}\beta a\\ \Psi_3&=\beta b\\ \Psi_4&=(1-\epsilon)^{1/2}\beta a-\epsilon^{1/2}\alpha b\end{aligned}\qquad(1)$$

where α and a are the electron and proton spin functions respectively, whose angular momentum projections in the direction of the dc field have the value $\frac{1}{2}$, and β and b are the functions with projections $-\frac{1}{2}$; $\epsilon=[1-x(x^2+1)^{-1/2}]/2$; $x=(1-g_J/g_P)(\nu_P/\nu_H)$; g_J and g_P are the electron and proton g factors; ν_H is the zero field hyperfine splitting frequency and $\nu_P=-g_P\mu_0 H_0/\hbar$; μ_0 is the Bohr magneton and H_0 the magnitude of the dc field. The energy levels U_i are given by the Breit-Rabi equation [8] and lie in the order $U_1>U_2>U_3>U_4$ for a nonzero field.

Following the treatment of Purcell and Field [9], we express the initial spin wave function for the two atoms as the product $\Psi_i(1)\Psi_j(2)$. This can be written as a superposition of singlet and triplet electron spin functions. For example, one might have

$$\begin{aligned}\Psi_{initial}=\Psi_1(1)\Psi_2(2)&=(1-\epsilon)^{1/2}\alpha(1)\alpha(2)a(1)b(2)\\ &+\tfrac{1}{2}\epsilon^{1/2}[\alpha(1)\beta(2)+\beta(1)\alpha(2)]a(1)a(2)\\ &+\tfrac{1}{2}\epsilon^{1/2}[\alpha(1)\beta(2)-\beta(1)\alpha(2)]a(1)a(2).\end{aligned}$$

The difference in the scattering potential for the singlet and triplet components produces a phase shift φ_{ts} between the amplitudes of the two components. This phase shift is given by the equation $\varphi_{ts}=\int(V_t-V_s)\,dt/\hbar$, where V_t and V_s are the energies of the triplet and singlet electronic states, and the integration is over the duration of the collision.

After the collision the wave function becomes,

$$\begin{aligned}\Psi_{final}&=(1-\epsilon)^{1/2}\alpha(1)\alpha(2)a(1)b(2)\\ &+\tfrac{1}{2}\epsilon^{1/2}[\alpha(1)\beta(2)+\beta(1)\alpha(2)]a(1)a(2)\\ &+\tfrac{1}{2}\epsilon^{1/2}[\alpha(1)\beta(2)-\beta(1)\alpha(2)]a(1)a(2)\exp(i\varphi_{ts}).\end{aligned}$$

The amplitude of the contribution of a particular product function $\Psi_k(1)\Psi_l(2)$ to Ψ_{final} is given by the integral $\int\Psi_k(1)\Psi_l(2)\Psi_{final}d\tau$, where the integration is over all space. The square of this amplitude gives the probability that after the collision the state $\Psi_{initial}$ becomes the state $\Psi_k(1)\Psi_l(2)$.

Performing this calculation for all possible combinations of initial product functions $\Psi_i(1)\Psi_j(2)$ and all possible final product functions $\Psi_k(1)\Psi_l(2)$, one obtains a 16×16 matrix of transition probabilities. Because of the small energy differences between the hyperfine levels this matrix is not quite symmetric. By detailed balancing, the rate of the transition $ij\rightarrow kl$, at equilibrium, must equal the rate of the reverse process $kl\rightarrow ij$. This can happen only if the matrix elements satisfy the relation $(kl,\ ij)=(ij,\ kl)\ \exp[(U_k+U_l-U_i-U_j)/kT]$, where $(ij,\ kl)$ is the probability for the transition $ij\rightarrow kl$, k is Boltzmann's constant, and T is the gas kinetic temperature. The error involved in calculating the transition probabilities in this manner is discussed by Purcell and Field. It is of the order $(U_k+U_l-U_i-U_j)/kT$ and thus quite small.

The nonzero elements of this matrix are given in table 1 as a function of the field strength parameter ϵ and a phase shift parameter $\Delta=\frac{1}{4}\sin^2(\varphi_{ts}/2)$. Only strong collisions for which $\varphi_{ts}\gg 1$ will be considered. In this case $\Delta=\frac{1}{4}$. Transition probabilities for the zero field case treated by Purcell and Field can be obtained from table 1 by letting $\epsilon=\frac{1}{2}$. For an EPR absorption at X band frequencies, $\epsilon\sim 0.5\times 10^{-2}$ for the high field H atom line. The matrix element $(ij,\ kl)$ is only the relative probability that $ij\rightarrow kl$ in a spin-exchange collision. The overall rate at which such collisions

occur will be specified by a rate constant S. A literature value will be used for this parameter.

The rates of change of the c_i are given by

$$\dot{c}_i S^{-1} = -\sum_j c_i c_j - \sum_{j \neq i} c_i c_j$$

$$+ \sum_{k,l} c_k c_l \Big\{ \sum_m (kl, im) + \sum_{m \neq i} (kl, mi) \Big\}$$

$$= \sum_{k,l} a_{kli} c_k c_l, \quad i = 1 \rightarrow 4 \tag{2}$$

where the coefficients a_{kli} are various linear combinations of the matrix elements (ij, kl). These equations represent changes in the c_i arising from spin-exchange collisions between the H atoms themselves. Let us now consider changes resulting from interactions of the atoms with the external system.

TABLE 1. *Nonzero transition probabilities for spin-exchange collisions between H atoms*, (ij, kl).

Transition [a]	Transition probability
(12, 14), (12, 41) (13, 22), (13, 44) (14, 21) (21, 41) (22, 31) (23, 34), (23, 43) (31, 44) (32, 34), (32, 43)	$\epsilon(1-\epsilon)\Delta$
(12, 21) (13, 24) (34, 43)	$\epsilon^2\Delta$
(13, 42) (14, 41) (23, 32)	$(1-\epsilon)^2\Delta$
(22, 24), (22, 42) (24, 44) (42, 44)	$\epsilon(1-\epsilon)\,(1-2\epsilon)^2\Delta$
(22, 44) (24, 42)	$4\epsilon^2(1-\epsilon)^2\Delta$
(11, 11), (33, 33)	1
(12, 12), (21, 21) (34, 34), (43, 43)	$1-2\epsilon(1-\frac{1}{2}\epsilon)\Delta$
(13, 13), (31, 31)	$1-\Delta$
(14, 14), (41, 41) (32, 32), (23, 23)	$1-(1-\epsilon^2)\Delta$
(22, 22), (44, 44)	$1-4\epsilon(1-\epsilon)$ $[1-\epsilon(1-\epsilon)]\Delta$
(24, 24), (42, 42)	$1-[1-4\epsilon^2(1-\epsilon)^2]\Delta$
$(kl, ij) = (ij, kl) \exp[(U_k + U_l - U_i - U_j)/kT]$	

[a] The matrix element (ij, kl) corresponds to the transition $\psi_i(1)\psi_j(2) \rightarrow \psi_k(1)\psi_l(2)$, where the numbers in parentheses label the two atoms involved in the collision.

2.2. Spin-Lattice Interactions

For H atoms in a nonpolar, nonparamagnetic carrier, the only important spin-lattice relaxation processes are spin-exchange collisions with paramagnetic impurities and wall collisions. The paramagnetic impurity is assumed to have orbital angular momentum so that its electron spin will be strongly coupled to the lattice. The spin temperature of this species will thus always remain at the temperature of the lattice [2]. We shall not try to specify the details of the impurity interactions, but shall simply let K_{ij} be an overall rate constant for a particular transition $\Psi_i \rightarrow \Psi_j$ produced by these interactions.

The total rate of change in the c_i resulting from these transitions will be

$$\dot{c}_i = \sum_{k \neq i} (K_{ki} c_k - K_{ik} c_i) = \sum_j R_{ij} c_j \tag{3}$$

where $R_{ij} = K_{ji}$ and $R_{ii} = -\sum_{j \neq i} K_{ij}$. From detailed balancing we have $K_{ij} = K_{ji} \exp[(U_i - U_j)/kT]$. One would expect the K_{ij} to be proportional to the concentration of a particular paramagnetic impurity and to depend on its nature.

Relaxation by wall collisions also yields terms which are first order in the c_i. If these were treated together with the gas phase interactions a single set of K_{ij} parameters could be used to represent both processes. It will be shown later that the wall relaxation process can be included explicitly by treating the interaction as a boundary condition on the rate equation when radial diffusion of the atoms is included.

2.3. Transitions Induced by an rf Magnetic Field

The rate of change in the c_i arising from absorption and induced emission by an rf magnetic field is given

$$\dot{c}_i = \sum_{k \neq i} (W_{ki} c_k - W_{ik} c_i) = \sum_j w_{ij} c_j \tag{4}$$

where the W_{ij} are rate constants for these transitions, $w_{ij} = W_{ji}$, and $w_{ii} = -\sum_{j \neq i} W_{ij}$. In the present experiment, the high field H atom line which arises from transitions between levels 2 and 3 was examined. For this case all $W_{ij} = 0$ except W_{23} and W_{32} which are equal. Let W_{23} and W_{32} equal W. The rate constant W is proportional to the rf power striking the sample. Because the rf field varies from point to point throughout the microwave cavity, W will be different at different points in the cavity. We have $W = h^{-2} H_1^2 \mu^2 g(\nu)$, where H_1 is the amplitude of the rf magnetic field, μ^2 is the square of the absolute value of the transition matrix element, and $g(\nu)$ is the normalized line shape function [10].

2.4. Effects of Mass Flow and Diffusion

To complete the rate equations for c_i, one must include a term which accounts for the flow of atoms

through the microwave cavity and another which represents their diffusion. The experimental arrangement consisted of a cylindrical flow tube running through a TE_{011} cavity with its axis coinciding with that of the cavity. Were relaxation on the walls as effective a 1 in 10 collisions in the present experiments, large radial gradients would arise in the population differences between the levels of interest during a saturation experiment. In this case both radial and axial diffusion terms should be included.

2.5. Complete Rate Equations and Their Linearization

The complete rate equations for the c_i are, in cylindrical coordinates

$$\frac{\partial c_i}{\partial t}=S\sum_{k,l}a_{kli}c_kc_l+\sum_j R_{ij}c_j+\sum_j w_{ij}c_j - v(r)\frac{\partial c_i}{\partial z}+D\left\{\frac{1}{r}\frac{\partial}{\partial r}\left(r\frac{\partial c_i}{\partial r}\right)+\frac{\partial^2 c_i}{\partial z^2}\right\} \quad (5)$$

where $v(r)=2v_0[1-(r/a)^2]$ the carrier flow velocity, v_0 is the average carrier velocity, a is the radius of the flow tube, and D is the atom's diffusion coefficient at the prevailing carrier pressure. The first term in the brackets represents radial diffusion and the second axial diffusion. The term containing $v(r)$ accounts for the effects of mass flow. For reasons discussed earlier, the coefficients w_{ij}, which represent the effect of rf power, are functions of r and z. The sum containing the parameters R_{ij} represents the effect of interactions with paramagnetic impurities and if desired, the effect of relaxation on the walls. The first sum represents the effect of spin-exchange collisions among the H atoms themselves.

Under all conditions experienced in a typical EPR experiment with H atoms, the c_i differ at most by several parts per thousand. The rate equations therefore can be linearized [11] by expressing the c_i in the form $c_i=\frac{1}{4}n(1+\xi_i)$, where n is the total H atom concentration and the ξ_i are very small numbers which will be considered only to first order. As a result of this definition, the relation $\sum_i \xi_i=0$ must always be satisfied.

With this substitution, the rate equations become.

$$\frac{\partial \xi_i}{\partial t}=\frac{1}{4}Sn\left\{\sum_{k,l}a_{kli}+\sum_j A_{ij}\xi_j\right\}+\sum_j R_{ij}(1+\xi_j) +\sum_j w_{ij}\xi_j-v(r)\frac{\partial \xi_i}{\partial z}+D\left\{\frac{1}{r}\frac{\partial}{\partial r}\left(r\frac{\partial \xi_i}{\partial r}\right)+\frac{\partial^2 \xi_i}{\partial z^2}\right\} \quad (6)$$

where the relation $\sum_j w_{ij}=0$ has been used. The A_{ij} are linear combinations of the a_{kli}, which in turn are linear combinations of the transition probabilities (ij, kl) from table 1.

The Boltzmann factors in the (ij, kl) and in the rate constants K_{ij} from which the R_{ij} are derived ensure that these rate equations will satisfy the proper equilibrium conditions. However, the equations are easier to handle if they are rewritten so that the equilibrium values of the ξ_i are included explicitly. This may be done in the following manner. For the system at thermal equilibrium, with no rf power applied, the rate equations become

$$\frac{1}{4}Sn\sum_{k,l}a_{kli}+\sum_j R_{ij}=-\frac{1}{4}Sn\sum_j A_{ij}E_j-\sum_j R_{ij}E_j$$

where the E_i are the equilibrium values of ξ_i for the particular lattice temperature and dc field.

Substituting this expression into (6) gives

$$\frac{\partial \xi_i}{\partial t}=\frac{1}{4}Sn\sum_j A_{ij}(\xi_j-E_j)+\sum_j R_{ij}(\xi_j-E_j) +\sum_j w_{ij}\xi_j-v(r)\frac{\partial \xi_i}{\partial z}+D\left\{\frac{1}{r}\frac{\partial}{\partial r}\left(r\frac{\partial \xi_i}{\partial r}\right)+\frac{\partial^2 \xi_i}{\partial z^2}\right\}. \quad (7)$$

In this form the equations give the correct equilibrium values of ξ_i even if the Boltzmann factors inherent in the A_{ij} and R_{ij} are neglected. The error in doing so will be very small since the factors are so close to unity.

2.6. Evaluation of the Coefficients A_{ij} and R_{ij}

The coefficients A_{ij} which account for the effects of H–H spin-exchange collisions are linear combinations of the transition probabilities (ij, kl) shown in table 1. They are given in table 2 in the form of a 4×4 matrix which is valid for all values of the dc field. Strong collisions, for which $\Delta=\frac{1}{4}$, have been assumed, and the Boltzmann factors neglected. In this table an additional field strength parameter, $\chi=8\epsilon(1-\epsilon)$ has been introduced. Lambe [11] has also determined the A_{ij} coefficients by a somewhat different method.

In the strong field limit, the coefficients R_{ij} which describe the spin-lattice interactions can easily be derived if we consider only interactions which change the electron spin state. These interactions could be with a gaseous paramagnetic impurity or with the walls of the flow tube. On changing the electron spin quantum number, the strong field wave functions for

TABLE 2. *The coefficients* A_{ij} *which describe the effects of* H–H *spin-exchange collisions.*

The parameter χ equals $8\epsilon(1-\epsilon)$.

i j	1	2	3	4
1	−1	1	−1	1
2	1	−(1+χ)	1	−(1−χ)
3	−1	1	−1	1
4	1	−(1−χ)	1	−(1+χ)

the four hyperfine states transform in the following way:

$$\Psi_1 = \alpha a \rightarrow \beta a = \Psi_4$$

$$\Psi_2 = \alpha b \rightarrow \beta b = \Psi_3$$

$$\Psi_3 = \beta b \rightarrow \alpha b = \Psi_2$$

$$\Psi_4 = \beta a \rightarrow \alpha a = \Psi_1.$$

The rates of change in the c_i produced by this interaction are thus

$$\begin{aligned}\dot{c}_1 &= K_{41}c_4 - K_{14}c_1\\ \dot{c}_2 &= K_{32}c_3 - K_{23}c_2\\ \dot{c}_3 &= K_{23}c_2 - K_{32}c_3\\ \dot{c}_4 &= K_{14}c_1 - K_{41}c_4.\end{aligned}$$

where $K_{ij} = \frac{1}{2}K$, and K is an overall rate constant for these interactions. The reason why the factor $\frac{1}{2}$ has been introduced will be discussed later. The R_{ij} can be derived from the K_{ij} by means of (3).

By considering only the strong field limit, one is assuming that the spin-lattice interaction effects only the electron spin. Although this leads to equilibration of the population *differences* $c_1 - c_4$ and $c_2 - c_3$ which are the ones involved in the EPR transitions, it will not by itself produce thermal equilibration of the c_i. This is because transitions between the states Ψ_1, Ψ_4 and Ψ_2, Ψ_3 have been neglected. Such transitions involve changes in the proton spin state. One way to estimate the relative K_{ij} for such changes is through an adaptation of the method used by Lambe [11] to determine the rate equations for H–H spin-exchange collisions. Consider the paramagnetic impurities to be a reservoir of electron spins in which P^+ and P^- are the probabilities of finding an electron with spin up and spin down, respectively. Since the impurity spins are assumed to be strongly coupled to the lattice, and thus always at thermal equilibrium, P^+ and P^- will be constant and have almost the same value, namely $\frac{1}{2}$, at the temperatures and field strengths used in the present experiments. Suppose that an H atom in state Ψ_1 exchanges its electron with one from the impurity reservoir. With probability P^+, Ψ_1 remains unchanged. With probability P^-, Ψ_1 goes to state βa which is a mixed state. We have

$$\beta a = (1-\epsilon)^{1/2}\Psi_4 + \epsilon^{1/2}\Psi_2.$$

so that with a probability ϵP^-, Ψ_1 goes to Ψ_2, and with a probability $(1-\epsilon)P^-$, to Ψ_4.

Following this procedure for all the states Ψ_i, one gets rate equations for the c_i. For example,

$$\begin{aligned}\dot{c}_1 &= -KP^-c_1 + K\epsilon P^+c_2 + K(1-\epsilon)P^+c_4\\ &= -\tfrac{1}{2}Kc_1 + \tfrac{1}{2}K\epsilon c_2 + \tfrac{1}{2}K(1-\epsilon)c_4\end{aligned}$$

where K is an overall rate constant for spin-exchange collisions between the H atoms and the paramagnetic impurity. It will be proportional to the impurity concentration.

On making the transformation $c_i = \frac{1}{4}n(1+\xi_i)$, and introducing the equilibrium parameters E_i, one obtains the rate equations in the desired form $\dot{\xi}_i = \sum_j R_{ij}(\xi_j - E_j)$, where the matrix R_{ij} is given in table 3. For the strong field case, $\epsilon \rightarrow 0$, and the R_{ij} reduce to the values obtained earlier. The factor $\frac{1}{2}$ in these coefficients arises because $\frac{1}{2}$ of the impurity spins in the strong field case will be in the same direction as the electron spin on the H atom and so no change in the state of H will occur during an electron exchange in one out of two collisions.

While the matrix R_{ij} in table 3 should be valid for all field strengths, only the strong field elements were used to analyze the experimental data. The H–H spin-exchange interactions also produce the transitions neglected in the strong field spin-lattice approximation. Since the H–H exchange dominates the spin-lattice interactions in the present experiments, the spin-lattice contributions to these transitions can be ignored.

TABLE 3. *The coefficients* R_{ij}, *which describe the spin-lattice interactions.*

The parameter χ equals $8\epsilon(1-\epsilon)$.

i \ j	1	2	3	4
1	$-\frac{1}{2}K$	$\frac{1}{2}\epsilon K$	0	$\frac{1}{2}(1-\epsilon)K$
2	$\frac{1}{2}\epsilon K$	$-\frac{1}{2}(1+\frac{1}{4}\chi)K$	$\frac{1}{2}(1-\epsilon)K$	$\chi K/8$
3	0	$\frac{1}{2}(1-\epsilon)K$	$-\frac{1}{2}K$	$\frac{1}{2}\epsilon K$
4	$\frac{1}{2}(1-\epsilon)K$	$\chi K/8$	$\frac{1}{2}\epsilon K$	$-\frac{1}{2}(1+\frac{1}{4}\chi)K$

2.7. Wall Relaxation as a Boundary Condition

If relaxation on the walls were rapid enough to produce radial concentration gradients, the rate equation (7) should be solved subject to the boundary conditions

$$\left\{\frac{\partial \xi_i}{\partial r}\right\}_{r=a} = -\frac{1}{2}aD\sum_j (R_w)_{ij}(\xi_j - E_j)$$

where the derivatives are evaluated at the wall of the flow tube, D is the diffusion coefficient for the atom in the carrier gas at the prevailing carrier pressure, and the $(R_w)_{ij}$ are coefficients for wall relaxation analogous to the R_{ij} defined for relaxation by paramagnetic impurities in the gas phase. In the present experiments wall relaxation cannot have been rapid. Therefore the radial diffusion term in (7) will be dropped, and any wall relaxation effects will be absorbed in the R_{ij} coefficients instead of being included explicitly as a boundary condition.

2.8. A Two-Level Spin Model

In order to examine the effects of axial diffusion, a two-level model consisting of particles with spin $^1/_2$ was

used. For such a system, the $A_{ij}=0$, while the matrices for R_{ij} and w_{ij} are simply

$$R_{ij}=\begin{pmatrix} -\frac{1}{2}K & \frac{1}{2}K \\ \frac{1}{2}K & -\frac{1}{2}K \end{pmatrix}, \tag{8a}$$

and,

$$w_{ij}=\begin{pmatrix} -W & W \\ W & -W \end{pmatrix} \tag{8b}$$

where K and W are analogous to the same quantities defined for the four-level model.

3. Apparatus and Experiments

The apparatus used was essentially that described in reference 1 except that the klystron frequency was now locked to the cavity resonance instead of to an external oscillator. Field modulation was at 400 Hz. Hydrogen atoms were produced outside the high field of the EPR magnet by passing Matheson[2] Ultra High Purity H_2 over a tungsten filament [6] heated to about 1600 °C. Only H_2 was used as a carrier. The walls of the 10 mm in diam quartz flow tube were poisoned against atom recombination with boric acid [12]. The amount of atom decay was measured by adding a trace of NO to the atom stream and observing the HNO emission [13]. Between the EPR cavity and the point of O_2 addition, the decay was less than 5 percent for all experiments. The length of flow tube in the high-field zone upstream from the cavity was estimated to be about 15 cm. Impurity O_2 was normally added at a point 45 cm downstream from the filament and 27 cm upstream from the cavity center in the form of a 1:500, O_2: Ar mixture. At H_2 flow rates of the order 3.5 atm cm^3s^{-1}, and pressures of 2 torr, a 2-fold enhancement of the *unsaturated* high field H atom EPR line was observed on addition of 15 ppm of O_2. Oxygen additions greater than this produced no further increase in the signal, nor did the addition of this same 15 ppm of O_2 further upstream.

At constant atom concentrations in the cavity, the amount of power required to produce a given degree of saturation was found to increase with increasing carrier flow velocity. Carrier velocities from 650 to 4400 cm s^{-1} were covered in these saturation experiments.

Analysis of these experiments indicated that T_1 in our system was of the order of 20 ms in the absence of added O_2, a value similar to that observed for N atoms. The neglect of the radial diffusion term in (7) is therefore justified, since even if a wall mechanism were the sole relaxation process, the radial gradients it would produce would be negligible at the flows and pressures used.

[2] Certain commercial products and instruments are identified in this paper in order to specify adequately the experimental procedure. In no case does such identification imply recommendation or endorsement by the National Bureau of Standards, nor does it imply that the products or equipment identified are necessarily the best available for the purpose.

4. Solution of the Rate Equations

Since a flow method was used, only steady-state solutions of the rate equations were required. The equations (7) for the four-level system were solved only under the following conditions: (a) radial and axial diffusion neglected; (b) for the unsaturated case, a uniform velocity profile for the carrier, and (c) for the saturated case, a zero carrier velocity. To examine the effects of axial diffusion at low and high power, and nonzero carrier velocity under saturation conditions, a two-level model was analyzed. Again radial diffusion was neglected, and a uniform carrier velocity assumed.

4.1. Unsaturated Four-Level System

For low power conditions such that the coefficients w_{ij} are negligible, diffusion is neglected, and the carrier velocity is assumed to be uniform, the steady-state solution of (7) is given by the set of equations,

$$\begin{aligned} \xi_1 &= E_1+\tfrac{1}{2}(V+Y) \\ \xi_2 &= E_2+\tfrac{1}{2}(U-V) \\ \xi_3 &= E_3+\tfrac{1}{2}(V-Y) \\ \xi_4 &= E_4+\tfrac{1}{2}(U+V) \end{aligned} \tag{9}$$

where,

$$V=V_0 \exp\left[-2(2\gamma+\tfrac{1}{2}K)(z/v_0)\right]$$

$$Y=\tfrac{1}{2}\zeta^{-1}\{(Y_0\theta^+-\tfrac{1}{2}KU_0)\exp(\Phi^-) + (Y_0\theta^-+\tfrac{1}{2}KU_0)\exp(\Phi^+)\}$$

$$U=\tfrac{1}{2}\zeta^{-1}\{(U_0\theta^--\tfrac{1}{2}KY_0)\exp(\Phi^-) + (U_0\theta^++\tfrac{1}{2}KY_0)\exp(\Phi^+)\}$$

and,

$$\begin{aligned} \gamma &= \tfrac{1}{4}Sn \\ \zeta &= (\eta^2-K\gamma\chi)^{1/2} \\ \eta &= \tfrac{1}{2}K+\gamma\chi \\ \theta^\pm &= \zeta\pm\gamma\chi \\ \Phi^\pm &= -(\eta\pm\zeta)(z/v_0). \end{aligned}$$

The subscript zero on the parameters U, V, and Y denotes their values at $z=0$, the start of the high field region. As mentioned earlier, the strong field values of the R_{ij} coefficients were used.

Calculated values of the ξ_i parameters are shown in figures 1 and 2 as functions of z/v_0. For this calculation the ξ_i values at the start of the high field region were taken to be the values corresponding to thermal equilibrium at zero field and 300 K, namely, $\xi_1^0=\xi_2^0=\xi_3^0=-0.572\times10^{-4}$, and $\xi_4^0=1.716\times10^{-4}$. An H atom concentration of 0.44×10^{14} cm^{-3} and a H—H spin-

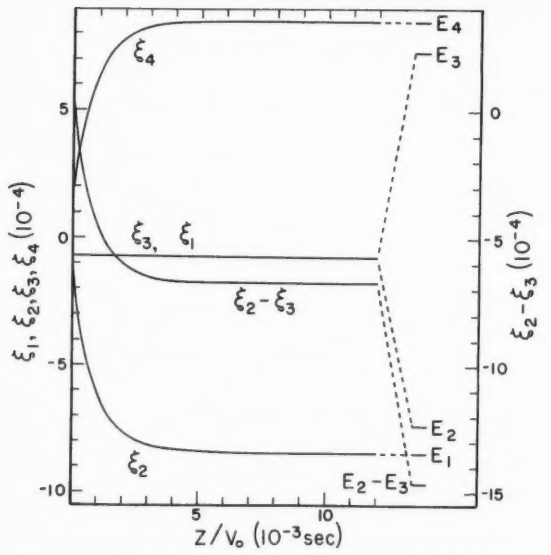

FIGURE 1. *Population parameters ξ_i versus z/v_0 calculated from eq 9.*

Parameter values used were $K=0$, $S=13\times10^{-10}$ cm^3 s^{-1}, $n=0.44\times10^{14}$ cm^{-3}, dc field = 3500 Gauss, and $T=300$ K. The difference $\xi_2-\xi_3$ is also plotted.

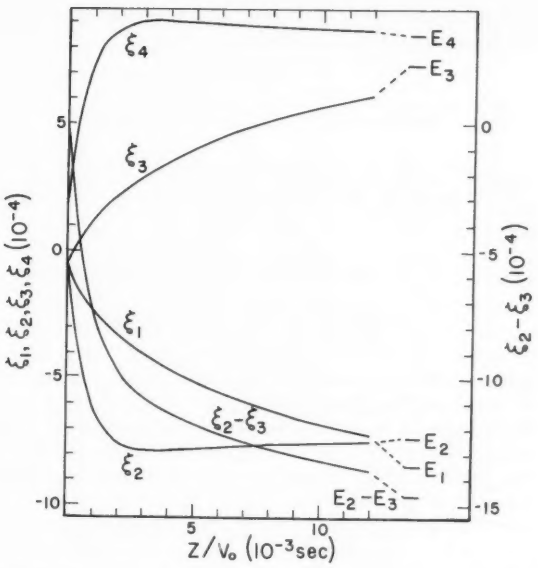

FIGURE 2. *Population parameters ξ_i versus z/v_0 calculated from eq 9.*

Parameter values used were $K=168$ s^{-1}, $S=13\times10^{-10}$ s^{-1}, $n=0.44\times10^{14}$ cm^{-3}, dc field = 3500 Gauss, and $T=300$ K. The difference $\xi_2-\xi_3$ is also plotted.

exchange rate constant of 13×10^{-10}cm^{3}s^{-1} were used. In the present apparatus the EPR cavity would lie at $z/v_0=12\times10^{-3}$s for $v_0=800$ cm s^{-1}. In figure 1, the spin-lattice relaxation parameter K has been set equal to zero, while in figure 2, it was given a value of 168 s^{-1}. Also shown in both figures is the difference $\xi_2-\xi_3$. The intensity of the high field EPR line will be proportional to the value of this difference at the cavity position. Thermal equilibrium values of the parameters at a field of 3500 Gauss and 300 K are shown as dotted lines.

In the absence of any spin-lattice relaxation, ξ_1 and ξ_3 remain unchanged, while H–H spin-exchange brings about rapid relaxation of ξ_2 and ξ_4 to their equilibrium values -8.431×10^{-4} and 8.490×10^{-4}, respectively. They approach to within 10 percent of their final values in a time of the order $1/3\gamma\chi$. Because χ is so small (~0.04), this is considerably slower than one might expect from the large value of γ at this particular H atom concentration. It is obvious that the strong field wave functions would not be suitable for this problem because they yield $\chi=0$ and thus no relaxation of ξ_2 and ξ_4.

The absolute value of $\xi_2-\xi_3$ for this partially relaxed condition is 6.77×10^{-4}, which is a factor of 2.16 smaller than the thermal equilibrium value. Therefore, unless one operates at considerably smaller H atom concentrations, or at much higher flow rates, the maximum enhancement of the EPR signal to be expected on addition of a paramagnetic impurity would be this factor of 2.16.

In case $\gamma\chi \gg K$, the solution for $\xi_2-\xi_3$ may be written approximately as

$$\xi_2-\xi_3=E_2-E_3+\tfrac{1}{2}\{Y_0-U_0\exp(-2\gamma\chi z/v_0)\}\exp(-\tfrac{1}{2}Kz/v_0).$$

The term in brackets quickly relaxes to the value Y_0 so that the process can be described by a single relaxation rate over the range of slow decay.

Let us now assume that K may be written as a sum of two terms, i.e., $K=K_0+Q[O_2]$, where Q is a rate constant for spin-exchange collisions between H and O_2, $[O_2]$ is the O_2 concentration, and K_0 is the value of K without added O_2, presumably arising from collisions with paramagnetic impurities and/or wall relaxation. From the observed values of the high-field line intensity as a function of added O_2, and the results of calculated ξ_i like those shown in figures 1 and 2, a value of $6.4\pm2.0\times10^{-10}$ cm^3 s^{-1} (corrected for axial diffusion as described in the next section) was found for Q, and a value of 50 ± 20 s^{-1} for K_0 at a H_2 flow of 3.5 atm cm^3 s^{-1} and a pressure of 2.2 torr. No measurements were made at other flows or pressures.

4.2. Unsaturated Two-Level System and Corrections for Axial Diffusion

For a two level system, a steady-state analytical solution of (7) is easily obtained if radial diffusion is neglected and a uniform carrier velocity is assumed.

The solution for the population difference $\delta\xi$ between the two levels in the unsaturated case is

$$\delta\xi = \delta E + (\delta\xi^0 - \delta E)\ \exp\left\{\frac{v_0 - (v_0^2 + 4KD)^{1/2}}{2D}\, z\right\}$$

where δE is $\delta\xi$ at equilibrium and $\delta\xi^0$ is $\delta\xi$ at $z=0$, the start of the high field region; $\delta\xi^0$ will be assumed to be zero.

If $v_0^2 \gg 4KD$, the solution may be approximated as

$$\delta\xi \sim \delta E + \delta E\ \exp\{-K[1-(KD/v_0^2)](z/v_0)\}.$$

This result was used to estimate the effects of axial diffusion in the four-level system. For the O_2 signal-enhancement experiment discussed in the preceding section, the correction for this axial diffusion to the rate constant Q was small, approximately + 10 percent.

4.3. Four-Level System With Saturation

Consider equations (7) at high microwave power levels where the factors w_{ij} cannot be neglected. For a nonflowing gas, without diffusion, the steady-state solution for the population difference of interest is

$$\xi_2 - \xi_3 = (E_2 - E_3)(1 + T_1 W)^{-1}$$

where T_1 is given by the expression

$$T_1 = K^{-1}(K/\gamma + 2)(\tfrac{1}{2}K/\gamma + 2)^{-1}. \qquad (10)$$

This parameter is equivalent to the reciprocal of the relaxation probability parameter W_r defined by Lloyd and Pake [10]. The factor multiplying K^{-1} ranges between the limits 1 and 2 according to whether the ratio K/γ is small or large. Although K/γ is much less than unity in the present experiments, large O_2 additions can easily make $K \gg \gamma$. In this situation, T_1 will not be strictly proportional to $[O_2]^{-1}$. It also is evident that when $K/\gamma \sim 1$, T_1 will be somewhat dependent, through γ, on the H atom concentration.

4.4. Two-Level System With Saturation

To estimate the effect of flow and axial diffusion on the amount of microwave power required to produce a given degree of saturation, the two-level model has been used. The parameter W has been assumed to be constant over the effective length L of the cavity ($\sim$ 2cm) and zero elsewhere. The spin-lattice parameter K has been assumed to be large enough to equilibrate the spins by the time the atoms reach the cavity. The EPR signal will be proportional to the average value of the population difference $\delta\xi$ in the cavity. This average over the length of the cavity is given by

$$\langle\delta\xi\rangle = F^+ + F^- + \tfrac{1}{2}K\delta E(\tfrac{1}{2}K + W)^{-1} \qquad (11)$$

where

$$F^{\pm} = 2(C^{\pm}/\mu^{\pm}L)\sinh(\mu^{\pm}\tfrac{1}{2}L)$$

$$C^{\pm} = \pm W\delta E(\tfrac{1}{2}K + W)^{-1}\{(\mu^{\mp} - \mu_0^+)\mu_0^-\exp(-\mu^{\pm}\tfrac{1}{2}L) - (\mu^{\mp} - \mu_0^-)\mu_0^+\exp(\mu^{\mp}\tfrac{1}{2}L)\}(G^+ + G^-)^{-1}$$

$$G^{\pm} = \pm(\mu^+ - \mu_0^{\mp})(\mu^- - \mu_0^{\mp})\exp[\pm(\mu^+ - \mu^-)\tfrac{1}{2}L]$$

$$\mu^{\pm} = v_0/2D \pm \lambda$$

$$\mu_0^{\pm} = v_0/2D \pm \lambda_0$$

$$\lambda = [v_0^2 + 8D(\tfrac{1}{2}K + W)]^{1/2}/2D$$

$$\lambda_0 = [v_0^2 + 8D\tfrac{1}{2}K]^{1/2}/2D.$$

This rather formidable expression was used to calculate $\langle\delta\xi\rangle$ as a function of W for various values of the parameters, v_0, D, and K. It was found that the relationship between $\langle\delta\xi\rangle$ and W could be represented to a very good approximation by the expression

$$\langle\delta\xi\rangle = \delta E(1 + T_1^* W)^{-1} \qquad (12)$$

where T_1^* depends on v_0, D, and K.

The relaxation time for the four-level model at high H atom concentrations will actually be equal to $\frac{1}{2}T_1^*$. This is because H–H spin-exchange collisions couple in the two unpumped levels which are also experiencing the same spin-lattice relaxation processes.

Some examples of how $\frac{1}{2}T_1^*$ depends on the various parameters are shown in figures 3 and 4. Figure 3 shows the variation of $2/T_1^*$ with D for a range of K values from 100 to 1600 s^{-1}. The flow velocity v_0 was varied over the range 100 to 500 cm s^{-1}. Over this interval the dependence on v_0 was small and is indicated by the width of the curves. It is evident that the effect of diffusion can be quite large even in the absence of any wall relaxation.

The variation of $2/T_1^*$ with v_0 at $D = 912$ cm^2 s^{-1} is shown is figure 4 for different values of K. It can be seen that for K values above 400 s^{-1}, the dependence of $2/T_1^*$ on v_0 is quite small for v_0 in the range 0 to 1000 cm s^{-1}.

4.5. Determination of T_1 by Saturation Methods

The fact that the population differences of the pumped levels for the models considered here are proportional to a quantity of the form $(1 + T_1 W)^{-1}$ means that the saturation theory for Lorentzian lines discussed by Westenberg and De Haas [5] is applicable. Caution must be observed in using this theory, however, as it applies only to homogeneously broadened lines and for field modulation frequencies ω_m such that $\omega_m \ll T_1^{-1}$. The 400 Hz modulation frequency used in the present experiment satisfied the latter condition when the carrier flow was sufficiently high,

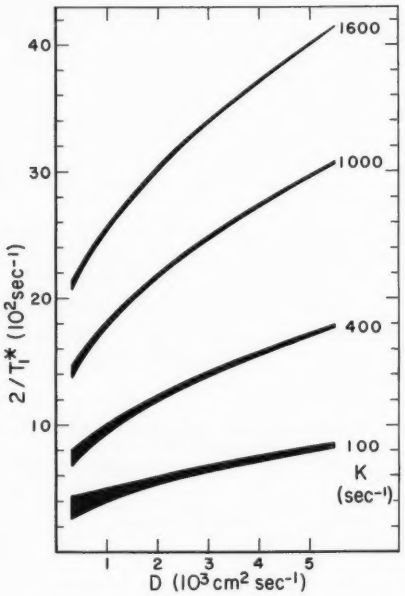

FIGURE 3. *Variation of* $2/T_1^*$ *versus* D *calculated from eqs 11 and 12 for different values of* K.

For each K value, v_0 was varied over the range 100 to 500 cm s^{-1}; the effect of this on $2/T_1^*$ is indicated by the width of each curve.

but the former requirement was not satisfied since the lines were asymmetrical and presumably broadened by field inhomogeneities.

4.6. Results of Saturation Experiment

The signal enhancement produced by traces of O_2 demonstrated that the H atom spin-lattice relaxation time in the present system was quite long. In this case, as can be seen from figure 4, the relaxation time observed in a saturation experiment should depend markedly on the rate at which unsaturated atoms enter the cavity. The effect of carrier velocity on the amount of saturation produced by a given microwave power level is shown in figure 5. Here, a H_2 carrier was used at 2 torr with $v_0 = 1160$ and 3239 cm s^{-1}. The high frequency H atom line is shown at a low power level at which saturation was negligible, and at a power level 20 dB higher for which considerable saturation was evident. In the double attenuator method used [1], the signal is proportional to χ'', the imaginary part of the magnetic susceptibility. It is obvious that there was considerably less saturation at the higher power level for the higher carrier flow. In this experiment, about 40 ppm O_2 was added to the carrier to ensure complete relaxation of the atoms arriving at the cavity so that the signal observed at low power would be proportional to the H atom concentration. This concentration was the same for both carrier velocities. The conditions of this experiment correspond to the third

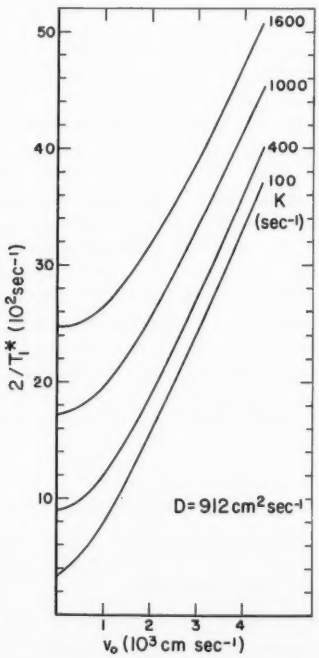

FIGURE 4. *Variation of* $2/T_1^*$ *with* v_0 *at* $D = 912\ cm^2\ s^{-1}$, *calculated from eqs* 11 *and* 12 *for different values of* K.

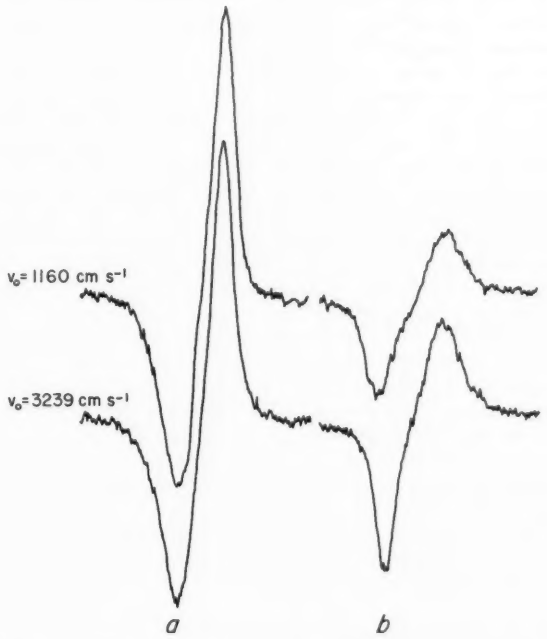

FIGURE 5. *Effect of carrier flow velocity on the power saturation of the high-field* H *atom EPR line.*

The two traces labeled (a) were recorded at low power where saturation was negligible. The H atom concentration is the same in both traces but the carrier velocity was different as shown. The traces (b) were recorded at a power level 20 dB higher. The lower trace in (b) corresponding to the higher carrier flow is less saturated than the one at the lower flow.

curve in figure 4, labeled $K=1000\ s^{-1}$. This calculation predicts that a given power input would produce roughly half the saturation at $v_0=3239$ cm s^{-1} that it would produce at 1160 cm s^{-1}. The results shown in figure 5 are in agreement with this prediction.

5. Discussion

The purpose of this work has been to show how the H atom hyperfine populations equilibrate when the atom is placed in a magnetic field. In the present experiments there were two major relaxation processes, (a) spin-exchange collisions between the H atoms, and (b) spin-exchange collisions between the H atoms and O_2 molecules added in trace amounts. The spin-exchange process conserves the component of angular momentum in the direction of the dc magnetic field, which we shall call the z-direction. Because states Ψ_2 and Ψ_4 have z angular momentum components of zero, spin-exchange collisions among the H atoms themselves can equilibrate [9] these levels without changing the net value of the z-component. The net magnetization of the system will change however, since these two states have nonzero magnetic moments at high field strengths. Thus, partial magnetization of the system will arise solely from H–H collisions. It is worth noting that this situation cannot occur for N atoms, because none of the hyperfine levels have zero values for the z-component.

The other two states have nonzero components $+\hbar$ and $-\hbar$ for Ψ_1 and Ψ_3, respectively. Thus, the relative populations of these two levels cannot change without changing the total value of the z-component for the H atom system. This can be changed only through an interaction with the surrounding system, i.e., with the "lattice". Spin-exchange collisions with impurity O_2 can provide the necessary spin-lattice interaction even though the z-component will be conserved during the collision. This is because any nonthermal spin orientation imparted to the O_2 will be rapidly destroyed because of the strong coupling of the electron spin on O_2 to its molecular framework. This is strongly coupled to the heat bath particles through collisions which change the O_2 rotational energy.

From the enhancing effect of O_2 on the H atom signal, a rate constant of 6×10^{-10} cm^3 s^{-1} was determined for the H–O_2 spin-exchange collision. Kleppner, Goldenberg, and Ramsey [14] examined the effect of O_2 on the radiating state of the atoms in a hydrogen maser, and reported a relaxation rate constant. To compare our value with theirs, it is necessary to solve (7) for the zero-field case. Letting $\epsilon=\frac{1}{2}$ in tables 1 and 2 for A_{ij} and R_{ij}, and neglecting diffusion and mass flow, one obtains for the population difference $\xi_2-\xi_4$ involved in the maser transition,

$$\xi_2-\xi_4=E_2-E_4+(\xi_2^0-\xi_4^0-E_2+E_4)\exp(-4\gamma t-Kt)$$

where t is the time, and ξ_i^0 are the values of ξ_i at $t=0$. If $4\gamma \ll K$ in the presence of added O_2, the relaxation will be represented by the change of exp $(-Kt)$ with time. Therefore the relaxation rate observed by these workers is equal to K as defined in the present work. Their value of $K[O_2]^{-1}=6.2\times10^{-10}$ cm^3 s^{-1} is in agreement with ours. Neither of these values is in agreement with that of Westenberg and De Haas [5], whose t_1 values should be equal to K^{-1} since their H atom concentration was kept high during O_2 addition. (See eq. 10.)

A collision cross section σ^2 can be derived from the observed rate parameter $K\sim Q[O_2]$ if one uses the kinetic-theory relation $K=\sigma^2(8\pi kT/\mu)^{1/2}[O_2]$, where k is the gas constant, T is the absolute temperature, and μ is the reduced mass of the colliding particles. The values of the rate constant Q and the cross section σ^2 are shown in table 4.

TABLE 4. *Rate constant and collision cross section for* H–O_2 *spin-exchange collisions.*

Q	σ^2	Reference
$6.4\pm2.0\times10^{-10}$ cm^3 s^{-1}	$8.0\pm2.5\times10^{-16}$ cm^2	This work.
6.2	7.7	[12]
35	44	[5]

The cross section determined in the present work and by Kleppner, et al., is smaller than that for H–H spin-exchange collisions. This may not be unreasonable since one would expect the attractive potential curve for H–O_2 to be considerably shallower than that for H–H and thus the phase shift between the attractive and repulsive potentials could be smaller. However, since it appears that the steepness of the repulsive state potential curve is also an important factor, at least in the H–H case [15], it is difficult to say anything definite about the H–O_2 system without a detailed knowledge of the states involved.

It is not clear why wall relaxation should have been so much more important in the experiments of Westenberg and De Haas than in ours. Nevertheless, our observations show that it is quite possible for wall relaxation to be negligible in some systems. In this situation some O_2 impurity must be present to achieve complete magnetization. The amount necessary at moderate carrier flows is very small however, of the order 15 to 30 ppm, so that it should not interfere with kinetic studies of moderately fast reactions. Under such conditions however, power saturation can still depend on the carrier flow rate. A line which is unsaturated at a high flow rate may be saturated at a lower one.

6. References

[1] Brown, R. L., and Brennen, W., J. Chem. Phys. **47,** 4697 (1967).
[2] McNeal, R. J., Bernheim, R. A., Bersohn, R., and Dorfman, M., J. Chem. Phys. **40,** 1678 (1964).
[3] Brown, R. L., and Brennen, W., J. Chem. Phys. **46,** 385 (1967).
[4] Breen, J. E., and Glass, G. P., J. Chem. Phys. **52,** 1082 (1970).
[5] Westenberg, A. A., and De Haas, N., J. Chem. Phys. **51,** 5215 (1969).
[6] Tollefson, E. L., and Leroy, D. J., J. Chem. Phys. **16,** 1057 (1948).

[7] Rony, R. P., and Hanson, D. N., J. Chem. Phys. **44,** 2536 (1966).
[8] Breit, G., and Rabi, I. I., Phys. Rev. **38,** 2082 (1931).
[9] Purcell, E. M., and Field, G. B., Astrophys. J. **124,** 542 (1956).
[10] Lloyd, J. P., and Pake, G. E., Phys. Rev. **94,** 579 (1954).
[11] Lambe, E. B., Thesis, Princeton University, 1959 (unpublished).
[12] Westenberg, A. A., and De Haas, N., J. Chem. Phys. **47,** 1393 (1967).
[13] Clyne, M. A. A., and Thrush, B. A., Trans. Faraday Soc. **57,** 1305 (1961).
[14] Kleppner, D., Goldenberg, H. M., and Ramsey, N. F., Phys. Rev. **126,** 603 (1962).
[15] Glassgold, A. E., and Lebedeff, S. A., Ann. Phys. **28,** 181 (1964).

(Paper 76A2–703)

JOURNAL OF RESEARCH of the National Bureau of Standards—A. Physics and Chemistry
Vol. 76A, No. 2, March–April 1972

Photoionization of $C_4H_8^+$ Isomers. Unimolecular and Bimolecular Reactions of the $C_4H_8^+$ Ions[1]

L. W. Sieck, S. G. Lias, L. Hellner,[2] and P. Ausloos

Institute for Materials Research, National Bureau of Standards, Washington, D.C. 20234

(November 4, 1971)

1-Butene, *cis*-2-butene, isobutene and methylcyclopropane have been photoionized with the resonance lines of krypton (10.0–10.6 eV) and argon (11.6–11.8 eV). We have determined that the internally excited 1-$C_4H_8^+$ ion and, to a much lesser extent, the *i*-$C_4H_8^+$ ion isomerizes to the 2-$C_4H_8^+$ structure. In both cases the extent of isomerization increases, approximately by a factor of ten when the photon energy is increased from 10 to 11.7 eV. An inert gas, neon, quenches the isomerization of the *i*-$C_4H_8^+$ ion and, to a much lesser rextent, that of the 1-$C_4H_8^+$ ion.

The unimolecular fragmentation of the $C_4H_8^+$ isomeric ions has been examined at 11.6–11.8 eV. In this energy range the dissociative lifetime of *i*-$C_4H_8^+$ was found to be at least 5×10^{-6} s, and collisional quenching of the dissociative process is already noticeable at pressures in the 10^{-3} torr range.

The rate coefficients for the reaction $C_4H_8^+$ (thermal) + $C_4H_8 \rightarrow (C_8H_{16}^+)^*$ occurring in the isomeric C_4H_8 systems have been determined under conditions where the structure of the reacting $C_4H_8^+$ ion is established. The values in cm^3/molecule · second are 1-$C_4H_8 - 6.0 \pm 0.5 \times 10^{-10}$, *cis*-2-$C_4H_8 - 0.37 \pm 0.1 \times 10^{-10}$, *i*-$C_4H_8 - 5.4 \pm 0.4 \times 10^{-10}$. At pressure below 10^{-3} torr, the internally excited $(C_8H_{16}^+)^*$ produced in the reaction dissociates along various channels with relative probabilities depending upon the structure of both the ionic and neutral reactant. Above 10^{-3} torr collisional quenching of $(C_8H_{16}^+)^*$ is noted.

Key words: C_4H_8 isomers; collisional stabilization; isomerization; photoionization; rate constants; vapor phase.

1. Introduction

The reactions of $C_4H_8^+$ ions have been examined in several laboratories. In most cases, the $C_4H_8^+$ ions were produced in the ion source of a mass spectrometer using electrons [1], and in some instances photons [2], as ionization sources. Several investigations have also involved the fate of $C_4H_8^+$ ions formed in the gamma radiolysis or vacuum ultraviolet photolysis of various compounds [3]. In many of these investigations, the structures of the $C_4H_8^+$ ions were not precisely established.

In a recent study [3d] the isomerization processes of the $C_4H_8^+$ ions formed in the irradiation of cyclobutane, methylcyclopropane, and in ethylene via the reaction

$$C_2H_4^+ + C_2H_4 \rightarrow C_4H_8^+$$

were explored and it was concluded that these relatively high energy $C_4H_8^+$ isomers rearrange to the thermodynamically more stable 2-$C_4H_8^+$, *i*-$C_4H_8^+$, and 1-$C_4H_8^+$ configurations. Furthermore, the extent of isomerization as well as the relative distributions of the final isomerization products were found to depend on the internal energy content of the rearranging species; i.e., the isomerization processes were dependent on the mode of ion formation (the initial energy content of the ion) as well as on the collision frequency.

In this related study, the isomerization processes of the lower energy isomeric $C_4H_8^+$, 1-$C_4H_8^+$, 2-$C_4H_8^+$, and *i*-$C_4H_8^+$ ions are examined, and the unimolecular fragmentation processes of the excited primary $(C_4H_8^+)^*$ ions are considered. Since the results of the earlier study would lead us to expect—and indeed this expectation is confirmed in the results reported here—that the structure of $C_4H_8^+$ ions observed in a given system will vary depending on the mode of formation of the ion, we have reexamined the often studied [1,2] reaction:

$$C_4H_8^+ + C_4H_8 \rightarrow (C_8H_{16}^+)^* \rightarrow \text{products} \qquad (2)$$

in systems where we know the structure(s) of the reacting ions.

[1] This research was supported by the U.S. Atomic Energy Commission.
[2] Guest Worker, 1970–1971. Permanent address: Equipe de Recherche du C.N.R.S., Paris, France.

453-425 OL - 72 - 4

2. Experimental Procedure

The ion-molecule reactions and fragmentation processes associated with the photoionization of the C_4H_8 isomers at various pressures were investigated with the NBS high pressure mass spectrometer. This instrument, which has been described in detail elsewhere [2b, 4], provides information concerning the reactivity of *thermal* ions at pressures up to approximately 1 torr. The detailed experimental techniques involved in deriving absolute rate parameters have also been discussed previously [2b, 4].

Isomerization reactions were examined by means of static system photolysis experiments, which were performed in the same manner as described in a previous publication [3d]. Some of the krypton resonance photolysis experiments were carried out with a light source emitting both the 123.6 and 116.5 nm (10.0 and 10.6 eV) resonance lines. A krypton lamp emitting only the 123.6 nm (10 eV) line was used in all mass spectrometric and some of the static system photoionization experiments. The argon resonance lamps emitted the 104.8 and 106.7 nm (11.6 and 11.8 eV) lines with about equal intensity. The construction of the light sources has been described [5]. In the static system experiments the yield of a product, X, in tables 1 and 2, is given in terms of the number of molecules (M(X)) produced per positive ion (N_+). This is designated as the ion pair yield ($M(X)/N_+$) of product X.

TABLE 1. *Yields of* C_4H_8 *Products formed in the photolysis of 1-butene*

	Pressure, torr			M/N$_+$	
	1-C_4H_8	DMA†	Ne	*trans*-2-C_4H_8	*cis*-2-C_4H_8
10.0–10.6 eV	0.75	0.70	.....	0.065	0.057
11.6–11.8 eV	1.0	.25	.....	.53	.35
	1.0	.58	.....	.54	.36
	0.5	.5	.....	.55	.38
	.5	.5	60.	.52	.37
	.5	.5	180.	.46	.34

† Dimethylamine.
All experiments are carried out in the presence of 5 percent oxygen added as a radical scavenger.

TABLE 2. *Yields of* C_4H_8 *products formed in the photolysis of isobutene*

	Pressure, torr			M/N$_+$	
	i-C_4H_8	DMA†	Ne	*trans*-2-C_4H_8	*cis*-2-C_4H_8
10.0–10.6 eV	1.0	.....	.....	0.007	0.005
	1.0	0.5	.....	.007	.005
11.6–11.8 eV	0.3	.....	.....	.071	.053
	1.0	.....	.....	.073	.056
	2.0	.....	.....	.072	.056
	2.2	.....	40	.036	.030
	2.1	.....	266	.0105	.009
	1.1	.2	.....	.072	.055
	1.1	.5	.....	.071	.053

† Dimethylamine.
All experiments are carried out in the presence of 5 percent oxygen added as a radical scavenger.

3. Results and Discussion

3.1. Isomerization of $C_4H_8^+$ Ions

a. 1-$C_4H_8^+$

In the earlier study [3d] results were obtained from which it was inferred that the high energy $C_4H_8^+$ ions formed in ethylene, cyclobutane, and methylcyclopropane rearranged to a 1-$C_4H_8^+$ structure which, unless deenergized by collisions, would rearrange further to the 2-$C_4H_8^+$ structure (and possibly also to the *i*-$C_4H_8^+$ structure). Therefore, it might be expected that sufficiently energetic $C_4H_8^+$ ions formed in the photoionization of 1-butene would undergo the exothermic ($\Delta H = -0.55$ eV) rearrangement:

$$(1\text{-}C_4H_8^+)^* \rightarrow (2\text{-}C_4H_8^+)^* \qquad (3)$$

which requires the displacement of only one hydrogen atom. When 1-butene is photolyzed in the presence of dimethylamine, any 2-$C_4H_8^+$ ions formed in isomerization process (3) would be expected [3] to undergo exothermic ($\Delta H = -0.27$ eV) charge transfer:

$$2\text{-}C_4H_8^+ + (CH_3)_2NH \rightarrow 2\text{-}C_4H_8 + (CH_3)_2NH^+ \qquad (4)$$

to form neutral 2-butene as a product. The results given in table 1 show the yields of *cis*- and *trans*-2-C_4H_8 formed in mixtures of 1-butene and dimethylamine irradiated with 10.0 and 11.6–11.8 eV photons. It is evident that the yield of 2-butene formed in reaction sequence (3)–(4) increases as the energy of the photon is increased. In the 10.0–10.6 eV photolysis, only about 10 percent of the 1-$C_4H_8^+$ ions isomerize to the 2-$C_4H_8^+$ structure, but at 11.6–11.8 eV, ~ 90 percent of the ions undergo this rearrangement. (Isomerization to the *i*-$C_4H_8^+$ structure can not be detected in this kind of experiment, since the analytical techniques used here do not distinguish between 1-C_4H_8 and *i*-C_4H_8.)

These conclusions are qualitatively confirmed in experiments in which the $C_4H_8^+$ ions abstract D_2^- from added methylcyclopentane-d_{12} to form butanes:

$$C_4H_8^+ + C_6D_{12} \rightarrow C_4H_8D_2 + C_6D_{10}^+ \qquad (5)$$

The D_2^- species is transferred across the unsaturated site in the $C_4H_8^+$ ion, so the isotopic structure of the partially deuterated butane product indicates the structure of the precursor $C_4H_8^+$ ion. When 1-butene-methylcyclopentane-d_{12} mixtures were irradiated with 10.0 eV photons in the presence of oxygen added to scavenge free radicals, 95 percent of the *n*-butane product had the structure, $CH_2DCHDCH_2CH_3$, indicating again that isomerization is relatively unimportant at this energy. The concentration of added methylcyclopentane in these experiments was varied from 10 to 80 mole percent, in order to confirm that the majority of the $C_4H_8^+$ ions were indeed intercepted. The fact that somewhat less isomerization was observed in this set of experiments than in the corresponding

experiments with added dimethylamine may be ascribed to the fact that the 10.6 eV krypton resonance line was filtered out by a calcium fluoride window in the methylcyclopentane experiments, so the ions may have had a slightly lower energy distribution. However, an exact quantitative treatment of the data in these experiments is difficult because of competition from the reaction of the $C_4H_8^+$ ions with the parent butene molecules.

As was found in the dimethylamine additive experiments, isomerization is more important when the photon energy is increased to 11.6–11.8 eV (in the methylcyclopentane-d_{12} experiments at this energy, 40–70 percent of the n-$C_4H_8D_2$ product consisted of $CH_3CHDCHDCH_3$). It should be mentioned that at this energy, a small amount of isobutane was also formed in reaction (5), but the yield was so small that it could not be accurately determined. We can conclude that isomerization of the 1-$C_4H_8^+$ ion to the i-$C_4H_8^+$ structure is unimportant at 11.6–11.8 eV. At 11.6–11.8 eV, the results are not quantitative because at these energies methylcyclopentane is ionized and the methylcyclopentane-d_{12} parent ions are known [6] to react with neutral 1-C_4H_8 molecules as follows:

$$C_6D_{12}^+ + 1\text{-}C_4H_8 \rightarrow CH_2DCHDCH_2CH_3 + C_6D_{10}^+ \quad (6)$$

The results given in table 1 show that when as much as 180 torr of neon are added to 1 torr of a 1-$C_4H_8^+$–$(CH_3)_2NH$ (1 : 1) mixture, the importance of isomerization to the 2-$C_4H_8^+$ structure is decreased by only 15 percent. The absence of a major effect indicates that the isomerization is relatively fast at this energy.

2-Butene is also produced in the absence of a charge acceptor, but its formation is entirely quenched upon addition of 400 torr of neon. It would seem therefore that a reaction mechanism involving internally excited 2-$C_4H_8^+$ ions would account for this observation.

b. i-$C_4H_8^+$

The results obtained in the photolysis of isobutene at 10.0 and at 11.6–11.8 eV, indicate that the isomerization of the i-$C_4H_8^+$ ion is unimportant at these energies. For example, experiments carried out in the presence of added dimethylamine as a charge acceptor (table 2) indicate that not more than 1.2 percent of the $C_4H_8^+$ ions isomerize as follows:

$$(i\text{-}C_4H_8^+)^* \rightarrow (2\text{-}C_4H_8^+)^* \quad (7)$$

followed by charge transfer reaction (4) at these two energies. However, it should be noted that at both energies, the yield of 2-C_4H_8 is nearly the same in the absence as in the presence of a charge acceptor. Since these products are not formed in the photolysis i-C_4H_8 below its ionization energy, we may infer that they do have $C_4H_8^+$ as precursors. Accepting that these products are formed by a process analogous to that described above for the 2-C_4H_8 products formed in the photolysis of 1-C_4H_8 in the absence of additives, the results given in table 2 indicate that the bulk of the 2-$C_4H_8^+$ ions formed in reaction (8) can transfer their charge to i-C_4H_8:

$$(2\text{-}C_4H_8^+)^* + i\text{-}C_4H_8 \rightarrow 2\text{-}C_4H_8 + i\text{-}C_4H_8^+$$

$$\Delta H = 0.1 \text{ eV} \quad (8)$$

and yield i-$C_4H_8^+$ ions containing less excess energy than those formed in the primary photoionization process.

Because it is difficult to analyze small quantities of 1-C_4H_8 in i-C_4H_8 using our analytical techniques, isomerization to the 1-$C_4H_8^+$ structure would not be detected in the charge transfer experiments given in table 2. However, when methylcyclopentane-d_{12} was added to isobutene at a total pressure of 2 torr, experiments at both energies failed to reveal the formation of any $CH_2DCHDCH_2CH_3$, which is the partially deuterated butane product that would be formed in reaction (5) if 1-$C_4H_8^+$ ions were present.

At 11.6–11.8 eV, an increase in the pressure of i-C_4H_8 from 0.3 to 2.0 torr has no obvious effect on the extent of isomerization. Addition of neon, however, strongly quenches the ion pair yield of 2-C_4H_8. An interpretation of this observation can be based on the occurrence of a stepwise deactivation of the $(i\text{-}C_4H_8^+)^*$ ions formed in the primary photoionization process by neon. The energy barrier for process (7), which requires carbon skeletal rearrangement, must be substantially higher than for process (3).

c. cis-2-$C_4H_8^+$

Photoionization of cis-2-C_4H_8 (in the presence of O_2 as free radical scavenger) at 10.0 eV and 11.6–11.8 eV results in the formation of $trans$-2-C_4H_8, with ion pair yields of 0.57 and 0.59 respectively. However, $trans$-2-C_4H_8 was also found (quantum yield = 0.05) when cis-2-C_4H_8 was photolyzed at 8.4 eV, which is below the energy threshold for ionization of 2-C_4H_8. A fraction of the $trans$-2-C_4H_8 product observed at 10 and 11.6–11.8 eV may therefore be produced in an unimolecular or bimolecular reaction which does not involve ions. If one assumes that the quantum yield of the neutral process is invariant with the photon energy, the ion pair yield of $trans$-2-C_4H_8, which may be ascribed to the reaction:

$$cis\text{-}2\text{-}C_4H_8^+ \rightarrow trans\text{-}2\text{-}C_4H_8^+ \quad (9)$$

is approximately equal to 0.4 for the ionizing wavelength regions.

When 38 mole percent methylcyclopentane-d_{12} is added to cis-2-butene at a total pressure of 2 torr, the butane formed in reaction (5) consists of at least 90 percent $CH_3CHDCHDCH_3$ at both 10.0 and 11.6–11.8 eV. Therefore, it may be concluded that the isomerization of cis-2-$C_4H_8^+$ to stable 1-$C_4H_8^+$ ions is unimpor-

tant. A small amount of isobutane-d_{12} ($M/N_+ = 0.01$) produced in the same experiment at 11.6–11.8 eV indicates that a minor fraction (< 5%) of the excited 2-$C_4H_8^+$ ions isomerize to the branched structure.

The addition of SF_6 as an electron scavenger in the photoionization of *cis*-2-C_4H_8 raises the ion pair yield of *trans*-2-C_4H_8 at least a hundredfold. A drastic effect of SF_6 was also noted by Hummel [7] in the radiolysis of C_4H_8-SF_6 mixtures and was ascribed to a perturbation of the π-bond in 2-C_4H_8 upon collision with SF_6^-:

$$cis\text{-}2\text{-}C_4H_8 + SF_6^- \rightarrow trans\text{-}2\text{-}C_4H_8 + SF_6^- \qquad (10)$$

3.2. Fragmentation Patterns of the $C_4H_8^+$ Isomers at 11.6–11.8 eV

Photoionization of the C_4H_8 isomers at 10.0 eV yields only parent ions since the appearance potentials of the possible fragment ions are higher than 11 eV [8]. At 11.6–11.8 eV, however, fragmentation of the $C_4H_8^+$ ions was observed in every case. The fragmentation patterns obtained at these energies are summarized in table 3. Also included are the ΔH_f values for the parent ions. The major dissociative processes found were:

$$(C_4H_8^+)^* \rightarrow C_4H_7^+ + H \qquad (11)$$

$$\rightarrow C_3H_5^+ + CH_3 \qquad (12)$$

The minor dissociation:

$$C_4H_8^{+}{}^* \rightarrow C_3H_4^+ + CH_4 \qquad (13)$$

was also observed for every isomer, and the fragment $C_2H_4^+$ ion was observed from *c*-C_4H_8.

It has been suggested [1f] that the proportion of $C_4H_8^+$ ions capable of dissociation increases with the heat of formation of the ground state parent ion. This trend is not confirmed by the results given in table 3. For instance, 1-$C_4H_8^+$ ($\Delta H_f = 9.6$ eV), 2-$C_4H_8^+$ ($\Delta H_f = 9.05$ eV), and *i*-$C_4H_8^+$ ($\Delta H_f = 9.05$ eV) all show more extensive fragmentation than the methylcyclopropane ion ($\Delta H_f = 10.18$ eV). Actually even the 70 eV mass spectral cracking patterns of the C_4H_8 isomers [1f] do not show a correlation between $\Delta H(C_4H_8^+)$ and the degree of fragmentation of the $C_4H_8^+$ ion. The results given in table 3 do indicate, however, that such a relation may hold when the cyclic $C_4H_8^+$ isomers and the open ring $C_4H_8^+$ isomers are considered separately. Partial retainment of the cyclic structure because of an activation energy requirement for ring opening might account for the higher relative stability of the methylcyclopropane and cyclobutane ions. Static system experiments [3d] have shown that in the case of cyclobutane, ring opening does occur effectively prior to or during reaction. A multitude of factors including bond strengths, Franck-Condon factors, rates of isomerization in the parent ions, etc., will influence the fragmentation patterns. For example only 12 percent of the parent ions from *i*-C_4D_8 fragment at 11.6–11.8 eV compared with approximately 29 percent of those derived from *i*-C_4H_8. Isotope effects of this magnitude in the isomerization and fragmentation processes are not surprising in these experiments since the average photon energy, and therefore the maximum available energy, is only slightly in excess of the threshold energies for the dissociation processes.

TABLE 3. *Fragmentation patterns of* C_4H_8 *isomers obtained at 106.7–104.8 nm*

	$\Delta H_f(C_4H_8^+)$	Percent distribution			
		$C_4H_8^+$	$C_4H_7^+$	$C_3H_5^+$	$C_3H_4^+$
Cyclobutane	[a] 10.57	48.5	12.7	32.3	5.2
Methylcyclopropane	[b] 10.18	77.3	8.9	11.9	1.9
1-butene	[c] 9.60	48.6	14.4	31.6	5.4
cis-2-butene	[c] 9.05	67.5	16.5	13.4	2.6
Isobutene	[c] 9.05	70.9	12.1	13.3	3.7

[a] Based on 10.3 eV for IP(C_4H_8) see Ref. 1d.
[b] Based on 9.9 eV for IP(C_4H_8) see Ref. 3d.
[c] K. Watanabe, T. Nakayama, and J. Mottel, J. Quant. Spectros. Radiative Transfer, **2**, 369 (1962).

3.3. Collisional Stabilization of the ($C_4H_8^+$) Ions Produced at 11.6–11.8 eV

a. 2-C_4H_8

Figure 1 presents the decay curves of $C_4H_8^+$ ions formed in the photoionization of *cis*-2-C_4H_8 at 10.0 and 11.6–11.8 eV. The obvious feature at the higher energy is the initial increase in the fractional yield of $C_4H_8^+$ as the total pressure is increased. Since none of the three fragment ions listed in table 3 can produce $C_4H_8^+$ by charge exchange (as verified experimentally by Abramson and Futrell [1b] in a tandem instrument) the increase in the fractional yield can only be ascribed to collisional quenching of the fragmentation processes which produce $C_3H_5^+$ and/or $C_4H_7^+$ (processes 11 and 12). It is of interest that competition between unimolecular dissociation and bimolecular reaction has also been observed in an electron impact mass spectrometric study [1g] of *cis*-2-C_4H_8, even though in that study the mean energy to the butene molecule was considerably higher than in the present investigation.

b. i-C_4H_8

The decay curves found for the major ions obtained

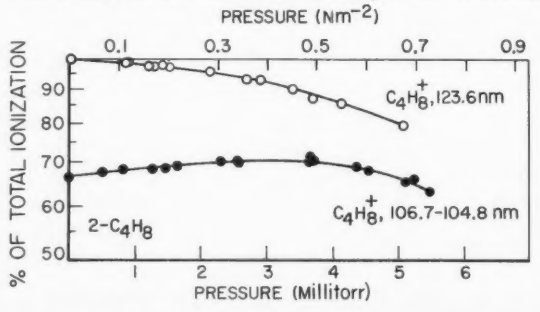

FIGURE 1. *Decay curves for* $C_4H_8^+$ *from* cis*-2-butene as a function of pressure at 123.6 and 106.7–104.8 nm.*

from the photoionization of i-C_4H_8 at 11.6–11.8 eV are given in figure 2. The decay curve for $C_4H_8^+$ found at 10.0 eV is also included for comparison. As was observed in 2-C_4H_8, the fractional yield curve for $C_4H_8^+$ at 11.6–11.8 eV exhibits pronounced curvature although the yield of this ion never exceeds the "zero pressure" value in this particular case. If the assumption is made that the differences in the contours of the decay curves at the two energies are due entirely to quenching of potentially dissociative $(C_4H_8^+)^*$ ions, it is possible to calculate an average half-life (lifetime) for the dissociation processes from the experimental data. As shown later in the discussion, isomerization of i-$C_4H_8^+$ to 2-$C_4H_8^+$ would result in a decreased reaction rate and therefore a reduced slope in figure 2. However the relatively small degree of isomerization which was shown to occur in this system (see sec. 3.1) would not have a noticeable effect on the $C_4H_8^+$ contour given in figure 2. If we assume that every collision deactivates the $C_4H_8^+$ ion to an energy level from which it can no longer dissociate, then the rate constant for deactivation may be taken as 2×10^{-9} cm³/molecule · s. and the lifetime of the $(C_4H_8^+)^*$ ions which dissociate prior to collision is approximately 5×10^{-6} s. This value for the deactivation rate constant is approximately equivalent to that expected for the charge-exchange reaction between i-$C_4H_8^+$ and i-C_4H_8, and exceeds the theoretical ion induced dipole rate constant for complex formation by a factor of two. If deactivation is less efficient than that assumed above the calculated lifetime would increase correspondingly. It is appropriate to compare this estimated lifetime with other lifetimes of more energetic $C_4H_8^+$ species which have been reported. Tiernan and Futrell [9] reported a unimolecular rate constant for dissociation of $C_4H_8^+$ ions formed in reaction (1) (ethylene ion + ethylene) which corresponded to a lifetime of 3×10^{-9} s. In these particular experiments the $C_4H_8^+$ ions were produced in a tendem mass spectrometer in which ionization of ethylene was induced by 100 eV electron impact. As a result these $C_4H_8^+$ ions most likely contained more internal energy than those characteristic of the other experiments we are comparing. It has recently been shown [3d] that $C_4H_8^+$ ions formed in reaction (1) contain more internal energy when ethylene is ionized by highly energetic electrons than when ionization is induced by absorption of 11.6–11.8 eV photons. Gorden and Ausloos [10] estimated an average dissociative lifetime of 5×10^{-8} s. for the $C_4H_8^+$ ion formed in the 11.6–11.8 eV photoionization of ethylene, and Meisels [11] estimated a lifetime of at least 2×10^{-8} s. for the $C_4H_8^+$ ion formed in the radiolysis of ethylene. It appears that the lifetime of the i-$C_4H_8^+$ ion formed when isobutene is ionized by 11.6–11.8 eV photons is approximately two orders of magnitude greater than that of the $C_4H_8^+$ ion formed in ethylene.

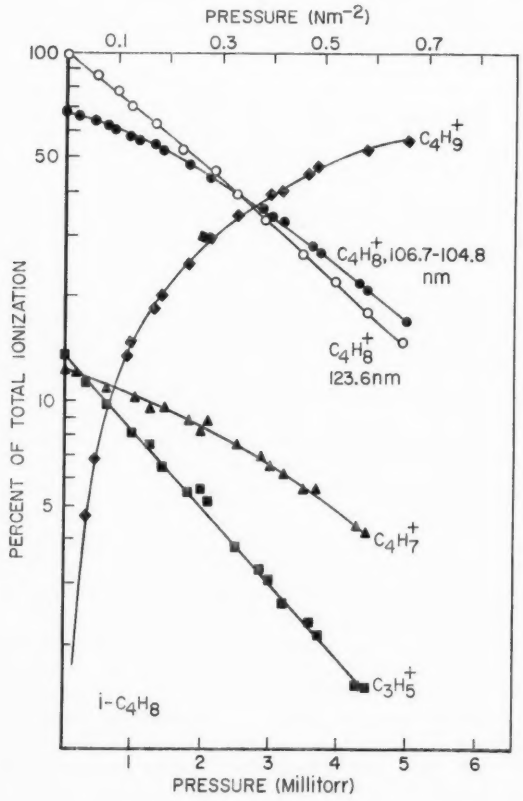

FIGURE 2. *Decay curves for major ions from photoionized* i-C_4H_8 *at 106.7–104.8 nm as a function of pressure.*

Also included (o) is the decay curve for $C_4H_8^+$ from i-C_4H_8 obtained at 123.6 nm.

c. 1-C_4H_8

In the 11.6–11.8 eV photoionization of 1-C_4H_8 (fig. 3) the initial slope of the decay curve is considerably lower than that obtained with 10.0 eV photons. The fact that the difference in slope is much more pronounced for this compound than for i-C_4H_8 (fig. 2) may be due to a longer dissociative lifetime of the $(1\text{-}C_4H_8^+)^*$ ion. However, in view of the results presented in section 3.1 which indicate that the structure of the reactant ion in 1-C_4H_8 at 11.6–11.8 eV is mainly 2-$C_4H_8^+$, the lower rate of reaction of this ion as compared to its precursor (1-$C_4H_8^+$) probably also contributes to the reduction in slope seen in figure 3.

3.4. Absolute Rate Coefficients of Reaction of $C_4H_8^+$ Ions

Rate coefficients for bimolecular reactions of primary $C_4H_8^+$ ions with their parent molecules were determined from the slopes of the semilogarithmic decay plots of the type displayed in figure 4. Only the 10.0 eV data, were considered, in view of the fact that at this energy fragmentation does not compete with the bimolecular reaction, and isomerization of the butene ions is relatively unimportant (see sec. 3.1). The decay curves are linear in the low pressure range for reactant ions of a single structure when the rate coefficient does not vary with the internal energy distribution of the

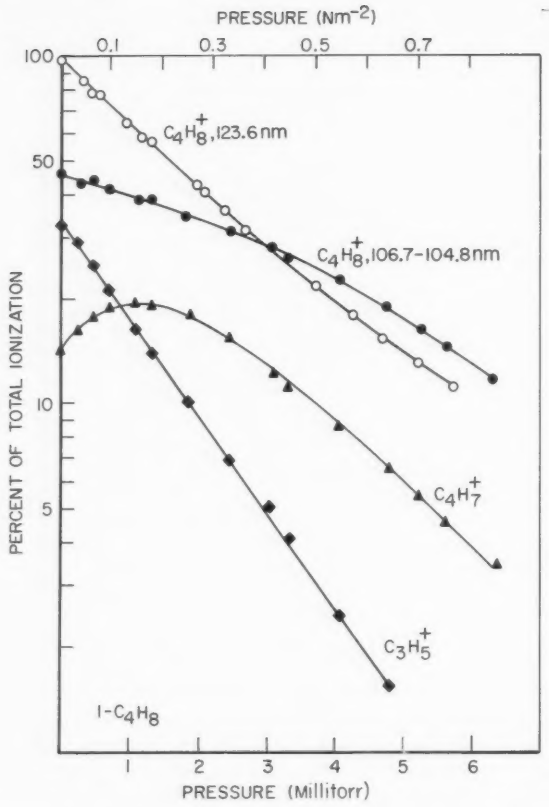

FIGURE 3. *Decay curves for major ions from photoionized* 1-C_4H_8 *at 106.7–104.8 nm as a function of pressure.*

Also included is the decay curve for $C_4H_8^+$ from 1-C_4H_8 obtained at 123.6 nm.

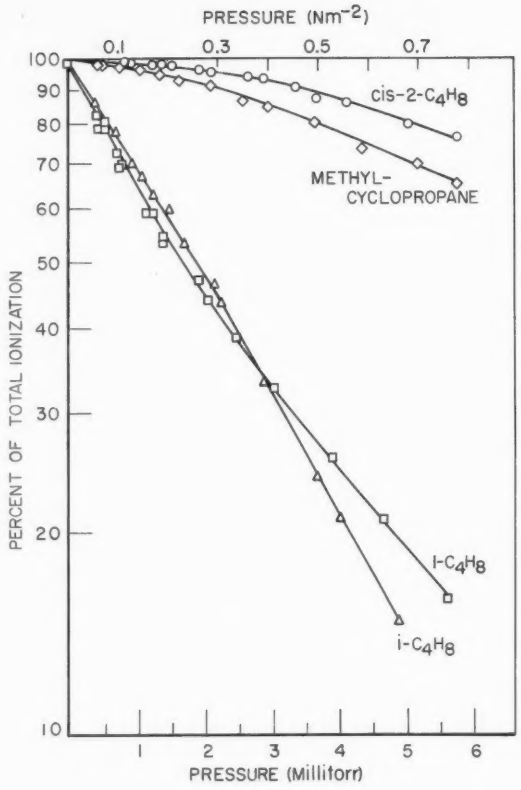

FIGURE 4. *Decay curves for* $C_4H_8^+$ *obtained from the photoionization of* cis-2-C_4H_8, *methylcyclopropane,* 1-C_4H_8, *and* i-C_4H_8 *at 123.6 nm as a function of pressure.*

reactant ion. Most experimental semilogarithmic decay curves will exhibit some downward curvature at higher pressures due to nonreactive scattering of ions, especially if the rate coefficient is relatively low. Alternatively, a decay curve which is concave upwards at higher pressures indicates that two or more ions of the same mass are reacting, and each exhibits a different overall reactivity. The experimental decay curves found for the $C_4H_8^+$ ions obtained from the photoionization of 1-C_4H_8, *i*-C_4H_6, methylcyclopropane, and 2-C_4H_8 at 10.0 eV as a function of pressure are given in figure 4. With the exception of 1-C_4H_8, all of the isomeric systems exhibit an increased slope at higher pressures due to nonreactive scattering of primary ions or other changes in the reaction mechanism. The contour of the experimental decay curve for $C_4H_8^+$ from 1-C_4H_8 indicates one or more minor $C_4H_8^+$ components in the composite signal which exhibit a reduced reactivity when compared to the bulk of the $C_4H_8^+$ ions. This is not unexpected because as shown earlier in the discussion, approximately 10 percent of the 1-$C_4H_8^+$ ions isomerize to the 2-$C_4H_8^+$ structure at 10.0 eV, and it is known [1e] that the latter ions react more slowly with 1-C_4H_8 than the 1-$C_4H_8^+$ ions. Due to the indeterminate effect of nonreactive scattering at higher pressures, however, no attempt was made to resolve the experimental curve into components. Absolute rate coefficients for the various isomers were derived from initial slopes using a best straight line fit through the low pressure points. A summary of these coefficients is given in table 4.

In agreement with earlier observations [1d, 2b, d] the $C_4H_8^+$ ion formed in the photoionization of cyclobutane was unreactive towards cyclobutane. At the pressures at which our experiments were carried out the *c*-$C_4H_8^+$ ion isomerizes to the 2-$C_4H_8^+$, *i*-$C_4H_8^+$, and *c*-$C_3H_5(CH_3)^+$ ion structures [2d].

The relative reaction rates are also given in table 4 and can be compared with those obtained by other investigators. Good agreement is seen between the rate data derived from ion cyclotron resonance experiments [1e] and those obtained in this study. Because the $C_4H_8^+$ ions in the cyclotron experiments were produced by impact with low energy electrons, it may be assumed that the structures of the reactant ions were not very different from those produced in the present 10.0 eV photoionization experiments. Agreement with the relative rate constants obtained

TABLE 4. *Absolute rate coefficients for the reaction:* $C_4H_8^+ + C_4H_8 \rightarrow$ *Products other than* $C_4H_8^+$

	Rate coefficient (cm^3/molecule·second)	Relative Rates		
		This work	[a] Ref. 1b	[b] Ref. 1e
cis-2-butene	$0.37 \pm 0.1 \times 10^{-10}$	1	1	1
Methylcyclopropane	$0.60 \pm 0.1 \times 10^{-10}$	1.6	.....	.....
Isobutene	$5.4 \pm 0.4 \times 10^{-10}$	14.5	5	.....
Isobutene-d_8	$5.4 \pm 0.4 \times 10^{-10}$	14.5	.....	.....
1-butene	$6.0 \pm 0.5 \times 10^{-10}$	16.2	2.5	14.0

[a] Tandem mass spectrometer. Kinetic energy 0.3 ± 0.3 eV, reactant ions produced by 100 eV electron beam.
[b] Ion cyclotron resonance mass spectrometer. Kinetic energy 0–0.1 eV. Ions produced by electrons whose energy is just above the threshold for ionization.

in the tandem mass spectrometer [1b] is, however, poor. The relatively low rate of reaction of the $C_4H_8^+$ produced from 1-C_4H_8 can in part be ascribed to the extensive isomerization to the 2-$C_4H_8^+$ structure which may be expected to occur when an 100 eV electron beam is used to produce $C_4H_8^+$ ions. The excess kinetic energy given to the ions in the tandem mass spectrometer will also tend to bring the rate coefficients closer together.

As shown in figure 2, the photoionization of *i*-C_4H_8 at 11.6–11.8 eV leads to the formation of $C_4H_9^+$ as the major ion at pressures above $4\text{–}5 \times 10^{-3}$ torr. This indicates the occurrence of the well-known reaction:

$$i\text{-}C_4H_8^+ + i\text{-}C_4H_8 \rightarrow C_4H_9^+ + C_4H_7 \qquad (14)$$

We have investigated the stereospecificity of this overall process via photoionization of $(CD_3)_2C=CH_2$ at both 10.0 eV and 11.6–11.8 eV. At each of these energies, the overall reaction gave 87 percent $C_4D_7H_2^+$ and 13 percent $C_4D_6H_3^+$. The invariance of this result with energy is not surprising in view of the fact that isomerization of the isobutene ion is unimportant in these energy regions (see Part 3.1). Exchange processes such as:

$$C_4D_7H_2^+ + (CD_3)_2C=CH_2 \rightarrow C_4D_8H^+ + C_4D_5H_3 \qquad (15)$$

were also observed under pressure conditions where consecutive reactions occur to a significant extent (that is, at pressures above $3\text{–}4 \times 10^{-3}$ torr).

3.5. Modes of Dissociation of the $(C_8H_{16}^+)^*$ Ions

The $C_4H_8^+$ ions have available to them as at least one possible reaction path, condensation with their parent C_4H_8 compounds:

$$C_4H_8^+ + C_4H_8 \rightarrow (C_8H_{16}^+)^* \qquad (16)$$

(The one exception to this is cyclobutane, which, as noted above, does not react with $C_4H_8^+$ ions.) The condensation ion $(C_8H_{16}^+)^*$, may be collisionally stabilized or undergo one of several possible dissociation processes, including regeneration of the original reactant partners. The major fragmentation channels observed to a greater or lesser extent at low pressures in the mass spectrometer reaction chamber for all of the isomers except cyclobutane, are:

$$C_8H_{16}^+ \rightarrow C_4H_9^+ + C_4H_7 \qquad (17)$$

$$\rightarrow C_5H_9^+ + C_3H_7 \qquad (18)$$

$$\rightarrow C_5H_{10}^+ + C_3H_6 \qquad (19)$$

$$\rightarrow C_5H_{11}^+ + C_3H_5 \qquad (20)$$

$$\rightarrow C_6H_{11}^+ + C_2H_5 \qquad (21)$$

$$\rightarrow C_6H_{12}^+ + C_2H_4 \qquad (22)$$

$$\rightarrow C_7H_{13}^+ + CH_3 \qquad (23)$$

It should be pointed out that proton (or H-atom) transfer reactions such as that shown in reaction (14) occur to some extent in all these systems (see table 5); this is an independent reaction channel of the $C_4H_8^+$-C_4H_8 reaction pairs, and not a mode of dissociation of the $C_8H_{16}^+$ ions. This will be discussed in more detail below.

Typical behavior is shown graphically in figure 5 which reproduces the data obtained as a function of pressure when 1-C_4H_8 was photoionized at 10.0 eV. Although only major ions are displayed, it is apparent that the ionic reaction mechanism is quite complex. The relative probabilities for production of $C_4H_9^+$, $C_5H_{10}^+$ etc., via unimolecular fragmentation of $(C_8H_{16}^+)^*$ may be obtained from such data by determining the relative rates of production of the various secondary ions as a function of pressure. The values for the relative rates were extrapolated to "zero pressure" and the intercepts were taken as the relative probabilities that the condensation ion as initially formed will dissociate via process (17) through (23). It was necessary to derive the zero pressure intercepts in every case since the C_4–C_7 product ions were also found to react further in each isomer. For example, it is evident from figure 5 that the relative rate of production of $C_5H_{10}^+$ decreases rapidly as the pressure of 1-C_4H_8 is increased in the reaction chamber. This behavior is indicative of further reaction of $C_5H_{10}^+$, presumably to produce C_7^+ ions. However, the exact

TABLE 5. *Distribution of product ions obtained from the overall reaction* $C_4H_8^+ + C_4H_8 \rightarrow$ *Products*

	Present work	Henis Ref. 1e	A and F Ref. 1b	Koyano Ref. 2a		Present work	Henis Ref. 1e	A and F Ref. 1b	Koyano Ref. 2a
	cis-2-butene					Isobutene			
$C_4H_9^+$	3.3	9.1	70	[a] 56	$C_4H_9^+$	91.7	n.d.	93	86
$C_5H_{10}^+$	5.8	12.4	4	n.d.	ΣC_5^+	4.5	n.d.	7	14
$C_5H_{11}^+$	3.5	6.2	10	n.d.	ΣC_6^+	3.4	n.d.	n.d.	n.d.
$C_6H_{11}^+$	42.3	31.0	10	n.d.	ΣC_7^+	0.4	n.d.	n.d.	n.d.
$C_6H_{12}^+$	45.1	41.3	6	n.d.					
	Methylcyclopropane					1-butene			
$C_4H_9^+$	< 1.0				$C_4H_9^+$	8.3	15.5	14	24.7
$C_5H_9^+$	8.8				$C_5H_9^+$	4.3	4.7	4	16.1
$C_5H_{10}^+$	69.0				$C_5H_{10}^+$	38.8	31.5	38	30.5
$C_6H_{11}^+$	8.0				$C_5H_{11}^+$	4.2	2.2	3	5.5
$C_6H_{12}^+$	7.6				$C_6H_{11}^+$	26.3	24.0	22	16.1
$C_7H_{13}^+$	6.3				$C_6H_{12}^+$	16.1	18.3	15	7.2
					$C_7H_{13}^+$	2.0	3.8	2	n.d.

a Koyano also observed 44 percent $C_3H_7^+$, which is a minor ion in all other studies.

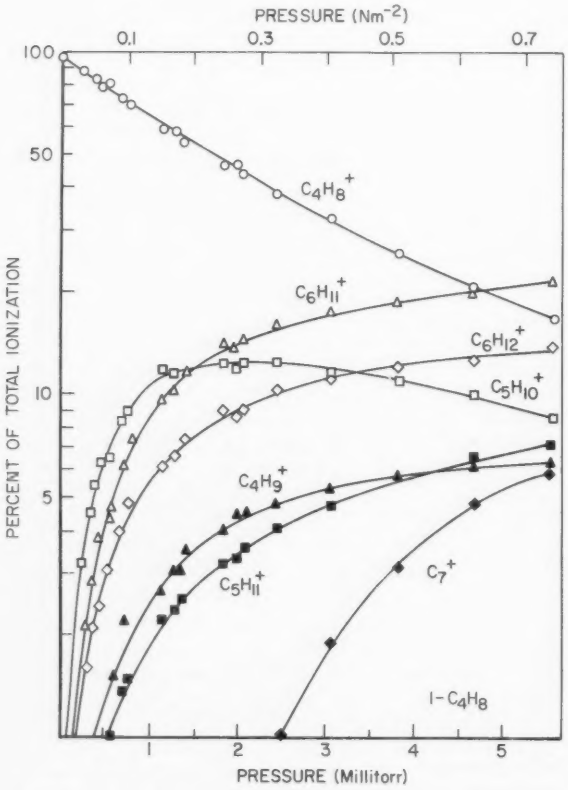

FIGURE 5. *Composite mass spectrum obtained following photoionization of* 1-C_4H_8 *as a function of pressure at 123.6 nm.*

mechanisms leading to consecutive reaction products could not be evaluated due to the complexity of the composite mass spectrum at higher pressures.

In kinetic mass spectrometry, there is a potential source of error in the use of "zero pressure" intercepts for the determination of unimolecular fragmentation patterns of condensation ions which are formed in slow reactions, especially if the precursor reactant ion ($C_4H_8^+$ in this case) isomerizes to a more or less reactive structure to any significant extent. That is, those condensation ions which are formed at very low pressures may result only from the interaction of those ions which for energetic and structural reasons were found to react quickly, and the fragmentation pattern obtained does not necessarily give the modes of dissociation of a condensation ion formed from the bulk of the ions in the system. In the experiments reported here, this effect was minimized by using 10.0 eV photons to generate the $C_4H_8^+$ ions. As indicated previously, isomerization is relatively unimportant at this energy. Included for comparison in table 5 are analogous data obtained by Henis [1e] using ICR techniques with ions at kinetic energies at or near kT, and by Abramson and Futrell [1b] using the ion-injection technique at any impacting energy of approximately 0.3 eV. Additional data obtained by Koyano [2a] using photoionization at 10.2 eV (Lyman α) at kinetic energies in excess of 0.5 eV are also tabulated.

In general our results agree best with those obtained by Henis, which is not unexpected in view of the fact that the ions have low internal and kinetic energies in both studies. However we do find a significantly lower probability for production of $C_4H_9^+$ in both 2-C_4H_8 and 1-C_4H_8 than that seen in the other studies. Abramson and Futrell [1b] have reported that this H^+ or H transfer process in olefins proceeds via a mechanism which does not involve the formation of C–C bonds in the collision complex. Herod and Harrison have actually found that the probability for the formation of the $C_3H_7^+$ ion in the $C_3H_6^+$-C_3H_6 reaction pair increases substantially with the kinetic energy of the $C_3H_6^+$ ion at the expense of the formation of condensation ions (reaction 16). It would seem therefore that the higher

$C_4H_9^+$ yield obtained in the other studies can mainly be ascribed to excess kinetic energy. The effect is particularly evident when comparing the results for 2-C_4H_8 in which Abramson and Futrell, and Koyano, observed 50–70 percent proton transfer.

It is seen (table 5) that for thermal $C_4H_8^+$ ions, the unimolecular fragmentation pattern of $C_8H_{16}^+$ varies considerably from one system to another. The structure of the reactant $C_4H_8^+$ ion and of the neutral molecule, as well as the internal energy content, will determine the fragmentation pattern of the $C_8H_{16}^+$. Henis [1e] has discussed some of these factors for a number of olefinic systems. Some of the main differences noted here can be rationalized in terms of the differences in structure of the $(C_8H_{16}^+)^*$ ions. For instance the much lower abundance of the $C_5H_{10}^+$ product ion in 2-C_4H_8 as compared to 1-C_4H_8 is due to the fact that the $C_8H_{16}^+$ ion resulting from a 2-$C_4H_8^+$-2-C_4H_8 encounter will be highly branched. The 70 eV mass spectral cracking patterns of linear and branched octenes show that process (19) is especially important only in those octenes which exhibit a linear portion of at least three carbon atoms.

The unusually high abundance of the $C_5H_{10}^+$ ion in the methylcyclopropane case would therefore indicate that the $C_4H_8^+$ ion (which as noted before exhibits mainly the 2-$C_4H_8^+$ structure under these conditions) reacts with the neutral methylcyclopropane molecule with ring opening in the 1–2 position.

3.6. Collisional Stabilization of $C_8H_{16}^{+*}$

Although stable $C_8H_{16}^+$ was not detected in any of the various perprotonated C_4H_8 isomers at pressures around 10^{-4} torr, the formation of $C_8D_{16}^+$ was observed in both 2-C_4D_8 and *i*-C_4D_8 in this pressure range. The relative probabilities for production of $C_8D_{16}^+$ at 10^{-4} torr were found to be 0.06 in *i*-C_4D_8 and 0.2 in 2-C_4D_8 when compared with the total probability for production of all other reaction product ions in these systems. The fact that formation of $C_8D_{16}^+$ ions was observed at lower pressures than the $C_8H_{16}^+$ ions is attributed to the theory that the dissociative lifetime of an internally excited deuterated molecule is higher than the protonated counterpart possessing the same amount of energy.

At higher pressures the relative yield of $C_8D_{16}^+$ product ions will increase because of collisional stabilization of the $(C_8D_{16}^+)^*$ condensation ions:

$$(C_8D_{16}^+)^* + M \rightarrow C_8D_{16}^+ + M \qquad (24)$$

which would otherwise dissociate. Experiments were carried out in which 2-C_4D_8 was photoionized in the presence of large excesses of several added gases which are not ionized at 10.0 eV; namely, C_3H_8, Xe, and Ne. The results of these experiments are displayed in figure 6 and were derived in the following manner. A mixture of approximately 2 percent 2-C_4D_8 in, for example, propane was photolyzed at various total chamber pressures in the range 0.001 to approximately

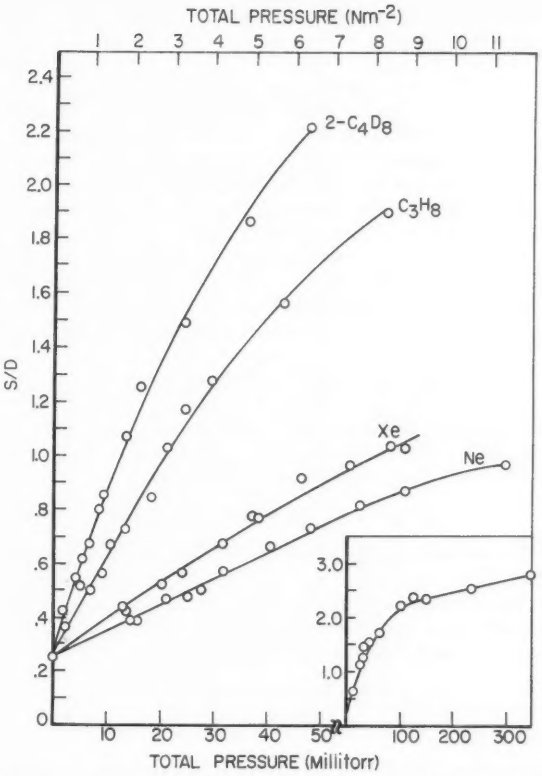

FIGURE 6. *Stabilization to decomposition ratio found for photoionized* 2-C_4D_8 *and mixtures of* 2-C_4H_8 *with* C_3H_8, Xe, *and* Ne *at 123.6 nm as a function of pressure.*

Insert shows ratio for pure 2-C_4D_8 on expanded pressure scale.

0.5 torr. The extent of stabilization of $C_8D_{16}^+$ in such an experiment is assumed to be represented by the sum of the fractional contributions of $C_8D_{16}^+$, $C_{12}D_{24}^+$, and $C_{16}D_{32}^+$ to the composite mass spectrum ($C_8D_{16}^+$ reacts further with 2-C_4D_8 at higher total pressures to form $C_{12}D_{24}^+$, etc.). The extent of dissociation of $C_8D_{16}^{+*}$ into carbon-containing ions other than $C_4D_8^+$ is reflected mainly (> 90 percent) by the sum of the fractional contributions of the C_6^+, C_{10}^+, and C_{14}^+ ions. In figure 6 the sum of the fractional intensities $(C_8^+ + C_{12}^+ + C_{16}^+)$ is represented by S (stabilization) while the parameter D represents $C_6^+ + C_{10}^+ + C_{14}^+$. The ratio S/D is a measure of the stabilization efficiency of the particular additive gas at a particular total pressure, and a plot of S/D versus total pressure yields the types of curves displayed in figure 6. Relative stabilization efficiencies were derived from the initial slopes found in pure 2-C_4D_8 and mixtures of 2-C_4D_8 with C_3H_8, Xe, and Ne. The relative efficiencies found were as follows: 2-C_4D_8, 1.0; C_3H_8, 0.56 ± 0.06; Xe, 0.20 ± 0.04; and Ne, 0.12 ± 0.03. The drop in the deactivating efficiencies from C_4D_8 to Ne cannot be entirely accounted for by a decrease in the collision rate (as calculated on the basis of the ion-induced dipole formulation). This is not unexpected since removal of internal energy by atoms may require several collisions.

3.7. Reaction of $C_8H_{16}^+$ with C_4H_8

Photoionization of i-C_4H_8 and i-C_4D_8 was also carried out at 10.0 eV at pressures up to 50 millitorr in order to investigate higher order processes. Representative results are given in figure 7, which reproduces the fractional intensities of major product ions as a function of pressure for i-C_4H_8. In agreement with previous mass spectrometric investigations of this system we observe the stepwise polymerization of $C_4H_9^+$, which is the major low pressure reaction product (see table 5), to yield $C_4H_9^+$ (C_4H_8) and, at higher pressures, $C_4H_9^+$ $(C_4H_8)_2$. In addition to these processes, however, we also observed the formation of stable $C_8H_{16}^+$ ions:

$$C_4H_8^+ + i\text{-}C_4H_8 \xrightarrow{i\text{-}C_4H_8} C_8H_{16}^+ + C_4H_8 \qquad (25)$$

At pressures greater than approximately 5 millitorr the dimer ion reacts further with i-C_4H_8 via an H_2 transfer reaction to yield $C_8H_{14}^+$ and i-C_4H_{10}

$$C_8H_{16}^+ + i\text{-}C_4H_8 \rightarrow C_8H_{14}^+ + i\text{-}C_4H_{10} \qquad (26)$$

At a pressure of 50 millitorr the sum of the fractional intensities of $C_8H_{16}^+$ and $C_8H_{14}^+$ is 0.31, and appears to be asymptotically approaching a constant value. Quantitative experiments could not be carried out at higher pressures due to the complexity of the composite mass spectrum under those conditions. Analogous experiments with i-C_4D_8 gave the same overall result [12], although the sum of $C_8D_{16}^+$ and $C_8D_{14}^+$ was approximately 0.5 at 50 millitorr. The observation of this reaction sequence accounts for the large ionic yields of isobutane obtained previously in the photoionization and radiolysis of isobutene-O_2 mixtures in closed systems. The analogous reaction scheme has been found in propylene, although the rate of dimer formation and its subsequent reaction was approximately a factor of four slower than found in isobutene. These results have recently been discussed [13].

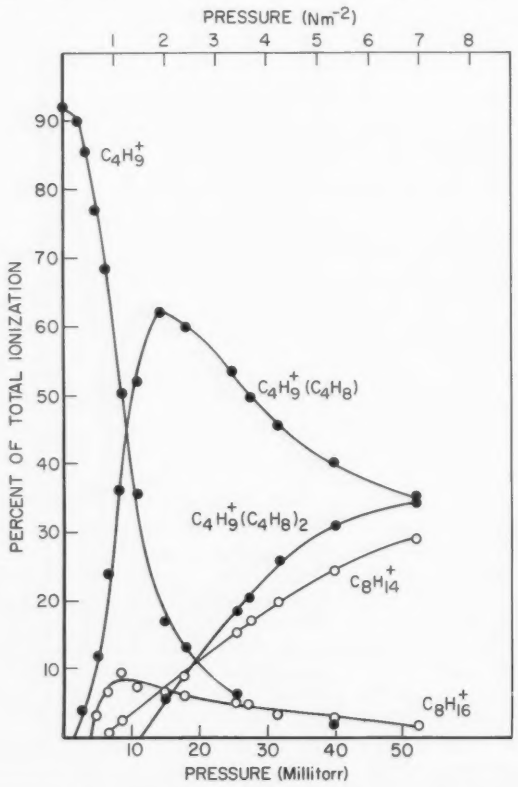

FIGURE 7. *Percentage composition of the product ion mass spectrum (major ions only) obtained from the photoionization of* i-C_4H_8 *at 123.6 nm as a function of pressure.*

The formation of stable dimeric ions and their subsequent reactions has not been considered previously when interpreting the radiation-induced polymerization of isobutene, but the present data indicate that this mechanism will contribute significantly to the chemical end-products. The failure of other mass spectrometric investigators to uncover this sequence is probably either due to the fact that ions were accelerated prior to reaction, the temperatures of the reaction chambers were excessively high, or the total pressures were too low, or some combination of these conditions.

4. References

Some of the more recent papers include:

[1a] Aquilanti, V., Galli, A., Giardini-Guidoni, A., and Volpi, G. G., Trans. Faraday Soc. **63,** 926 (1967).
[1b] Abramson, F. P., and Futrell, J. H., J. Phys. Chem. **72,** 1944 (1968).
[1c] Sieck, L. W., and Futrell, J. H., J. Chem. Phys. **48,** 1409 (1968).
[1d] Hughes, B. M., and Tiernan, T. O., J. Chem. Phys. **51,** 4373 (1969).
[1e] Henis, J. M. S., J. Chem. Phys. **52,** 282 (1970); Ibid. **52,** 292 (1970).
[1f] Meisels, G. G., Park, J. Y., and Giessner, B. G., J. Am. Chem. Soc. **92,** 254 (1970).
[1g] Wisniewsky, S. J., Clow, R. P., and Futrell, J. H., J. Phys. Chem. **74,** 2234 (1970).
[1h] Irie, M., et al., Bull. Chem. Soc. Japan **44,** 2261 (1971).
[2a] Koyano, I., J. Chem. Phys. **45,** 706 (1966).
[2b] Sieck, L. W., Searles, S. K., and Ausloos, P., J. Am. Chem. Soc. **91,** 7627 (1969).
[3a] Lias, S. G., and Ausloos, P., J. Am. Chem. Soc. **92,** 1840 (1970).
[3b] Herman, J., Herman, K., and Ausloos, P., J. Chem. Phys. **52,** 28 (1970).
[3c] Gill, P. S., Inel, Y., and Meisels, G. G., J. Chem. Phys. **54,** 2811 (1971).
[3d] Lias, S. G., and Ausloos, P., Nat. Bur. Stand. (U.S.), J. Res. **75A,** No. 6 589 (1971).
[4] Searles, S. K., and Sieck, L. W., J. Am. Chem. Soc. **92,** 2937 (1970).
[5] Gorden, R., Jr., Rebbert, R. E., and Ausloos, P., Nat. Bur. Stand. (U.S.), Tech. Note 496 55 pages (1969).
[6] Ausloos, P., Progress in Reaction Kinetics, Chapter 3, 113–179, Ed. G. Porter (Pergamon Press Ltd., London, 1970).
[7] Hummel, R. W., Nature **218,** 1050 (1968).
[8] Franklin, J. L., Dillard, J. G., Rosenstock, H. M., Herron, J. T., Draxl, K., and Field, F. H., Nat. Stand. Ref. Data Ser., Nat. Bur. Stand. (U.S.), NSRDS–26, 289 pages (June 1969).
[9] Tiernan, T. O., and Futrell, J. H., J. Phys. Chem. **72,** 3080 (1968).
[10] Gorden, R., Jr., and Ausloos, P., Nat. Bur. Stand. (U.S.), J. Res. **75A,** No. 3, 141 (1971).
[11] Meisels, G. G., Advan. in Chem. **58,** 243 (1966).
[12] Sieck, L. W., and Ausloos, P., J. Chem. Phys. (To be published).
[13] Sieck, L. W., and Ausloos, P., Nat. Bur. Stand. (U.S.), J. Res. 76A, No. 3, (May-June 1972).

(Paper 76A2–704)

JOURNAL OF RESEARCH of the National Bureau of Standards—A. Physics and Chemistry
Vol. 76A, No. 2, March–April 1972

Theoretical Investigation of the Odd Configurations of Ni II .*

Y. Shadmi and E. Caspi****

(December 20, 1971)

Two groups of odd levels in Ni II were investigated: those belonging to the complex $3d^84p + 3d^74s4p + 3d^85p$ and those belonging to the configuration $3d^84f$. In the first group the calculated positions of the levels were fit to the positions of the 174 observed levels with an rms error of 133 cm^{-1}. The fit for the second group was based on 60 observed levels and had an rms error of 25 cm^{-1}. The predictions of this investigation helped in the discovery of many of the observed levels.

Key words: Energy levels; g-factors; nickel; parameters, theory.

1. Introduction

The configuration $3d^84p$ has been well known, and many of its observed levels have been reported in AEL [1].[1] Theoretical interpretations of the $3d^84p$ level structure were performed by various investigators [2–4].

About four years ago Professor A. G. Shenstone informed us of some newly discovered odd levels, presumably belonging to the configurations $3d^74s4p$, $3d^85p$, and $3d^8nf$ $(n=4, 5, 6, 7)$. This paper is the result of his suggestion that a theoretical investigation of these configurations be made to help him with his experimental investigation. The companion paper containing Shenstone's experimental results has already been published [5].

Our calculations involved the diagonalization of the energy matrices of the $3d^84p$, $3d^74s4p$, and $3d^85p$ configurations calculated as one complex, and the energy tions calculated as one complex, and the energy matrices associated with the $3d^84f$ configuration. In the case of the $3d^84p + 3d^74s4p + 3d^85p$ complex, we were able to fit the 174 observed levels to the calculated ones with an rms error of 133 cm^{-1}. For the $3d^84f$ configuration, the 60 observed levels could be fitted to the calculated ones with an rms error of 25 cm^{-1}. All the levels were designated in a well defined coupling scheme.

2. Notations and Definitions

In the text and tables Slater parameters and spin-orbit parameters are designated in the usual way. Other symbols and abbreviations used in the text have the following meanings:

B, C = linear combinations of Slater parameters $F_2(dd)$ and $F_4(dd)$; (see, for example, ref. [7]).

α, β, T = effective interactions among d electrons; [9].

H, J, K = parameters of configuration interaction which are appropriate linear combinations of Slater integrals; (see, for example, refs. [4] and [8]).

Δ = root mean square error ("rms error").

"Diag.", "L.S." = abbreviations for "Diagonalization" and "Least-squares calculation," respectively.

In cases where several configurations have analogous parameters, the configuration is also explicitly specified.

3. The Theoretical Interpretation of the Configurations $3d^84p + 3d^74s4p + 3d^85p$

We shall use the following abbreviations:

$$d^8p = 3d^84p,$$

$$d^7sp = 3d^74s4p,$$

$$d^8p' = 3d^85p.$$

In his first letter, Professor Shenstone supplied us with 17 levels belonging to the d^7sp configuration; 9 of them were low and were assumed to be based on $d^7s(^5F)$; 8 of them were high and it was supposed that they were based on d^7s (^3P).

In the first stage of our calculations only the two configurations $d^8p + d^7sp$ were included. The interaction parameters of d^8p are well known [2–4]. For an estimate of initial parameters for d^7sp, we were able to use analogous calculations performed by C. Roth [4] on the Cu II and Zn II spectra and by A. Schwimmer [6] on Sc II, Ti II and V II. It is well known

*An invited paper. This paper was partially supported by the National Bureau of Standards, Washington, D.C. 20304.
**Present Address: The Hebrew University of Jerusalem, Israel.
[1]Figures in brackets indicate the literature references at the end of this paper.

from works on the even configurations in the iron group [7, 8] and from reference (4) that the electrostatic interaction parameters change linearly along sequences of spectra with constant ionization. The behavior of D', defined as the separation between the centers of the configurations $d^{n-1}sp$ and d^np, and the behavior of the spin-orbit interaction parameters are also approximately linear.

Hence we could interpolate the values of D' and the d-p interaction parameters from the spectra of Sc II, Ti II, V II, Cu II, and Zn II mentioned above. For the G_1 (sp) parameter we could rely upon the spectra of the right hand side of the period. Values for the parameters B, C, G_2 (ds) and H were simply taken from the even configurations of Ni II [10]. J and K were also extrapolated from the right hand side of the period.

The first diagonalization was performed using the described above parameters. The nine low observed levels of Shenstone's first list were quartets. It also became evident that the correct coupling for the d^7sp configuration is the following: first the s and p electrons are coupled and then the resulting term is coupled with a term of d^7. Such a coupling was already used by C. Roth [4]. Using this scheme we found that all the nine low-lying levels reported by Shenstone are based on the combination $d^7(^4\mathrm{F})sp(^3\mathrm{P})$.

After our initial diagonalization, additional observed levels were provided by Professor Shenstone to bring the total number of observed levels which were fitted to calculated levels of $d^8p + d^7sp$ up to 78. In the final least-squares calculation based on the previously described interaction parameters, 43 levels were found to belong to the d^8p configuration and 35 to the new configuration d^7sp. The rms error was 100 cm^{-1} for the calculated levels.

The observed levels in the range 110,000–120,000 cm^{-1} could not be satisfactorily fitted in the previous diagonalization. The reason for this was rather clear: in the same energy range some levels belonging to the d^8p' configuration were also observed. This means that in order to obtain good results, one has to include the interaction between the configurations d^7sp and d^8p' as well. Because such an extended calculation requires quite a number of additional new parameters, we first performed a separate calculation on the d^8p' configuration in which we included only the levels which we believed not to be strongly perturbed by d^7sp. This auxiliary calculation provided initial values for the $3d-5p$ interaction parameters and for ζ_{5p}; for B and C we used the same values as for the d^8p configuration.

The extended energy matrix of the three configurations was diagonalized using the approximated values for the parameters found in the previous calculations and estimates for the initial values for J' and K'. In the subsequent least-squares calculations we gradually fitted more and more observed levels to the calculated ones and reached a stage at which 109 observed levels were fitted unequivocally to the calculated ones with an rms error of 70 cm^{-1}. A considerable improvement of the fit between the observed and calculated levels was achieved in the previously problematic range 110,000–120,000 cm^{-1}.

These results enabled Professor Shenstone to supply us with an improved and extended list of observed levels. This new list of levels was used in a new series of iterated diagonalizations. In the final least-squares calculation of this stage, which included the effective-interaction parameters β and T, 132 levels were fit with an rms error of 112 cm^{-1}.

We were not able to include in the fit ten levels of the experimental list. Of these levels, seven were considered by Professor Shenstone to be of doubtful identification. The inclusion of any of the remaining three in the least-squares calculation increases the rms error considerably and forces some of the parameters to assume unreasonable values.

In subsequent correspondence with Professor Shenstone a final level list was constructed. The ten problematical levels were reassigned—some to other configurations and others to different J values. Also, the list was amended by addition of 40 new levels to bring the total up to 174. A new iteration was performed, and the observed levels were fitted to the calculated values with an rms error of 133 cm^{-1}. The parameters of this final calculation are given in table 1, Column L.S. 1a.

The parameters β and T could not both be derived directly from the least squares calculation. Instead, the value of T was fixed at a value obtained from our calculations on the even third spectra of the iron group [8]. When T and β were not included in the calculation, the rms error increased to 145 cm^{-1} as indicated in table 1, column L.S. 2.

Table 2 contains the list of observed and calculated levels of the configurations $d^8p+d^7sp+d^8p'$. The spectral purities of the reported assignments are given only when at least one level of the term has a purity of less than 60 percent. In a few cases the parent term was strongly mixed and was not included in the designation. Four observed levels which were assigned to these configurations by Professor Shenstone could not be fit into the scheme on calculated levels. They are:

1) The level $d^7sp^2\mathrm{D}_{5/2}$ observed at 135258.88 cm^{-1} with a deviation of about 600 cm^{-1} from the calculated value;
2) the levels $d^7sp\ ^4\mathrm{P}_{5/2}$ 131834.94 cm^{-1}
$^4\mathrm{P}_{3/2}$ 132225.15 cm^{-1}
$^4\mathrm{P}_{1/2}$ 132120.70 cm^{-1}

which differ from the calculated values by about 1,200 cm^{-1}. When these levels are included in the iterative fitting procedure, the ^{4}P levels disagree by about 700 cm^{-1} and the mean error increases to 188 cm^{-1}. (See table 1, column L.S. 1b; these levels are those in table 2 which are enclosed by parentheses.)

4. The Theoretical Interpretation of the Configuration $3d^84f$

The abbreviation d^8f will be used for the configuration $3d^84f$. The treatment of this configuration was relatively simple. Initial values for the parameters B, C, and ζ_d were taken from the configuration d^8 of Ni III. [8] A rough first estimate for the parameters

TABLE 1. *Parameters of the configurations* $d^8p + d^7sp + d^9p$.

All values are in units of cm^{-1}

P	Diag. 1	L.S. 1a	L.S. 1b	Diag. 2	L.S. 2
$A(3d^74s4p)$	120990	120980 ± 80	120775 ± 110	120830	120815 ± 85
$A(d^7sp) - A(3d^84p)$	58350	58335 ± 105	58170 ± 145	58540	58500 ± 120
$A(d^7sp) - A(3d^85p)$	7785	7755 ± 95	7550 ± 130	7950	7940 ± 100
$B - d^7sp$	1113	1112 ± 3	1108 ± 4	1130	1131 ± 3
$B - d^8p$	1046	1047 ± 4	1046 ± 5	1073	1075 ± 4
$B - d^8p'$	1046			1073	
$C - d^7sp$	4875	4888 ± 23	4928 ± 31	4550	4550 ± 14
$C - d^8p$	4535	4547 ± 27	4549 ± 37	4170	4172 ± 28
$C - d^8p'$	4535			4170	
$G_2(ds) - d^7sp$	1755	1756 ± 30	1752 ± 42	1770	1751 ± 32
$F_2(dp) - d^7sp$	478	477 ± 6	455 ± 8	478	481 ± 6
$F_2(dp) - d^8p$	352	353 ± 5	353 ± 8	352	351 ± 7
$F_2(dp) - d^8p'$	87	85 ± 7	87 ± 10	87	87 ± 8
$G_1(sp) - d^7sp$	10220	10192 ± 31	10076 ± 42	10290	10306 ± 34
$G_1(dp) - d^7sp$	359	362 ± 9	353 ± 13	346	352 ± 12
$G_1(dp) - d^8p$	295	293 ± 6	296 ± 8	300	299 ± 7
$G_1(dp) - d^8p'$	88	88 ± 7	90 ± 10	97	98 ± 9
$G_3(dp) - d^7sp$	42	42 ± 3	43 ± 3	40	41 ± 3
$G_3(dp) - d^8p$	42			40	
$G_3(dp) - d^8p'$	7	8 ± 4	8 ± 5	8	9 ± 4
α	29	27 ± 3	28 ± 4	78	76 ± 2
β	−900	−1230 ± 160	−1370 ± 230	.....	.....
T	−5.7	Fixed	Fixed	.....	.....
H $d^7sp - d^8p$	185	220 ± 40	175 ± 55	120	135 ± 55
J $d^7sp - d^8p$	1650	1830 ± 330	1755 ± 465	1300	1290 ± 370
J $d^7sp - d^8p'$	400	410 ± 80	475 ± 110	485	465 ± 85
K $d^7sp - d^8p$	2850	2620 ± 370	2730 ± 525	2965	2875 ± 425
K $d^7sp - d^8p'$	1035	1005 ± 75	1015 ± 110	1070	1050 ± 85
$\zeta_d - d^7sp$	749	744 ± 21	748 ± 29	749	748 ± 23
$\zeta_d - d^8p$	663	662 ± 18	664 ± 25	663	657 ± 20
$\zeta_d - d^8p'$	663			663	
$\zeta_p - d^7sp$	630	640 ± 70	720 ± 100	595	605 ± 75
$\zeta_p - d^8p$	455	450 ± 50	450 ± 75	455	450 ± 55
$\zeta_p - d^8p'$	140	130 ± 55	130 ± 75	155	135 ± 60
Δ		133 cm^{-1}	188 cm^{-1}		145 cm^{-1}
Number of levels		174	178		174

TABLE 2. Ni II—*Observed and calculated energy levels* $3d^84p + 3d^85p + 3d^74s4p$ *in units of* cm^{-1}

THEORETICAL ASSIGNMENT		*J*	OBS.	CALC.	O−C	CALC. *g*
MAIN COMPONENT	ADDITIONAL					
$3d^8(^3F)4p\,^4D$		7/2	51557.85	51701	−143	1.423
		5/2	52738.45	52846	−108	1.359
		3/2	53634.62	53721	−86	1.187
		1/2	54176.26	54252	−76	.003
$3d^8(^3F)4p\,^4G$		11/2	53496.49	53364	132	1.273
		9/2	53365.17	53367	−2	1.180
		7/2	54262.63	54205	58	1.021
		5/2	55018.71	54931	88	.620
$3d^8(^3F)4p\,^4F$		9/2	54557.05	54523	34	1.288
		7/2	55417.83	55342	76	1.185
		5/2	56075.26	55990	85	.987
		3/2	56424.49	56352	72	.423
$3d^8(^3F)4p\,^2G$		9/2	55299.65	55315	−15	1.148
		7/2	56371.44	56478	−107	.936
$3d^8(^3F)4p\,^2F$		7/2	57080.55	57103	−22	1.119
		5/2	58493.21	58471	22	.934
$3d^8(^3F)4p\,^2D$		5/2	57420.16	57376	44	1.132
		3/2	58705.95	58647	59	.797

TABLE 2. Ni II—*Observed and calculated energy levels* $3d^84p + 3d^85p + 3d^74s4p$ *in units of* cm^{-1}—Continued

THEORETICAL ASSIGNMENT		J	OBS.	CALC.	O–C	CALC. g
MAIN COMPONENT	ADDITIONAL					
$3d^8(^3P)4p\ ^4P$		5/2	66571.35	66599	−28	1.487
		3/2	66579.71	66584	−4	1.564
		1/2	67031.02	66998	33	2.267
$3d^8(^1D)4p\ ^2F$		5/2	67694.64	67666	29	.938
		7/2	68131.21	68053	78	1.179
$3d^8(^1D)4p\ ^2D$		3/2	68154.31	68235	−81	1.050
		5/2	68735.98	68796	−60	1.258
$3d^8(^1D)4p\ ^2P$		1/2	68281.62	68118	164	1.070
		3/2	68965.65	68831	135	1.264
$3d^8(^3P)4p\ ^4D$		7/2	70778.11	70759	19	1.390
		5/2	70635.55	70626	10	1.334
		3/2	70706.74	70672	35	1.189
		1/2	70748.66	70718	31	.012
$3d^8(^3P)4p\ ^2D$		5/2	71770.83	71909	−138	1.206
		3/2	72375.42	72449	−74	.850
$3d^8(^3P)4p\ ^2P$		3/2	72985.65	72963	23	1.309
		1/2	73903.25	73886	17	.926
$3d^8(^3P)4p\ ^2S$		1/2	74283.33	74399	−116	1.721
$3d^8(^3P)4p\ ^4S$		3/2	74300.93	74304	−3	1.968
$3d^8(^1G)4p\ ^2H$		9/2	75149.55	75190	−40	.910
		11/2	75721.71	75705	17	1.091
$3d^8(^1G)4p\ ^2F$		7/2	75917.61	75977	−59	1.143
		5/2	76402.04	76395	7	.858
$3d^8(^1G)4p\ ^2G$		7/2	79823.03	79874	−51	.890
		9/2	79923.88	79977	−53	1.110
$3d^7(^4F)^4sp(^3P)\ ^6F$		11/2	86343.21	86645	−302	1.450
		9/2	86870.03	86956	−86	1.458
		7/2	87538.09	87599	−61	1.417
		5/2	88128.56	88170	−41	1.332
		3/2	88582.01	88608	−26	1.084
		1/2	88881.59	88884	−2	−.619
$3d^7(^4F)sp(^3P)\ ^6D$		9/2	88171.88	88272	−100	1.519
		7/2	89100.47	89213	−113	1.541
		5/2		89900		1.590
		3/2		90374		1.742
		1/2		90654		3.285
$3d^7(^4F)sp(^3P)\ ^6G$		13/2		88787		1.384
		11/2	89460.35	89327	133	1.345
		9/2	89918.47	89795	123	1.281
		7/2	90275.30	90164	111	1.164
		5/2	90526.18	90428	98	.903
		3/2		90595		.106
$3d^7(^4F)sp(^3P)\ ^4F$		9/2	94283.94	94262	22	1.295
		7/2	94705.93	94701	5	1.214
		5/2	95332.53	95324	9	1.001
		3/2	95893.76	95878	16	.423
$3d^7(^4F)sp(^3P)\ ^4G$		11/2	94396.74	94363	34	1.274
		9/2	95017.71	94989	29	1.208
		7/2	95573.39	95572	1	1.027
		5/2	96052.48	96056	−4	.625
$3d^7(^4F)sp(^3P)\ ^4D$		7/2	96535.87	96629	−93	1.407
		5/2	97273.83	97376	−102	1.346
		3/2	97799.66	97917	−117	1.178
		1/2	98122.63	98250	−127	.003

TABLE 2. Ni II—*Observed and calculated energy levels* $3d^84p + 3d^85p + 3d^74s4p$ *in units of* cm^{-1}—Continued

THEORETICAL ASSIGNMENT		J	OBS.	CALC.	O–C	CALC. *g*
MAIN COMPONENT	ADDITIONAL					
$3d^7(^4F)sp(^3P)\,^2G$		9/2	98276.70	98301	−24	1.115
		7/2	99844.13	99857	−13	.908
$3d^7(^4P)sp(^3P)\,^6S$		5/2		98759		1.997
$3d^7(^4F)sp(^3P)\,^2F$		7/2	99418.61	99222	196	1.130
		5/2	100609.01	100430	179	.876
$3d^7(^4F)sp(^3P)\,^2D$		5/2	101754.80	101718	37	1.186
		3/2	102742.74	102733	10	.803
$3d^8(^3F)5p\,^4D$		7/2	103653.03	103741	−88	1.414
		5/2	104503.22	104590	−87	1.310
		3/2	105439.85	105478	−38	1.125
		1/2	106022.79	106086	−63	.013
$3d^8(^1S)4p\,^2P$		1/2		103459		.667
		3/2		104087		1.329
$3d^8(^3F)5p\,^4G$		11/2	104147.29	104066	81	1.273
41%	38% ^2G	9/2	105588.89	105496	93	1.164
55%	24% ^2G	7/2	105499.05	105429	70	1.006
		5/2	106283.16	106228	55	.701
$3d^8(^3F)5p\,^2G$	60% 32% ^4G	9/2	104081.04	104045	36	1.181
	58% 24% ^4G	7/2	106620.53	106525	96	.964
$3d^8(^3F)5p\,^4F$		9/2	104298.23	104285	13	1.271
39%	33% ^2F	7/2	104646.52	104646	1	1.157
53%	24% ^4G	5/2	105668.78	105673	− 4	.931
		3/2	106369.30	106399	−30	.463
$3d^8(^3F)5p\,^2D$		5/2	105861.19	106017	−156	1.178
		3/2	107142.12	107313	−171	.822
$3d^8(^3F)5p\,^2F$	46% 32% ^4F	7/2	105838.06	105825	13	1.144
		5/2	107082.21	107080	2	.913
$3d^7(^4P)\ sp\ (^3P)\ ^6D$		9/2	105981.50	105888	93	1.554
		7/2		105817		1.585
		5/2		105863		1.654
		3/2		105971		1.837
		1/2		106106		3.296
$3d^7(^4P)sp\,(^3P)\,^4S$		3/2	107737.81	107835	−97	1.851
$3d^7(^4P)\ sp\ (^3P)\ ^6P$		7/2		108783		1.705
		5/2		108873		1.869
		3/2	109038.84	108901	138	.982
$3d^7(^2G)\,sp\,(^3P)\,^4F$		9/2	109148.05	109136	12	1.324
		7/2	109846.00	109892	−46	1.163
		5/2	110573.36	110573	0	1.022
		3/2	111120.54	111068	53	.518
$3d^7(^2G)\ sp\ (^3P)\ ^4H$		13/2		109796		1.228
		11/2		109673		1.135
		9/2		109780		.977
		7/2		110088		.744
$3d^7(^2P)\,sp\,(^3P)\,^4P$		1/2		111112		2.458
44%	30% ^4D	3/2		111724		1.519
48%	30% ^4D	5/2		111917		1.506
$3d^7(^2G)\,sp\ (^3P)\,^4G$		11/2		111634		1.263
		9/2		111850		1.160
		7/2	111783.79	112087	−303	.975
		5/2		112329		.584

TABLE 2. Ni II—*Observed and calculated energy levels* $3d^84p + 3d^85p + 3d^74s4p$ *in units of* cm^{-1}—Continued

THEORETICAL ASSIGNMENT			J	OBS.	CALC.	O–C	CALC. g
MAIN COMPONENT		ADDITIONAL					
$3d^7(^4P)\,sp\,(^3P)\,^4D$			7/2		111437		1.427
	56%	25% ^4P	5/2		111233		1.437
	44%	24% ^4P	3/2		111271		1.258
			1/2		111497		.166
$3d^7(^4F)\,sp\,(^1P)\,^4G$			11/2	112422.19	112549	−127	1.272
	67%	28% ^4F	9/2	113753.04	113728	25	1.214
	41%	44% ^4F	7/2		114531		1.124
	50%	28% ^2F	5/2	115108.09	115173	−65	.820
$d^7sp\,^4D$			7/2		112683		1.421
			5/2		113262		1.380
	65%	24% ^4P	3/2		113846		1.309
	65%	28% ^4P	1/2		114523		.843
$3d^7(^2G)\,sp\,(^3P)\,^2H$			9/2		113082		.904
			11/2		113952		1.085
$3d^7(^4F)\,sp\,(^1P)\,^4F$	63%	34% ^4G	9/2	113321.95	112935	387	1.275
	28%	29% ^4G + 29% ^2G	7/2	114052.21	113788	264	1.056
	61%	16% ^2F	5/2	115120.00	114836	284	1.046
	60%		3/2		115149		.761
$3d^7(^2G)\,sp\,(^3P)\,^2G$	58%	25% ^4G + 14% ^4F	7/2		113765		.970
			9/2		114276		1.119
$3d^7(^4P)\,sp\,(^3P)\,^2S$			1/2		113841		1.925
$3d^7(^4P)\,sp\,(^3P)\,^4P$	61%		5/2		114043		1.456
	53%	40% ^4D	3/2		114387		1.495
	38%	40% ^4D + 20% ^2S	1/2		114378		1.459
$3d^7(^2G)\,sp\,(^3P)\,^2F$	29%	46% ^4G	5/2		114229		.831
	51%	22% ^4D	7/2	115000.25	114866	134	1.209
$3d^7(^2H)\,sp\,(^3P)\,^4G$			11/2	114858.88	114996	−137	1.269
			9/2	116087.38	115720	367	1.139
			7/2	116275.81	116379	−103	1.019
			5/2	116824.15	116833	−9	.643
$d^7\,sp\quad ^2D$	62%		3/2	114869.35	115018	−149	.923
	50%	33% ^4D	5/2	116893.98	117046	−152	1.237
$d^7\,sp\quad ^4D$	78%		1/2		115177		.461
	30%	42% ^4F	3/2	115592.25	115568	24	.834
	32%	25% ^4F + 23% ^2D	5/2	115565.98	115340	226	1.154
	55%	18% ^2F	7/2	115209.98	115321	−111	1.298
$3d^7(^2H)\,sp\,(^3P)\,^4I$			15/2		115245		1.200
			13/2		115237		1.109
			11/2		115440		.977
			9/2		115784		.785
$3d^7(^4P)\,sp\,(^3P)\,^2D$	61%	27% ^4D	5/2		115868		1.245
	43%	25% ^2P	3/2		117094		1.057
$d^7\,sp\quad ^4D$			7/2	116512.06	116603	−91	1.408
	50%	23% ^4F	5/2		117595		1.242
	40%	23% ^4S + 21% ^2P	3/2		117989		1.384
	38%	26% ^2P + 23% ^2S	1/2		118159		.758
$3d^7(^2P)\,sp\,(^3P)\,^4S$	37%	12% ^2D + 12% ^4F	3/2	117662.11	117460	202	1.417
$d^7\,sp\quad ^2P$	41%	23% ^2S	1/2		117478		.984
	27%	29% ^4D + 21% ^4F	3/2		118284		1.118
$3d^7(a^2D)\,sp\,(^3P)\,^4F$			9/2	117593.68	117552	42	1.333
			7/2	117972.47	117993	−21	1.250
	48%	24% ^2D	5/2		118627		1.094
	32%	32% ^2D + 17% ^2P	3/2		118786		.874

TABLE 2. Ni II—*Observed and calculated energy levels* $3d^84p + 3d^85p + 3d^74s4p$ *in units of* cm^{-1}—Continued

THEORETICAL ASSIGNMENT			J	OBS.	CALC.	O–C	CALC. g
MAIN COMPONENT		ADDITIONAL					
$3d^8(^1D)5p\ ^2D$	36%	12%$(^1D)^2P$	3/2	117763.91	117858	−94	1.165
	65%		5/2	117872.78	117995	−122	1.271
$3d^7(^2H)\,sp\,(^3P)^2I$			11/2	118248.98	118305	−56	.928
			13/2	119010.21	118992	18	1.085
$3d^8(^1D)5p\ ^2F$			5/2	118379.11	118389	−10	.979
			7/2	118563.39	118542	21	1.193
$3d^8(^1D)\,5p\ ^2P$	37%	35%$(^1D)^2D$	3/2	118442.81	118510	−67	1.158
	50%	29%$d^7\,sp\,^4D$	1/2	118631.95	118503	128	.606
$3d^7(^2P)\,sp\,(^3P)\,^2S$	36%	44%^2P	1/2		119423		1.438
$3d^7(^2H)\,sp\,(^3P)\,^4H$			13/2		119729		1.226
			11/2		120027		1.133
			9/2		120280		.976
			7/2		120498		.692
$3d^8\,(^3P)\,5p\ ^4P$	51%	19%$(^1D)^2D$	5/2	119796.98	119905	−108	1.518
	36%	17%$(^1D)^2P$	3/2	120166.52	120221	−54	1.534
			1/2	120316.02	120260	56	2.406
$3d^7\,(^2P)sp\,(^3P)\,^2P$	54%		1/2		119906		.679
	31%	36%d^85p^4P	3/2		119945		1.385
$3d^7\,(a^2D)sp\,(^3P)\,^4P$			5/2		120612		1.527
	44%	17%^2P	3/2		121766		1.535
			1/2		122378		2.393
$3d^8\,(^3P)\,5p\ ^4D$	81%		7/2	120903.31	121052	−149	1.387
	63%	27%$(^3P)^2D$	5/2	121325.09	121302	23	1.322
	54%		3/2	121385.80	121307	79	1.227
	83%		1/2	121561.06	121445	116	.064
$3d^8\,(^3P)5p\ ^2P$	35%	18%^2D + 17%^2S	3/2	121042.57	121091	−48	1.260
			1/2		121917		.751
$3d^8\,(^3P)5p\ ^2D$	57%	20%$(^3P)\,^4D$	5/2	121050.66	121007	44	1.216
	28%	32%$(^3P)^2P$	3/2	121800.34	121662	138	1.260
$3d^8\,(^3P)5p\ ^4S$	43%	23%$(^3P)^2D$	3/2	121456.30	121409	47	1.509
$3d^7\,(^2H)sp\,(^3P)\,^2G$			9/2	121692.55	121749	−56	1.108
			7/2	121862.57	121882	−19	.873
$3d^7\,(a^2D)sp\,(^3P)\,^2F$			5/2		121963		.914
			7/2		122670		1.150
$3d^8\,(^3P)5p\ ^2S$			1/2		122063		1.883
$3d^7\,(a^2D)sp\,(^3P)\,^2D$			3/2		122131		.930
			5/2		122277		1.204
$3d^7(a^2D)sp\,(^3P)\,^2P$			1/2		124474		.751
			3/2		124771		1.362
$3d^7\,(^2H)sp\,(^3P)\,^2H$			9/2	124652.00	124787	−135	.911
			11/2	125003.41	125159	−156	1.092
$3d^8\,(^1G)5p\ ^2F$			7/2	127219.57	126938	282	1.142
			5/2	127331.60	127071	261	.858
$3d^8\,(^1G)5p\ ^2H$			9/2	126679.98	126895	−215	.910
			11/2	126857.97	127061	−203	1.091

453-425 OL - 72 - 5

TABLE 2. Ni II—*Observed and calculated energy levels* $3d^84p + 3d^85p + 3d^74s4p$ *in units of* cm^{-1}—Continued

THEORETICAL ASSIGNMENT		J	OBS.	CALC.	O–C	CALC. g
MAIN COMPONENT	ADDITIONAL					
$3d^7(^4P)sp(^1P)\ ^3S$		3/2	126738.82	126903	−164	1.990
$3d^8(^1G)5p\ ^2G$		9/2	127885.86	127896	−10	1.110
		7/2	127895.33	127888	7	.890
$3d^7(^4P)sp(^1P)\ ^3D$		7/2	129782.07	129925	−143	1.427
		5/2	129988.05	130121	−133	1.366
		3/2	130331.78	130372	−40	1.200
		1/2	130570.42	130595	−25	.037
$3d^7(^2G)sp(^1P)\ ^2H$		11/2	131424.32	131131	293	1.086
		9/2	132311.98	132116	196	.915
$3d^7(^2F)sp(^3P)\ ^4G$		5/2		132462		.611
		7/2		132685		1.012
		9/2		133035		1.188
		11/2	133625.96	133567	59	1.272
$3d^7(^4P)sp(^1P)\ ^4P$		5/2	(131834.94)	132957	(−1122)	1.548
		3/2	(132225.15)	133323	(−1098)	1.681
		1/2	(132120.70)	133328	(−1208)	2.490
$3d^7(^2G)sp(^1P)\ ^2F$		7/2	133169.92	132917	253	1.138
		5/2	134208.30	134110	98	.994
$3d^7(^2F)sp(^3P)\ ^4F$		3/2	133190.19	132894	296	.425
		5/2	133209.30	133179	30	1.021
		7/2	133528.02	133541	−13	1.214
		9/2	133853.04	133898	−45	1.303
$3d^7(^2G)sp(^1P)\ ^2G$		9/2	133445.75	133676	−230	1.116
		7/2	134380.82	134783	−402	.891
$3d^7(^2F)sp(^3P)\ ^4D$		7/2	133850.83	133888	−37	1.417
		5/2	133973.33	133885	87	1.225
		3/2	134156.28	134113	43	1.198
		1/2	134283.76	134215	69	.047
$3d^7(^2F)sp(^3P)\ ^2D$		5/2	134783.14	134841	−58	1.205
		3/2	134964.78	135024	−59	.913
$3d^7(^2P)sp(^1P)\ ^2P$		1/2		135549		.776
		3/2	135382.53	135661	−278	1.169
$3d^7(^2F)sp(^3P)\ ^2G$		7/2	135746.06	135737	9	.894
		9/2	136076.26	135942	134	1.112
$3d^7(^2P)sp(^1P)\ ^2D$		5/2	(135258.92)	135900	(−741)	1.200
		3/2		137089		.826
$3d^7(^2H)sp(^1P)\ ^2I$		13/2		136509		1.077
		11/2		137494		.929
$3d^7(a^2D)sp(^1P)\ ^2D$		5/2		138244		1.154
		3/2		139402		.864
$3d^7(^2H)sp(^1P)\ ^2G$		9/2	138495.84	138613	−117	1.109
		7/2		139322		.906
$3d^7(^2F)sp(^3P)\ ^2F$		7/2		138858		1.138
		5/2		139447		.889
$3d^7(^2P)sp(^1P)\ ^2S$		1/2		139683		1.911
$3d^7(a^2D)sp(^1P)\ ^2F$		7/2		139904		1.140
		5/2		141012		.902
$3d^7(^2H)sp(^1P)\ ^4H$		11/2		141873		1.091
		9/2		142868		.913

TABLE 2. Ni II—*Observed and calculated energy levels* $3d^84p + 3d^85p + 3d^74s4p$ *in units of* cm^{-1}—Continued

THEORETICAL ASSIGNMENT		J	OBS.	CALC.	O–C	CALC. g
MAIN COMPONENT	ADDITIONAL					
$3d^7(a^2D)sp(^1P)\ ^2P$		3/2		142107		1.332
		1/2		143961		.738
$3d^7(b^2D)sp(^3P)\ ^4P$		5/2		151277		1.598
		3/2		151257		1.730
		1/2		151281		2.661
$3d^7(b^2D)sp(^3P)\ ^4F$		3/2		152576		.403
		5/2		152859		1.029
		7/2		153254		1.237
		9/2		153760		1.330
$3d^8(^1S)5p\ ^2P$		1/2		153513		.667
		3/2		154114		1.148
$3d^7(^2F)\ sp\ (^1P)\ ^2G$		7/2		154379		.890
		9/2		154810		1.114
$3d^7(^2F)\ sp\ (^1P)\ ^2D$		3/2		154619		.986
		5/2		154998		1.078
$3d^7(^2F)\ sp\ (^1P)\ ^2F$		5/2		155556		.979
		7/2		155892		1.143
$3d^7(b^2D)\ sp\ (^3P)\ ^2P$		3/2		156895		1.330
		1/2		157329		.623
$3d^7(b^2D)\ sp\ (^3P)\ ^2F$		5/2		157904		.869
		7/2		158157		1.166
$3d^7(b^2D)\ sp\ (^3P)\ ^4D$		1/2		158243		.048
		3/2		158398		1.200
		5/2		158717		1.359
		7/2		159298		1.405
$3d^7(b^2D)\ sp\ (^3P)\ ^2D$		5/2		161296		1.200
		3/2		161382		.803
$3d^7(b^2D)\ sp\ (^1P)\ ^2P$		1/2		173566		.667
		3/2		174048		1.332
$3d^7(b^2D)\ sp\ (^1P)\ ^2F$		5/2		174919		.858
		7/2		175397		1.142
$3d^7(b^2D)\ sp\ (^1P)\ ^2D$		3/2		179748		.800
		5/2		180530		1.199

of the $d-f$ interaction and for ζ_f was done by direct observation of the experimental level values. The final parameters which we obtained for these configurations are given in table 3. In column L.S.a, all the parameters were set free, and the rms error is 25.6 cm^{-1}. We can see that the parameters $F_4(df)$, $G_3(df)$ and ζ_f are equal to zero within their statistical accuracy. Column L.S.b of table 3 gives the results of a calculation in which the above-mentioned parameters were fixed at zero. In this case the rms error is 25.2 cm^{-1}. The observed and calculated levels of d^8f are given in table 4.

We would like to emphasize that the d^8f configuration was calculated independently without including any interaction with any other configuration. This simple treatment is justified to some extent by the small mean error.

In all, 60 experimental levels of d^8f were fitted to the calculated ones. Three observed levels could not be fitted. They are:

132729.48 cm^{-1} with $J = 5/2$,

135954.09 cm^{-1} with $J = 7/2$,

135580.25 cm^{-1} with $J = 9/2$.

TABLE 3. *Parameters of the Configuration* d^8f

All values are in units of cm^{-1}

P	Diag.	L.S.a	L.S.B
$A-3d^84f$	128190	128189. ±	128186 ±5
B	1035	1035.4±0.6	1035.5±0.6
C	4080	4086 ±6	4086 ±6
$F_2(df)$	8.5	8.4±0.5	8.3±0.4
$F_4(df)$	0	0.1±0.1	.....
$G_1(df)$	1	1.6±0.8	1.4±0.6
$G_3(df)$	0	0.3±0.3	.....
$G_5(df)$	0	0.03±0.05	.....
ζ_d	670	668 ±3	668 ±3
ζ_f	0	3 ±2	.....
Δ	.....	25.6 cm^{-1}	25.2 cm^{-1}

The coupling for this configuration is the $J-l$ coupling; that is: the S' and L' of the d^8 parent term first combine to form J''. Then J'' is combined with the $l=3$ of the f electron forming K and finally the spin of this electron is added to K and the total J is formed. This is the coupling used in table 4.

The authors wish to express their deep gratitude to Professor Shenstone for the special pleasure and benefit of his kind and useful cooperation.

TABLE 4. *Ni* II *—Observed and calculated energy levels* $3d^84f$

THEORETICAL ASSIGNMENT		J	OBS.	CALC.	O–C	CALC. g
d^8 PARENT	K					
$^3F_4$	7	13/2	118803.82	118837	−33	1.086
		15/2	118848.92	118837	12	1.200
	1	3/2	118809.34	118800	9	1.779
		1/2	118774.76	118805	−30	1.523
	2	5/2	118828.61	118833	−4	1.448
		3/2	118877.09	118853	24	1.143
	3	7/2	118874.11	118871	3	1.329
		5/2	118897.94	118900	−2	1.094
	6	11/2	118892.99	118909	−16	1.081
		13/2	118893.24	118909	−16	1.212
	4	9/2	118914.34	118905	9	1.269
		7/2	118923.20	118924	−1	1.082
	5	9/2	118927.02	118924	3	1.081
		11/2	118939.53	118924	16	1.234
$^3F_3$	0	1/2	120189.55	120170	20	2.043
	1	3/2	120199.18	120194	5	1.379
		1/2	120203.49	120181	22	.704
	2	5/2	120203.49	120222	−19	1.244
		3/2	120222.89	120224	−1	.861
	6	11/2	120211.30	120205	6	.970
		13/2	120218.22	120205	13	1.117
$^3F_3$	3	7/2	120250.17	120249	1	1.176
		5/2	120271.97	120265	7	.909
	4	7/2	120268.81	120281	−12	.938
		9/2	120281.11	120272	9	1.146
	5	11/2	120270.44	120265	5	1.124
		9/2	120272.53	120265	8	.949
$^3F_3$	1	3/2	121042.52	120092	−49	1.540
		1/2	121090.71	121092	−1	1.059
	5	11/2	121120.88	121122	−1	.976
		9/2	121125.41	121122	3	.771
	2	5/2	121146.98	121146	1	1.181
		3/2	121161.81	121147	15	.763

TABLE 4. *Ni* II—*Observed and calculated energy levels* $3d^8 4f$—Continued

THEORETICAL ASSIGNMENT		J	OBS.	CALC.	O–C	CALC. g
d^8 PARENT	K					
	4	7/2	121178.56	121192	−13	.762
		9/2	121180.54	121190	−9	1.008
	3	7/2	121192.32	121183	9	1.063
		5/2	121194.14	121188	6	.753
$^1D_2$	4	9/2	132818.16	132855	−37	1.138
		7/2	132846.53	132857	−10	.933
	3	5/2	(132729.48)	132875	(−146)	.878
		7/2	132869.16	132889	−20	1.148
$^1D_2$	2	5/2	132912.15	132944	−32	1.197
		3/2	132927.97	132940	−12	.793
	1	3/2	132982.51	133005	−23	1.283
		1/2	133001.47	133005	−4	.564
	5	11/2	133014.08	132950	64	1.119
		9/2	133031.00	132950	81	.943
$^3P_2$	3	7/2	135400.67	135438	−37	1.179
		5/2	135461.55	135452	10	.979
	4	9/2	135435.26	135414	21	1.283
		7/2	135444.47	135430	14	1.127
	2	3/2	135493.26	135485	8	.515
		5/2	135512.92	135501	12	.976
	5	11/2	135538.61	135582	−43	1.243
		9/2	135558.80	135582	−23	1.092
	1	3/2	135652.93	135661	−8	1.057
		1/2	135670.49	135659	11	.106
$^3P_1$	2	5/2		135784		1.255
		3/2	135746.13	135784	−38	.885
	4	9/2	(135580.35)	135773	(−193)	1.179
		7/2	(135464.86)	135776	(−311)	.976
	3	5/2	135849.41	135866	−17	.895
		7/2	135879.41	135864	15	1.174
$^3P_0$	3	7/2	(135954.09)	136055	(−101)	1.176
		5/2	136122.61	136056	67	.905
$^1G_4$	1	3/2		140232		1.334
		1/2		140233		.667
	2	5/2		140345		1.200
		3/2		140347		.800
	7	13/2		140355		.933
		15/2		140355		1.067
	3	7/2		140491		1.143
		5/2		140492		.857
	4	9/2		140632		1.111
		7/2		140632		.889
	6	11/2		140643		.923
		13/2		140643		1.077
	5	11/2		140708		1.091
		9/2		140708		.909
$^1S_0$	3	7/2		171363		1.143
		5/2		171364		.857

5. References

[1] Moore, C. E., Atomic Energy Levels, NBS Circ 467, II (1949).
[2] Steinberger, H., Msc. Thesis, The Hebrew University of Jerusalem, 1958.
[3] Shimoni, Z., Msc. Thesis, The Herbrew University of Jerusalem, 1959.
[4] Roth, C., J. Res. Nat. Bur. Stand. (U.S.), **73A** (Phys. and Chem.) No. 2, 129, (1969).
[5] Shenstone, A. G., J. Res. Nat. Bur. Stand. (U.S.), **74A** (Phys. and Chem.) No. 6, 801, (1970).
[6] Schwimmer, A., Msc. Thesis, The Hebrew University of Jerusalem (1967).
[7] Racah, G., and Shadmi, Y., Bull. Res. Counc. of Israel **8F**, 15 (1959).
[8] Shadmi, Y., and Caspi, E., Oreg J. Res., Nat. Bur. Stand. (U.S.), **73A** (Phys. and Chem.) No. 2, 173, 1969.
[9] Shadmi, Y., Phys. Rev. **139A**, 43 (1965).
[10] Shadmi, Y., Oreg, J., Stein, J., J.O.S.A. **58**, 7, 909–914 (1968).

(Paper 76A2–705)

JOURNAL OF RESEARCH of the National Bureau of Standards—A. Physics and Chemistry
Vol. 76A, No. 2, March–April 1972

The Characterization of Linear Polyethylene SRM 1475. I. Introduction.

C. A. J. Hoeve,* Herman L. Wagner, and Peter H. Verdier

Institute for Materials Research, National Bureau of Standards, Washington, D.C. 20234

(December 15, 1971)

The National Bureau of Standards has issued a linear polyethylene standard reference material, SRM 1475. In this report a general description of the sample is given, and the characterization work described in the subsequent reports is outlined. Some pellet-to-pellet variability was found and estimated.

Key words: Fractionation; linear polyethylene; molecular weight; molecular weight distribution; National Bureau of Standards; pellet variability; standard reference material.

1. Purpose

The National Bureau of Standards has issued a linear polyethylene standard reference material, SRM 1475,** to fill the need for a well-characterized sample of this polymer. The sample may be used for the calibration of instruments for measuring molecular weight and molecular weight distribution, such as light scattering photometers and gel permeation chromatographs. It should also be useful in other areas of polymer research such as dilute solution studies, polymer rheology, and polymer crystal physics.

2. Properties Measured

The characterization results which are described in the succeeding papers in this series [1][1] include a determination of:

(1) Weight average molecular weight by light scattering,
(2) molecular weight distribution by gel permeation chromatography and, from this distribution, weight average, number average, and Z average molecular weights,
(3) limiting viscosity number in 1-chloronaphthalene, 1,2,4-trichlorobenzene, and decalin,
(4) melt flow rate by a melt index type apparatus,
(5) density by ASTM procedures.

No attempt was made to determine number average molecular weight of this whole polymer by osmometry since diffusion of even small amounts of low molecular weight species through the membrane makes such a determination meaningless. However, by calibration of the gel permeation chromatograph with fractions that were well characterized by light scattering and osmometry, it was possible to determine number average molecular weight as well as weight average and molecular weight distribution. With these data, SRM 1475 may be used conveniently for the precise calibration of other gel permeation chromatographs.

In the papers which follow, the various techniques are described. More detail is given in those cases where there has been some deviation from the usual procedure. The certificate for SRM 1475 is reproduced at the end of this paper.

3. Sample Description

The sample of linear polyethylene chosen for SRM 1475, an ALATHON 7050, was kindly donated by the E. I. duPont Company, Wilmington, Delaware.* The material is in the form of pellets, each weighing about 20 mg. An antioxidant, tetrakis[methylene-3-(3′,5′-di-*t*-butyl-4′-hydroxyphenyl)propionate]methane, known commonly as Irganox 1010 (Geigy Chemical Company), was added to the polymer at a concentration of 111 ppm by the manufacturer. The linearity of the polymer is demonstrated, as shown in part II [1], by infrared analysis. Ash content, determined by ashing a 10-gram portion of the sample at 750 °C, was found to be 0.002 percent.

*Present address: Department of Chemistry, Texas A & M University, College Station, Texas 77843.

**Available through the Office of Standard Reference Materials, National Bureau of Standards, Washington, D.C. 20234.

[1] Figures in brackets indicate the literature references at the end of this paper.

*Certain commercial equipment, instruments, or materials are identified in this paper in order to adequately specify the experimental procedure. In no case does such identification imply recommendation or endorsement by the National Bureau of Standards, nor does it imply that the material or equipment identified is necessarily the best available for the purpose.

The determination of volatile components, or at least those components soluble in xylene, was made as follows. Three grams of polyethylene and 7 grams of xylene were sealed in one container and 7 grams of xylene was sealed in another as a control. These containers were heated at 140 °C until the contents dissolved. They were cooled to precipitate the polyethylene, opened, and samples of liquid from each were analyzed by gas chromatography.

It is estimated that any xylene-soluble volatiles that amounted to as much as $^1/_2$ percent of the polyethylene could be readily detected by this method. No evidence of such volatile material was found.

4. Sampling

The sample was received in forty 50-lb bags. To determine the conditions necessary for uniform sampling, polymer variability from pellet-to-pellet and bag-to-bag was determined. The bags were numbered at random from 1 to 40 and samples were taken from the top and bottom of each of bags 1 to 20. Several grams of each of these were mixed and samples drawn from this "pool" to make up blended samples for light scattering, limiting viscosity number, and gel permeation chromatography. These blends were made up of several hundred pellets dissolved in xylene at 140 °C and precipitated in ethanol at room temperature.

Pellet-to-pellet variability was determined by solution viscosity measurements [1d] in 1-chloronaphthalene at concentrations of from 0.06 to 0.12 g/dl at 130 °C on individual pellets and on samples of the blends. The viscosity number, $(\eta - \eta_0)/(\eta_0 c)$, in dl/g, where η is the viscosity of the solution, η_0 is the viscosity of the solvent, and c is the concentration in g/dl, is plotted against concentration in figure 1. The viscosity numbers obtained for the blended samples were fitted by least squares to a linear function of concentration, yielding the straight line shown in the figure. The standard deviation in viscosity number obtained from the least-squares analysis for the blended samples was 0.0034 dl/g (0.38%). The root-mean-square deviation from the straight line of the viscosity numbers obtained for solutions made up from individual pellets was found to be 0.028 dl/g (3.1%). Thus the standard deviation of a single measurement is 0.38 percent and the standard deviation due to pellet-to-pellet variation is

$$[(3.1)^2 - (0.38)^2]^{1/2} = 3.1\%.$$

Since the coefficient of variation is 3 percent, it is recommended that all determinations be performed on samples containing at least 50 pellets or one gram of polymer (or material from a blend of one gram). This will reduce the expectation of the standard error due to pellet variability to less than 0.5 percent.

Details of the method of measurement of melt flow rate and the results obtained are discussed elsewhere [1c]. These measurements were employed to investigate variations in material taken from different regions of the entire material. Forty-two samples for melt flow rate determination were taken from 13 different regions in seven of the bags. The standard deviation for samples within a region was found to be 2.1 percent, based on 29 degrees of freedom. The standard deviation between regions was found to be 1.7 percent, based on 12 degrees of freedom. We conclude that variations from region to region are too small to be detected by this method.

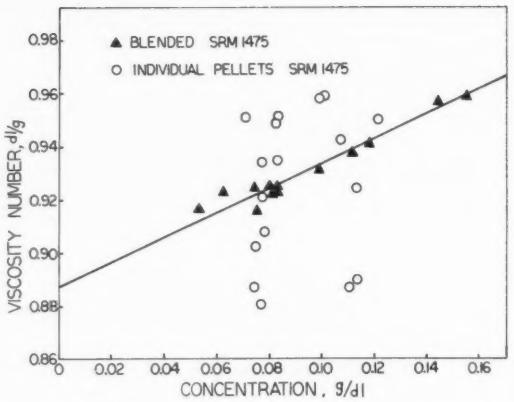

FIGURE 1. *The viscosity number of a blended sample and of individual pellets of SRM 1475 plotted against concentration.*

5. References

[1] The Characterization of Linear Polyethylene 1475:

(a) Brown, J. E., Paper II, Determination of Total Methyl Content by Infrared Spectrophotometry, J. Res. Nat. Bur. Stand. (U.S.), **76A** (Phys. and Chem.), No. 2, 141–142 (Mar.–Apr. 1972).

(b) Brown, J. E., Paper III, Density Determination, Ibid, **76A** (Phys. and Chem.), No. 2, 143–144 (Mar.–Apr. 1972).

(c) Maurey, J. R., Paper IV, Melt Flow Rate, Ibid, **76A** (Phys. and Chem.), No. 2, 145–146 (Mar.–Apr. 1972).

(d) Christensen, R. G., Paper V, Solution Viscosity Measurements, Ibid, **76A** (Phys. and Chem.), No. 2, 147–149 (Mar-Apr. 1972).

(e) Christensen, R. G., Paper VI, Preparation of Calibrating Fractions, Ibid, **76A** (Phys. and Chem.), No. 2, 149–150 (Mar.–Apr. 1972).

(f) Wagner, H. L., Paper VII, Differential Refractive Index of Polyethylene Solutions, Ibid, **76A** (Phys. and Chem.), No. 2, 151–155 (Mar.–Apr. 1972).

(g) Frolen, L. J., Ross, G. S., Wims, A. M., and Verdier, P. H., Paper VIII, Light Scattering Studies on Polyethylenes in 1-Chloronaphthalene, Ibid, **76A** (Phys. and Chem.), No. 2, 156–160 (Mar.–Apr. 1972).

(h) Brown, J. E., and Verdier, P. H., Paper IX, Number Average Molecular Weight of Fractions by Membrane Osmometry, Ibid, **76A** (Phys. and Chem.), No. 2, 161–163 (Mar.–Apr. 1972).

(i) Ross, G. S. and Frolen, L. J., Paper X, Gel Permeation Chromatography, Ibid, **76A** (Phys. and Chem.), No. 2, 163–170 (Mar.–Apr. 1972).

(Paper 76A2–706)

U. S. Department of Commerce
Maurice H. Stans
Secretary

National Bureau of Standards
L. M. Branscomb, Director

National Bureau of Standards Certificate

Standard Reference Material 1475

Linear Polyethylene

(Whole Polymer)

C. A. J. Hoeve, H. L. Wagner, J. E. Brown,
R. G. Christensen, L. J. Frolen, J. R. Maurey, G. S. Ross, and P. H. Verdier

This Standard Reference Material is intended for the calibration of instruments used in polymer science and technology for the determination of molecular weight and molecular weight distribution.

Quantity		Average Values	Estimated Standard Deviation of Average
Molecular Weight			
Weight-average molecular weight[a]		52,000	2,000
Number-average molecular weight	[b]	18,310	360
Weight-average molecular weight	[b]	53,070	620
Z-average molecular weight	[b]	138,000	3,700
Ratio of molecular weights $M_z:M_w:M_n$	[b]	7.54:2.90:1	
Molecular weight distribution	[b]	See Table 1	
Limiting Viscosity Number (dl/g)			
In 1-chloronaphthalene at 130 °C		0.890	0.0032
In 1,2,4-trichlorobenzene at 130 °C		1.010	.0086
In decahydronaphthalene[c] at 130 °C		1.180	.0032
Melt-Flow Rate (g/10 min)[d]		2.07	.0062
Density (g/cm^3)[e]		0.97844	.00004

[a] By light scattering in 1-chloronaphthalene at 135 °C.
[b] By gel-permeation chromatography.
[c] "Technical" grade, which assayed at approximately equal proportions of cis- and trans- decahydronaphthalenes.
[d] By a procedure similar to Procedure A, ASTM Method D1238-65T, Test Condition D, 190 °C, load 325 g.
[e] By ASTM Method D1505-67; sample prepared by Procedure A, ASTM Method D1928-68.

Measurements leading to the certification of this material were performed in the Molecular Properties and Characterization Section of the Polymer Division.

Washington, D.C. 20234
November 6, 1969
(Revised December 2, 1971)

J. Paul Cali, Chief
Office of Standard Reference Materials

(over)

The methyl group content as determined by ASTM Method D2238-68 is 0.15 methyl groups per 100 carbon atoms. This shows the polyethylene to be essentially linear. A pellet to pellet coefficient of variation of 3 percent in the limiting viscosity number was found. All determinations should consequently be performed on samples containing at least 50 pellets or one gram of polymer (or material from a blend of one gram). This will reduce the expectation of the standard error due to pellet variability to less than 0.5 percent.

Table 1. Cumulative Molecular Weight Distribution by Gel-Permeation Chromatography

log M	Wt. %	log M	Wt. %	log M	Wt. %
2.800	0.0	4.014	15.2	5.065	90.7
2.865	0.005	4.070	18.1	5.113	92.2
2.929	0.020	4.126	21.5	5.161	93.7
2.992	0.052	4.182	25.2	5.209	94.8
3.056	0.105	4.237	29.3	5.256	95.8
3.119	0.185	4.292	33.7	5.303	96.6
3.181	0.343	4.346	38.5	5.349	97.3
3.243	0.475	4.400	43.4	5.395	97.9
3.305	0.706	4.454	48.5	5.440	98.4
3.366	0.999	4.507	53.5	5.485	98.7
3.427	1.38	4.560	58.3	5.530	99.1
3.488	1.88	4.612	62.9	5.574	99.3
3.548	2.51	4.664	67.3	5.618	99.5
3.607	3.30	4.715	71.4	5.662	99.7
3.667	4.28	4.766	75.1	5.705	99.8
3.725	5.46	4.817	78.5	5.789	99.9
3.784	6.87	4.868	81.6	5.87	100.0
3.842	8.56	4.918	84.4		
3.900	10.50	4.967	86.7		
3.957	12.7	5.016	88.9		

The sample of linear polyethylene was obtained from E. I. du Pont de Nemours and Company of Wilmington, Delaware.

This sample of linear polyethylene has an ash content of 0.002 percent. No volatiles were detected by a gas-chromatographic procedure capable of detecting 0.5 percent volatiles. The manufacturer added 111 ppm of the antioxidant, Irganox 1010 (Geigy), which is tetrakis [methylene-3-(3′,5′-di-t-butyl-4′-hydroxyphenyl)propionate] methane.

The differential refractive index in 1-chloronaphthalene, required for the calculation of molecular weight by light scattering, was found to be −0.193 ml/g at 135 °C and 546 nm.

The maximum rate of shear in the Ubbelohde viscometer was about 1500 sec^{-1}. All measurements were carried out at specific viscosities (0.1 or less) which were sufficiently low for negligible dependence on rate of shear.

A series of reports describing investigations required for this certificate will be published in the Journal of Research of the National Bureau of Standards, Volume 76 A, No. 2, 1972.

The Characterization of Linear Polyethylene SRM 1475. II. Determination of Total Methyl Content by Infrared Spectrophotometry.

James E. Brown

Institute for Materials Research, National Bureau of Standards, Washington, D.C. 20234

(December 15, 1971)

An ASTM method was used to determine the methyl content of linear polyethylene SRM 1475 by measuring the absorbance at 1378 cm^{-1} (7.25 nm) of methyl groups on compensated infrared spectra. The methyl content of this polymer was found to be 0.15 methyls per 100 carbon atoms. Considering the methyls to be polymer end groups, the number average molecular weight computed approximates that determined by gel permeation chromatography within the experimental error. These values indicate that the polymer is essentially free of branching.

Key words: Infrared; linear polyethylene; methyl; methylene; number average molecular weight; spectra; spectrophotometry.

1. Introduction

The total methyl group content in polyethylene may be used to estimate the amount of branching in the polymer. If, for example, it is assumed that all chain-ends are methyl groups, then the methyl-group content of the polymer may be combined with its number-average molecular weight, M_n, to yield an estimate of the average number of chain ends per molecule.

In the characterization of SRM 1475, the total methyl content was determined to obtain an estimate of the polymer's linearity. Infrared spectrophotometry was used to determine the methyl content from the absorbance at about 1378 cm^{-1} due to methyl groups. This band is overlapped by bands at 1368 and 1352 cm^{-1}, and therefore cannot be used directly to estimate methyl group content. However, it has been shown [1–5][1] that both the latter two bands and another band at 1304 cm^{-1} arise from methylene-groups in the amorphous or disordered regions only, while the 1378 cm^{-1} band arises from methyl groups in both amorphous and crystalline regions. If we assume [5] that the spectrum of solid polyethylene is a superposition of contributions from amorphous and crystalline regions, then the spectrum arising from methyl groups alone may be obtained as a difference spectrum between two films of the same polymer, but different degrees of crystallinity and appropriately different thicknesses.

In this paper, we report the results for total methyl content in SRM 1475 by the method described in American Society for Testing and Materials (ASTM) Designation: D 2238–68, "Standard Method of Test for Absorbance of Polyethylene Due to Methyl Groups at 1378 cm^{-1}."[2] By this method, the absorbance is measured at the methyl frequency (1378 cm^{-1}) on films which are largely crystalline while compensating for the amorphous methylene absorbance with thinner, less crystalline films. Graphically, the absorbance resulting only from methyl groups is interpolated to the point of zero methylene absorbance at 1304 cm^{-1}. Each of the absorbances at 1378 and 1304 cm^{-1} is corrected for the effect produced by the difference in thickness and density of the crystalline and amorphous films. The resulting absorbance at 1378 cm^{-1} is then used to calculate the number of methyl groups per 100 carbon atoms. The conversion of absorbance to methyls per 100 carbon atoms is computed from the absorbance at 1378 cm^{-1} due to methyl groups in *n*-hexadecane (cetane).

2. Experimental Procedure

Films were prepared from SRM 1475 pellets taken from each container and blended as described in the first paper of this series [6]. In accordance with the ASTM procedure, several films ranging in thickness from 0.01 to 0.04 cm were molded in a hydraulic press heated to 168 °C. The molten polyethylene in the mold assembly was then quenched in an ice-water mixture. Films prepared in this manner are designated reference films. Four films about 0.05 cm thick were also molded from the SRM pellets by the above procedure except that these films were annealed so as to produce an increase in density of at least 0.02 g/cm^3 greater than the density of the quenched reference films. The annealed films will later be referred to as

[1] Figures in brackets indicate the literature references at the end of this paper.

[2] Available from American Society for Testing and Materials, 1916 Race Street, Philadelphia, Pennsylvania 19103.

samples I through IV. Difference spectra of each sample (high crystalline content) were obtained with three or four of the thinner reference films (low crystalline content). The spectra were recorded in the region from about 1430 to 1250 cm^{-1} using the prism optics of a double-beam, infrared spectrophotometer, (Perkin-Elmer Model 221).[3] From these spectra, which range from partial to over-compensation of the absorption due to amorphous methylene groups, the absorbance at the methyl frequency, A_{1378}, and that at the methylene frequency, A_{1304}, were determined as directed by the ASTM method.

3. Results and Discussion

Effective absorptivities, α, at 1378 and 1304 cm^{-1} were calculated from the difference spectrum of each sample-reference pair by the relation $\alpha = A/(d_s t_s - d_r t_r)$, where A is absorbance and d_s, t_s, d_r and t_r are sample density, sample thickness, reference density, and reference thickness, respectively. The resulting pairs, (α_{1304}, α_{1378}), were plotted as shown in figure 1, together with the straight line determined by a linear least squares fit. The value of α_{1378}, on the least squares line, corresponding to $\alpha_{1304} = 0$ is the absorbtivity in cm^2/g at 1378 cm^{-1} at which the methylene absorptivity at 1304 cm^{-1} is completely compensated. This quantity is designated K' in table 1. The number of methyl groups per 100 carbon atoms is also shown in table 1. The methyl concentration is computed from the product of K' and a calibration factor derived from measurements on cetane, as described in the ASTM procedure.

High density (linear) polyethylene chains may be presumed to be terminated with methyl groups as demonstrated by Willbourn [4] in a study of chain branching in polyethylene. If we assume two methyl groups per chain, then our estimate of 0.15 methyl groups per 100 carbon atoms leads to an estimate of 18,700 for the number-average molecular weight, M_n. This value closely approximates the M_n (18,310) from the gel permeation chromatography measurement as shown in Paper X of this series [7]. This correlation and the density [8] suggests that the polymer, SRM 1475, is essentially free of branching.

[3] Certain commercial equipment, instruments, or materials are identified in this paper in order to adequately specify the experimental procedure. In no case does such identification imply recommendation or endorsement by the National Bureau of Standards, nor does it imply that the material or equipment identified is necessarily the best available for the purpose.

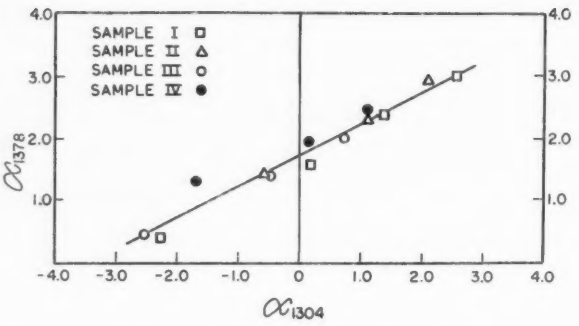

FIGURE 1. *Ordinate: Absorptivity, α_{1378}, cm^2/g; Abscissa: Absorptivity, α_{1304}, cm^2/g.*

The line shown in this graph represents a least squares fit of the absorptivity at 1378 cm^{-1} resulting from methyl groups against the absorptivity at 1304 cm^{-1} arising from amorphous methylene groups. The slope is equal to 0.51 ± 0.03 with the intercept at 1.74 ± 0.05 where the symbol $\pm$ stands for the standard deviation in these quantities inferred from the linear least-squares fit. The intercept represents the methyl absorption at perfect compensation for the methylene groups.

TABLE 1. *Results of methyl group determination from compensated spectra*

Absorptivity K', cm^2/g	Sample standard deviation of K'	CH_3 groups per 100 C atoms
1.74	0.053	0.15

K' in cm^2/g is the reduced absorptivity of methyl groups, at complete compensations for the absorption due to methylene groups determined for SRM 1475.

4. References

[1] Cross, L. H., Richard, R. B., and Willis, H. A., Discussions Faraday Soc., No. **9**, 235 (1950).
[2] Nielson, J. R. and Holland, R. F., J. Mol. Spectr. **4**, 488 (1960).
[3] Okada, T. and Mandelkern, L., J. Polymer Sci. A-2 **5**, 239 (1967).
[4] Willbourn, A. H., J. Polymer Sci. **34**, 569 (1959).
[5] Krimm, S., Liang, C. Y., and Sutherland, G. B. B. M., J. Chem. Phys. **25**, 549 (1956).
[6] Hoeve, C. A. J., Wagner, H. L., and Verdier, P. H., J. Res. Nat. Bur. Stand. (U.S.), **76A** (Phys. and Chem.), No. 2, 137–140 (Mar.–Apr. 1972). Paper I of this series.
[7] Ross, G. S. and Frolen, L. J., J. Res. Nat. Bur. Stand. (U.S.), **76A** (Phys. and Chem.), No. 2, 163–170 (Mar.–Apr. 1972). Paper X of this series.
[8] Brown, J. E., J. Res. Nat. Bur. Stand. (U.S.), **76A** (Phys. and Chem.), No. 2, 143–144 (Mar.–Apr. 1972). Paper III of this series.

(Paper 76A–707)

The Characterization of Linear Polyethylene SRM 1475. III. Density Determination

James E. Brown

Institute for Materials Research, National Bureau of Standards, Washington, D.C. 20234

(December 15, 1971)

The density of SRM 1475 at 23 °C was determined by ASTM method D 1505–67 on samples prepared by Procedure A of ASTM method D 1928–68, with the result 0.9784 g/cm³.

Key words: Crystallization; degree of crystallinity; density; linear polyethylene; polymer; recrystallization.

1. Introduction

The density of polyethylene crystallized from its melt is sensitive to a number of factors which influence the degree of crystallinity. Among these factors are: the polymer's previous thermal history and crystallization temperature which affect the perfection and rate of crystal growth [1–4],[1] the average molecular weight and its distribution [3], and the amount of branching [5–6].

In this paper we report the results of the density measurements on linear polyethylene SRM 1475. The density measurements and the sample preparation were performed using standard methods of the American Society for Testing and Materials (ASTM). It was necessary to specify closely the preparation of the samples used in this determination since the density of polyethylene depends to such an important extent on the polymer's previous history. From our experience, it should be possible to duplicate these results closely provided that the same methods are followed.

2. Experimental Procedure

Three composite samples, weighing about 100 g each, were made up separately as described in the first paper of this series [7] by blending equal amounts of the SRM 1475 pellets taken from the tops and bottoms of each of the original containers. These three composite samples will subsequently be referred to as blend I, II, and III.

Test samples (plaques) were prepared from blend I by Procedure A of ASTM Designation: D 1928–68, "Standard Method for Preparation of Compression-Molded Polyethylene Test Samples." [2] In accordance with this procedure, the pellets of blend I were made into a crepe on a roll mill. The polyethylene was milled for about four minutes at a temperature sufficiently high to cause the polymer to flux but not to drip. Pieces were cut from the cooled crepe and compression molded into 3 mm thick plaques at 178 °C using picture-frame-like chases.[3] The mold assembly containing the molten polyethylene was removed from the press and quenched to room temperature in a water bath. The mold assemblies containing the quenched plaques were then placed in a heated oven and maintained at 170 °C, well above the crystal melting point, for 1 h or more in order to destroy the polymer's previous thermal history. The temperature of the oven was then lowered to 50 °C at a rate of 5 °C/hr. After the plaques had come to room temperature, several specimens (2–3 mm on a side) were cut from each plaque for the density measurements.

As a check on the sensitivity of the ASTM procedure to variations in the preparative technique, plaques of blends II and III were prepared somewhat differently. Plaques of blend II were prepared as described above except that the milling time (about 2 minutes) was just long enough at about 125 °C to cause the pellets to fuse into a sheet. The plaques of blend III were not molded from a milled crepe. These plaques were compression-molded from the pellets. Except for the milling process, the test samples (plaques) of blend III were quenched, recrystallized, and cooled to room temperature by the same techniques described for blends I and II.

The density of the three blends was determined by the procedure given in ASTM Designation: D1505–67, "Standard Method of Test for Density of Plastics by the Density-Gradient Technique." [2] The density of each specimen taken from the recrystallized plaques was determined by graphical interpolation of its equilibrium height in the density-gradient liquid

[1] Figures in brackets indicate the literature references at the end of this paper.

[2] Available from the American Society for Testing and Materials, 1916 Race Street, Philadelphia, Pennsylvania 19103.

[3] Although paragraph 5.6 of the ASTM procedure calls for a preheating period of 5 min, we have employed a time of 15 s.

maintained at 23 ± 0.1 °C. Isopropanol and water were used as the density-gradient liquids. The column was calibrated by a series of glass beads whose density was known to within ±0.0001 g/cm³. The sensitivity of the column was found to be about 0.0002 g/cm³ per mm column height, and the position of beads and specimens could be read to about 1 mm.

3. Results and Discussion

The molding and recrystallization of the plaques and the density measurements were performed on several different days according to ASTM procedures for sample preparation and density measurement. No significant day-to-day variation was found in the results. It was concluded that the preparation and recrystallization of the samples were consistent from one experiment to the next to within the precision of the density determination. The average density of twelve specimens taken from five samples (plaques) of blend I was found to be 0.97844 g/cm³ with a sample standard deviation of a single determination of 0.00014 g/cm³. The sample standard deviation of the mean of the twelve determinations is therefore 0.00004 g/cm³. These values of the mean density and the sample standard deviation of the mean are reported on the certificate for SRM 1475. The range of the measurements was from 0.9784 to 0.9786 g/cm³.

The average of ten density measurements on blend II was found to be 0.97817 g/cm³ with a standard deviation of a single determination of 0.00010 g/cm³. The density measurements for blend III gave a result of 0.97493 g/cm³ with a standard deviation of a single measurement of 0.00045 g/cm³, based on 21 measurements. These results are summarized in table 1. From the sample standard deviations and the systematic uncertainties associated with the calibrating beads, we conclude that the overall accuracy of our measurements is well within the 0.05 percent limit cited in the ASTM procedure.

TABLE 1. *Density at 23 °C of Linear Polyethylene SRM 1475*

	Blend I	Blend II	Blend III
Average density, g/cm³	*0.97844	0.97817	0.97493
Standard deviation of a single measurement	0.00014	0.00010	0.00045
Number of measurements	12	10	21

* Certificate value.

The samples of blend I were prepared from pellets of polyethylene which had been fluxed and milled twice as long (about 4 minutes) as blend II. The samples of blend III were molded from the polyethylene pellets.

Although the 0.03 percent difference between the densities of blends I and II is statistically significant, for practical purposes this difference is unimportant in view of the 0.05 percent estimate of accuracy given in the ASTM procedure. On the other hand, the density of blend III (unmilled samples) is materially lower than that of blends I and II, and its standard deviation of a single measurement is much larger than those of blends I and II. These differences cannot be ascribed to differences in the crystallinity of the samples, for the parts of the procedure which might be expected to affect crystallinity (molding, quenching, recrystallization) were identical for all three blends. Nor can the differences be attributed to the lack of mixing of the individual pellets during the preparation of blend III, since pellet-to-pellet variation would be expected to yield a larger sample standard deviation for blend III than for blends I and II, but the same mean density. The most likely explanation of both the lower mean density of blend III and its larger sample standard deviation seems to be the presence of small voids resulting from the lack of milling and fluxing. This explanation is reinforced by the fact that specimens taken from plaques of blend III, even though carefully selected, appeared to contain small regions of entrapped air.

We conclude that the preparatory milling and fluxing stipulated in the ASTM procedure is essential if the stated precision of the procedure is to be realized.

4. References

[1] Mandelkern, L., in Growth and Perfection of Crystals, Ed. R. H. Doremus, B. W. Roberts, and D. Turnbull, p. 467 (John Wiley and Sons, Inc., New York, N.Y., 1958).
[2] Mandelkern, L., Posner, A. S., Diorio, A. F., and Roberts, D. E., J. Appl. Phys. **32**, 1509 (1961).
[3] Chiang, R. and Flory, P., J. Am. Chem. Soc. **83**, 2857 (1961).
[4] Weeks, J. J., Jr., J. Res. Nat. Bur. Stand. (U.S.), **67A** (Phys. and Chem.), No. 5, 441–451 (Sept.–Oct. 1963).
[5] Stella, C., Compt. Rend. **248**, 1819 (1959).
[6] Sperati, C. A., Franta, W. G., and Starkweather, H. W., Jr., J. Am. Chem. Soc. **75**, 6157 (1953).
[7] Hoeve, C. A. J., Wagner, H. L., and Verdier, P. H., J. Res. Nat. Bur. Stand. (U.S.), **76A** (Phys. and Chem.), No. 2, 137–140 (Mar.–Apr. 1972). Paper I of this series.

(Paper 76A2–708)

The Characterization of Linear Polyethylene SRM 1475. IV. Melt Flow Rate.

John R. Maurey

Institute for Materials Research, National Bureau of Standards, Washington, D.C. 20234

(December 15, 1971)

The melt flow rate of SRM 1475 was determined to be 2.07 g/10 min at 190 °C under a load of 325 g by a method similar to procedure A of ASTM method D 1238–65T. This value is the average of determinations on 42 samples with a standard deviation of a single measurement of 0.040 g/10 min, and a range of 1.991 g/10 min to 2.132 g/10 min.

Key words: Extrusion plastometer; load; melt flow rate; orifice; orifice die; preliminary extrudate; test extrudate.

1. Introduction

Melt flow rate is widely used in polymer technology as a product specification since this value, which includes a statement of the load and temperature under which it is obtained, gives an indication of the processing properties of the polymer. The value of melt flow rate is expressed as the mass of polymer melt pushed from the heated cylinder of the extrusion plastometer through its precision bore orifice by its piston in a period of time, the standard units of the value being grams per ten minutes (g/10 min).

In this paper, we report the determination of melt flow rate for linear polyethylene SRM 1475. Use of the same measurements to investigate the uniformity of the material is described elsewhere [1].[1]

2. Experimental Procedure

2.1. Instrument and Method

The melt flow rate determinations were made with a commercial extrusion plastometer,[2,3] by a method similar to Procedure A described in "Tentative Method of Measuring Flow Rates of Thermoplastics by Extrusion Plastometer," ASTM Designation: D 1238–65T.[4]

The dimensions of the plastometer cylinder, piston assembly and orifice, and the combined masses of the piston and passenger weight were found to comply with the instrument specifications described by the ASTM method.

In compliance with the ASTM method, the temperature indicator of the extrusion plastometer was calibrated with respect to a standardized iron-constantan thermocouple mounted in an undisturbed column of polymer melt in the plastometer cylinder. The thermocouple junction was fixed at the axis of the cylinder, 12.7 mm above the top surface of the orifice die in the bottom of the cylinder. An equilibrium temperature reading of 189.9 °C was observed on the mercury column thermometer in the cylinder while the thermocouple indicated the equilibrium temperature of the polyethylene melt to be 190.0 °C at the prescribed calibration point. Thus, prior to each series of flow rate determinations, the cylinder of the extrusion plastometer was brought to thermal equilibrium with a constant reading of 189.9 °C on the mercury column thermometer.

Further study of the temperature at other distances up to 48 mm above the orifice, under conditions required by the calibration procedure, indicated that the temperature was uniform above the 12.7 mm height in the undisturbed melt column. However, the temperature of the melt 1 mm above the orifice was 0.7 deg lower than the temperature of the melt 12.7 mm above the orifice. This thermal gradient at the bottom of the undisturbed melt column is probably at least partially erased in an actual flow rate determination by the downward flow of the piston-driven melt through the orifice.

A separate study of the effect of temperature indicated that the flow rate of SRM 1475 was not significantly altered by a temperature change of 1 deg from the specified test temperature, 190 °C.

The orifice die was found to have a bore diameter of 2.096 mm, well within the ASTM specification tolerance limits. Bore diameter tolerance gauges were used to test the bore of the orifice die frequently between series of flow rate determinations. According to this test, no detectable change occurred in

[1] Figures in brackets indicate the literature references at the end of this paper.

[2] Certain commercial equipment, instruments, or materials are identified in this paper in order to adequately specify the experimental procedure. In no case does such identification imply recommendation or endorsement by the National Bureau of Standards, nor does it imply that the material or equipment identified is necessarily the best available for the purpose.

[3] Model 3, Tinius Olsen Testing Machine Company, Willow Grove, Pennsylvania 19090.

[4] Available from the American Society for Testing and Materials, 1916 Race Street, Philadelphia, Pennsylvania 19103.

maintained at 23 ± 0.1 °C. Isopropanol and water were used as the density-gradient liquids. The column was calibrated by a series of glass beads whose density was known to within ± 0.0001 g/cm³. The sensitivity of the column was found to be about 0.0002 g/cm³ per mm column height, and the position of beads and specimens could be read to about 1 mm.

3. Results and Discussion

The molding and recrystallization of the plaques and the density measurements were performed on several different days according to ASTM procedures for sample preparation and density measurement. No significant day-to-day variation was found in the results. It was concluded that the preparation and recrystallization of the samples were consistent from one experiment to the next to within the precision of the density determination. The average density of twelve specimens taken from five samples (plaques) of blend I was found to be 0.97844 g/cm³ with a sample standard deviation of a single determination of 0.00014 g/cm³. The sample standard deviation of the mean of the twelve determinations is therefore 0.00004 g/cm³. These values of the mean density and the sample standard deviation of the mean are reported on the certificate for SRM 1475. The range of the measurements was from 0.9784 to 0.9786 g/cm³.

The average of ten density measurements on blend II was found to be 0.97817 g/cm³ with a standard deviation of a single determination of 0.00010 g/cm³. The density measurements for blend III gave a result of 0.97493 g/cm³ with a standard deviation of a single measurement of 0.00045 g/cm³, based on 21 measurements. These results are summarized in table 1. From the sample standard deviations and the systematic uncertainties associated with the calibrating beads, we conclude that the overall accuracy of our measurements is well within the 0.05 percent limit cited in the ASTM procedure.

Table 1. *Density at 23 °C of Linear Polyethylene SRM 1475*

	Blend I	Blend II	Blend III
Average density, g/cm³	*0.97844	0.97817	0.97493
Standard deviation of a single measurement	0.00014	0.00010	0.00045
Number of measurements	12	10	21

* Certificate value.

The samples of blend I were prepared from pellets of polyethylene which had been fluxed and milled twice as long (about 4 minutes) as blend II. The samples of blend III were molded from the polyethylene pellets.

Although the 0.03 percent difference between the densities of blends I and II is statistically significant, for practical purposes this difference is unimportant in view of the 0.05 percent estimate of accuracy given in the ASTM procedure. On the other hand, the density of blend III (unmilled samples) is materially lower than that of blends I and II, and its standard deviation of a single measurement is much larger than those of blends I and II. These differences cannot be ascribed to differences in the crystallinity of the samples, for the parts of the procedure which might be expected to affect crystallinity (molding, quenching, recrystallization) were identical for all three blends. Nor can the differences be attributed to the lack of mixing of the individual pellets during the preparation of blend III, since pellet-to-pellet variation would be expected to yield a larger sample standard deviation for blend III than for blends I and II, but the same mean density. The most likely explanation of both the lower mean density of blend III and its larger sample standard deviation seems to be the presence of small voids resulting from the lack of milling and fluxing. This explanation is reinforced by the fact that specimens taken from plaques of blend III, even though carefully selected, appeared to contain small regions of entrapped air.

We conclude that the preparatory milling and fluxing stipulated in the ASTM procedure is essential if the stated precision of the procedure is to be realized.

4. References

[1] Mandelkern, L., in Growth and Perfection of Crystals, Ed. R. H. Doremus, B. W. Roberts, and D. Turnbull, p. 467 (John Wiley and Sons, Inc., New York, N.Y., 1958).
[2] Mandelkern, L., Posner, A. S., Diorio, A. F., and Roberts, D. E., J. Appl. Phys. **32**, 1509 (1961).
[3] Chiang, R. and Flory, P., J. Am. Chem. Soc. **83**, 2857 (1961).
[4] Weeks, J. J., Jr., J. Res. Nat. Bur. Stand. (U.S.), **67A** (Phys. and Chem.), No. 5, 441–451 (Sept.–Oct. 1963).
[5] Stella, C., Compt. Rend. **248**, 1819 (1959).
[6] Sperati, C. A., Franta, W. G., and Starkweather, H. W., Jr., J. Am. Chem. Soc. **75**, 6157 (1953).
[7] Hoeve, C. A. J., Wagner, H. L., and Verdier, P. H., J. Res. Nat. Bur. Stand. (U.S.), **76A** (Phys. and Chem.), No. 2, 137–140 (Mar.–Apr. 1972). Paper I of this series.

(Paper 76A2–708)

The Characterization of Linear Polyethylene SRM 1475. IV. Melt Flow Rate.

John R. Maurey

Institute for Materials Research, National Bureau of Standards, Washington, D.C. 20234

(December 15, 1971)

The melt flow rate of SRM 1475 was determined to be 2.07 g/10 min at 190 °C under a load of 325 g by a method similar to procedure A of ASTM method D 1238–65T. This value is the average of determinations on 42 samples with a standard deviation of a single measurement of 0.040 g/10 min, and a range of 1.991 g/10 min to 2.132 g/10 min.

Key words: Extrusion plastometer; load; melt flow rate; orifice; orifice die; preliminary extrudate; test extrudate.

1. Introduction

Melt flow rate is widely used in polymer technology as a product specification since this value, which includes a statement of the load and temperature under which it is obtained, gives an indication of the processing properties of the polymer. The value of melt flow rate is expressed as the mass of polymer melt pushed from the heated cylinder of the extrusion plastometer through its precision bore orifice by its piston in a period of time, the standard units of the value being grams per ten minutes (g/10 min).

In this paper, we report the determination of melt flow rate for linear polyethylene SRM 1475. Use of the same measurements to investigate the uniformity of the material is described elsewhere [1].[1]

2. Experimental Procedure

2.1. Instrument and Method

The melt flow rate determinations were made with a commercial extrusion plastometer,[2,3] by a method similar to Procedure A described in "Tentative Method of Measuring Flow Rates of Thermoplastics by Extrusion Plastometer," ASTM Designation: D 1238–65T.[4]

The dimensions of the plastometer cylinder, piston assembly and orifice, and the combined masses of the piston and passenger weight were found to comply with the instrument specifications described by the ASTM method.

In compliance with the ASTM method, the temperature indicator of the extrusion plastometer was calibrated with respect to a standardized iron-constantan thermocouple mounted in an undisturbed column of polymer melt in the plastometer cylinder. The thermocouple junction was fixed at the axis of the cylinder, 12.7 mm above the top surface of the orifice die in the bottom of the cylinder. An equilibrium temperature reading of 189.9 °C was observed on the mercury column thermometer in the cylinder while the thermocouple indicated the equilibrium temperature of the polyethylene melt to be 190.0 °C at the prescribed calibration point. Thus, prior to each series of flow rate determinations, the cylinder of the extrusion plastometer was brought to thermal equilibrium with a constant reading of 189.9 °C on the mercury column thermometer.

Further study of the temperature at other distances up to 48 mm above the orifice, under conditions required by the calibration procedure, indicated that the temperature was uniform above the 12.7 mm height in the undisturbed melt column. However, the temperature of the melt 1 mm above the orifice was 0.7 deg lower than the temperature of the melt 12.7 mm above the orifice. This thermal gradient at the bottom of the undisturbed melt column is probably at least partially erased in an actual flow rate determination by the downward flow of the piston-driven melt through the orifice.

A separate study of the effect of temperature indicated that the flow rate of SRM 1475 was not significantly altered by a temperature change of 1 deg from the specified test temperature, 190 °C.

The orifice die was found to have a bore diameter of 2.096 mm, well within the ASTM specification tolerance limits. Bore diameter tolerance gauges were used to test the bore of the orifice die frequently between series of flow rate determinations. According to this test, no detectable change occurred in

[1] Figures in brackets indicate the literature references at the end of this paper.

[2] Certain commercial equipment, instruments, or materials are identified in this paper in order to adequately specify the experimental procedure. In no case does such identification imply recommendation or endorsement by the National Bureau of Standards, nor does it imply that the material or equipment identified is necessarily the best available for the purpose.

[3] Model 3, Tinius Olsen Testing Machine Company, Willow Grove, Pennsylvania 19090.

[4] Available from the American Society for Testing and Materials, 1916 Race Street, Philadelphia, Pennsylvania 19103.

the bore diameter during the entire course of the flow rate study.

2.2. Procedure

Because of the relatively high fluidity of the melt of the linear polyethylene, the light load of conditions D of the ASTM method was chosen for the flow rate determination. Conditions D of the ASTM method specify the temperature of the melt to be 190 °C, and the load (combined apparent masses of piston assembly and passenger weight) to be 325 grams.

In accordance with the ASTM procedure, each sample was first preheated in the plastometer for 6 minutes, and the preliminary extrudate cut from the bottom of the orifice. Test segments were then cut from the extrudate at 1 minute intervals for 11 minutes, and were examined for bubbles as they emerged from the plastometer. The ASTM procedure calls for the use of bubble-free samples obtained during the first 3 minutes. We found, however, that it was virtually impossible to obtain bubble-free samples of SRM 1475 within 3 minutes. Attempts were therefore made, as suggested in the ASTM procedure, to eliminate the bubbles by manually forcing out some of the melt during the preheat period. These attempts were unsuccessful and this modification was therefore not employed. Among the first five segments collected, however, at least two were completely free of bubbles, and generally one or two additional segments contained only bubbles so few and small that their individual flow rate values were not distinguishable from the values for the completely bubble-free segments. The extrudate from the fourth through the eleventh 1 min intervals contained no bubbles. In order to obtain measurements on bubble-free materials while staying as close as possible to the conditions specified by the ASTM procedure, we therefore determined flow rate for the certificate from the bubble-free segments obtained during the first 5 min. In order to investigate the effect of exceeding the prescribed time of 3 min, we also determined the flow rate from all the bubble-free segments obtained during the entire 11 min interval. The results obtained are described in the following section.

It was found unnecessary to apply the severe orifice-cleaning techniques, described in the ASTM method, between flow rate determinations of this particular polyethylene. It was found satisfactory to ram out the residual polyethylene with a soft copper wire of diameter nearly as large as that of the orifice bore, while the die was still hot. No effect on the flow rate values could by detected when this technique was applied between determinations.

3. Results and Discussion

Flow-rate measurements were obtained on a total of 42 samples, taken from thirteen different regions of the total supply of SRM 1475. As described elsewhere [1], no variation could be found from region to region. The results for the 42 samples were therefore pooled. The mean flow rate, based on segments obtained during the first 5 min as described in the preceding section, was found to be 2.07 g/10 min, with a sample standard deviation of 0.040 g/10 min, a range of 1.991 to 2.132 g/10 min, and a sample standard deviation of the mean of 0.0062 g/10 min. The mean value and the sample standard deviation of the mean are the values reported on the certificate for SRM 1475.

Measurements on segments collected during the entire 11 min period, well beyond the 3 min limit specified in the ASTM procedure, yielded a mean flow rate of 2.06 g/10 min, with a sample standard deviation of 0.038 g/10 min and a range of 1.987 to 2.142 g/10 min. The close agreement between the two calculations in mean value, standard deviation, and range suggests that either a longer preheat period or a longer measurement period could be used for this material without affecting the observed flow rate.

4. References

[1] Hoeve, C. A. J., Wagner, H. L., and Verdier, P. H., J. Res. Nat. Bur. Stand. (U.S.), NBS **76A**, (Phys. and Chem.), No. 2, 137–140 (Mar.–Apr. 1972). Paper I of this series.

(Paper 76A2–709)

The Characterization of Linear Polyethylene SRM 1475. V. Solution Viscosity Measurements

Richard G. Christensen

Institute for Materials Research, National Bureau of Standards, Washington, D.C. 20234

(December 15, 1971)

The limiting viscosity numbers of linear polyethylene SRM 1475 were determined at 130 °C in 1,2,4-trichlorobenzene, 1-chloronaphthalene, and decalin. Technique, including use of a novel solution transfer method, is described.

Key words: 1-chloronaphthalene; decalin; linear polythylene; limiting viscosity number; solution viscosity; 1,2,4-trichlorobenzene; viscometer.

1. Viscosity Measurements

Limiting viscosity number is a readily measured physical property which can be related empirically to molecular weight. A number of empirical relationships between limiting viscosity number and molecular weight of polyethylenes have been published [1–6].[1]

The limiting viscosity number $[\eta]$ is defined as the limit as the concentration c approaches zero of the viscosity number, $(\eta_s - \eta_0)/(\eta_0 c)$, where η_s and η_0 are the viscosities of the solution and solvent, respectively, in the limit of zero shear rate. Thus, $[\eta]$ may be determined by measuring the viscosity number over a range of finite concentrations and extrapolating to zero concentration, provided the solution and solvent viscosities are independent of shear rate.

The limiting viscosity number of SRM 1475, described in Part I of this series [7], has been determined in several solvents so that data can be compared with that already published, and also so that the sample can serve as a basis for interlaboratory comparison of technique.

Viscosity measurements were made in a Ubbelohde viscometer fitted with a removable sintered glass filter in the neck through which the viscometer is filled. Such a viscometer is described in ASTM D 1601–61.[2] Solutions were made up by weight in 25 cm^3 flasks. The solvents used and their densities at 130 °C were: 1-chloronaphthalene, 1.098 g/cm^3; 1,2,4-trichlorobenzene, 1.323 cm^3; and decalin, 0.801 g/cm^3. The polymer was weighed on an electric microbalance. Dissolution of the polymer was accomplished by heating at 140 °C with occasional vigorous agitation by magnetic stirrer. Usually an hour of heating and stirring sufficed.

The 1-chloronaphthalene was carefully purified and appeared to be about 99.5 percent pure by gas chromatographic analysis. The 1,2,4-trichlorobenzene was technical grade and appeared to be about 98.5 percent pure by gas chromatographic analysis. The decalin used was technical grade which had been subjected to a simple vacuum distillation to remove gross impurities. An assay showed approximately equal proportions of *cis*- and *trans*-decahydronaphthalenes.

All solvents used contained 0.1 percent 2,6-*di*-*tert*-butyl-4-methylphenol (Ionol) as an antioxidant, and the automatic viscometer used kept the solutions under nitrogen during measurement. It is believed that degradation of the polymer was negligible under these conditions, since little change in the flow times occured even when the solutions were left in the viscometer as long as overnight. Also, dilutions were not made, but rather a separate solution was used for each concentration. Under conditions such as long heating to dissolve high molecular weight fractions, significant degradation can occur. This is usually evinced by much larger scattering of points in the plot for the extrapolation to limiting viscosity number, since the extent of degradation is likely to vary from sample to sample.

The solutions were transferred into the viscometer by a wash-bottle-like siphon (see fig. 1) which was found to be more convenient than a heated pipette. Due to the low thermal mass of the fine glass tubing, it was found unnecessary to preheat the siphon. The viscometer was rinsed twice with about 4 cm^3 of the solution, then about 10 cm^3 was siphoned in for the flow time measurement. An automatic viscometer timer (Hewlett-Packard Model 5901B Autoviscometer[3]) was used to operate the viscometer and measure the flow times, while the viscometer was thermostatted in a Hewlett-Packard 5901A Constant Temperature Bath.[3]

[1] Figures in brackets indicate the literature references at the end of this paper.

[2] Available from the American Society for Testing and Materials, 1916 Race Street, Philadelphia, Pennsylvania 19103.

[3] Certain commercial equipment, instruments, or materials are identified in this paper in order to adequately specify the experimental procedure. In no case does such identification imply recommendation or endorsement by the National Bureau of Standards, nor does it imply that the material or equipment identified is necessarily the best available for the purpose.

453-425 OL - 72 - 6

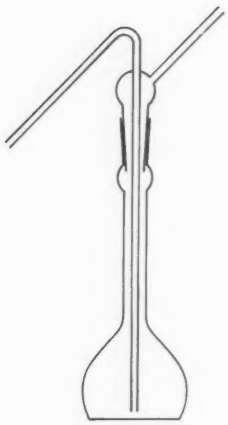

FIGURE 1. *Solution transfer siphon.*

Advantages of an automatic viscometer timer are that the same amount of liquid is automatically drawn up to each time and that the flow time is measured to 0.001 seconds. The former contributes to the uniformity of the measurement, the latter makes possible the use of very dilute solutions, which greatly facilitates reliable extrapolations to zero concentration. A third advantage is that the cleanliness of the viscometer can be judged by the reproducibility of the flow times. Ordinarily, flow times will fall in a range of 0.03 seconds or less. In the presence of lint or dust the flow time will drift or will be randomly erratic with a range of up to 0.2 seconds.

Kinetic energy corrections were made in all cases [8]. These amounted to about 1.2 percent for 1,2,4-trichlorobenzene solutions, and about 0.3 percent for the decalin and 1-chloronaphthalene solutions. The rate of shear in the Ubbelohde viscometer used was about 1000–1500 seconds^{-1}. Measurements on a higher molecular-weight linear polyethylene fraction (M_n=355,300, M_w=688,000) at shear rates from 20 to 1500 s^{-1} reveal no dependence of measured viscosity number on shear rate. We therefore assume that the measured viscosity numbers of SRM 1475 exhibit no shear-rate dependence in this region.

Since the flow time (corrected to allow for kinetic energy of the effluent from the capillary) in a Ubbelohde viscometer is proportional to solution viscosity, the viscosity number can be written $(t_s-t_0)/(t_0c)$, where c is concentration and t_s and t_0 are flow times for solution and solvent respectively. The standard deviation in the viscosity number of aliquots of the same solution was found to be slightly less than 0.3 percent. The viscosity numbers were fitted by least squares to linear functions of concentration; the limiting viscosity numbers were obtained as the resulting constant terms. The results are given in table 1. The viscosity numbers are plotted against concentration in figure 2, which also shows the straight lines obtained from the least-squares analysis.

Considerable care must be exercised in making viscosity measurements when decalin is used as the solvent. Errors can easily arise due to the widely differing properties of the *cis*- and *trans*-isomers of decahydronaphthalene. The *cis*-isomer has a boiling point about 10 °C higher, a density about 3 percent greater, and a viscosity about 20 percent higher than the *trans*-isomer. If the solutions are made up by weight, density must be measured for each batch of solvent. Since the isomers differ in volatility, condensation in the upper part of the viscometer can change the isomeric composition in the solution. The resulting error in flow time can cause errors of 5 percent or more in the viscosity number. These errors were minimized in he present work by repeatedly equilibrating the viscometer with fresh portions of solvent. After reproducible solvent flow times were obtained, the flow times of the solutions were measured. We believe that by the use of these techniques, the errors due to the variable composition of decalin have been reduced to less than 1 percent.

TABLE 1.

Solvent	Limiting viscosity number, dl/g	Slope of viscosity number versus concentration, (dl/g)^2
1-chloronaphthalene	[a] 0.890 ± 0.0032	0.48
1,2,4-trichlorobenzene	1.010 ± .0086	.55
decahydronaphthalene[b]	1.180 ± .0032	.72

[a] Uncertainties quoted are estimated standard deviations obtained from linear least squares fits of viscosity number versus concentration.

[b] Technical grade, which assayed at approximately equal proportions of *cis*- and *trans*-decahydronaphthalenes.

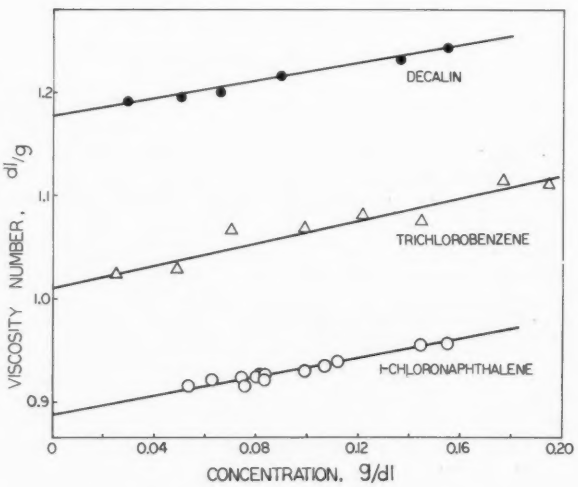

FIGURE 2. *Limiting viscosity numbers of SRM 1475.*

2. References

[1] Wesslau, H., Makromol. Chem. **20**, 111 (1956).
[2] Francis, P., Cooke, R., Jr., and Elliott, J., J. Polymer Sci. **31**, 453 (1958).
[3] Kotera, A., et al., Rept. Progr. Polymer Phys. Japan **3**, 58 (1960).
[4] Chiang, R., J. Polymer Sci. **36**, 91 (1959).
[5] Tung, L., J. Polymer Sci. **36**, 287 (1959).
[6] de la Cuesta, M., and Billmeyer, F. Jr., J. Polymer Sci. A **1**, 1721 (1963).
[7] Hoeve, C. A. J., Wagner, H. L., and Verdier, P. H., J. Res. Nat. Bur. Stand. (U.S.), **76A** (Phys. and Chem.), No. 2, 137–140 (Mar.–Apr. 1972). Paper I of this series.
[8] Allen, P. W., Techniques of Polymer Characterization, p. 180 (Butterworths, London, 1959).

(Paper 76A2–710)

The Characterization of Linear Polyethylene SRM 1475. VI. Preparation of Calibrating Fractions

Richard G. Christensen

Institute for Materials Research, National Bureau of Standards, Washington, D.C. 20234

(December 15, 1971)

Fractions for use in calibrating a gel permeation chromatograph were prepared by a Desreux column extraction method. The construction and operation of the fractionating system are described.

Key words: Column extraction fractionation; fractionation; linear polyethylene.

1. Introduction

In the process of determining the molecular weight distribution of SRM 1475 [1][1] it was necessary to calibrate a gel permeation chromatograph [2] with linear polyethylene. Fractions of linear polyethylene were used for this purpose. The fractions were subsequently used to establish relations between limiting viscosity number (intrinsic viscosity) and molecular weight [3]. The requisite fractions were prepared by a column extraction [4] technique, using a solvent system which has been described in considerable detail by Chiang [5] and others.

2. Experimental Procedure

The fractionation apparatus was constructed as depicted in figure 1. The column temperature is maintained by surrounding it with a narrow, deep oil bath, $20 \times 20 \times 90$ cm. The stirrer and heater are placed inside a long tube to promote efficient thermal exchange between the top and bottom of the tank.

The solvent inlet to the column is a small concentric tube reaching to the bottom of the packed column. The efflux collects above the column packing and is periodically drawn off through a slightly larger tube concentric with the inlet tube. The liquid is forced out by nitrogen pressure. The 8 cm diameter column is packed

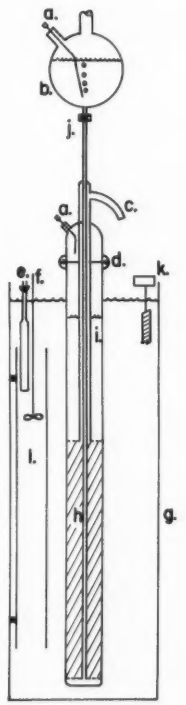

FIGURE 1. *Section of fractionation apparatus.*

(a) nitrogen inlets; (b) preheating flask; (c) efflux siphon; (d) o-ring flange; (e) heater; (f) stirrer; (g) tank; (h) packed column; (i) effluent liquid; (j) inlet tube; (k) thermoregulator; (l) circulating tube.

[1] Figures in brackets indicate the literature references at the end of this paper.

with Johns-Manville Celite No. 545[2] to a depth of about 55 cm. The free liquid volume of the packed column is about 2000 cm^3.

In operation, the column was heated to 127 °C, the polymer in xylene was allowed to flow in, and the column was allowed to cool slowly overnight. All of the polyethylene except a small amount of low molecular weight was thereby precipitated in the column. The cooling rate at 90 °C was about 0.2 °C/min. The cooled (50 °C) xylene was displaced by a poor solvent, 2-butoxyethanol, while the precipitated polyethylene was retained in the column. The column was reheated to 127 °C, causing the polyethylene to melt and swell with the poor solvent. The column was then extracted with mixtures of xylene and 2-butoxyethanol which were successively better solvents. The solutions of extracted polyethylene were siphoned into flasks containing cold ethanol. The polyethylene was filtered out, washed with ethanol, air dried, and then dried in vacuum at 50 °C.

All solvents contained 0.1 percent Ionol (2,6-di-tert.-butyl-4-methylphenol) as an antioxidant. They were preheated under nitrogen to over 130 °C before being admitted to the column. This served to degas the solvent, preventing the formation of bubbles in the column. Typical input concentration was 1 percent polymer in xylene. Extracting mixtures were 15–55 percent xylene. Recovery was ordinarily 97–98 percent, but no great effort was made to obtain absolutely quantitative recovery of material.

Samples PE 7 to PE 180 were prepared by fractionating SRM 1475. Yield was three to six grams of each sample. Samples PE 200 to PE 600 were prepared from Phillips Marlex 6002. These fractions contained two to four grams each.

Light-scattering [6], osmometry [7], and gel permeation chromatography [2] studies were carried out with these samples. The final results are tabulated in paper X of this series [2].

[2] Certain commercial equipment, instruments, or materials are identified in this paper in order to adequately specify the experimental procedure. In no case does such identification imply recommendation or endorsement by the National Bureau of Standards, nor does it imply that the material or equipment identified is necessarily the best available for the purpose.

3. References

[1] Hoeve, C. A. J., Wagner, H. L., and Verdier, P. H., J. Res. Nat. Bur. Stand. (U.S.), **76A,** (Phys. and Chem.), No. 2, 137–140 (Mar.–Apr. 1972). Paper I of this series.

[2] Ross, G. S., and Frolen, L. J., J. Res. Nat. Bur. Stand. (U.S.), **76A,** (Phys. and Chem.) No. 2, 163–170 (Mar.–Apr. 1972). Paper X of this series.

[3] Hoeve, C. A. J., and Wagner, H. L., to be published.

[4] Desreux, V., Rec. Trav. Chim. **68,** 789 (1949).

[5] Chiang, R., J. Polymer. **36,** 91 (1959).

[6] Frolen, L. J., Ross, G. S., Wims, A. M., and Verdier, P. H., J. Res. Nat. Bur. Stand. (U.S.), **76A,** (Phys. and Chem.), No. 2, 156–160 (Mar.–Apr. 1972). Paper VIII of this series.

[7] Brown, J. E., and Verdier, P. H., J. Res. Nat. Bur. Stand. (U.S.), **76A,** (Phys. and Chem.), No. 2, 161–163 (Mar.–Apr. 1972). Paper IX of this series.

(Paper 76A2–711)

The Characterization of Linear Polyethylene SRM 1475. VII. Differential Refractive Index of Polyethylene Solutions

Herman L. Wagner

Institute for Materials Research, National Bureau of Standards, Washington, D.C. 20234

(December 15, 1971)

The value of *dn/dc* for polyethylene in 1-chloronaphthalene at 135 °C, required for the determination of molecular weight by light scattering, was found to vary with molecular weight. Similar changes were found in 1,2,4-trichlorobenzene, the gel permeation chromatograph solvent. The absolute value of *dn/dc* decreases by about 2 percent as the polymer molecular weight increases from 12,000 to 110,000.

Key words: 1-chloronaphthalene; *dn/dc*; differential refractive index; refractometer; refractive index; 1,2,4-trichlorobenzene.

1. Introduction

Since the change of refractive index with concentration, *dn/dc* (differential refractive index), enters as a squared term in the light scattering equation, its accuracy is of considerable importance for obtaining reliable values of molecular weight of polymers. The first determination of *dn/dc* of polyethylene in 1-chloronaphthalene (table 1) found in the literature was by Nichols and was reported by Billmeyer [1].[1] It was measured at 90 °C and 125 °C using a divided cell technique, giving values of −0.199 ml/g and −0.191 ml/g respectively. The latter value is the one most often quoted. Kobayashi, Chitale, and Frank [2], using an interferometer technique, obtained a somewhat lower value at 90 °, namely −0.183. Nicholas [3] found a very low value (−0.257 at 125 °C) using a Rayleigh differential refractometer at concentrations of 0.15 to 0.7 g/100 ml. This result seems to be completely out of line with the other values reported and may be due to the greater errors incurred working at low concentrations. The use of such low concentrations would appear to be unnecessary inasmuch as *dn/dc* is found to be constant at the concentrations used in this work, which range from 0.5 g/100 ml to 4 g/100 ml.

Most of the other literature values fall in the range of −0.188 to −0.199 [4,5,6]. The recent data are those of Drott and Mendelson [7], Chiang and Rhodes [8] and Benoit et al. [9]. Drott and Mendelson provide considerable detail about their procedure, which appears to

TABLE 1. *Literature values of* dn/dc *for polyethylene in 1-chloronaphthalene*

	dn/dc in ml/g							
Refs.	1	2	3	6	22	7	8	9
Temp. °C								
90	−0.199	−0.183			−0.198			
99.5							−0.1924	
104.5							−.1927	
105				−0.188				
109							−.1934	
114							−.1927	−0.1957
120							−.1917	
125	−.191		−0.257		−.195	−0.195	−.1911	
127								−.1967
128								−.1955
135							−.190	
139								−.1956
140						−.191		−.1961
145								−.1967

[1] Figures in brackets indicate the literature references at the end of this paper.

be thorough and careful, and obtained a value of −0.191 at 140 °C and −0.195 at 125 °C. Chiang believes his values for a low molecular weight branched sample of −0.195 at 80 °C [10] are consistent with his values for higher molecular weights which range from −0.193 at 100 °C to −0.190 at 135 °C. Benoit et al. measured dn/dc between 141 °C and 150 °C finding values about $2\frac{1}{2}$ percent higher than those of Chiang and Billmeyer. The change in dn/dc with temperature is insignificant in this temperature range.

In view of the uncertainties described above and the importance of accurate values of dn/dc, it appeared necessary to make as accurate a determination as possible for the Standard Reference Materials Program. It soon became evident that dn/dc was to some extent a function of molecular weight. This may account for some of the discrepancies in the literature but these could not be readily resolved because in most cases no characterization is provided for the polyethylene used in the dn/dc measurement. It was also necessary to measure the variation with molecular weight in 1,2,4-trichlorobenzene since this solvent is used in gel permeation chromatography with the assumption that dn/dc is constant.

2. Experimental Procedure

The determination of the change of refractive index with concentration is most conveniently accomplished by a differential refractometer. The instrument employed here was the image displacement type, in which light passes through a cell consisting of two adjacent prismatic compartments, one containing solvent, the other dilute solution. It may be easily shown that in the limit as the difference Δn between the refractive index of solution and of solvent becomes small, the displacement Δd of the imaged light source from its position with pure solvent in both compartments of the cell becomes proportional to Δn, i.e.,

$$\Delta n = k\Delta d$$

where k is the proportionality constant and is determined by calibration with a substance of known refractive index.

2.1. Optical System

The optical system, consisting of the elements shown in figure 1, is mounted on an optical bench 125 cm long. Light from an air cooled mercury lamp passes through a combination of filters which transmits green monochromatic light at 5460 Å. This light enters a slit, passes through the collimating lens, L_1, then through the cell, where the deviation due to the refractive index difference takes place. The displaced slit, imaged by the lens, L_2, is observed with a micrometer eyepiece having a 10 mm scale and a drum divided to 0.01 mm. The entire optical system is carefully aligned so that the collimated beam is normal to the face of the cell. The system was stable in that once the optical components were fixed the reading did not change over a period of several days with a given solvent in both compartments of the cell.

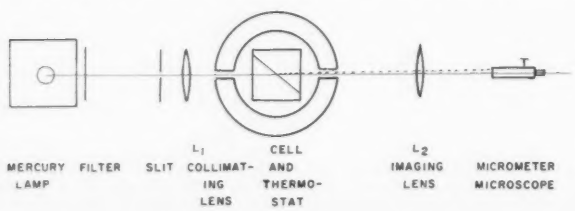

FIGURE 1. *Optical system, schematic.*

2.2. Glass Cell

The sample cell, supplied commercially [11][2] is a sinter fused Pyrex optical cell 15 mm square with plane parallel windows. The partition is set at such an angle that the light beam forms an angle of incidence of approximately 69° with the normal to the surface of the partition. This cell is provided with a fused top with openings which are closed by Teflon stoppers, thus eliminating the problem of evaporation which in the past has caused troublesome temperature gradients at high temperatures.

2.3. Cell Holder

In order to achieve temperature stability over long periods of time and to keep the temperature difference between the two compartments of the cell down to a few hundredths of a degree, considerable care was necessary in the design of the cell holder. As in the apparatus discussed by Benoit et al. [9], the cell is set into a rectangular opening in the center of a cylindrical aluminum block, 4 in in diameter and 5 in high (fig. 2) containing a $\frac{3}{8}$ in hole for passage of the light beam. Aluminum 1100 was used because of its superior heat conductivity. The aluminum block is positioned by three bakelite pins inside a $\frac{1}{8}$ in thick brass shell of 5 in diameter, leaving a half inch air space to minimize heat loss. Both the aluminum block and the brass shell are heated by coils of wire embedded in silicone rubber. Additional heat is supplied by means of four rod heaters inserted into holes in the block and by another coil heater, also embedded in silicone rubber, underneath the brass shell. The temperature of the cell holder is maintained by a thermistor temperature controller. The entire assembly is insulated by a laminate composed of eight layers of balsa wood alternating with aluminum foil. Short term temperature fluctuations of the aluminum block were of the order of 0.001 °C. Drift during a set of measurements was no greater than 0.01 °C.

Brice [12] recommends that the temperature difference between solvent and solution should be no greater than 0.01 °C. Attempts to measure this difference by simply inserting thermocouples into each

[2] Certain commercial equipment, instruments, or materials are identified in this paper in order to adequately specify the experimental procedure. In no case does such identification imply recommendation or endorsement by the National Bureau of Standards, nor does it imply that the material or equipment identified is necessarily the best available for the purpose.

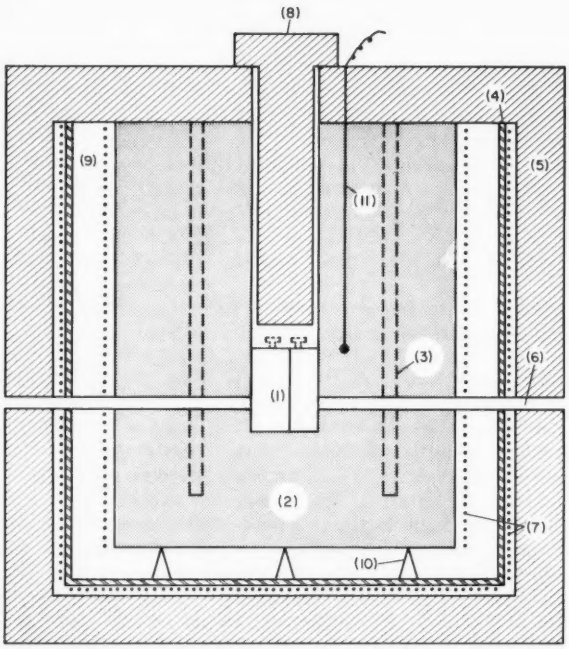

FIGURE 2. *Heating block for cell.*

(1) Divided cell, (2) aluminum cylinder, (3) cartridge heaters, (4) brass shell, (5) balsa wood-aluminum foil laminate, (6) opening for light path, (7) heaters embedded in silicone rubber, (8) balsa wood cap, (9) air space, (10) bakelite positioning pins, (11) thermistor.

compartment were unsuccessful, probably because of heat loss through the openings for the thermocouple leads and through the leads themselves. In view of the construction described above it is doubtful that a significant difference existed. In any case the effect of such a difference would be cancelled since measurements were made first with solution on one side and solvent on the other and again with solution and solvent reversed.

3. Materials

3.1. Solvents

Reagent grade 1-chloronaphthalene was double distilled, center cuts being taken each time. Observable impurities were less than 0.05 percent by gas liquid chromatography. The 1,2,4-trichlorobenzene, technical grade, was not further purified and 0.05 percent Ionol (2,6-di-*tert.*-butyl-4-methylphenol) was added as an antioxidant in order to use the same material used in the gel permeation apparatus [13]. Gas liquid chromatography revealed only a single major peak containing at least 99 percent of the material.

3.2. Polymers

Measurements of dn/dc were made on several polyethylenes. They are: (1) SRM 1475, the linear polyethylene standard reference material described previously [14]; (2) fractions of SRM 1475 obtained by column extraction of this polyethylene [15]; (3) SRM 1476, the branched polyethylene standard reference material. The available data are provided in the certificate for this material. Additional details will be given in a forthcoming publication; (4) fraction R 1201–7 is a linear polyethylene supplied by the Monsanto Chemical Company; (5) AC–6 is a polyethylene wax obtained from the Allied Chemical Corporation.

The number average molecular weights of these materials were obtained in various ways, as indicated in tables 2 and 3. Some were obtained by direct measurement by osmometry [16]; others were determined by gel permeation chromatography (G.P.C.) [13]. The number average molecular weights of fractions 12x and 7y were estimated from molecular weight measurements made on other fractions prepared by the same process. For three of the samples (AC–6, R 1201–7, and SRM 1476), the values supplied by the manufacturer were used.

4. Procedure

For each concentration two readings of the displacement of the light beam were made. The first was taken with the solvent on one side and solution on the other and another reading was taken with these reversed. One-half the difference between the two readings multiplied by the calibration constant gave the value of the refractive index difference Δn. This is similar to the procedure of Brice and Halwer [12] ex-

TABLE 2. dn/dc *of Polyethylenes in 1-Chloronaphthalene at 135 °C*

Sample	M_n	dn/dc, ml/g	Stand. dev. of dn/dc,[e] ml/g	No. of points[e]
SRM 1475	[a] 18,310	−0.1932	0.00016	5
SRM 1476	[b] 25,200	−.1916	.00028	5
Fraction R 1201–7	[b] 12,300	−.1931	.00042	3
Fraction PE 15	[c] 13,500	−.1929	.00035	3
Fraction 12x	[d] 110,000	−.1883	.00088	2
Fraction PE 120	[c] 112,200	−.1879	.00059	4

[a] Value obtained from Gel Permeation Chromatography [13].
[b] Value provided by manufacturer.
[c] Determined by osmometry [16].
[d] Estimated as described in text.
[e] The estimated standard deviation of the slope, calculated by linear regression of the refractive index difference, Δn, on the concentration c, assuming a zero intercept. The number of points in each regression line is shown in column 5.
For convenience all standard deviations are given to two significant figures, with no implication that such precision is warranted.

TABLE 3. dn/dc *of Polyethylenes in 1,2,4-Trichlorobenzene at 135 °C*

Sample	M_n	*dn/dc*, ml/g	Stand. dev. of *dn/dc*,[d] ml/g	No. of points [d]
AC–6	[b] 2,000	−0.1085	0.00028	3
SRM 1475	[a] 18,310	−.1085	.00015	5
Fraction 12 AC	[a] 34,800	−.1082	.00019	3
Fraction 7y	[c] 77,000	−.1073	.00038	3
Fraction 12x	[c] 110,000	−.1063	.00014	4

[a] Value obtained from Gel Permeation Chromatography [13].
[b] Approximate value, supplied by manufacturer.
[c] Estimated as described in text.
[d] The estimated standard deviation of the slope, calculated by linear regression of the refractive index difference, Δn, on the concentration c, assuming a zero intercept. The number of points in each regression line is shown in column 5.
For convenience all standard deviations are given to two significant figures, with no implication that such precision is warranted.

cept that since it is not possible, as in their apparatus, to rotate our cell housing because of its large bulk, the cell is kept fixed and the contents reversed. Readings with solvent on both sides were made occasionally to make certain that the beam's position through the center of the cell had not shifted.

Solutions were made up by weight, and concentrations were calculated from measurements of solvent densities and partial specific volumes. The densities at 135 °C of 1-chloronaphthalene and 1,2,4-trichlorobenzene were found to be 1.095 g/ml and 1.315 g/ml respectively. The partial specific volumes were approximated from measurements of the change in density on dissolving the polymer to specified concentrations. The values obtained were 1.29 ml/g in 1-chloronaphthalene at a concentration of 0.03 g/ml and 1.30 ml/g in 1,2,4-trichlorobenzene at a concentration of 0.01 g/ml. It was assumed that at the low concentrations employed here the partial specific volume is constant, so that the volume increase on dissolving polymer is equal to the weight of the polymer multiplied by this approximate partial specific volume. The polymer was dissolved in the solvent at 140 °C and about 1.5 ml was transferred by a heated hypodermic syringe to the cell. The compartment was not cleaned and dried when its content was changed but was thoroughly rinsed beforehand with solvent and solution of the new concentration. A period of at least 15 min was allowed after transfer for temperature equilibration before readings were taken. The standard error (15 readings) was about 2×10^{-6} in Δn or about 0.2 percent. The least square slopes computed from these data show a standard deviation of the slope of from 0.1 to 0.5 percent, as shown in tables 2 and 3. The standard deviation of the slope for the standard reference sample is about 0.1 percent.

No refractive index data at 135 °C are available for calibration of differential refractometers. We therefore calibrated our instrument with aqueous solutions of NBS sucrose at 25 °C and assumed the calibration did not change with temperature. The most likely cause for a change in calibration would be a change in the angle of the glass partition of the cell. Measurements in a cell similar to ours by Benoit et al. [9] of sodium chloride solutions up to 70 °C did not reveal any changes with temperature.

The partial specific volume of sucrose in water was taken as 0.618 ml/g at 25 °C [19]. The value of 0.1429 ml/g for *dn/dc* at 5460 Å at 25 °C, obtained by Norberg and Sundeloff [18], was employed in the calibration of the apparatus. This value agrees very well with the results of other authors [19–21]. Bodmann [21] has shown that *dn/dc* is constant up to concentrations of at least 0.025 g/ml. We found that the displacement Δd of the light beam is linear with concentration for concentrations as high as 0.04 g/ml and displacements up to 5 mm, the limit of our instrument scale. The calibration constant k for our instrument was found to be 1.1417×10^{-3} refractive index units per mm deflection, with a standard deviation of 0.1 percent.

5. Results and Discussion

The values of *dn/dc* for various polyethylenes in 1-chloronaphthalene are listed in table 2. The value for the linear sample, SRM 1475 at 135 °C is −0.193 ml/g and for the branched sample, SRM 1476, is −0.192. The numbers fall into two groups: values of −0.192 to −0.193 for low number average molecular weights (11,000–25,000) and a decidedly higher value, −0.188 for the higher molecular weights. In order to obtain a better idea of the molecular weight dependence and to determine whether gel permeation chromatography intensities need to be corrected for molecular weight, *dn/dc* was measured in 1,2,4-trichlorobenzene over a range of molecular weights. These are enumerated in table 3 and a plot of these values against $1/M_n$ is shown in figure 3. The change in *dn/dc* in going from an M_n of 12,000 to 110,000 is about the same in both solvents, a decrease of about 2 percent in absolute value. Several

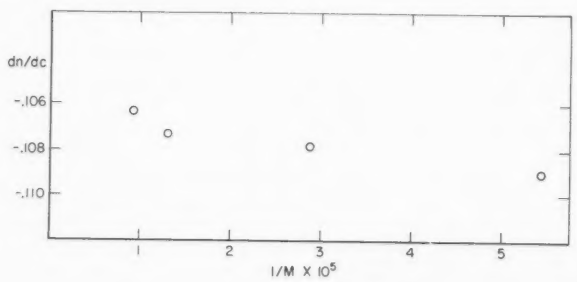

FIGURE 3. *Differential refractive index in 1,2,4-trichlorobenzene.*

factors contribute to the belief that this is a real change. It is outside the limits of error of the determination, for which the standard deviation is of the order of 0.5 percent. Different fractions of the same molecular weight, such as 12x and PE 120 in one case, and R 1201–7 and PE 15 for another, the latter two coming from different starting polymers, have the same values of dn/dc. The infrared spectra of the whole polymer SRM 1475 and a high molecular weight fraction, showing a smaller dn/dc, are similar, indicating the absence of some chemical group which might account for the difference in dn/dc.

Unfortunately it was not possible to measure dn/dc for fractions of M_n greater than 110,000 because of the difficulties of handling the extremely high viscosities of these fractions at the concentrations needed to give meaningful results. For most determinations concentrations ran between 0.5 to 4 g/100 ml but were limited to no greater than 2 g/100 ml for the high molecular weight samples.

6. Conclusion

Because dn/dc changes with molecular weight, it is necessary to use the correct value of dn/dc in light scattering work, as is done in Paper VIII of this series [23]. Although 1-chloronaphthalene measurements were not made for the intermediate molecular weight range, the measurements in trichlorobenzene are extensive enough to show that dn/dc changes continually so that interpolation should provide sufficiently precise values for the former solvent. No data are available, however, at number averages greater than 110,000, and since it can not be assumed that the absolute value of dn/dc decreases without limit, the value at high molecular weights is taken, for the present, as constant at -0.188 ml/g in 1-chloronaphthalene.

7. References

[1] Billmeyer, F., J. Am. Chem. Soc. **75,** 6118 (1953).
[2] Kobayashi, T., Chitale, A., and Frank, H. P., J. Polymer Sci. **24,** 156 (1957).
[3] Nicolas, L., J. Polymer Sci. **29,** 191 (1958).
[4] Chiang, R., J. Polymer Sci. **36,** 91 (1959).
[5] Duch, E. and Kűchler, L., Z. Electrochem. **60,** 218 (1956).
[6] Trementozzi, Q. A., J. Polymer Sci. **36,** 113 (1959).
[7] Drott, E. E. and Mendelson, R. A., Polymer Letters **2,** 187 (1964).
[8] Chiang, R. and Rhodes, J. H., Polymer Handbook, Editors J. Brandrup and E. D., Immergut, p. 14–282, (Interscience, 1966).
[9] Ehl, J., Louchaux, C., Reiss, C., and Benoit, H., Makromol. Chem. **75,** 35 (1964).
[10] Chiang, R., J. Polymer Sci. **C8,** 295 (1965).
[11] Phoenix-Precision Optical Company, Philadelphia, Pa.
[12] Brice, B. A., and Halwer, M., J. Optical Soc. of America **41,** 1033 (1951).
[13] Ross, G. S. and Frolen, L. J., J. Res. Nat. Bur. Stand (U.S.)., **76A,** (Phys. and Chem.), No. 2, 163–170 (Mar.–Apr. 1972). Paper X of this series.
[14] Hoeve, C. A. J., Wagner, H. L., and Verdier, P. H., J. Res. Nat. Bur. Stand. (U.S.)., **76A,** (Phys. and Chem.), No. 2, 137–140 (Mar.–Apr. 1972). Paper I of this series.
[15] Christensen, R. G., J. Res. Nat. Bur. Stand. (U.S.)., **76A,** (Phys. and Chem.), No. 2, 149–150 (Mar.–Apr. 1972). Paper VI of this series.
[16] Brown, J. E. and Verdier, P. H., J. Res. Nat. Bur. Stand. (U.S.), **76A,** (Phys. and Chem.), No. 2, 161–163 (Mar.–Apr. 1972). Paper IX of this series.
[17] Bates, F. J., et al., NBS Circular C440 (May 1, 1942).
[18] Norberg, P. H. and Sundelof, L. A., Makromol. Chem. **77,** 77 (1964).
[19] Gosting, L. J. and Morris, M. S., J. Am. Chem. Soc. **71,** 1998 (1949).
[20] Maron, S. H. and Lou, R. L. H., J. Phys. Chem. **59,** 231 (1955).
[21] Bodmann, O., Chemie-Ing.-Tech. **29,** 468 (1957).
[22] Tung, L. H., J. Polymer Sci. **36,** 287 (1959).
[23] Frolen, L. J., Ross, G. S., Wims, A. M., and Verdier, P. H., J. Res. Nat. Bur. Stand. (U.S.), **76A,** (Phys. and Chem.), No. 2, 156–160 (Mar.–Apr. 1972). Paper VIII of this series.

(Paper 76A2–712)

The Characterization of Linear Polyethylene SRM 1475

VIII. Light-Scattering Studies on Polyethylenes in 1-Chloronaphthalene

Lois J. Frolen, Gaylon S. Ross, Andrew M. Wims*, and Peter H. Verdier

Institute for Materials Research, National Bureau of Standards, Washington, D.C. 20234

(December 15, 1971)

Light-scattering measurements have been made on a series of linear polyethylene fractions and a linear polyethylene standard reference material (SRM 1475). All measurements were made in 1-chloronaphthalene at 135 °C, and over an angular range from 45° to 135°. The data were analyzed to obtain the weight average molecular weights, second virial coefficients and root-mean square end-to-end distances.

Key words: End-to-end distance; light scattering; linear polyethylene; polyethylene fractions; M_w; second virial coefficient; solution properties.

1. Introduction

Several investigators [1, 2][1] have used the technique of light scattering to obtain weight-average molecular weights, second virial coefficients and radii of gyration for polyethylene in dilute solutions. In this paper, we report the results of light scattering studies on a series of linear polyethylene fractions with molecular weight ranging from about 1.9×10^4 to about 6.9×10^5. The weight-average molecular weights reported here were employed in the calibration of a gel permeation chromatograph used [3] to obtain the molecular weight distribution of Standard Reference Material 1475, Linear Polyethylene. We also report the direct determination of weight-average molecular weight for SRM 1475 by light scattering.

2. Experimental Procedure

2.1 Apparatus

The light scattering photometer described by McIntyre and Doderer [4] was used for most of the studies reported here. However, a few measurements were made on a modified Brice-Phoenix Photometer (Phoenix Precision Instrument Company, Philadelphia, Pa.).[2] Consistent results were obtained from the two instruments, and data from both instruments are included in the analysis of results.

All measurements on polyethylene solutions were made at 135 °C, using a heated cell holder [5] designed and constructed in this laboratory. A schematic drawing of the cell holder is shown in figure 1. It consists of two concentric cylinders wrapped with heating wire, insulated with alternating layers of balsa wood and aluminum foil bonded together with silicone rubber adhesive. A slot, not shown in the figure, extends slightly more than halfway around the oven at the height of the sample cell to provide paths for the in-

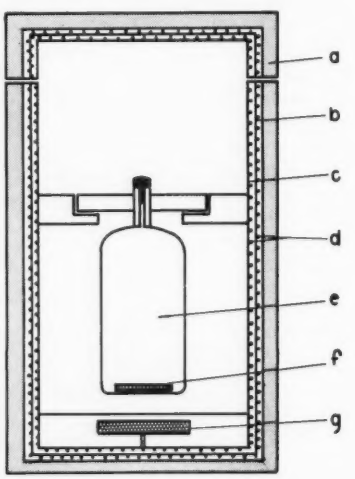

FIGURE 1. *Schematic drawing of high temperature oven for light scattering cells.*

a. Insulation, b. outer cylinder, c. inner cylinder, d. heating wire, e. light scattering cell, f. stirring bar, g. rotatable magnet.

* Present address: General Motors Research Laboratory, Warren, Michigan 48092

[1] Figures in brackets indicate the literature references at the end of this paper

[2] Certain commercial equipment, instruments, or materials are identified in this paper in order to adequately specify the experimental procedure. In no case does such identification imply recommendation or endorsement by the National Bureau of Standards, nor does it imply that the material or equipment identified is necessarily the best available for the purpose.

cident, transmitted and scattered light. A small rotatable magnet under the sample cell permits stirring when desired. The scattering cells used with the oven are clear Pyrex cylindrical cells fitted with capillary necks and Teflon stoppers to minimize contamination by dust.

Measurements on polyethylene were made with the outer cylinder heated to 130 °C and the temperature of the inner cylinder controlled to maintain the sample at 135 °C. No attempt was made to monitor the temperature of the solutions in the light scattering cell while measurements were being taken. However, in preliminary tests, the temperature at various points in the stirred solvent was monitored with thermocouples. The liquid attained a steady temperature of 135 ° in 15 minutes and thereafter showed temperature variations of less than ± 0.05 °C during a period of one hour.

A solution of polystyrene in toluene was used as a working standard to calibrate the instrument. Measurements of absolute scattering on the working standard were made at room temperature (about 25 °C) in a semi-octagonal sample cell with a clear (unblackened) back surface. The temperature control employed for the higher-temperature measurements on polyethylene was felt to be unnecessary for the room-temperature reference measurements. The oven and cell holder described above were therefore not used for the reference measurements.

2.2. Preparation of Samples

The preparation of the linear polyethylene fractions is described in paper VI of this series [6]. The solvent employed was Fisher Reagent Grade 1-chloronaphthalene which was passed through activated 28–200 mesh silica gel before use. Gas chromatographic analysis of the solvent showed less than 0.1 percent observable impurity. Before being filled with solution, the light scattering cells were cleaned with hot chromic acid, rinsed with distilled water, dried in a dust-free atmosphere, and rinsed from three to five times with filtered 1-chloronaphthalene.

Each sample was prepared by adding approximately 10 cm^3 of solvent to a weighed amount of polyethylene, stirring at 130–135 °C until the polyethylene dissolved (usually 1 to 1½ h) and weighing the resulting solution. The sample was then filtered as described below into a weighed scattering cell. After light scattering measurements had been taken, second and third concentrations were prepared for measurement by adding approximately 5 cm^3 increments of filtered solvent, weighing the scattering cell before and after each addition. Weight per unit volume concentrations were calculated from the weights of solvent and solute, solvent density, and partial specific volume [7] of polyethylene in 1-chloronaphthalene. For some representative samples, the final concentration was checked by evaporating 10 cm^3 of the solution and weighing the residue. In all cases, the concentration so obtained agreed with that calculated from the known dilutions to within 1 percent.

The samples were filtered with a heated 40 cm^3 hypodermic syringe fitted with a "Swinney Adapter" filter holder (Millipore Corp., Bedford, Mass. 01730). A ball joint sealed to the top of the syringe allowed the rate of filtration to be controlled with nitrogen gas under pressure. The nitrogen pressure was adjusted to give a flow rate of approximately 1 drop per second. Faster flow rates resulted in less clean samples as determined by their erratic scattering at low angles. Two Metricel type, Alpha–6 filter discs with a nominal pore size of 0.4 μm (Gelman Instrument Co., Ann Arbor, Mich. 48106) were used for each filtration. These discs had been found to be resistant to 1-chloronaphthalene and could be used at temperatures up to 150 °C without apparent damage. They were rinsed with the material to be filtered before use, and were changed after each filtration.

During filtration, the syringe was heated by placing it in a glass tube wrapped with heating wire and maintained at 135–140 °C. The needle of the syringe was inserted into the capillary neck of the light-scattering cell, and the filtration was carried out in a stagnant air box to minimize contamination by dust.

2.3. Scattering Measurements

Scattered intensities were measured at eleven scattering angles ranging from 45° to 135°. Measurements on SRM 1475 were made at 25 concentrations, in the range from 1.7×10^{-3} to 20.8×10^{-3} g/cm^3. Measurements on each of the seven fractions listed in table 1 were made at six concentrations. The concentrations chosen varied with the molecular weights of the fractions, from a range of 1.8×10^{-2} to 5.7×10^{-2} g/cm^3 for PE 15 to a range of 0.7×10^{-3} to 2.6×10^{-3} g/cm^3 for PE 600. Measurements were also made on pure solvent. The incident illumination in all cases was the mercury green line of wavelength 5461 Å, plane-polarized with its electric vector perpendicular to the scattering plane.

As mentioned previously, a solution of polystyrene in toluene was used as a working standard. The absolute scattering of the working standard at 90° was first determined. As each polyethylene solution was measured, the scattered intensity from the working standard at 90° was also recorded. Thus, the quantity actually obtained was the ratio of the scattering from the solution (or solvent) at each angle to that of the working standard at 90°.

3. Treatment of the Data

The use of light scattering to determine molecular weight and size parameters of macromolecules in dilute solution is well established [8]. At sufficiently low concentrations and small scattering angles, the ratio of solution concentration to scattered light intensity may be expanded in a Taylor series in concentration and in the sine of half the scattering angle. For plane-polarized monochromatic light scattered through an angle θ, the result for a solution of monodisperse

material may be expressed in the form [9]:

$$\frac{Kc}{R_\theta} = \frac{1}{M} + \frac{h^2 R_G^2}{3M} + 2A_2 c + \ldots, \quad (1)$$

with:

$$K = (4\pi^2 n^2/\lambda_0^4 N_A)(dn/dc)^2(1-\cos^2\psi\sin^2\theta), \quad (2)$$

$$R_\theta = r^2[I(\theta,c) - I(\theta,0)]/(vI_0), \quad (3)$$

and

$$h = (4\pi/\lambda)\sin(\theta/2) = (4\pi n/\lambda_0)\sin(\theta/2), \quad (4)$$

where

c is solution concentration (weight per unit volume),
M is the molecular weight of the solute,
R_G is the radius of gyration of the solute,
A_2 is the second virial coefficient of the solution,
λ_0 is the wavelength *in vacuo* of the radiation,
n is the index of refraction of the solvent at wavelength λ_0,
$\lambda = \lambda_0/n$ is the wavelength of the radiation in the solvent,
N_A is Avogadro's number,
dn/dc, the so-called differential refractive index, is the derivative (at constant temperature and pressure and in the limit of zero concentration) of solution refractive index with respect to concentration,
θ is the angle between the incident and scattered wave vectors,
ψ is the angle between the electric vector of the incident radiation and the plane containing the incident and scattered wave vectors,
I_0 is the intensity of the incident radiation,
$I(\theta,c)$ is the scattered intensity at angle θ for a solution of concentration c,
r is the distance from the scattering center to the point at which the scattered intensity is observed, and
$v = v(n,\theta)$ is the volume of solution from which the scattered radiation is observed.

For the special cases $\psi = \pi/2$ and $\psi = 0$ (so-called vertical and horizontal polarization), the last factor in eq (2) becomes unity and $\cos^2\theta$, respectively. (The usually-quoted result for unpolarized incident radiation is obtained by averaging over all possible values of ψ, in which case the factor becomes $(1+\cos^2\theta)/2$.)

For a solution of polydisperse material, it can be shown [10, 11] that eq (1) still holds at sufficiently small scattering angle and low concentration, provided M is replaced by M_w, the weight-average molecular weight, R_G^2 is replaced by its z-average, $\langle R_G^2 \rangle_z$ [12], and A_2 is replaced by an "effective" value without simple interpretation [11].

In order to use eqs (1)–(4) to relate observed scattering to molecular parameters, it is necessary to know the functional dependence of the scattering volume, v, upon n and θ. For the geometry of our instrument, the scattering volume is inversely proportional to the square of the index of refraction of the material in the scattering cell [13,14]. A simple geometrical argument suggests that for scattering angles not too close to 0° or 180°, the scattering volume should vary as the cosecant of the scattering angle. (The validity of the approximation was established for the present work, in the course of checking the alignment of the instrument, by measurements on fluorescein solutions.) Thus we can write

$$v(n,\theta) = v_0 n^{-2}\csc\theta. \quad (5)$$

Finally, the observed intensities must be corrected for the effects of reflections at the entrances and exits of the scattering cells, as discussed by Kratohvil [15]. When light impinges perpendicularly upon an interface between two regions with indices of refraction n_1 and n_2, the fraction f reflected is given by Fresnel's formula: $f = [(n_1-n_2)/(n_1+n_2)]^2$. In the light-scattering experiment, such interfaces occur at both the inside and the outside surfaces of the walls of the scattering cells. If we make the usual assumption that the difference between the index of refraction of the solution inside the scattering cell and the index of the glass in the cell walls is so small as to cause negligible reflection, we are left with only the interfaces between the cell walls and the air outside the cell to consider. By counting up the various possible paths resulting from multiple reflections of the incident and scattered beams, we can readily show that for a circularly cylindrical scattering cell, the observed intensity $I'(\theta,c)$ is related to the "true" intensity $I(\theta,c)$ (i. e., that which would be observed in the absence of reflections) by

$$I(\theta,c) = (1-f)^{-2}[(1+f^2)I'(\theta,c) - 2fI'(\pi-\theta,c)], \quad (6)$$

where $f = [(n_g-1)/(n_g+1)]^2$, and n_g is the index of refraction of the cell wall glass. Equation (6) is in agreement, to first order in f, with the approximate result obtained by Kratohvil [15] for this case.

For the semioctagonal cell used to determine absolute scattering by the working standard, only the intensity of the beam scattered through an angle $\theta = \pi/2$ and the intensity I_0 of the incident (unscattered) beam need be considered. For right-angle scattering, the light paths for this cell are identical with those for a circularly cylindrical cell, and the special case $I = I'$ obtained from eq (6) for $\theta = \pi/2$ also applies to this cell. For the incident beam, observed after passage through the semioctagonal cell, it can easily be shown that

$$I_0 = I_0'(1+f)/(1-f). \quad (7)$$

For the present work, the quantity $R_{\pi/2,s} = r^2 I_s/(vI_0)$, where we denote by I_s the intensity of right-angle scattering from the working standard, was first determined as described by McIntyre [13]. The intensity ratio I_s/I_0 was measured with the use of a set of calibrated filters, and was corrected for reflections as described above. For the semioctagonal cell employed, the quantities r and v_0 were obtainable from the

instrument geometry, and the scattering volume v was obtained from eq (5).

For measurements made on the working standard at 90° in the circularly cylindrical scattering cells, we can use the definition of $R_{\pi/2,s}$ and eq (5) to write

$$v_0 I_0 / r^2 = I_s n_s^2 / R_{\pi/2,s}, \tag{8}$$

where n_s is the index of refraction of the working standard. With the use of eqs (2)–(6), the left-hand side of eq (1) can be rewritten in the form

$$\frac{Kc}{R_\theta} = \frac{4\pi^2 n_s^2 c(1-\cos^2\psi \sin^2\theta)\ \csc\theta (dn/dc)^2}{\lambda_0^4 N_A R_{\pi/2,s}} \times \left(\frac{I_s}{I(\theta, c) - I(\theta, 0)}\right). \tag{9}$$

Thus, measurement of the scattering of the solution relative to that of the working standard (the last factor on the right-hand side of eq (9)), together with the value of dn/dc for the solution, yields Kc/R_θ. Equation (1) may then be used to determine M_w, $\langle R_G^2\rangle_z$, and A_2 from the dependence of Kc/R_θ upon c and θ.

In order to extract molecular parameters from experimental values of Kc/R_θ, we employ the well-known Zimm method [16]. If we plot Kc/R_θ as a function of $\sin^2(\theta/2)+kc$, where k is a constant chosen for convenience, we obtain an array of points through which lines of constant concentration and lines of constant angle can be drawn, as exemplified in figure 2. Extrapolation of each of the constant-concentration lines to zero angle gives a set of points which constitute a plot of Kc/R_0 versus kc. According to eq (1), such a plot intersects the Kc/R_θ-axis at $1/M_w$, with a limiting slope of $2A_2/k$. In the same way, extrapolation of each of the constant-angle lines to zero concentration yields a plot of $\lim_{c\to 0}[Kc/R_\theta]$ versus $\sin^2(\theta/2)$. Combining eqs (1) and (4), we find:

$$\lim_{c\to 0}[Kc/R_\theta] = M_w^{-1}[1+(16/3)\pi^2\lambda^{-2}\langle R_G^2\rangle_z \sin^2(\theta/2)].$$

The intercept is therefore again $1/M_w$, and the limiting slope is a measure of $\langle R_G^2\rangle_z$. In the special case of a linear random-coil chain one can estimate the mean-square distance, $\langle L^2\rangle$, between the ends of the chain by using the relation [17] $\langle L^2\rangle = 6\langle R_G^2\rangle$, although this relation has been established only for chains with Gaussian random-flight statistics.

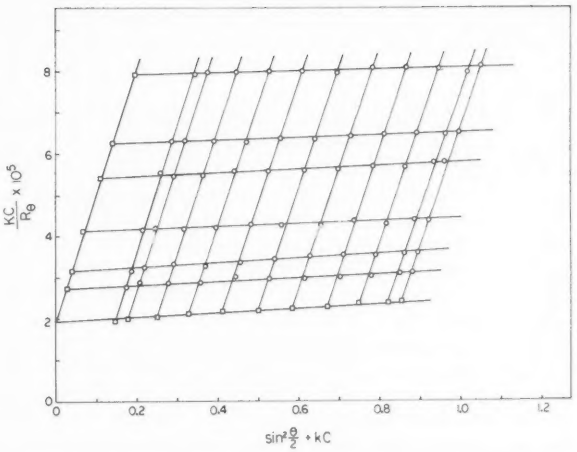

FIGURE 2. *Typical Zimm plot* (Kc/R_θ *versus* $\sin^2(\theta/2)+kc$) *obtained for linear polyethylene in 1-chloronaphthalene at 135 °C.*

The concentration c is expressed in g/cm³; the arbitrary constant k was chosen to have a value of 10 cm³/g. The other symbols are explained in the text. The circles are experimental values; the squares are extrapolations to zero angle at constant concentration and to zero concentration at constant angle.

4. Results

The results obtained for the linear polyethylene fractions and for SRM 1475 are summarized in table 1, together with the values of dn/dc used in calculating Kc/R_θ. For SRM 1475 and the fractions with M_w less than 200,000, measured values [7] of dn/dc were used. For fractions with M_w greater than 200,000, measured values of dn/dc were not available, but measurements on the lower-molecular-weight fractions appeared to suggest that by this point, dn/dc had reached a constant value of −0.188 ml/g independent of molecular weight. This value of dn/dc was therefore used in calculating Kc/R_θ for the fractions of M_w above 200,000.

Values of Kc/R_θ for each fraction and for SRM 1475 were analyzed by the Zimm technique, as described in the preceding section. In all cases, plots of Kc/R_θ versus $\sin^2(\theta/2)+kc$ were found to be linear throughout the entire angular range. A typical plot, obtained for SRM 1475, is shown in figure 2. For clarity, the plot

TABLE 1. *Weight-average molecular weights* M_w, *second virial coefficients* A_2, *and rms end-to-end lengths* $\langle L^2\rangle^{1/2}$, *for linear polyethylenes in 1-chloronaphthalene at 135 °C.*

The uncertainties shown are estimates of the standard deviations obtained from linear least squares analyses of the corrected experimental scattering intensities, as described in the text.

Sample	dn/dc, ml/g	$M_w \times 10^{-3}$, g/mol	$A_2 \times 10^3$, mol · cm³/g²	$\langle L^2\rangle^{1/2} \times 10^{-3}$, Å
PE 15	−0.193	19.1 ± 2.4	1.9	0.4
PE 40	−.191	49.4 ± 2.0	1.6	.6
PE 60	−.190	82.2 ± 7.1	1.6	.6
PE 120	−.188	170 ±16	1.4	.7
PE 180	−.188	210 ±30	1.2	.9
PE 350	−.188	520 ±42	1.3	1.4
PE 600	−.188	688 ±67	1.2	2.1
SRM 1475	−.193	52.0 ± 2.0	.....	.....

shows the data for only six of the 25 concentrations actually employed. The lack of downward curvature in the plots suggests that the samples were adequately cleaned [18].

The linear extrapolations necessary to obtain M_w, $\langle R_G^2 \rangle_z$, and A_2 were carried out by unweighted linear least-squares analyses. The results are given in table 1, together with estimates of the standard deviation in M_w inferred from the least-squares analyses. The values of the rms end-to-end length, $\langle L^2 \rangle^{1/2}$, given in table 1 were obtained from the values found for $\langle R_G^2 \rangle_z$ by use of the approximate relation $\langle L^2 \rangle = 6 \langle R_G^2 \rangle$, as described in the preceding section. It is clear from the lack of smoothness in the variation of A_2 and $\langle L^2 \rangle^{1/2}$ with molecular weight that they are to be regarded as no more than crude estimates. Estimates of the standard deviations in $\langle R_G^2 \rangle_z$ and A_2 from the least-squares analyses were unrealistically low (typically, about 5 per cent for A_2 and 50–100 Å for $\langle L^2 \rangle^{1/2}$), and are therefore not shown in the table. Values of $\langle R_G^2 \rangle_z$ and A_2 were not calculated for SRM 1475.

5. References

[1] DeLaCusta, M. O., and Billmeyer, F. W., Jr., J. Polymer Sci. **A1**, 1721 (1963).
[2] Chiang, R., J. Phys. Chem. **69**, 1645 (1965).
[3] Ross, G. S., and Frolen, L. J., J. Res. Nat. Bur. Stand. (U.S.), **76A** (Phys. and Chem.), No. 2, 163–170 (Mar.–Apr. 1972). Paper X of this series.
[4] McIntyre, D., and Doderer, G. C., J. Res. Nat. Bur. Stand. (U.S.), **62**, 153 (1959).
[5] Wims, A., and Ross, G. S., unpublished work.
[6] Christensen, R. G., J. Res. Nat. Bur. Stand. (U.S.), **76A**, (Phys. and Chem.), No. 2, 149–150 (Mar.–Apr. 1972). Paper VI of this series.
[7] Wagner, H. L., J. Res. Nat. Bur. Stand. (U.S.), **76A**, (Phys. and Chem.), No. 2, 151–155 (Mar.–Apr. 1972). Paper VII of this series.
[8] See, for example, Kerker, M., The Scattering of Light (Academic Press, New York, 1969); Tanford, C., Physical Chemistry of Macromolecules, John Wiley and Sons, New York, 1961; Flory, P. J., Principles of Polymer Chemistry (Cornell University Press, Ithaca, New York, 1953).
[9] The notation used here is essentially that used by Kerker (*op. cit.*, Ch. 8), but is written for plane-polarized incident radiation rather than for unpolarized radiation.
[10] Kerker, *op. cit.*, Ch. 8.
[11] Fujita, H., Mathematical Theory of Sedimentation Analysis, p. 268 f. (Academic Press, New York, 1962).
[12] We define the z-average of the square of the radius of gyration of a polydisperse material as

$$\langle R_G^2 \rangle_z = \sum_i n_i M_i^2 R_{Gi}^2 \Big/ \sum_i n_i M_i^2 ,$$

where n_i is the number of molecules of the i-th component, of molecular weight M_i and radius of gyration R_{Gi}.
[13] McIntyre, D., J. Res. Nat. Bur. Stand. (U.S.), **68A**, (Phys. and Chem.) 87 (1964).
[14] Herman, J. J. and Levinson, S., J. Opt. Soc. Am. **41**, 460 (1951).
[15] Kratohvil, J. P., J. Colloid and Interface Science **21**, 498 (1966).
[16] Zimm, B. H., J. Chem. Phys. **16**, 1099 (1948).
[17] See, for example, Flory, P. J., *op. cit.*
[18] Muus, L. T., and Billmeyer, F. W., Jr., J. Am. Chem. Soc. **79**, 5079 (1957).

(Paper 76A2–713)

The Characterization of Linear Polyethylene SRM 1475. IX. Number Average Molecular Weight of Fractions by Membrane Osmometry

James E. Brown and Peter H. Verdier

Institute for Materials Research, National Bureau of Standards, Washington, D.C. 20234

(December 15, 1971)

The number average molecular weights of a series of fractions of linear polyethylene have been determined using a high speed membrane osmometer. The M_n values of the fractions, which were prepared by an elution technique, were used in GPC calibration and subsequent characterization of linear polyethylene SRM 1475. The molecular weights, measurement techniques, and the precision of the measurements are presented.

Key words: Concentration dependence; linear polyethylene; membrane; number average molecular weight; osmometer; osmotic pressure; virial coefficient.

1. Introduction

In the course of the characterization of the linear polyethylene Standard Reference Material 1475 described in this series of papers [1],[1] the molecular weight distribution was determined [2] by gel permeation chromatography. The gel permeation chromatograph was calibrated with linear polyethylene fractions obtained [3] by a column elution technique. These fractions were characterized for use in the calibration procedure by determining their number- and weight-average molecular weights. Determination of the weight-average molecular weights from light-scattering studies is described elsewhere [4]. In the present paper, we report the determination of the number-average molecular weights, M_n, ranging from about 8,000 to about 350,000, from osmotic pressure measurements.

2. Experimental Procedure

2.1. Apparatus

Osmotic pressure measurements were made with a Hewlett-Packard Mechrolab Membrane Osmometer, Model 502[2]. This instrument, which has been described elsewhere [5], consists essentially of a photocell for detecting liquid flow across a semipermeable membrane, monitored by the motion of a bubble in a capillary tube, and a servomechanism for balancing the osmotic pressure by varying the liquid level on the solvent side of the membrane. It is characterized by rapid response time (of the order of a few minutes with a suitable membrane), negligible solvent transfer across the membrane [6], and small sample volume (about 0.3 ml).

2.2. Membranes

The semipermeable membranes employed were gel cellophane membranes, type 450D, obtained from Arro Laboratories, Inc. When received, they were swollen in an isopropanol-water solution. The following procedure was used to condition them to 1-chloronaphthalene, the solvent used in this work: 24 hours in 50 percent ethanol solution; rinsing with ethanol; 48 hours in ethanol; 24 hours in a 1:1 mixture of ethanol and acetone; 24 hours in a 1:1 mixture of acetone and toluene; rinsing with toluene; 24 hours in toluene; rinsing with 1-chloronaphthalene; heating (with an infrared lamp) in 1-chloronaphthalene under reduced pressure for a minimum of 1 hour, to drive off dissolved gases.

2.3. Procedure

Polyethylene solutions were made up by weight in distilled Fisher reagent grade 1-chloronaphthalene, in concentrations ranging from 0.5 to 12 g/l. Osmotic pressure measurements were made by first placing pure solvent in both sides of the osmometer and recording the level on the solvent side, then flushing out and filling the sample side with one of the solutions and recording the new solvent level. Several measurements were made for each solution. The reference solvent height was checked between solutions by flushing and refilling the sample side with pure solvent. The osmotic pressure for each solution is then given directly as the hydrostatic pressure

[1] Figures in brackets indicate the literature references at the end of this paper.

[2] Certain commercial equipment, instruments, or materials are identified in this paper in order to adequately specify the experimental procedure. In no case does such identification imply recommendation or endorsement by the National Bureau of Standards, nor does it imply that the material or equipment identified is necessarily the best available for the purpose.

difference between solvent and solution. All measurements were made at a temperature of 130 °C.

3. Results and Discussion

In order to obtain values of M_n from the variation of osmotic pressure with solution concentration, we start with the familiar virial expansion, expressed in one of the two equivalent forms:

$$\pi/c = RT\left[\frac{1}{M_n} + A_2c + A_3c^2 \ldots\right],$$

$$= (\pi/c)_0\left[1 + \Gamma_2c + \Gamma_3c^2 + \ldots\right], \qquad (1)$$

where π is the osmotic pressure of a solution of concentration c (weight per unit volume), relative to that of pure solvent, R and T are the gas constant and absolute temperature, respectively, the A's and Γ's are the virial coefficients, and the subscript zero denotes the limit of zero concentration.

According to eq (1), M_n is obtained directly from the zero-concentration intercept of a plot of π/c versus c. Such plots are shown in figure 1 for three typical fractions, PE 7, PE 120, and PE 350. Although the plot for PE 7, the lowest molecular-weight fraction, is essentially linear, the plots for the higher molecular-weight fractions show distinct curvature, and extrapolation to zero concentration presents a problem. In principle, the extrapolation may be performed by fitting π/c to a polynomial in c, thus determining some of the virial coefficients higher than the second. In the present case, however, the precision of the data and the concentration range spanned do not appear to warrant the determination of more than two parameters. We therefore resort to the approximate relationship $\Gamma_3 = \frac{1}{4}\Gamma_2^2$, which is frequently found to give satisfactory results for polymer solutions in good solvents at sufficiently low concentrations [5, 7]. With the aid of this relation, and neglecting terms beyond the third virial coefficient, eq (1) may be rewritten in the form:

$$(\pi/c)^{1/2} = (\pi/c)_0^{1/2}(1 + \tfrac{1}{2}\Gamma_2c). \qquad (2)$$

To the extent that the approximations implied in obtaining eq (2) are justified, a plot of $(\pi/c)^{1/2}$ versus c should yield a straight line with a zero-concentration intercept of $(RT/M_n)^{1/2}$ and a slope of $(RT/M_n)^{1/2}\Gamma_2/2$. Figure 2 shows the data of figure 1 replotted as $(\pi/c)^{1/2}$ versus c. The plot is clearly much more nearly linear than that of figure 1. We have therefore used a linear least-squares analysis to fit $(\pi/c)^{1/2}$ to a linear function of concentration, according to eq (2). The dashed lines in figure 1 are plots of eq (2), using the parameters obtained from the least-squares analysis. It is clear that for the higher molecular-weight fractions, use of a simple linear plot would introduce significant errors into the limiting zero-concentration value of π/c, and therefore of M_n.

The results of the least-squares analyses are shown in table 1. The standard deviations for the values of M_n range from about 0.1 percent for PE 7 to 2–4 percent for the higher molecular-weight fractions. For the lower molecular-weight fractions, accuracy is limited by the diffusion of solute through the membrane, as discussed by Staverman et al. [8, 9] and by Tung [10]. From observation of the drift in hydrostatic pressure over periods of an hour or more, we conclude that errors arising from this source are much smaller than the reproducibility of the measurements, even for the lowest molecular-weight fractions reported here. The accuracy of the M_n values for the high molecular-weight fractions is limited primarily by uncertainties arising from the use of the approximate eq (2) to fit the data. In the absence of information on the behavior of the higher virial coefficients, it is very difficult to estimate the uncertainty introduced by the use of eq (2). It is our feeling, however, that for all the fractions, the errors in M_n from all sources are unlikely to exceed 10 percent.

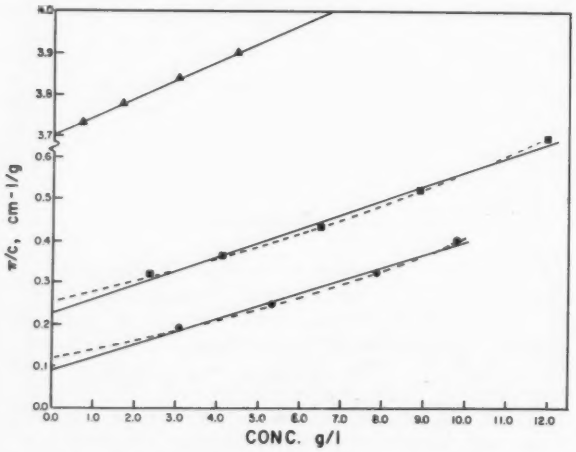

FIGURE 1. *Plots of π/c versus c, where π is osmotic pressure and c is concentration, for solutions of three fractions of linear polyethylene, PE 7 (△), PE 120 (□), and PE 350 (○), in 1-chloronaphthalene.*
The solid lines are the results of linear least-squares fits of π/c versus c; the dashed lines are the results of linear least-squares fits of $(\pi/c)^{1/2}$ versus c.

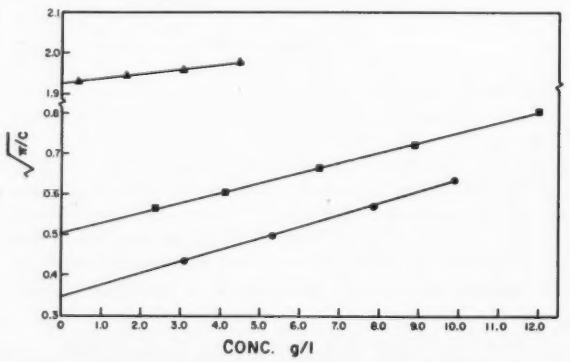

FIGURE 2. *The data of figure 1, replotted as $(\pi/c)^{1/2}$ versus c.*
The solid lines are the results of linear least-squares fits of the data in this form, and are equivalent to the dashed lines in figure 1.

TABLE 1. *Values of number-average molecular weight, M_n, and second virial coefficient, A_2, for solutions of polyethylene in 1-chloronaphthalene at 130 °C, inferred from measurements of osmotic pressure, π, versus concentration, c, by linear least-squares fit of the data to the form* $(\pi/c)^{1/2} = (RT/M_n)^{1/2}(1 + M_n A_2 c/2)$, *where R and T are the gas constant per mole and the absolute temperature, respectively.*

Number in parentheses following the M_n values are the standard deviations in M_n obtained from the linear least-squares analyses. The last column shows the number of solution concentrations at which each sample was measured.

Sample	M_n	$A_2 \times 10^4$, mol cm³/g²	Number of concentrations
PE 7.....	7,730(10)	15.78	4
PE 15.....	13,500(60)	11.48	5
PE 20.....	20,700(240)	11.16	4
PE 40.....	49,700(1,350)	10.29	5
PE 60.....	61,000(2,400)	9.00	5
PE 120.....	112,200(1,900)	8.74	5
PE 180.....	142,800(3,400)	8.44	5
PE 200.....	200,600(5,800)	8.44	4
PE 350.....	241,400(8,300)	7.05	4
PE 600.....	355,300(1,400)	6.46	5

Values of the second virial coefficient, A_2, obtained in the least-squares analyses are also shown in table 1. Because of the uncertainties introduced by the use of eq (2) and by the precision of the experimental data, they should be regarded only as rough estimates of A_2 for these systems.

4. References

[1] Hoeve, C. A. J., Wagner, H. L., and Verdier, P. H., J. Res. Nat. Bur. Stand. (U.S.), **76A,** (Phys. and Chem.), No. 2, 137–140, (Mar.–Apr. 1972). Paper I of this series.

[2] Ross, G. S., and Frolen, L. J., J. Res. Nat. Bur. Stand. (U.S.), **76A,** (Phys. and Chem.), No. 2, 163–170, (Mar.–Apr. 1972). Paper X of this series.

[3] Christensen, R. G., J. Res. Nat. Bur. Stand. (U.S.), **76A,** (Phys. and Chem.), No. 2, 149–150, (Mar.–Apr. 1972). Paper VI of this series.

[4] Frolen, L. J., Ross, G. S., Wims, A. M., and Verdier, P. H., J. Res. Nat. Bur. Stand. (U.S.), **76A,** (Phys. and Chem.) No. 2, 156–160 (1972). Paper VIII of this series.

[5] See, for example, Coll, H. and Stross, F. H., Determination of Molecular Weights by Equilibrium Osmotic-Pressure Measurements, in Characterization of Macromolecular Structure (Publication 1573, National Academy of Sciences, Washington, D.C., 1968).

[6] Steele, R. E., Walker, W. E., Burge, D. E., and Ehrmantraut, H. C., Paper presented at the Pittsburgh Conference on Analytical Chemistry and Applied Spectroscopy, March, 1963.

[7] Flory, P. J., Principles of Polymer Chemistry, p. 533ff. (Cornell University Press, 1953).

[8] Staverman, A. J., Rec. Trav. Chim. **70,** 344 (1951).

[9] Staverman, A. J., Pals, D. T. F., and Kruissink, C. A., J. Polymer Sci. **23,** 57 (1957).

[10] Tung, L. H., J. Polymer Sci. **32,** 477 (1958).

(Paper 76A2–714)

The Characterization of Linear Polyethylene SRM 1475. X. Gel Permeation Chromatography

Gaylon Ross and Lois Frolen

Institute for Materials Research, National Bureau of Standards, Washington, D.C. 20234

(December 15, 1971)

The determination of the integral molecular weight distribution (*MWD*) of the linear polyethylene sample (SRM 1475) by means of gel permeation chromatography (GPC) is described. Both the experimental and mathematical details of column calibration and sample analysis are included.

Key words: Gel permeation chromatography (GPC); linear polyethylene; molecular weight distribution (MWD); number average; weight average.

1. Introduction

Heretofore the molecular weight characterization of polymer samples issued by the National Bureau of Standards has been primarily limited to the reporting of the number average molecular weight, M_n, and the weight average molecular weight, M_w. This paper describes the determination of the integral molecular weight distribution (*MWD*) of the linear polyethylene sample (SRM 1475) using the technique of gel permeation chromatography (GPC).

Prior to 1964 the determination of the *MWD* of a polymer was a tedious, time-consuming task. The first step was to fractionate the polymer using either batch fractionation or elution chromatographic techniques, both of which take advantage of changes in solution properties as a function of molecular weight. Then M_n and M_w measurements were made on each fraction, and, by knowing the weight percent of each fraction and by making certain simplifying assumptions about the molecular weight distribution of each fraction, the *MWD* was constructed.

In 1964, J. C. Moore first published his work on a process which he called gel permeation chromatography [1].[1] In GPC a dissolved sample of polymer

[1] Figures in brackets indicate the literature references at the end of this paper.

453-425 OL - 72 - 7

is carried into and through a packed column by an appropriate solvent stream. The packing is such that the polymer is separated by molecular size, the larger molecules eluting first. By using the appropriate sensing devices, a function of the quantity of each molecular species is graphically displayed on a strip-chart recorder against the volume of solution emerging from the column (elution volume).

Thus, providing the system has been calibrated, one can determine the *MWD* for a given polymer sample in a very short time (usually less than one day). In the past, for each polymer system, the calibration procedure has required the use of well-characterized fractions of the polymer. This paper describes the techniques for the use of such fractions to provide a calibration curve, as well as the methods used to determine the *MWD* of our linear polyethylene whole polymer (SRM 1475). This Standard Reference Material, with its certified *MWD*, may then be used to calibrate other gel permeation chromatographs without requiring the use of fractions.

2. Description of Apparatus

The particular gel permeation chromatographic apparatus used was the Waters Model 200 (analytical scale) GPC.[2, 3] This instrument is designed to analyze samples in the milligram range. The range of molecular weights which can be analyzed is dependent upon column selection. The pertinent features of the apparatus include, in order of flow: (1) a solvent reservoir, (2) a solvent degasser and preheaters, and (3) a precision metering pump with an adjustable pumping rate. The solvent flow emerging from the pump is split, one portion going into a set of columns being used for sample injection, and the other portion flowing through a second set of columns (reference set). Multi-port valving is used to inject the dissolved sample into the appropriate set of columns for analysis. The materials emerging from the two sets of columns pass through the two sides of a differential refractometer cell. The refractometer is stated by the manufacturer to be capable of detecting a difference of 10^{-7} in refractive index. The electronic output from the refractometer is recorded on a chart recorder, providing a continuous record of the difference in refractive index between the two streams. From the refractometer the sample-solvent mixture flows directly into a dump-syphon (5 ml capacity). When the syphon empties a spike is displayed on the recorder trace. In GPC language each spike or pip is referred to as a "count," and the sample injection is timed to coincide with a count, labeled the zeroth one. Temperature controls are provided for regulating the temperature throughout the column, detector, and syphon system. The one modification made to the Model 200 GPC was to provide a Teflon cover for the top of the syphon, to minimize solvent evaporation.

[2] Certain commercial materials and equipment are identified in this paper in order to specify adequately the experimental procedures. In no case does such indentification imply recommendation or endorsement by the National Bureau of Standards, nor does it imply that the material or equipment is necessarily the best available for the purpose.

[3] Waters Associates, 61 Fountain Street, Framingham, Mass. 01701

In the Model 200 GPC, each column is a 4-foot long, thin (3/8 in diameter) stainless steel tube packed with beads of a rigid, crosslinked polystyrene gel. The gel was prepared, characterized, and packed in the columns by Waters Associates, Inc. Five such columns were connected in series to form the column set used for the analysis. The columns had nominal exclusion limits of 1×10^7, 1×10^6, 1×10^5, 1×10^4, and 1×10^3 angstroms. This particular nomenclature [1] describes the minimal length in angstroms of a polystyrene molecule which will be excluded from permeation into the pores of the particular bead packing. The reference column set was a five column set having similar nominal exclusion limits.

3. Column Broadening Effects

From the cursory information in the introduction one might assume that a sample of monodisperse material injected into the GPC column would emerge from the column without change in concentration, producing a rectangular area as a recorder trace, having a base length equal to the volume of the sample injected. However, as is well known [2], in any chromatographic procedure the elution profile is broadened due to longitudinal diffusion in the column, producing, in the case of a single component, a bell-shaped curve. Therefore, in the case of a polydisperse polymer the height of the chromatogram at any point is due to the cumulative effect of the presence of many neighboring molecular weights. The amount of broadening observed is a function of the molecular weight, becoming larger as the molecular weight increases. The observed width is due to: (1) the actual *MWD*, (2) the spreading which occurs during flow through connecting tubing, (3) the effect due to spreading in the interstitial volume of the column packing, (4) the diffusional spreading within the pores, and (5) the effects of any adsorption within the system. The combined result may be not only spreading or broadening, but also skewing of the chromatogram.

Attempts to obtain analytical and numerical corrections for column broadening have been made by Tung and others [3–5], and the general state-of-the-art of GPC correction of broadening and skewing has been discussed by Hamielec [6, 7]. Fortunately, these effects tend to cancel out when the molecular weight distribution of a relatively broad material is obtained on a GPC column calibrated with much narrower fractions of the same material. Since the work reported here meets this condition, throughout this paper we assume that column broadening effects can be neglected. The validity of this assumption is discussed in section 9.

4. The Molecular Weight Distribution

In this section we describe the method used to calibrate the GPC. As stated in the preceding section, we assume that column broadening effects are not

significant. In the notation of Frank [8], the calibration curve and the elution chromatogram are respectively:

$$m = m(v) \tag{1}$$

$$Z(m) = N(v). \tag{2}$$

In (1) the molecular weight, m, is a function of the elution volume, v. $Z(m)$ is the number of molecules in the particular sample having molecular weights which are greater than m; conversely $N(v)$ is the number of molecules in the sample which elute at volumes which are less than or equal to v. We define $z(m)dm$ as the number of molecules having molecular weights between m and $m+dm$, such that:

$$-z(m) = dZ(m)/dm = (dN/dv)(dv/dm)$$

$$= (1/m')(dN/dv), \tag{3}$$

where m' is the slope of the calibration curve, $m(v)$ versus v.

For this development we assume that the height, h, of the chromatogram from the base line results solely from the presence of molecules all having the same molecular weight, m, for each corresponding elution volume, v. In particular it is assumed that the detector responds linearly to the mass of the sample. Thus:

$$mdN(v)/dv = kh(v) \tag{4}$$

Combining (3) with (4), we obtain:

$$z(m) = -kh/mm' \tag{5}$$

Here k is an unknown instrumental scaling factor. The number-, weight-, and z-average molecular weights M_n, M_w, and M_z are given by:

$$M_n = \frac{\int mz(m)dm}{\int z(m)dm} = \frac{\int (h/m')dm}{\int (h/mm')dm}$$

$$= \frac{\int h(v)dv}{\int [h(v)/m(v)]dv}, \tag{6}$$

$$M_w = \frac{\int m^2 z(m)dm}{\int mz(m)dm} = \frac{\int (mh/m')dm}{\int (h/m')dm}$$

$$= \frac{\int m(v)h(v)dv}{\int h(v)dv}, \tag{7}$$

$$M_z = \frac{\int m^2(v)h(v)dv}{\int m(v)h(v)dv}. \tag{8}$$

The integral *MWD* is obtained in the following fashion. We define a function $w(m)$ by

$$w(m) = kh(v) \tag{9}$$

Then the cumulative weight percent, i.e., the weight percent of polymer of molecular weight less than M, is given by

$$100 \int_0^M w(m)dm \Big/ \int_0^\infty w(m)dm.$$

The integral *MWD* is usually given as cumulative weight percent versus log molecular weight.

5. The Calibration Curve

In this section we will presuppose that the column selection has been made such that log m is a nearly linear function of v in the molecular weight range of interest. Further, we will assume that we already have a calibration curve for polystyrene using the same column set.

The development of the calibration curve for any particular polymer usually starts from the preparation and characterization of narrow molecular weight fractions. The molecular weight range covered by the fractions should at least encompass the expected distribution of any samples to be subsequently analyzed. By *classical* characterization methods such as osmometry and light scattering, the average molecular weights M_n and M_w are determined for each fraction. One of two general methods is then used in producing a reliable calibration. In the first method we define M_0 as being that molecular weight species which elutes at the peak of a chromatogram, and we assume that a reasonable value of M_0 can be assigned by knowing both M_n and M_w. In the second method we assume that, for each fraction, we know the general form of the calibration curve, eq (1).

A. Method One

In this development we assume that the peak molecular weight, M_0, can be approximated by:

$$(M_n + M_w)/2 = M_0. \tag{11}$$

This assumption would appear reasonable to a first approximation providing that the polydispersity, M_w/M_n, is sufficiently close to unity, and that the chromatogram is symmetrical and single-peaked. From the individual chromatograms of the fractions we can determine the elution volume v_0 corresponding to M_0.

A preliminary calibration curve is constructed using the pairs of M_0 and v_0 values, and a least-squares fitting routine is employed to determine whether the points can be best described by a first, a second, or a third degree polynomial. Comparison of this preliminary calibration curve with the polystyrene calibration curve obtained with the same column set, should show qualitative similarity, i.e., the inflection points and general curvature at all elution volumes should be similar. Next equations (6) and (7), in conjunction with the preliminary calibration curve, are used to calculate M_n's and M_w's from the GPC chromatograms of the individual fractions, and from the preliminary calibration curve we determine the corresponding elution volumes. We now use the values of M_n and M_w (classically determined) together with the elution volumes (GPC determined) and plot these points on the preliminary calibration curve. This type of plot should reveal that most of the calculated points fall on or near the calibration curve. However, if all the number-average molecular weight points lie on one side of the curve and all of the weight-average molecular weight points lie on the other side, this is usually an indication of extreme broadening and skewness of the chromatograms resulting from poor column selection or poorly chosen operational parameters.

Assuming that this latter possibility did not arise, we now refit the data, using only the classically determined M_n's and M_w's and their calculated elution volumes (GPC), and at this point we consider that the best fit has been obtained.

B. The Second Calibration Method

In this method we assume that for our narrow distribution fractions (M_w/M_n from 1.1 to 1.7) the portion of the calibration curve for each fraction will be adequately represented by the relationship:

$$m(v) = \exp(a - bv). \tag{12}$$

Of course we do not assume that the parameters a and b are the same for all fractions. Again following the development by Frank [8], we incorporate eq (12) into eqs (6) and (7). By using eq (12) in the denominator of (6) and in the numerator of (7), we obtain two expressions for the parameter a:

$$a_n = \ln M_n + \ln \int_0^\infty e^{bv} h(v)\, dv - \ln \int_0^\infty h(v)\, dv \tag{13}$$

and

$$a_w = \ln M_w + \ln \int_0^\infty h(v)\, dv - \ln \int_0^\infty e^{-bv} h(v)\, dv. \tag{14}$$

After equating a_n with a_w, simultaneous solution of eqs (13) and (14) yields unique values for the parameters a and b. If this were done for each fraction, a plot using eq (12) over the particular molecular weight range involved should result in a collection of straight lines which define the calibration curve exactly.

Both the first and second methods herein described have the disadvantage that M_n and M_w have to be known for each fraction; further, an error in either M_n or M_w seriously affects the calculation. A modification of the second method allows calibrational information to be obtained when only M_n or only M_w is known for a fraction, and, in addition, may provide insight into the question of whether or not error exists in M_n or M_w as determined classically.

Rather than solving eqs (13) and (14) simultaneously to obtain a unique pair of values for the parameters a and b, we can, by treating each equation separately, obtain the functional dependence of a_n and a_w on b over the range of values for which b may be expected to lie. Either equation (13) or equation (14) implies a functional relationship between a and b, i.e., $a = a(b)$. The calibration curve (or rather, our estimate of it based on one determination of M_n or M_w) is then one of the family of curves.

$$\ln m(v) = a(b) - bv, \tag{15}$$

and must therefore be tangent to the envelope of the family at some point. The envelope is easily obtained, in the usual way, as the simultaneous solution of eq (15) and the result of partial differentiation of eq (15) with respect to b at constant m and v, i.e.,

$$v = da/db. \tag{16}$$

For each point (v, $m(v)$) on the calibration curve, the abscissa v is given by eq (16) and the ordinate $m(v)$ by eq (15). A calibration curve may then be estimated from measurements of M_n and/or M_w on a series of fractions by plotting the envelope obtained for each measurement and requiring that the calibration curve be tangent or nearly so to each envelope at some point. Since this technique uses each experimental value of M_n and M_w independently, it can be useful in identifying individual molecular weight measurements which may be in error.

6. Experimental Procedures

All samples were dissolved in nitrogen-saturated, 1,2,4-trichlorobenzene (TCB) (filtered technical grade) at 135 °C using magnetic stirring. They were then filtered under nitrogen pressure through regenerated cellulose filters having an average pore size of 0.45 microns. The GPC column oven was operated at approximately 135 °C, and nitrogen-saturated TCB was used. Five hundredths of one percent by weight of 2,6-*di-tert.*-butyl-4-methylphenol was added to the TCB as an antioxidant.

We assumed that the calibration curve for polyethylene would be similar to that for polystyrene and hence selected the column combinations used herein because they produced a nearly linear polystyrene calibration curve.

The degree of replication which can be achieved in successive chromatograms resulting from a series of

identical experiments appears to be almost totally dependent upon base-line stability. Of the various factors affecting this stability, we found that the constancy of both fluid flow and temperature was the most important. We were fortunate in that our GPC was in an area in which both the air temperature and air circulation were well controlled, and this, coupled with stable line voltages, gave good temperature stability throughout the system. We found that the constancy of solvent flow could be improved upon by keeping both of the column throttle valves in their open position, regulating solvent flow solely by adjustment of the pumping stroke. Under these conditions a point by point comparison of the heights of the chromatograms resulting from supposedly identical experiments showed maximum deviations of approximately ± 1 percent, and a comparison of the areas of the chromatograms showed a maximum deviation of less than ± 2 percent. Uncertainties of this magnitude could be explained almost completely by the observed base-line instability.

A change in operating parameters may result in a change of the chromatogram obtained with gel permeation chromatography. Ideally, perhaps, one would like to use samples of very small size and of vanishing concentration together with very small flow rates, but, practically, one compromises by using samples whose size and concentration are such that good detector response is obtained, and a flow rate such that the experiment can be run in a reasonable amount of time. A large number of experiments were run, varying each of the operating parameters in turn. We found that between the extremes of 0.2 and 2.0 ml/minute no discernible change occurred in the chromatograms resulting from replicate experiments. We therefore chose to use 0.5 ml/minute as the flow rate which would be used. With the whole polymer (SRM 1475) a change in the concentration from 0.02 to 0.2 weight percent caused no observable change in the calculated weight versus elution volume distribution. We therefore chose to use a 0.1 weight percent concentration for the whole polymer. The acceptable range of concentration varied for each fraction, but we found that the use of concentrations such that the resulting viscosities were similar to that of the 0.1 weight percent of the whole polymer was a good workable rule. The detector response was such that for a 0.1 weight percent concentration of whole polymer, an injection time of two minutes was required to produce a 1/2 to 2/3 full scale deflection of the recorder pen at the peak elution, and this injection time was used throughout.

For the final calibration, three independently prepared concentrations of each calibrating material were used. For each material, the three concentrations were such as to cause peak heights of nearly full scale, one-half of full scale, or one-quarter of full scale. When any two chromatograms within each triplicate set were compared in respect to height ratio at each elution volume, or in respect to area ratios, these were, within the precision of the experiment, identical to the ratios of the known concentrations. Therefore, within the limits of our sensitivity, we believe that there was no dn/dc (refractive index change in respect to concentration) dependence with molecular weight. This observation is not in conflict with paper VII of this series [9], wherein, when greater sensitivity and precision was used, there indeed was shown to be a dn/dc dependence with molecular weight.

The integration of the chromatograms was performed numerically using Simpson's one-third rule, using an elution increment of 0.2 count.

7. Determination of the Calibration Curve

We used both polyethylene fractions and linear hydrocarbon samples in the determination of the calibration curve. Zone-refined samples of n-$C_{36}H_{74}$ and n-$C_{94}H_{190}$ were used. The values assigned to the hydrocarbon samples were the calculated molecular weights, and these calculated molecular weights were assigned to the peak elution volumes. Table 1 lists these materials together with the M_n and M_w values associated with each. These were determined by membrane osmometry and light scattering experiments. For details of the fractionation and of the determination of the molecular weights see papers VI, VIII and IX of this series [10–12]. Included also in table 1 are the GPC determined moments using the final calibration curve.

The calibration curve used in this work was determined by the use of method 1. For the preliminary determination of the calibration curve the chromatograms of the hydrocarbon samples and those of the fractions for which both M_n and M_w had been determined were used. As can be seen from table 1, the differences between the classical and GPC values of M_w for PE 350 and PE 60 do not appear consistent with those for the other fractions. The same discrepancies are shown when method 2 is employed (see fig. 2), and as a result we did not use the M_w values for these two fractions in the final determination of the calibration curve. In addition the M_w values for PE 200 and PE 20 were not available and only M_n values were employed. A plot of the final calibration curve is shown in figure 1, together with the points corresponding to M_0, M_n, and M_w for the fractions and the hydrocarbons.

The best least squares fit, using Method 1, was found to be a quadratic of the form ($\log M = a + bv + cv^2$), having the following coefficients and standard deviations:

$$\begin{aligned} a &= 7.4 \quad \pm 1.2 \\ b &= 0.106 \pm 0.07 \\ c &= -0.0051 \pm 0.0009 \end{aligned}$$

The standard deviation of the molecular weight was ± 0.047 $\log M$ units. The volume v is in units of count.

Method 2 was also investigated. Figure 2 shows the calibration curve as derived by method 1, together with the envelope plots for each material used in the calibration. Figure 3 shows the same calibration curve, superimposed on which are the individual line segments calculated for the individual calibrating materials. The unusual behavior associated with the two

TABLE 1. *Classic versus gel permeation chromatographic analysis of polyethylene fractions used in calibration procedure*

Sample	$M_n \times 10^{-4}$ [a]	$M_w \times 10^{-4}$ [b]	M_w/M_n	GPC analysis[c] $M_n \times 10^{-4}$	GPC analysis[c] $M_w \times 10^{-4}$	GPC analysis[c] M_w/M_n
PE600	35.5	68.8	1.9	39	67	1.7
PE350	24.1	[d] 52.0	2.2	26	40	1.5
PE200	20.1	.....	.....	21	32	1.5
PE180	14.3	21.0	1.5	14.0	21	1.5
PE120	11.2	17.0	1.5	12.2	16	1.3
PE60	6.1	[d] 8.22	1.3	6	6.9	1.2
PE40	4.97	4.94	1.0	4.6	5.2	1.1
PE20	2.07	.....	.....	2.2	2.5	1.1
PE15	1.35	1.91	1.4	1.4	1.6	1.1
C_{94} Calc $M = 0.132 \times 10^4$			(1.00)	0.146	0.154	1.05
C_{36} Calc $M = 0.0506 \times 10^4$			(1.00)	.047	.049	1.04

[a] = results from membrane osmometry.
[b] = results from light scattering.
[c] = results of using the samples to calibrate the GPC, then analyzing the samples using calculated calibration curve.
[d] Not employed in construction of calibration curve. See text.

hydrocarbon samples results from using their calculated molecular weight to describe both M_n and M_w in eqs (13) and (14), and the slopes of these lines probably reflect the column dispersion. While the calibration curve was determined solely by method 1, it is obvious from figures 2 and 3 that method 2 would have produced a nearly identical curve.

It was interesting to note that the polyethylene calibration curve remained unchanged for approximately a year of continuous running. Immediately after starting up there would be an apparent shift of calibration, but the columns would return to their previous state after approximately 48 hours of running time. During this year the solvent and the general operational parameters were not changed.

8. Analysis of SRM 1475

The data in table 2 result from the analysis of twelve samples of SRM 1475, listed as samples 1 through 12. Each of the twelve samples was prepared from 25–75 pellets as described in section 6. The mean values and sample standard deviations of the mean for M_n, M_w,

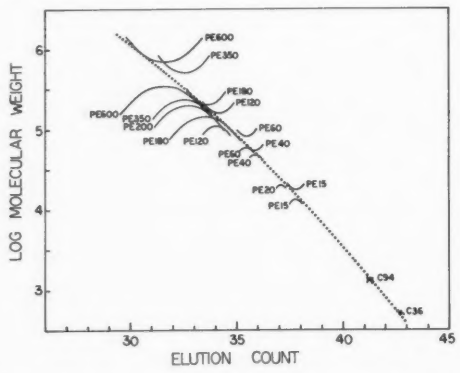

FIGURE 2. *The calibration curve derived by use of Method One (dotted line) together with the calculated envelopes for each calibration sample.*

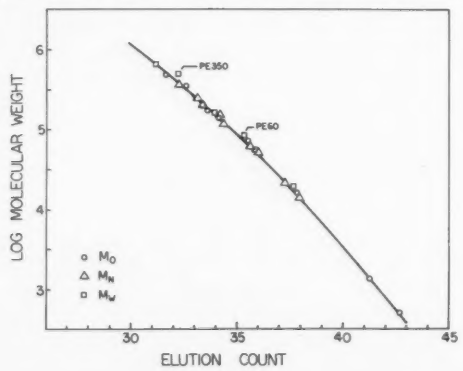

FIGURE 1. *The calibration curve derived by use of Method One, showing all calibration points.*

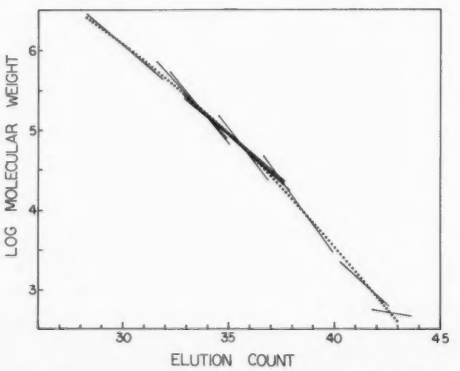

FIGURE 3. *The calibration curve derived by use of Method One (dotted line) together with the calculated line segments for each calibration sample for which both* M_n *and* M_w *are known.*

and M_z are those shown on the certificate for SRM 1475.

TABLE 2. *Gel permeation chromatographic analysis of SRM 1475*

Sample number	$M_n \times 10^{-4}$	$M_w \times 10^{-4}$	$M_z \times 10^{-5}$
1	1.833	5.503	1.518
2	1.789	5.309	1.490
3	1.681	5.013	1.291
4	1.726	5.247	1.369
5	1.921	5.451	1.351
6	2.019	5.149	1.200
7	2.068	5.400	1.243
8	1.820	5.065	1.220
9	1.883	5.538	1.534
10	1.789	5.310	1.489
11	1.657	5.032	1.277
12	1.789	5.669	1.583
Mean	1.831	5.307	1.380
Estimated standard deviation	0.125	0.214	0.127
Estimated standard deviation of mean	.036	.062	.037

Samples 1 through 4 were also subjected to a modified treatment, in order to check the effects of the handling procedure. After the solutions had been made up as described in section 6, and aliquots taken for the original chromatograms, the remaining portions of the solutions were allowed to cool to room temperature, precipitating the polymer, reheated and stirred as before to redissolve the material, and fresh aliquots rerun on the GPC column. The results obtained for the original and rerun materials are shown in table 3. If degradation or other modification of the sample occurred in the handling procedure, one might expect to find trends in the results for the original and rerun materials. No such trends are apparent, and the differences between original and rerun values are not inconsistent with the sample-to-sample spreads implied by the sample standard deviations given in table 2. We conclude that the effects of our sample handling procedure are not observable.

TABLE 3. *Effect of rerunning SRM 1475 samples*

Sample Number	$M_n \times 10^{-4}$	$M_w \times 10^{-4}$	$M_z \times 10^{-5}$
1	1.833	5.503	1.518
1, rerun	1.852	5.374	1.363
2	1.789	5.309	1.490
2, rerun	1.741	5.296	1.469
3	1.681	5.013	1.291
3, rerun	1.674	5.196	1.410
4	1.726	5.247	1.369
4, rerun	1.745	5.276	1.395

The integral *MWD* was obtained by summing the chromatograms for samples 1 through 12. In view of the lack of trend in the reruns of samples 1 through 4 described above, the rerun chromatograms were included in the final sums. The resulting molecular weight distribution is given in table 4 and on the certificate for SRM 1475. Since this distribution is based on an "average" chromatogram, the values of M_n, M_w, and M_z obtained from it will not necessarily agree precisely with those quoted in table 2, which are obtained by averaging molecular weights from the individual chromatograms. From the *MWD*, we obtain values of 17,900, 52,900, and 139,000 respectively for M_n, M_w, and M_z. These may be compared with the values 18,310, 53,070, and 138,000, respectively, shown in table 2.

TABLE 4. *Cumulative molecular weight distribution of SRM (1475) by gel permeation chromatography*

log M	Wt. percent	log M	log M percent	log M	Wt. percent
2.800	0.0	4.014	15.2	5.065	90.7
2.865	.005	4.070	18.1	5.113	92.2
2.929	.020	4.126	21.5	5.161	93.7
2.992	.052	4.182	25.2	5.209	94.8
3.056	.105	4.237	29.3	5.256	95.8
3.119	.185	4.292	33.7	5.303	96.6
3.181	.343	4.346	38.5	5.349	97.3
3.243	.475	4.400	43.4	5.395	97.9
3.305	.706	4.454	48.5	5.440	98.4
3.366	.999	4.507	53.5	5.485	98.7
3.427	1.38	4.560	58.3	5.530	99.1
3.488	1.88	4.612	62.9	5.574	99.3
3.548	2.51	4.664	67.3	5.618	99.5
3.607	3.30	4.715	71.4	5.662	99.7
3.667	4.28	4.776	75.1	5.705	99.8
3.725	5.46	4.817	78.5	5.789	99.9
3.784	6.87	4.868	81.6	5.87	100.0
3.842	8.56	4.918	84.4		
3.900	10.50	4.967	86.7		
3.957	12.7	5.016	88.9		

9. Discussion and Conclusion

For both calibration and analysis, no corrections have been applied to take into account the effects of column broadening in the GPC system. While such effects are obviously present, it would appear that in this particular case, they do not significantly affect the validity of the analysis. Evidence to this effect may be found in the general agreement between values of M_w/M_n obtained from the chromatograms of the individual fractions and the classically determined ratios. Since SRM 1475 is substantially broader than the individual fractions, we conclude that column broadening effects are not likely to introduce serious errors into the molecular weight distribution obtained for SRM 1475.

The internal consistency of the experiment was checked by comparing chromatograms obtained from sixteen fractions of a sample of SRM 1475 with the chromatogram of the whole polymer. The polymer was fractionated into sixteen fractions using a conventional column elution technique [10]. The fractions were analyzed using GPC, and the areas under the result-

ing chromatograms were normalized to the weight of the respective fraction. These normalized curves were summed. When this reconstructed "whole polymer" was analyzed, the number- and weight-average molecular weights were calculated to be 17,400 and 53,300 respectively, whereas the best GPC values for the whole polymer were calculated as 18,300 and 53,100.

The results given herein reflect primarily on the precision of the measurement. A statement as to the absolute accuracy is impossible at this time; however, it is our opinion that the errors reflected in the uncertainty of the GPC analysis are largely those associated with the light scattering and membrane osmometry analyses of the calibrating samples.

Individual credit has not been given to some of the specific experimental and analytical details used herein. In many instances original credit is not known, but a great many of these details are to be found in references [8, 13, and 14].

10. References

[1] Moore, J. C.: J. Polymer Sci. A **2**, 835 (1964).

[2] Determan, H., Gel Chromatography, Chap. 3 (Springer-Verlag, New York, N.Y. 1968).

[3] Tung, L. H., J. Appl. Polymer Sci. **10**, 375 (1966).

[4] Tung, L. H., Moore, J. C., and Knight, G. W., J. Appl. Polymer Sci. **10**, 1261 (1966).

[5] Hess, M., and Kratz, R., J. Polymer Sci. A 2, **4**, 731 (1966).

[6] Hamielec, A., Proceedings of the 6th International GPC Seminar, Miami Beach, Fla. (1968).

[7] Duerksen, J. H., and Hamielec, A. C., J. Polymer Sci. C **21**, 83 (1968).

[8] Frank, F. O., Ward, I. M., and Williams, T., Proceedings of the 5th International GPC Seminar, London (1968).

[9] Wagner, H. L., J. Res. Nat. Bur. Stand. (U.S.), **76A** (Phys. and Chem.), No. 2, 151–155 (Mar.–Apr. 1972). Paper VII of this series.

[10] Christensen, R. G., J. Res. Nat. Bur. Stand. (U.S.), **76A**, (Phys. and Chem.), No. 2, 149–150 (Mar.–Apr. 1972). Paper VI of this series.

[11] Frolen, L. J., Ross, G. S., Wims, A., and Verdier, P. H., J. Res. Nat. Bur. Stand. (U.S.). **76A** (Phys. and Chem.), No. 2, 156–160 (Mar.–Apr. 1972). Paper VIII of this series.

[12] Brown, J. E. and Verdier, P. H., J. Res. Nat. Bur. Stand. (U.S.), **76A** (Phys. and Chem.), No. 2, 161–163 (Mar.–Apr. 1972). Paper IX of this series.

[13] Moore, J. C., Proceedings of the 4th International GPC Seminar, Miami Beach, Fla. (1967).

[14] Yau, W. W., Suchan, H. L., Malone, C. P., and Fleming, S. W., Proceedings of the 5th International GPC Seminar, London (1968).

(Paper 76A2–715)

JOURNAL OF RESEARCH of the National Bureau of Standards—A. Physics and Chemistry
Vol. 76A, No. 2, March–April 1972

Publications of the National Bureau of Standards*

Selected Abstracts

Abramowitz, S., Levin, I. W., **Raman spectra of the hexahalogenated benzenes in the solid phase,** *Spectrochim. Acta* **26A,** *2261–2268 (1970).*

Key words: Hexahalogenated benzenes; molecular structure; Raman spectra; vibrational assignment.

Solid Raman spectra of the hexahalogenated benzenes are examined at both room and liquid nitrogen temperatures. Tentative assignments for C_6Cl_6, C_6Br_6, and C_6I_6 are proposed on the basis of a puckered (D_{3d}) geometry.

Alexandropoulos, N. G., Parks, S. H., Kuriyama, M., **Polarization of the x-ray Compton-Raman radiation,** *Physics Letters* **35A,** *No. 5, 369–370 (June 28, 1971).*

Key words: Azimuthal angle; Compton-Raman interaction; Hamiltonian; polarization; radiation; spectrometer.

The spectrum of x-ray Compton-Ramon scatter at 90° has been analyzed at several azimuthal angles. The relation between the recorded intensity and the angle is given as $\cos^2 \Phi$ dependence. The reported observation indicates that the A^2 term of the coupling Hamiltonian is the leading one.

Baker, M. A., **1939 Exposure test of porcelain enamels on steel 30-year inspection,** *Nat. Bur. Stand. (U.S.), Bldg. Sci. Ser.* **38,** *9 pages (Aug. 1971) 25 cents, SD Catalog No. C13.29/2:38.*

Key words: Acid resistance; color; gloss; porcelain enamel; weather resistance.

The weather resistance of 192 porcelain enameled panels representing 14 enamel types was evaluated after being exposed for 30 years at Washington, D.C. A direct correlation was found between the acid resistance and weather resistance of the enamels tested. The porcelain enamel protected the base metal from corrosion if the initial coverage was complete.
Similar evaluations and findings were made on 58 panels representing 13 enamel types that were added to this test in 1947.

Bardos, D. I., Waterstrat, R. M., Rowland, T. J., Darby, J. B., Jr., **The magnetic susceptibility of transition-metal A15-type phases,** *J. Low Temp. Phys.* **3,** *No. 5, 509–518 (1970).*

Key words: Atomic ordering; intermetallic compounds; magnetic susceptibility; superconductors.

The temperature dependence of the paramagnetic susceptibility was measured for several binary A15–type compounds of transition elements. Measurements were made between room temperature and either 3 K or the super-conducting transition temperature, whichever was higher. The susceptibilities were found to have, in most cases, a small linear temperature dependence. Molar susceptibilities χ_M, superconducting transition temperatures T_c, and electronic specific-heat coefficients γ for these compounds, when plotted as a function of the valence electron concentration e/a, reveal peaks at an e/a of about 6.5 for all three properties. Compounds containing the 4*d* series transition elements molybdenum or niobium have higher T_c and lower χ_M values than compounds containing the 3*d* transition element chromium or vanadium. It appears that an increased mixing of atoms on either of the two crystallographic sites in the A15-type structure can be associated with a significant decrease in the paramagnetic susceptibility of the compound.

Benjamin, I. A., **Research needs in fire and smoke control,** *Proc. Symp. Fire Hazards in Buildings, Semiannual Meeting, American Society of Heating, Refrigerating and Air-Conditioning Engineers, San Francisco, Calif., Jan. 19–22, 1970, pp. 35–38 (1971).*

Key words: Building design; dampers; ducts; fire control; fire spread; smoke movement.

The author discusses problems associated with the movement of smoke and fire in buildings and reviews some of the current design requirements. Selected areas of needed research are pointed out and mention is made of some of the work being conducted by the Fire Research Section of the National Bureau of Standards.

Bennett, H. S., **Two-electron F^- centers in the alkaline-earth fluorides,** Phys. Rev. B. **4,** *No. 4, 1327–1335 (August 15, 1971).*

Key words; Alkaline earth; color centers; fluorides; F^- centers.

The Hartree-Fock-Slater equations for the two electron orbitals localized about an anion vacancy in CaF_2, SrF_2, and BaF_2 have been solved numerically in the point-ion-lattice potential. It is found that only the ground state ^1S (1*s*, 1*s*) contains spatially compact (bound) electronic orbitals. The existence of bound excited states for the F^- center in these crystals has been investigated. However, definitive statements on such excited states are not available at present.

Blunt, R. F., Candela, G. A., Forman, R. A., Kahn, A. H., Mangum, B. W., **Magnetic susceptibility and optical studies of Cr^{3+} in Al_2O_3 (Ruby): Magnetic method for determining concentration,** *J. Appl. Phys.* **42,** *No. 8, 3058–3062 (July 1971).*

Key words: Concentration determination; magnetic susceptibility; optical absorption coefficient; radiation damage; ruby.

Magnetic susceptibility and optical absorption measurements were performed on ruby samples of varying chromium concentration. Susceptibilities were measured by the Faraday method, both with and without selective microwave saturation of the Cr^{3+} susceptibility at resonance. The susceptibility values were used to calculate the Cr^{3+} concentrations, and these together with the optical absorption used to obtain the "molar" absorption coefficients. The absorption coefficient of 56.8 ± 0.2 cm^{-1} per wt % equivalent Cr_2O_3, for both the 0.40 and 0.56 μm band maxima ($E \perp c$) resulted. A Co^{60} γ-irradiation was performed and the susceptibility was unchanged within experimental error.

Bowen, R. L., Argentar, H., **Amine accelerators for methacrylate resin systems,** *J. Dental Res.* **50,** *No. 4, 923–928 (July–August 1971).*

Key words: Amine accelerators; aromatic amines; color stability; methacrylate esters; polymerization; synthesis.

Tertiary aromatic amines were synthesized with various nitrogen and ring substituents, They were compared with commercial homologues using composites based on dimethacrylate monomer formulations containing benzoyl peroxide. Equimolar amounts of the different amines were the only variables. Although accelerating ability was a function of both ring and nitrogen substitution, color stability was influenced more by the substituents on the ring than by the substituents on the nitrogen.

Boyd, M. E., Larsen, S. Y., **First quantum-mechanical correction to the classical viscosity cross section of hard spheres,** *Phys. Rev. A.* **4,** *No. 3, 1155–1163 (Sept. 1971).*

Key words: Boltzmann gas; cross-section for viscosity; hard sphere gas; quantum corrections; statistical mechanics; viscosity.

The classical and first quantum correction terms in a high-energy expansion of the viscosity cross section $Q^{(2)}$ for a Boltzmann gas of hard spheres is derived. The first correction is found to be proportional to $(1/k\sigma)^{4.3}$, which is a term nonanalytic in $\hbar$ (i.e., $\hbar^{4.3}$), and the results from scattering near the edge of the sphere. A bound is established showing the remainder of the asymptotic series to be of $0[\ln(k\sigma)/(k\sigma)^2]$. This asymptotic formula is compared with calculations based on the exact phase-shift expressions and its range of validity is established. The next correction terms are deduced to be proportional to $(\ln k\sigma)/(k\sigma)^2$ and $1/(k\sigma)^2$ which involve $\hbar^2 \ln h$ and $\hbar^2$, respectively.

Breden, L. H., Technical Standards Coordinator, **Fluorinated ethylene-propylene (FEP) plastic tubing,** *Nat. Bur. Stand. (U.S.), Prod. Stand. 43–71, 12 pages (Sept. 1971) 10 cents, SD Catalog No. C13.20/2:43–71.*

Key words: Chemical, mechanical, and electrical tubing; FEP tubing; fluorocarbon plastic tubing; plastic tubing, fluorinated ethylene-propylene; tubing, FEP-fluorocarbon.

This Voluntary Product Standard covers plastic tubing made from fluorinated ethylene-propylene (FEP) resin intended for chemical, mechanical, or electrical use. It provides requirements and methods of test for materials, dimensions, and physical and chemical properties of FEP tubing. A method for identifying products which comply with this standard is provided.

Breden, L. H., Technical Standards Coordinator, **Heat-shrinkable fluorocarbon plastic tubing,** *Nat. Bur. Stand. (U.S.), Prod. Stand. 47–71, 14 pages (Sept. 1971) 20 cents, SD Catalog No. C13.20/2:47–71.*

Key words: FEP heat-shrinkable tubing; fluorocarbon plastic heat-shrinkable tubing; plastic tubing, fluorocarbon; PTFE heat-shrinkable tubing; tubing, heat-shrinkable fluorocarbon plastic.

This Voluntary Product Standard covers commercially available PTFE and FEP plastic tubing which can be reduced to a predetermined inside diameter by the application of heat. Included are requirements and methods of test for materials, dimensions, and physical and electrical properties. A method for identifying products which comply with this standard is provided.

Brenner, A., Sligh, J. L., **Electrodeposition of magnesium and beryllium from organic baths,** *Trans. Inst. Metal Finishing* **49,** *71–78 (May 1971).*

Key words: Beryllium; beryllium azide; beryllium thiocyanate; decaborane; dimethyl beryllium; electrodeposition of; Grignard reagents; magnesium; non-aqueous plating baths; organic plating baths; triethylboron.

Solutions that are feasible for electrodepositing magnesium were prepared from Grignard reagents with the addition of boranes in ether solutions. A typical bath consisted of methylmagnesium chloride, 3-molar, (dissolved in tetrahydrofuran) and 1-molar in triethylboron. The deposits were white, ductile and contained at least 99% of Mg. Cathode and anode current efficiencies were 100%. A similar beryllium plating solution, prepared with beryllium dimethyl and decaborane, yielded dark grey, coherent deposits containing 85% to 90% beryllium.

Broadhurst, M. G., Mopsik, F. I., **Normal mode calculation of Grüneisen thermal expansion in *n*-alkanes,** *J. Chem. Phys.* **54,** *No. 10, 4239–4246 (May 15, 1971).*

Key words: Entropy; Grüneisen relation; quasiharmonic; semirigid; specific heat; thermodynamic.

The normal mode problem is solved for a semirigid chain of beads in a quasiharmonic potential in order to separate the inter- and intrachain parts of the specific heat. The effects of lattice vibrations are included in an approximate way. The usual Grüneisen relation, $\alpha B_T = \gamma C_v/V$, valid only for acoustical modes, is generalized for optical modes to give $\alpha B_T = \Sigma_j(\gamma_j/V)\ (\partial S_j/\partial \ln \omega_{j\max})$, where S_j and $\omega_{j\max}$ are the entropy and frequency cutoff of mode j. The predicted thermodynamic properties of the system are unusually sensitive to chain length because of interchain thermal energy effects. The parameters are given values from independent solid *n*-alkane data, and the calculated results are shown to predict quite well experimental C_p and V–T behavior of the *n*-alkanes.

Cali, J. P., Seward, R. W., **The challenge of the 70's NBS standard reference materials program,** *Am. Lab.* **3,** *No. 6, 10–14 (June 1971).*

Key words: Agriculture; air and water pollution; biology; botany; health and medicine; instrument calibration; metrology; research materials; standard reference materials; SRM's; Standard Reference.

The direction the National Bureau of Standards' Standard Reference Materials program will take in the next decade is outlined with emphasis on those areas that have only recently been included in the SRM program such as health, pollution, botany, biology and agriculture, and also on areas in which no SRM's now exist. As the program moves into these new areas, the traditional industry-oriented aspects of the program will be maintained and improved through close cooperation with such standards-making bodies as ASTM and ANSI.

Carter, R. S., **The NBS reactor as a source of neutrons,** *Proc. American Nuclear Society Topical Meeting on Neutron Sources and Applications, April 19–21, 1971, Augusta, Ga.,* 2, 1-10-1–17 *(April 1971).*

Key words: High flux; irradiation facilities; neutron source; and reactor.

The NBS Reactor (NBSR) is a 10 Mw D_2O moderated and reflected reactor. The fuel elements are located seven inches apart in hexagonal arrays around experimental irradiation facilities. In order to support the broad range of research programs typical of a laboratory like the NBS the reactor has extensive in-core, beam tube, and pneumatic tube facilities. Thermal neutron fluxes in the beam tubes and higher-flux irradiation facilities are about 10^{14} n/cm^2-s. Several unique features of the NBSR contribute to its versatility. They include a thermal column with cadmium ratios for gold foils as high as 30,000 to 1, a split core to minimize the intensity of very high energy neutrons in the beam tubes, and a cold neutron source to enhance the intensity of very low energy neutrons available for certain inelastic scattering experiments. Extensive, automated experimental facilities have been developed to fully utilize the neutron beams and irradiations provided by the NBSR.

Cassidy, E. C., Cones, H. N., Booker, S. R., **Development and evaluation of electrooptical high-voltage pulse measurement techniques,** *IEEE Trans, Instr. Meas.* **IM-19,** *No. 4, 395-402 (Nov. 1970).*

Key words: Electro-optical measurements; high voltage measurements; Kerr cell; pulse measurements.

Use of the Kerr electrooptical effect for time-resolved pulse measurements is extended to the 300-kV level. Pulse durations are as short as 5 μs. The performance of systems equipped with Kerr cells of various designs is investigated under a variety of operating conditions. Calibrations are achieved using both pulse-divider and high direct-voltage techniques. Methods are devised for measurement and correction of errors resulting from the fringing electric field at the ends of the Kerr-cell electrodes. Measurements of the temperature coefficient of the Kerr-cell constant are also included.
The pulse waveform is reconstructed from typical Kerr-system results by automatic computation and compared with simultaneous time-resolved pulse-divider measurements. Comparisons at the peak

of the pulse, where a "slideback" technique is used to enhance the resolution of the divider measurement, demonstrate agreement to better than 1 percent.
In addition, a novel technique is developed for measurement of the pulse magnitude from photographs of the Kerr-effect fringe patterns produced by passing an expanded, pulsed laser beam through the system. By this approach, voltage is measured optically without use of sophisticated electrical metering instrumentation.

Cezairliyan, A., **Measurement of the variation of normal spectral emittance of tantalum during melting by a pulse heating method,** *High temperatures-High Pressures* **2,** *501–506 (1970).*

Key words: Emittance; high-speed measurements; melting; normal spectral emittance; tantalum; thermal radiation properties.

A pulse heating method was used to measure the change in normal spectral emittance (at 650 nm) of tantalum as a function of the change in electrical resistance during the initial melting period. Duration of an individual experiment in which the specimen was heated from room temperature to its melting point was approximately 400 ms. The partial melting period was approximately 100 ms. A millisecond resolution photoelectric pyrometer was used for temperature measurements. The recordings of experimental quantities were made with a digital data acquisition system which has a full-scale signal resolution of approximately one part in 8000 and a time resolution of 0.4 ms. It was found that normal spectral emittance decreased by approximately 3.5 percent during the initial one third of the melting period.

Chandler, H. H., Bowen, R. L., Paffenbarger, G. C., **Method for finishing composite restorative materials,** *J. Am. Dental Assoc.* **83,** *No. 2, 344–348 (August 1971).*

Key words: Composite restorative materials; finishing; operative dentistry; polishing; surface finish.

An instrument, designed to finish the surface of composite restorative materials, was made by bonding 1μ to 5μ diamond particles to flexible paper disks. The surface finish produced by this instrument was superior to that obtained by fine cuttlefish disks and inferior to surfaces obtained by the hardening of the material in contact with polished glass. Results are presented with use of scanning electron photomicrographs.

Chandler, H. H., Bowen, R. L., Paffenbarger, G. C., **Physical properties of a radiopaque denture base material,** *J. Biomed. Mater. Res.* **5,** *335–357 (July 1971).*

Key words: Composite materials; denture base materials; physical properties; prosthetic materials; radiopacity-radiopaque.

Physical properties were determined for radiopaque composite denture base materials consisting of poly(methyl methacrylate) as the matrix and 30, 40, and 50% by weight of a silane-treated barium fluoride-containing glass powder as the reinforcing filler. Specimens without glass were included for comparison.
All of the materials met the requirements of ADA Spec. No. 12 for Denture Base Polymer except that the material containing 50% glass had less deflection than the minimum required at the 5000-g load in transverse testing.
There was little or no difference among the materials with respect to hardness, indentation resistance, water sorption, color stability, and resistance to drop impact.
Addition of glass to the 30% level decreased the transverse strength while 50% glass specimens had slightly greater transverse strengths as compared to specimens with no glass. In general, the addition of glass increased the time to reach the packing stage, densities, and Young's bulk, shear, and flexural moduli, had only slight effect on solubility and decreased the cold-cure repairability and the coefficient of linear thermal expansion.
The solubility of the glass powder was about four times that of powdered porcelain teeth after 24 h, and totaled 0.55% after 5 days.

Chandler, H. H., Bowen, R. L., Paffenbarger, G. C., **Radiopaque denture base materials technic dentures,** *J. Biomed. Mater. Res.* **5,** *359–371 (July 1971).*

Key words: Composites; dentures; denture base materials; dimensional stability; foreign bodies; prosthetics; radiopacity; silane bonding.

Technic dentures were made using composite base materials containing 30, 40, and 50 wt % of a silane-treated, radiopaque, powdered glass as the reinforcing filler and poly(methyl methacrylate) as the matrix. Dentures containing no glass were included for comparison. Molar-to-molar dimensional changes, effects of silane treatment of the porcelain teeth and handling and finishing characteristics were determined.
Dentures containing glass had less dimensional change during curing and subsequent water storage than those without glass. Thick upper dentures exhibited the least change and thin lowers, the most. The differences in the magnitudes of the changes would not be clinically noticeable.
Silane treatment of the porcelain teeth in thick upper dentures resulted in breakage of the posterior teeth in almost all instances. Posterior teeth also fractured in thick upper dentures containing 40 and 50% of the silane-treated glass even though the teeth were not treated with silane.
Mixing and molding properties of the composite materials, while accepting characteristics were definitely inferior in that it was more difficult and time-consuming to attain the final surfaces and these surfaces were not as smooth as those in dentures without glass.

Chang, S. S., Bestul, A. B., **Heat capacities of cubic monoclinic, and vitreous arsenious oxide from 5 to 360 °K,** *J. Chem. Phys.* **55,** *No. 2, 933–946 (July 15, 1971).*

Key words: Arsenious oxide; crystalline; cubic crystal; entropy; heat capacities; transition.

Experimentally determined heat capacities, C_p, precise to better than 0.1%, and derived thermal data are reported for cubic and monoclinic crystalline and vitreous arsenious oxide at temperatures from 5 to 360 °K. C_p for the glass is higher than for either crystal at all temperatures. C_p's for the cubic crystal are lower than those for the monoclinic between about 20 and 310 °K and higher at temperatures below and above this range. C_p/T^3 for the glass is still increasing with decreasing temperature at 5 °K, although C_p/T^3 for both crystals peaks a few degrees above this. C_p's reported here for the monoclinic crystal are grossly different from those previously reported by Stranski's school. The corresponding entropy difference between the two crystals at 298.15 °K reported here is 5.9 ± 0.2 J deg^{-1} · mol^{-1}, whereas that previously reported from C_p measurements by Stranski's school was 14.4 J deg^{-1} · mol^{-1}. Combined with a value newly obtained elsewhere for the enthalpy difference between the two crystals at 298.15 °K, the value reported here for the entropy difference yields a transition temperature between them of 311 ± 30 °K, which is in the range currently cited on other bases. C_p values reported here for the cubic crystal and the glass are consistently 4%–5% lower than those previously reported by Tarasov's school, suggesting a systematic proportional effect of the magnitude in those previous values. The proportionality of C_p to T for the cubic crystal from 65 to 160 °K, previously erroneously attributed to the monoclinic crystal by Tarasov on the basis of Anderson's C_p data, are discussed.

Chang, T-T, Cohen, M. I., Hosler, W. R., **Superhyperfine interactions in CdF_2 : Yb,** *J. Chem. Phys.* **54,** *No. 10, 4278–4280 (May 15, 1971).*

Key words: Cadmium fluoride; EPR; superhyperfine interaction; ytterbium.

The superhyperfine structure of Yb^{3+} in CdF_2 has been observed. Fitting of the structure was done according to the model of Ranon and Hyde. The principal values of the interaction tensor T were approximated to be -16.7 MHz for $T_\perp$ and 37.8 MHz for $T_{||}$.

Clifton, J. R., Mathey, R. G., **Interrelations between cement and concrete properties, Part 6,** *Nat. Bur. Stand. (U.S.), Bldg. Sci. Ser. 36, 118 pages (Aug. 1971) $1.25, SD Catalog No. C13.29/36.*

Key words: Cement; chemical composition; concrete; durability; material properties; physical properties.

Data are presented on the properties of Portland cements, mortars and concretes from a long term study reported principally by Blaine and Arni.
These data are from laboratory studies and cover a wide range of cements and concretes. A total of 199 different cements were included in the study.

Cohen, J., Edelman, S., Vezzetti, C. F., **Pyroelectric effect in polyvinylfluoride, Nature (London),** *Phys. Sci.* **233,** *12 (Sept. 6, 1971).*

Key words: Infrared; piezoelectricity; polyvinylfluoride; pyroelectricity.

Significant infra-red sensitivity has been obtained in oriented polyvinylfluoride, apparently due to pyroelectricity.

Creutzberg, F., Hougen, J. T., **Rotational line intensities for singlet-triplet transitions in molecules belonging to the point groups D_{2h}, C_{2v}, and D_2,** *J. Mol. Spectry.* **38,** *No. 2, 257–272 (1971).*

Key words: Asymmetric rotors; matrix elements; rotational line intensities; singlet-triplet transitions; spin forbidden transitions; transition calculations.

Explicit expressions are presented for transition moment matrix elements and Hamiltonian matrix elements which can be used directly in computer programs for calculating rigid rotor line intensities for singlet-triplet transitions in molecules belonging to the point groups D_{2h}, C_{2v}, and d_2. The calculational procedure outlined and the various matrix elements presented can be used for triplet states exhibiting large or small spin splittings in the nonrotating molecule.

Devereux, C. W., Technical Standards Coordinator, **Body measurements for the sizing of women's patterns and apparel,** *Nat. Bur. Stand. (U.S.), Prod. Stand. 42–70, 29 pages (Sept. 1971) 40 cents, SD Catalog No. C13.20/42–70.*

Key words: Apparel, women's; body measurements, women's; classifications, women's size; grading charts, women's size; pattern size, women's; size designations, women's; span charts, women's sizing.

This Voluntary Product Standard covers standard size classifications, size designations, and body measurements to aid in the consistency of sizing of women's apparel and, by doing so, provides a means for the consumer to identify her body type and size for proper fit. This standard also covers applications of the system, definitions, methods of measurement, adjustments to compensate for the effect of foundation garments, spanning charts, and a recommended method of identification. The measurements given in this standard are body, not garment, measurements.

Durst, R. A., Duhart, B. T., **Ion-selective electrode study of trace silver ion adsorption on selected surfaces,** *Anal. Chem.* **42,** *No. 9, 1002–1004 (1970).*

Key words: Electrometric study of silver adsorption; silver adsorption; silver ion-selective electrode; trace silver determination.

This study demonstrates the feasibility of using a silver ion-selective electrode for monitoring silver ion losses in long-term investigations of trace silver adsorption on various container surfaces. The electrometric technique offers the advantages of less complex and costly equipment, simplified procedure, and improved precision over the radiometric method. Nernstian electrode response was observed down to 4×10^{-7} M silver. For maximum sensitivity, 2×10^{-6} M (0.2 ppm) silver was selected as the concentration for the test solution which was placed in Pyrex, Desicoted Pyrex, polyethylene, Vycor, and Teflon containers. At various intervals up to 46 days, duplicate EMF readings were made on each of the five solutions with periodic restandardization of the electrode to permit drift corrections. Adsorption levels at the end of 30 days increased in the order: Vycor < polyethylene ≈ Teflon < Desicoted Pyrex < Pyrex; ranging from 28% adsorption for Vycor to 48% for Pyrex. Although for periods of up to a day, silver losses on Teflon were less than 2%, this study indicates that none of the above materials is suitable for long-term storage of solutions containing low levels of silver.

Evans, J. P., Wood, S. D., **An intercomparison of high temperature platinum resistance thermometers and standard thermocouples,** *Metrologia* **7,** *No. 3, 108–130 (July 1971).*

Key words: Calibration; fixed point; freezing point; furnaces; high temperature; IPTS–68; platinum resistance thermometer; temperature scale; thermocouple; triple point.

To obtain some of the information necessary for redefining a practical temperature scale in terms of resistance thermometry up to the gold point, we have intercompared nine high temperature platinum resistance thermometers and eight standard thermocouples at 50 degree intervals over the range 630.74 to 1064.43 °C. Values of temperature were derived from "before and after" calibrations of the instruments at the freezing points of gold, silver, antimony, zinc, and tin, and at the triple point of water.—Analysis of the data showed that the standard deviation of temperatures measured with thermometers was about 4 mK, while with thermocouples it ranged from 25 to 30 mK. When systematic errors were accounted for, we found that values of temperature on IPTS–68 could be determined with a single thermometer, using an interpolation formula analogous to that used below 630.74 °C, with about one-third the uncertainty usually attributed to a single thermocouple determination (±200 mK). The data also revealed that there is a lack of "smoothness" in the scale at 630.74 °C—first derivatives with respect to t_{68} are discontinuous by about 0.1 percent at this temperature.—We conclude from the results of this work that if a practical temperature scale were redefined in terms of presently available high temperature platinum resistance thermometers, it could be realized with significantly less uncertainty (±12 mK for a single determination) than IPTS–68, as it is now realized with thermocouples (±200 mK for a single determination). We recommend, however, that the adoption of such a scale be deferred until indicated improvements in thermometers have been made, and until current researches in gas thermometry have provided new values of thermodynamic temperatures for calibrating fixed points.

Fatiadi, A. J., **Evidence for adsorption as the first step in the solid-state oxidation of benzenehexol with active manganese dioxide,** *J. Chem. Soc. Section B. 889–894 (1971).*

Key words: Adsorption; benzenehexol; chain-structure; concerted; free-radical; ionic; manganese dioxide; mechanism; polycrystalline.

Oxidation of benzenehexol on the surface of amorphous, precipitated (active) manganese dioxide proceeds by a concerted mechanism, involving ionic and free-radical pathways, to give a crotonic acid derivative. This manganese dioxide has a polycrystalline chain structure, in contrast to the crystalline oxidant prepared in deuterium oxide.

Fetters, L. J., Yu, H., **Equilibrium conformation and "worm-like coil" configuration of poly(n-alkyl isocyanates),** *Macromolecules* **4,** *No. 4, 385–389 (July–August 1971).*

Key words: Configuration; conformation; equilibrium; poly(n-alkyl isocyanates); worm-like coil.

Osmotic pressure and light-scattering measurements of the polymers of *n*-butyl, *n*-hexyl, and *n*-octyl isocyanates are presented. The molecular weight dependence of the osmotic second virial coefficients and the radii of gyration is analyzed in terms of the worm-like-coil model of Kratky and Porod. The characterization of the *n*-butyl polymer, which has been studied most extensively, results in 500–600 Å for the persistence length and 1.8–2.1 Å for the monomeric projection along the contour direction of the chain. The

dependence of the radii of gyration on the weight-average molecular weights for the *n*-hexyl and *n*-octyl polymers is found to be similar to that for the *n*-butyl polymer. Thus, although our analysis has focused on the *n*-butyl species, it appears that a similar set of Kratky-Porod parameters should be applicable to the other polymers with normal aliphatic side chains of moderate length.

Flynn, J. H., **The historical development of applied nonisothermal kinetics,** (*Proc. 2nd Intern. Conf. on Thermal Analysis, Holy Cross College, Worcester, Mass., Aug. 19–23, 1969*), *Thermal Analysis* **2,** *1111–1126* (*Academic Press, Inc., New York, N.Y., 1969*).

Key words: Applied non-isothermal kinetics; historical review; isoconversional and isokinetic methods; kinetic parameters; thermogravimetric analysis.

In spite of a surprisingly extensive literature prior to 1950 on non-isothermal kinetic methods, this field was long ignored by chemical kineticists who were preoccupied with simple systems in the gas phase or in homogeneous solution. In such systems, the equations of state of each involved species change with temperature so that isothermal restrictions were often necessary.
However, the advent of wide interest in thermogravimetric techniques applied to condensed phase volatilization reactions has helped the kineticist shake off the shackles of isothermicity and has fostered the development of new and powerful methods of kinetic analysis.
The neglected early literature is reviewed briefly in light of modern developments. Generalized techniques for determining kinetic parameters under isothermal, isoconversional and isokinetic conditions are outlined and illustrated.

Fong, E., **A survey of selected document processing systems,** *Nat. Bur. Stand. (U.S.), Tech. Note 599, 67 pages (October 1971) 65 cents, SD Catalog No. C13.46:599.*

Key words: Bibliographic system; computer package; data base; document processing; information retrieval; document storage and retrieval; text; text processing.

There are many document processing systems that are commercially available or government-owned. These systems emerged in the evolution from early efforts in library automation to current on-line systems. Due to the diverse nature of the facilities provided in the document processing systems, it is difficult to evaluate them. The purpose of this paper is to present a list of features as a set of dimensions along which to compare the surveyed systems. The feature list is also developed to serve as a common basis for describing document processing systems. Another purpose of this paper is to provide a reference tool for the eight systems surveyed. They are CIRCOL, DDC ITIRC, The Mead Data Central, MEDLARS II, New York Times Information Bank, ORBIT II, and RECON/STIM. This paper first explored the characteristics of available, large document processing systems in general. An overview of the eight systems surveyed is presented. The paper then defines the feature list. The description of the eight systems surveyed according to the feature list outline is included as an Appendix.

Fraker, A. C., Ruff, A. W., Jr., **Observations of hot saline water corrosion of aluminum alloys,** *Corrosion* **27,** *No. 4, 151–156 (April 1971).*

Key words: Aluminum alloys; hot saline; oxide films; precipitates; transmission microscopy; water corrosion.

Corrosion films formed on aluminum in hot salt water (100 to 177 C) after short time tests of thirty seconds to one hour were studied by transmission electron microscopy and diffraction. It was concluded from observation of 6061, 5454, 2024, Al–1.52Mn and Al–1.66Ni alloys that one controlling factor in the initiation and growth of the outer film of the duplex oxide film is the alloy composition. The outer film formed earlier on alloys containing copper and the film growth was also more rapid on these alloys. Additions of magnesium, manganese and nickel retarded this outer film formation but with nickel additions, pitting attack was more severe and deposition of copper from solution was increased. The formation and growth of the outer film was slowest on the 5454 alloy which was also the most resistant alloy tested.

Franklin, A. D., Crissman, J., **Reorientation of trivalent cation-interstitial fluorine pair in CaF_2,** *Letters to the Editor J. Phys. C: Solid State Phys.* **4,** *L239–242 (July 12, 1971).*

Key words: Anelastic relaxation; calcium fluoride; defect pairs; dielectric relaxation; relaxation modes; reorientation.

Anelastic relaxation measurements are reported for CaF_2 containing 0.45 mole percent GdF_3 as a function of heat treatment of the crystals prior to measurement. Two main relaxation modes were found whose intensities were influenced by heat treatment in the same way as were tetragonal centers observed in the EPR spectrum. Treating these centers as pairs formed of Gd^{3+} ions plus nearby F^- interstitials, a two-shell relaxation mode analysis accounts quantitatively for the relaxation times observed by anelastic and dielectric relaxation and by EPR line-broadening. An additional relaxation mode, excited by ⟨100⟩ longitudinal stress, was observed but not identified. It was uninfluenced by heat treatment.

Frenkiel, F. N., Klebanoff, P. S., **Statistical properties of velocity derivatives in a turbulent field,** *J. Fluid Mech.* **48,** *Part 1, 183–208 (July 13, 1971).*

Key words: Computer; correlations; grid; intermittency; isotropy moments; probability-distributions; turbulence; velocity-gradients.

High-speed digital computing methods are applied to the study of the statistical behavior of turbulent velocity derivatives in a nearly isotropic turbulent field downstream of a grid. Higher-order correlations of turbulent velocity gradients, up to the eighth order, are measured. Contrary to the case of *velocities*, the higher even-order correlations of *velocity gradients* more clearly evidence the departure from a two-dimensional Gaussian probability distribution. Using non-Gaussian probability distribution laws the relations between different odd- and even-order correlations are obtained and compared with the experimental measurements. The conditions of similarity and isotropy are evaluated for the small-scale structure as evidenced by the behavior of the turbulent velocity gradients. The concept of intermittency of the small-scale structure is also discussed.

Fuhr, J. R., Wiese, W. L., **Bibliography on atomic transition probabilities, July 1969 through June 1971,** *Nat. Bur. Stand. (U.S.), Spec. Publ. 320 Suppl. 1, 67 pages (Sept. 1971) 65 cents, SD Catalog No. C13.10:320 Suppl. 1.*

Key words: Allowed; atomic; discrete; forbidden; transition probability.

This is the first supplement to the NBS Special Publication 320, "Bibliography on Atomic Transition Probabilities," and it covers the most recent literature on the subject from July 1969 through June 1971. The papers are arranged according to elements and stages of ionization, and the method employed and classification of transitions are indicated for each reference. Only articles on discrete transistions, both allowed and forbidden, are listed. Papers containing data for many elements within isoelectronic sequences are collected separately in front of the list in order to keep this bibliography to a reasonable size. Also included is a selected list of new papers dealing with the subject of atomic transition probabilities from a general point of view.

Fussell, W. B., **Effect of ceramic spectral emissivity variations on the computed luminous emissivity of the NBS standard of light,** *Nat. Bur. Stand (U.S.), Tech. Note 595, 58 pages (Sept. 1971) 65 cents, SD Catalog No. C13.46:595.*

Key words: Ceramic; light; photometry; radiometry; spectral emissivity; standard.

A simplified model of the National Bureau of Standards (NBS) 1970 design for the standard of light (platinum point blackbody)

is introduced. This model is used to calculate the apparent luminous emissivity of the base of the sighttube of the standard of light, and of the wall near the base, by two different methods. The first method includes the effect of variations with wavelength in the spectral emissivity of the ceramic composing the sighttube; the second method does *not* include the effect of ceramic spectral emissivity variations. The results of the two methods are compared and their difference (about 6×10^{-6}) is found to be negligible for the NBS 1970 design when the sighttube is made of alumina, compared with other uncertainties and the precision of measurement.

A formula is derived for estimating the apparent luminous emissivity of a standard of light, given: a., the length-to-diameter ratio of the sighttube; b., the half-angle of the conical base; c., the wall thickness of the sighttube; d., the thermal conductivity of the sighttube ceramic; e., the average thermal and luminous emissivities of the sighttube ceramic.

Gadzuk, J. W., Hartman, J. K., Rhodin, T. N., **Approach to alkali-metal chemisorption within the Anderson model,** *Phys. Rev. B.* **4,** *No. 2, 241–255 (July 15, 1971).*

Key words: Chemisorption; magnetic impurities; surface physics and electron emission.

A theory of chemisorption relevant to alkali atoms on metal surfaces is presented. The virtual-impurity-state problem is modeled in the manner presented by Kjöllerström, Scalapino, and Schrieffer for solving the Anderson impurity problem in the low-density approximation (LDA). It is assumed that the binding or chemisorption energy of the alkali metal is composed of two parts, a metallic and an ionic component. Since considerable charge transfer from the alkali atom to the metal occurs, the LDA is appropriate for describing the metallic part of the binding. Another consequence of the large charge transfer is that the major portion of the binding results from an ionic type of bond between the partially charged alkali ion on the surface and a polarization or screening charge inside the metal. The results of the theoretical calculations indicate that binding energies for alkali atoms adsorbed the clean single-crystal faces of metals generally fall within the range of 1.5–2.5eV, in accord with available experimental data on metals such as W, Mo, Ta, and Ni.

Gebbie, K. B., **The Menzel symposium on solar physics, atomic spectra, and gaseous nebulae,** *Nat. Bur. Stand. (U.S.), Spec. Publ. 353, 213 pages (Aug. 1971) $1.75, SD Catalog No. C13.10:353.*

Key words: Atomic energy levels; transition probabilities; solar physics; gaseous nebulae; non-LTE thermodynamics.

A symposium in honor of Donald H. Menzel's contributions to astrophysics was held on his 70th birthday at the Harvard College Observatory, Cambridge, Massachusetts, 8–9 April 1971. Menzel and his school have made distinguished contributions to the theory of atomic physics, solar physics, and gaseous nebulae. The work on planetary nebulae represented the first investigations of non-equilibrium thermodynamic conditions in astronomy; the solar work extended these investigations to stellar atmospheres. The applied atomic physics laid the basis for what we now call laboratory astrophysics and, together with work on non-equilibrium thermodynamics, inspired the founding of the Joint Institute for Laboratory Astrophysics. Menzel has served as a distinguished consultant to the National Bureau of Standards, and publication of this volume represents a grateful acknowledgment of his service to the Bureau. The papers summarize the current status of work in the three fields he pioneered.

Grabner, L., Stokowski, S. E., **Photoluminescence of Cr-doped $CaTiO_3$,** *Phys. Rev. B.* **2,** *No. 11, 4351–4353 (Dec. 1, 1970).*

Key words: Cr^{3+}; energy transfer; excitation; lifetime; photoluminescence.

At 4° K and 77° K photoluminescence from nominally undoped and $CaTiO_3$:0.0025% Cr show identical spectra in the infrared with an intensity ratio of 1 : 2. The emission is attributed to the $^2E \rightarrow {}^4A_2$ transition of the Cr^{3+} ion at a Ti^{4+} site. At 4° K it consists of a single nophonon line at 1.744eV of half-width 1.5meV and a complex vibronic spectrum which is anomalously intense. Data at 77° K shows a splitting of the ^2E state of 2 meV. The absorption spectrum of $CaTiO_3$: Cr is dominated by a "background absorption" by unknown defects. From the coincidence of the excitation spectrum with the absorption spectrum, we conclude that the excitation is dominated by absorption by unknown defects which transfer energy into Cr^{3+}, presumably by resonant energy transfer. In undoped $CaTiO_3$ a single exponential decay of the emission of $700_{\mu sec}$ is reported. In $CaTiO_3$: 0.0025% Cr, on the other hand, two exponentials of 700 μsec and 11 msec were observed. The former is assigned to Cr^{3+}, the latter to the time of energy transfer from defects responsible for the background absorption to the Cr^{3+}.

Grabner, L., Stokowski, S. E., Brower, W. S., Jr., **No-phonon $^4T_{2g} = {}^4A_{2g}$ transitions of Cr^{3+} in TiO_2,** *Phys. Rev. B.* **2,** *No. 3, 590–598 (August 1, 1970).*

Key words: Absorption; defect phonon; emission; excitation; lifetime; $^4T_2$ state.

Absorption and emission at 4° K and 77° K are observed in Cr-doped TiO_2 consisting of two sharp no-phonon lines at 12685 cm^{-1} and 12732 cm^{-1} and vibronic side bands with an integrated intensity 10^4 that of the no-phonon lines. In undoped TiO_2, identical spectra are observed but are a factor of 100 less intense. The center responsible for these spectra is identified as substitutional Cr^{3+} by observing, in emission, a splittering of the 12685 cm^{-1} line of 1.4 cm^{-1}, a value previously determined by EPR measurements. The vibronic side bands have some structure superposed on a broad band. The vibronics are different in emission and absorption and have a lifetime of 45 μ-sec, equal to that of the no-phonon line. They are shown to be principally due to defect induced phonons arising from the Cr^{3+} defect. We argue that the spectra observed are not characteristic of the usual ^2E_g—$^4A_{2g}$ transition and propose that the $^4T_2$ lies lower in energy than the ^2E_g state. If so, the new results of this work are: (1) no-phonon line emission for the $^4T_2 - {}^4A_2$ transition, and (2) defect phonon states which are different for the $^4A_2$ and $^4T_2$ states. The excitation spectrum is also presented. It shows that the excitation of the Cr^{3+} emission occurs mainly by the transfer of energy from excited trapping centers rather than by direct excitation.

Grimes, D. N., **Measurement of the second-order degree of coherence by means of a wavefront shearing interferometer,** *Appl. Opt.* **10,** *No. 7, 1567–1570 (July 1971).*

Key words: Coherence; coherence measurement; interferometry; wavefront shearing interferometer.

A method of measuring the second order degree of coherence in an arbitrary plane by means of a compact wavefront shearing interferometer is described. The prism interferometer previously described by Saunders produces two sheared images which interfere allowing measurement of the degree of spatial coherence. If the degree of coherence is a function of co-ordinate differences only, the visibility is constant over the field. Otherwise it varies point-to-point. Experimental results are given.

Grimes, D. N., **Imaging of tri-bar targets and the theoretical resolution limit in partially coherent illumination,** *J. Opt. Soc. Am.* **61,** *No. 7, 870–876 (July 1971).*

Key words: Coherence; difffraction; resolution.

In viewing systems that employ critical, Kohler, or collimated illumination, the illumination may frequently be characterized by the complex degree of coherence in the form of a first-order Bessel function divided by its argument. The anomalies that occur in the image of a tri-bar target viewed in partially coherent illumination of this form are discussed for a two-dimensional circular diffraction-limited imaging system. The Sparrow criterion, which in this case correlates with experimental measurements of resolving power, is applied to determine the resolution limit. The computed resolution-limit curve for a tri-bar target is shown and compared to the previously published two-point resolution-limit curve for a one dimen-

sional system and to the limiting values obtained in a two-dimensional system for coherent and incoherent illumination. In the latter case, the full curve is shown as a special case of the application of the Sparrow criterion to the partially coherent imaging equations for a circular two-dimensional system. Experimental confirmation of the calculations is given.

Heinrich, K. F. J., Myklebust, R. L., Rasberry, S. D., Michaelis, R. E., **Standard Reference Materials: Preparation and evaluation of SRM's 481 and 482 gold-silver and gold-copper alloys for microanalysis,** *Nat. Bur. Stand. (U.S.), Spec. Publ. 260–28, 100 pages (Aug. 1971) $1.00, SD Catalog No. C13.10:260–28.*

Key words: Alloys; corrections; electron probe; homogeneity; matrix scanner; microanalysis; quantitative analysis; standard reference materials; x-ray emission.

The reasoning behind the choice of the systems Au-Ag and Au-Cu for SRM's, and their suggested uses are described. We also report on the preparations of the materials, their chemical analysis, the tests performed to ascertain macroscopic and microscopic homogeneity, and on relative x-ray intensity measurements at various x-ray lines and voltages. A description of the instrumentation (matrix scanner), techniques, and programs employed in the homogeneity studies, as well as tables and graphs of the x-ray intensity measurements, are appended.

Heydemann, P. L. M., **A fringe-counting pulsed ultrasonic interferometer,** *Rev. Sci. Instr.* **42,** *No. 7, 983–986 (July 1971).*

Key words: Phase sensitive detection; speed of sound; ultrasonic interferometer; ultrasonics.

A new ultrasonic interferometer for the automatic measurement of transit times is described. Its main advantage is its ability to follow very large changes of the transit time (1–20) and still maintain a resolution of typically 2.5 x 10^{-10} s. The method is based on the phase sensitive detection of multiple echoes, counting of the output signal at the rate of four counts per full cycle, and an additional interpolation.

Hougen, J. T., **Interpretation of molecular-beam radiofrequency orthopara transitions in methane,** *J. Chem. Phys.* **55,** *No. 3, 1122–1127 (August 1, 1971).*

Key words: Group theory; inversion splitting; methane molecular-beam data; ortho-para transitions; radiofrequency.

A modified formalism, involving primarily changes in certain group-theoretical arguments, is presented for the data leading to the recent report of the observation of the inversion splitting in methane has been resolved.

Hudson, R. D., **Critical review of ultraviolet photoabsorption cross sections for molecules of astrophysical and aeronomic interest,** *Nat. Stand. Ref. Data Ser., Nat. Bur. Stand. (U.S.), 38, 106 pages (Aug. 1971) $1.00, SD Catalog No. C13.48:38.*

Key words: Aeronomic; Astrophysical; Partial; Photoabsorption cross sections; Photodissociation; Photoexcitation; Photoionization; Photon-scattering; Total; Ultraviolet cross sections.

This paper is devoted to a critical review of photoabsorption cross sections for molecules of aeronomic and astrophysical interest at wavelengths less than 3000 A. A discussion of the relative merits of various experimental techniques is given along with possible systematic and random errors that may be associated with them. The problems in data analysis associated with finite spectral bandwidths are reviewed, with special emphasis on the interpretation of published absorption cross sections. This review does not contain a complete set of cross-section-versus-wavelength values for each molecule; the prepared figures are used to compare the results of several determinations or to point out where difficulties of interpretation might arise. However, references to all papers believed to contain the more reliable data are given.

Hussmann, E. K., McLaughlin, W. L., **Dose-distribution measurement of high-intensity pulsed radiation by means of holographic interferometry,** *Radiation Res.* **47,** *No. 1, 1–14 (July 1971).*

Key words: Calorimetry; depth dose; dosimetry; holography; interferometry; isodose.

A novel calorimetric method has been developed for evaluating the spatial distribution of radiation absorbed dose in transparent liquids, particularly for dosimetry of pulsed, high-intensity electron beams. Local temperature change is determined without the introduction of temperature sensors that may disturb the radiation field. The change in a liquid's refractive index, which is a function of temperature, is measured by an interferometric method employing holographic wavefront reconstruction. For radiation beams essentially symmetric to the direction of propagation, the three dimensional dose distribution can be derived from the information given by the interferogram. Dose distributions in water have been evaluated for short electron pulses of different energy spectra.

Johnson, D. R., Powell, F. X., Kirchhoff, W. H., **Microwave spectrum, ground state structure, and dipole moment of thioformaldehyde,** *J. Mol. Spectry.* **39,** *No. 1, 136–145 (July 1971).*

Key words: Dipole moment; microwave spectrum; reactive species; rotational spectra; structure thioformaldehyde.

The microwave spectrum of the reactive species thioformaldehyde (H_2CS) has been studied in the ground vibrational state. Rotational transitions in $H_2{}^{12}C^{32}S$, $H_2{}^{13}C^{32}S$, $H_2{}^{12}C^{34}S$, and $D_2{}^{12}C^{32}S$ have been measured and assigned. A detailed centrifugal distortion analysis has been carried out on the species $H_2{}^{12}C^{32}S$ with a total of 27 transitions up to $J=27$ fit to a standard deviation of 26 kHz. Rotational constants obtained from these four isotopic species have been used to obtain the following completely substituted structure: $r_{S=C}=1.6108(9)$ Å, $r_{C-H}=1.0925(9)$ Å, and $<HCH=116.87(5)°$. The dipole moment of H_2CS was found to be $\mu=1.6474(14)$ Debye from Stark effect measurements on the $J=1_{01}\leftarrow 0_{00}$ transition. The typical reactive half-life of this new species was found to be about 6 min in a static system.

Kirstein, A. F., **Universal testing machine of 12-million-lbf capacity at the National Bureau of Standards,** *Nat. Bur. Stand. (U.S.), Spec. Publ. 355, 18 pages (Sept. 1971) 30 cents, SD Catalog No. C13.10:355.*

Key words: Force calibration; large test facilities; structural testing; universal testing machine.

A 12-million pounds-force capacity universal testing machine, which is believed to be the largest of its kind in the world, has been put into operation in the Engineering Mechanics Laboratory of the National Bureau of Standards in Gaithersburg, Maryland. This hydraulically operated machine, which has an overall height of over 100 feet, was designed to test full scale structural components and to apply the forces needed to calibrate large capacity force measuring devices. The testing machine is capable of applying axial forces of 12,000,000 lbf in compression, 6,000,000 lbf in tension, and a transverse force of 4,000,000 lbf to a flexural specimen.

Krauss, M., Maldonado, P., Wahl, A. C., **Interaction energy curves of LiHe and NaHe ($X\,^2\Sigma^+$, $A\,^2\Pi$, $B\,^2\Sigma^+$) and $X\,^1\Sigma^+$ ions,** *J. Chem. Phys.* **54,** *No. 11, 4944–4953 (June 1, 1971).*

Key words: Hartree-Fock; interaction energy; LiHe; NaHe; transition probabilities.

Hartree-Fock interaction energy curves have been calculated for the $X^2\Sigma^+$, $A^2\Pi$, and $B^2\Sigma^+$ states of neutral LiHe and NaHe as well as for the ground state of $X^1\Sigma^+$ ions over a range of distances from 3 to 10 a.u. Since it is intended to apply these results to scattering problems, the variation of the dipole and quadrupole moments and the electronic transition probabilities with internuclear distance were also obtained. Both Slater-type functions and Gaussian-type functions were used as variational trial functions with the intention

of gauging the efficacy of the Gaussian basis. Except for situations involving small energy minima the Gaussian basis yielded results accurate relative to the Slater basis. The features of the Hartree-Fock interaction energy curves can be summarized as follows:
(1) The $X^2\Sigma^+$ interaction energy is purely repulsive for both molecules to the accuracy of the present calculation.
(2) The $A^2\Pi$ and $X^1\Sigma^+$ curves are strikingly similar for both Li and Na confirming the penetration of the He for this interatomic orientation.
(3) The long-range repulsive behavior of the $B^2\Sigma^+$ curve compared with estimates of the correlation energy shows that the internuclear distance dependence of the energy in the region of 10 a.u. is dominated by the Hartree-Fock repulsive curve.
Charge-density plots have been obtained for all states and distances. These are used to illustrate the physical basis of the energy curves.

Krauss, M., Mielczarek, S. R., Neumann, D., Kuyatt, C. E., **Mechanism for production of the fourth positive band system of CO by electron impact on CO_2,** *J. Geophys. Res.* **76,** *No. 16, 3733–3737 (June 1, 1971).*

Key words: CO; CO_2; electron impact; fourth positive bands; oscillator strength; Rydberg state; valence state.

The electron impact energy loss spectrum for CO_2 is presented over an energy range of 10 to 20 eV. Analysis of this spectrum and molecular orbital calculations indicate that valence state perturbers of $^1\Sigma_u^-$ and $^1\Pi_u$ symmetry contribte significantly to the oscillator strength in the range from 11 to 14 eV. The $^1\Sigma_u^-$ state is then determined to be the predominant contributor to the reaction $CO_2 + e \rightarrow CO_2(^1\Sigma_u^-) + e \rightarrow CO(A^1\Pi) + O(^3P) + e$. Unusual intensity distributions in the observed fluorescence of the vibrational states of $CO(A^1\Pi)$ observed by M. J. Mumma, E. J. Stone, and E. C. Zipf (1970) are explained on the basis of competition between predissociation and autoionization from this single excited state. This mechanism would be one means for production of the fourth positive bands of CO in the ultraviolet dayglow of the upper atmosphere of Mars.

Lafferty, W. J., Ritter, J. J., **Microwave spectrum, dipole moment, and structure of ethynyldifluoroborane,** *J. Mol. Spectry.* **38,** *No. 1, 181–194 (April 1971).*

Key words: Dipole moment; ethynyldifluoroborane; microwave spectrum; molecular structure; rotational spectrum; stark effect

The microwave spectrum of ten isotopic species of ethynyldifluoroborane ($HCCBF_2$) has been measured. Rotational constants of the ground state and the lowest excited vibrational state have been obtained. Structural parameters obtained are: $r_{C-H} = 1.058 \pm 0.003$ Å, $r_{C\equiv C} = 1.206 + 0.003$ Å, $r_{C-B} = 1.513 \pm 0.005$ Å, $r_{B-F} = 1.323 \pm 0.005$ Å, and $< FBF = 116.5 \pm 1.0°$. The dipole moment is $1.87_6 \pm 0.010$ D.

Langenberg, D. N., Taylor, B. N., **Precision measurement and fundamental constants.** *Proceedings of the International Conference held at the National Bureau of Standards Gaithersburg, Maryland, August 3–7, 1970, Nat. Bur. Stand. (U.S.), Spec. Publ. 343, 543 pages (Aug. 1971) $6.00, SD Catalog No. C13.10:343.*

Key words: Fundamental constants; least-squares adjustments; precision measurements.

This volume presents the Proceedings of the International Conference on Precision Measurement and Fundamental Constants, held at the National Bureau of Standards in Gaithersburg, Maryland, from August 3 through August 7, 1970. The conference brought together theoretical, experimental, and applied scientists for the purpose of discussing modern techniques of precision physical measurement and their application, along with modern theoretical developments, to the determination of the fundamental constants. The topics covered were: frequency and time standards; length standards; the velocity of light; the Rydberg constant; electrical standards; the proton gyromagnetic ratio; the Faraday constant; atomic masses; the proton magnetic moment; Josephson effects; x-rays; fine and hyperfine structure in simple atoms; lepton g-factor anomalies; the gravitational constants; least squares adjustments of the constants. These proceedings contain the invited tutorial talks as well as the contributed papers presented at the conference. Also included are the post-paper discussions and a panel discussion entitled "Should Least Squares Adjustments of the Fundamental Constants be Abolished?"

Laufer, A. H., Okabe, H., **Heat of formation and bond dissociation energy of diazomethane by a photodissociation method.** *J. Am. Chem. Soc.* **93,** *4137–4140 (1971).*

Key words: Bond dissociation energy; diazomethane; heat of formation; vacuum ultraviolet.

A lower limit for the heat of formation of diazomethane has been obtained from measurement of the minimum energy required to produce the $A^2\Delta$ state of CH in the low-intensity vacuum-ultraviolet photolysis of diazomethane. The value obtained is $\Delta H_{f_0}°(CH_2N_2) \geq 51.3$ kcal/mol (2.22 eV). In conjunction with $\Delta H_{f_0}° - (CH_2) = 93.0$ kcal/mol, the dissociation energy of the C=N bond in diazomethane is <41.7 kcal/mol (1.81 eV). Reasonable upper limits for $\Delta H_{f_0}°$ (CH_2N_2) are discussed.

Lawless, W. N., Radebaugh, R., Soulen, R. J., **Studies of a glass-ceramic capacitance thermometer between 0.025 and 2.4 K,** *Rev. Sci. Instr.* **42,** *No. 5, 567–570 (May 1971).*

Key words: Capacitance thermometer; refrigeration; $SrTiO_{3+}$; thermometer.

Capacitance measurements from 0.025 to 2.4 K are reported for capacitance thermometers (made from an $SrTi0_3$ glass-ceramic crystallized at 1100 and 1203 °C) two of which were the ones reported in the previous article. It was found that the 1200 type thermometer has a useful thermometric range down to 0.06 K and a linear C–T region down to 0.5 K. The 1100-type thermometer has a useful range down to 0.110 K and a linear region down to 1.1 K. The measured data do not appear to be influenced by self-hearing or adiabatic correction effects. Both thermometers display an unexpected increase in capacitance with decreasing temperature below their monotonically decreasing ranges. The 1100-type thermometer displays the more pronounced increase, with $C \propto T^{-1}$ from 0.100 to 0.025 K. It is argued that this T^{-1} behavior is due to crystallized $SrTi0_3$ and the possibility of using this effect to achieve adiabatic depolarization cooling is discussed.

Leasure, W. A., Jr., **Truck tire noise—preliminary results of a field measurement program,** *Proc. Purdue Noise Control Conference, Purdue University, West Lafayette, Indiana, July 14–16, 1971, pp. 41–48 (July 1971).*

Key words: Acoustics; noise measurement; noise pollution; noise (sound); sound transmission; tires; transportation noise.

This paper presents an inventory of peak A-weighted sound levels measured during an extensive parametric study conducted to characterize the noise generated by typical rib, cross-bar, and retread type truck tires in actual use. A test sample of nine tread designs, estimated to represent 70–80% (these exact designs) of the truck tire population on the road today, was investigated considering the following variables: wear, loading, speed, pavement surface, and tire location. Test vehicles included both single-chassis vehicles and a tractor-trailer.
The results show that the A-weighted sound level increased with either an increase in load or speed. The pocket retread design always produced the highest level followed by the cross-bar tires and then the rib tires. This ranking held for both new and half-worn tires. The influence of wear and pavement surface is more complex. For all of the tread designs except one there was an increase in noise level between the new and half-worn states. The results for different pavement surfaces are much the same as with wear. The generated noise appears to depend on both the specific tread design and the surface roughness. Individual tires do contribute differently to the overall level depending on their location on the vehicle. In some cases, significant reductions in the noise

level were observed when "noisy" tires were mounted inboard of "quieter" tires.
The paper includes a discussion of the measurement and analysis techniques utilized for the establishment of this data base.

Loebenstein, W. V., **Calculations and comparisons of nonideal gas corrections for use in gas adsorption,** *J. Colloid Interface Sci.* **36,** *No. 3, 397–400 (July 1971).*

Key words: Adsorption; correction for gas; gas; gas law correction; imperfect gas; nonideal gas; second virial coefficient.

Volumetric gas adsorption measurements have become increasingly popular in recent years. The techniques for determination of surface area and pore size distribution have become so commonplace that they can almost be termed routine. At the temperature of the adsorption experiment, it is necessary at each equilibrium pressure to correct for the nonideal behavior of the gas surrounding the sample in order to obtain by difference an accurate evaluation of the amount of gas actually adsorbed. The correction factors that are continually used by most adsorption chemists have not been critically re-examined by these ultimate users since they were originally recommended more than thirty years ago. Indeed, textbooks published more than 25 years later continue to perpetuate the same correction factors. It is the purpose of this paper, by comparing correction factors derived from various sources, to avoid gross inaccuracies and to suggest a procedure whereby the investigator may estimate his own factor in instances where tabulated values are not readily available to him.

McNesby, J. R., Kelly, R. V., **Abstraction of hydrogen by methylene,** *Intern. J. Chem. Kinetics* **3,** *293–305 (1971).*

Key words: Ketene; kinetics; methyl; methylene; neopentane.

The photolysis of CD_2CO at 313 nm in the presence of neopentane was carried out over the temperature range 576–706 K. Analysis of the products and isotopic analysis of the methanes demonstrate abstraction of H from neopentane and D from CD_2CO by methylene. The relative kinetics of abstraction of H and D have been measured over the temperature range, and the absolute value for the collision yield of the abstraction of H from neopentane by CD_2 at 653 K has been estimated to be about 1.5×10^{11} mol^{-1} cm^3 s^{-1}, a value 10^3 times larger than the corresponding reaction of CH_3.

Madey, T. E., Yates, J. T., Jr., **Electron-stimulated desorption as a tool for studies of chemisorption: A review,** *J. Vacuum Sci. Technol.* **8,** *No. 4, 525–555 (July/August 1971).*

Key words: Adsorption; chemisorption; cross section; desorption; electron stimulated desorption; hydrogen, nickel, nitrogen, oxygen, surface constants.

Bombardment of solids by low-energy electrons (< 500 eV) can cause various changes in the surface region, particularly if the surface contains an adsorbed layer. Electron bombardment can promote the desorption of energetic neutral and ionic fragments from the surface, can alter the bonding of surface species, and in some cases can cause decomposition of the surface region. These processes are termed electron-stimulated desorption (ESD) phenomena, and this review is primarily concerned with the use of ESD in studies of species adsorbed on surfaces. Topics covered include experimental methods, a theoretical discussion of physical mechanisms, and a detailed discussion of certain specific and well-studied adsorbate-substrate systems.

Mandel, J., **Repeatability and reproducibility,** *Mater. Res. Stand.* **11,** *No. 8, 8–16 (August 1971).*

Key words: Evaluation of; interlaboratory testing; precision, repeatability; reproducibility; test methods.

A simple method is presented for the evaluation of the repeatability and the reproducibility of test methods. The method obviates such difficulties as transformations of scale or weighted analysis of variance.

It is shown, furthermore, that the concepts of repeatability and reproducibility are, by themselves, insufficient to answer the major questions related to interlaboratory testing. Alternative procedures are mentioned. Finally, the paper presents a rationale for a proper choice of the number of laboratories and the number of replicate determinations required for an adequate interlaboratory study.

Marlow, W. F., LaFleur, P. D., **Standard reference materials for analysis of environmental samples,** *Proc. Symp. Nuclear Techniques in Measurement and Control of Environmental Pollution, Salzburg, Austria, Oct. 26–30, 1970, pp. 91–94 (International Atomic Energy Agency, Vienna, Austria, March 1971).*

Key words: Activation analysis; biological; botanical; environment; Standard Reference Material.

As is evidenced by the large number of publications on the subject, especially at this Symposium, many groups are engaged in the analysis of environmental samples of all kinds for their trace element content, as well as for their major constituent content. Perhaps the most versatile and popular method for the rapid, economical analysis of environmental samples for a large number of elements is neutron activation analysis. Also extensively used are x-ray fluorescence analysis, atomic absorption spectroscopy, spark-source mass spectrometry, and emission spectrometry. In many cases, meaningful results for multi-element analysis have been difficult to obtain because of the lack of adequate standard materials, despite the limited efforts by some investigators to produce them. Particularly, in the cases of neutron activation analysis and spark-source mass spectrometry the matrix of the sample can have a pronounced effect upon the analysis. It is extremely important that the standard material have a matrix as similar as possible to that of the sample. At present such suitable standard materials are not widely available. Therefore, the U.S. Atomic Energy Commission and the U.S. National Bureau of Standards have instituted a program for the production of a series of special Standard Reference Materials, fully characterized for at least 22 and possibly 30 elements, suitable for use in the analysis of environmental samples, particularly biological samples. These Standard Reference Materials will be available for purchase by all laboratories. Multi-laboratory intercomparisons of these Standard Reference Materials will be encouraged.
Details of the nature of these materials, elements for which they will be characterized and analytical techniques used in standardizing them will be discussed.

Marshall, R. D., **Surface pressure fluctuations near an axisymmetric stagnation point,** *Nat. Bur. Stand. (U.S.), Tech. Note 563, 67 pages (Aug. 1971) 70 cents, SD Catalog No. C13.46:563.*

Key words: Disk; pressure fluctuations; stagnation point; turbulence.

Surface pressure fluctuations on a circular disk placed normal to a turbulent air stream have been investigated. Turbulence intensities of approximately 10% were produced by a coarse grid installed at the test-section entrance. The turbulent field in the neighborhood of the disk was homogeneous and nearly isotropic.
Experimental results indicate that existing linear theories which do not consider distortion of the flow fail to predict the nature of surface pressure fluctuations on a bluff body. Only for wavelengths which are large compared to the body do these theories yield satisfactory results. A strong attenuation of the high frequency components occurs as the flow stagnates. This is accompanied by a transfer of energy from short to long wavelengths. The opposite effect is observed as the flow attains a radial direction and approaches the edge of the disk. A neutral wavelength which undergoes little change in energy was observed. Integral scales of surface pressure fluctuations are much larger than the lateral integral scale of the free-stream turbulence.

Menis, O., Iyer, C. S. P., **Spectrophotometric determination of vanadium and iron with β-isopropyltropolone,** *Anal. Chim. Acta* **55,** *89–95 (1971).*

Key words: Analysis of steel samples; extraction with β-isopropyltropolone; simultaneous determination of vanadium and iron; spectrophotometric determination of vanadium.

A spectrophotometric procedure is described for the determination of vanadium and for the simultaneous determination of iron and vanadium using two wavelength measurements, at 470 and 540 nm or 418 and 470 nm. It is based on the formation of chelate complex with β-isopropyltropolone. The complex is extracted with chloroform and in the presence of alcohol the color develops rapidly and is stable for at least 24 hours. The precision of the calibration curve is 1 percent relative standard deviation. The application and results of the analysis of NBS Standard Reference Material steel samples are presented.

Milligan, D. E., Jacox, M. E., **Infrared spectrum and structure of the SO_2^- radical ion,** *J. Chem. Phys.* **55,** *No. 3, 1003–1012 (August 1, 1971).*

Key words: Alkali metal reactions; charge transfer; electron capture; infrared spectrum; matrix isolation; molecular orbital; SO_2^- anion; sulfur dioxide.

When a sample of SO_2 in a large excess of argon is codeposited at 4 K or at 14 K with an atomic beam of an alkali metal, prominent new absorptions appear near 500 cm^{-1} and between 975 and 1100 cm^{-1}. The pattern of absorptions is somewhat dependent both upon the alkali metal and upon the temperature at which the sample is deposited. Product absorptions which appear at 495, 985, and 1042 cm^{-1} in samples containing a small concentration of cesium atoms have been demonstrated to be contributed by a single species, shown by isotopic substitution studies to contain one sulfur and two oxygen atoms. A slight splitting in the absorptions of the mixed oxygen-isotopic species indicates that the two oxygen atoms are not symmetrically equivalent, either because of a site perturbation or because of a slight nonequivalence of the two S–O bonds. The absorptions have been assigned to the three SO_2^- vibrational fundamentals of a charge-transfer complex in which the residual interaction of the cation is sufficiently small that all of the vibrational data can be fitted within experimental error without considering the motion of the cation. The data are consistent with an O–S–O valence angle of 110°±5°. The S–O stretching force constant is significantly lower than that of SO_2, consistent with the addition of an electron to an orbital which is antibonding between the sulfur and two oxygen atoms.

Milligan, D. E., Jacox, M. E., **Infrared spectrum of the $BrHBr^-$ ion isolated in an argon matrix,** *J. Chem. Phys.* **55,** *No. 5, 2550–2560 (Sept. 1, 1971).*

Key words: Alkali metal reactions; $BrHBr^-$; charge transfer; $ClHCl^-$; electron attachment; infrared spectrum; matrix isolation; molecular rotation; vacuum-ultraviolet photolysis; vibrational potential function.

Infrared absorptions assigned to ν_3, $(\nu_3+\nu_1)$, and $(\nu_3+2\nu_1)$ of $BrHBr^-$ have been observed in samples of HBr in an argon matrix which have been subjected to 1216-Å photolysis or which have been co-deposited with an alkali metal atomic beam and then subjected to mercury-arc radiation. The corresponding experiments on deuterium-enriched samples support this identification. Mechanisms by which $BrHBr^-$ is produced in these experiments are considered in detail. An atomic mechanism leading to the stabilization of the uncharged species is shown to be inadequate. However, several ionic processes may contribute to the observed production of the anion. As previously postulated, dissociative electron attachment to $(HBr)_2$ may occur. In addition, it is necessary to postulate the production of Br^- by various charge-transfer processes, followed by the reaction of Br^- with HBr. Analysis of the infrared spectra of $BrHBr^-$ and of $BrDBr^-$ indicates that the vibrational potential function must include significant contributions from both cubic and quartic terms.

Ming, T-K, Tauber, S. J., **Chemical structure and substructure search by set reduction,** *J. Chem. Doc.* **11,** *No. 1, 47–51 (Feb. 1971).*

Key words: Chemical search; chemical substructure; set reduction; structure.

The set reduction method by Sussenguth for chemical structure and substracture searching has been adapted: Structure search and substructure search have been separated into distinct subroutines; first-order and second-order degree have been included in the control vector. This method has been tested on structures with greater symmetry than has been done previously, and it has been verified for disjoint substructures. A method has been demonstrated for removing and ambiguity inherent in using a bond adjacency matrix.

Moore, C. E., **Selected tables of atomic spectra, atomic energy levels and multiplet tables, N IV, N V, N VI, N VII,** *Nat. Stand. Ref. Data Ser., Nat. Bur. Stand. (U.S.), 3, Sec. 4, 46 pages (Aug. 1971) 55 cents, SD Catalog No. C13.48:3/Sec. 4.*

Key words: Atomic energy levels, N IV–N VII; Multiplet tables, N IV–N VII; Nitrogen spectra, N IV–N VII; Spectra, N IV–N VII; Wavelengths, nitrogen spectra N IV–N VII.

The present publication is the fourth Section of a series being prepared in response to the persistent need for a current revision of two sets of tables containing data on atomic spectra as derived from analyses of optical spectra. As in the previous Sections, Part A contains the atomic energy levels and Part B the multiplet tables. Four spectra of nitrogen, N IV, N V, N VI, and N VII, are included. The form of presentation is described in detail in the text to Section 1.

Mountain, R. D., Raveché, H. J., **Entropy and molecular correlation functions in open systems. II Two- and three-body correlations,** *J. Chem. Phys.* **55,** *No. 5, 2250–2255 (Sept. 1, 1971).*

Key words: Configuration entropy; correlation function; entropy; hard sphere; liquid state; neon; Percus-Yevick equation.

We consider the contributions from the correlation of pairs and triples of molecules to the configurational entropy per molecule of a simple fluid system. Using numerical values of the pair function and only certain moments of the triplet function, we have computed the first few terms in an expression for the entropy in terms of the correlation functions. The results, which compare favorably with experimental values over a range of densities including that of the liquid, indicate that contributions from the correlations of triples of molecules can be appreciable. The computations are done for a fluid of hard spheres and liquid neon and the results are discussed in terms of the molecular correlations in a simple fluid.

Newman, M., **Invariant factors of combinatorial matrices,** *Israel J. Math.* **10,** *No. 1, 126–130 (1971).*

Key words: Designs; incidence matrices; invariant factors; Smith normal form.

The Smith normal forms of an Hadamard matrix of order $4m(m$ square-free), and of the incidence matrix of a v, k, λ configuration $(n=k-\lambda$ square-free, $(n, \lambda)=1)$, are determined.

Oberholtzer, B. L., **Publications of the National Bureau of Standards 1970,** *Nat. Bur. Stand. (U.S.), Spec. Publ. 305 Suppl. 2, 378 pages (July 1971) $3.25, SD Catalog No. C13.10:305 Suppl. 2.*

Key words: Abstracts; key words; NBS publications; publications.

This Supplement to Special Publication 305 Supplement 1 of the National Bureau of Standards lists the publications of the Bureau issued between January 1, 1970 and December 31, 1970. It includes an abstract of each publication (plus some earlier papers omitted from Special Publication 305 Supplement 1), key-word and author indexes; and general information and instructions about NBS publications. Previous catalogs of NBS publications referenced in Special Publication 305, Supplement I remain in effect.

Page, C. H., **External field of an ideal toroid,** *Am. J. Phys.* **39,** *No. 9, 1039–1043 (Sept. 1971).*

Key words: Leakage flux; magnetic field; toroid; transformer; vector potential.

The external magnetic field of an ideal toroid vanishes for dc excitation but not for ac excitation. The external static field has a non-

vanishing vector potential; the emf in a transformer winding is due to the time variation of this vector potential. An expression for the external flux density is a negligible fraction of the flux density in the core.

Page, C. H., **On the external magnetic field of a closed-loop core,** *Am. J. Phys.* **39,** *No. 10, 1206–1209, October 1971.*

Key words: Magnetic field; solenoid; toroid; transformer; vector potential.

An infinite solenoid, or a toroidal coil, has no external magnetic field for dc excitation but has a nonvanishing vector potential field. The development of the steady-state condition from the transient response to step excitation is discussed. Under ac excitation, an external magnetic field must be present, but in practical cases its magnitude is negligible.

Raveché, H. J., **Entropy and molecular correlation functions in open systems I. Derivation.** *J. Chem. Phys.* **55,** *No. 5, 2242–2250 (Sept. 1, 1971).*

Key words: Activity derivatives; closed system; correlation functions; entropy; open system; potentials of mean force.

A method is presented for obtaining an expression for the entropy in terms of molecular correlation functions defined in the grand canonical ensemble. The procedure is for a system of a single molecular species whose dynamics are determined by classical equations of motion. The entropy is obtained as a sum of two different classes of functions each involving the correlations between n-tuples of molecules. One class contains logarithmic terms similar to those obtained for the closed system; the other class involves isothermal activity derivatives of potentials of mean force. The latter terms, which are moments of the correlations between disjoint sets of molecules, can make appreciable contributions to the entropy. The method leads to results similar to those obtained from a different procedure by Nettleton and Green. The expression for the entropy is obtained and properties of the results are discussed for a simple fluid system.

Reed, R. P., Durcholz, R. L., Schramm, R. E., Patrician, T. J., **Study of cyrogenic storage tank fatigue life,** *Nat. Bur. Stand. (U.S.), Tech. Note 609, 86 pages (Aug. 1971) 75 cents, SD Catalog No. C13.46:609.*

Key words: Fatigue; fracture; impact; low temperature; mechanical property equipment; stainless steel.

Two 300 series stainless steels were tested for impact-fatigue life and tensile properties as a function of temperature, percent transformed phase (martensite), stress level, and specimen geometry. These alloys were studied to predict the fracture characteristics of parent material and weld joints in large cryogenic dewars which are subjected to periodic stresses. Normally, AISI 304 is employed in the construction of such dewars. Under fatigue loading conditions at cryogenic temperatures, the behavior of AISI 304 is complicated by the gradual transformation to a martensitic structure. The influence of this transformation on the fracture characteristics was studied. For this purpose, a new impact-fatigue test and necessary equipment were developed.
The fatigue strength of AISI 304 and 310 exhibit similar trends, but at a given fatigue life and temperature, the fatigue strength of AISI 304 is slightly superior. AISI 310 displays an endurance limit of about 20,000 psi; the 304 limit is 25–30,000 psi. However, the lowest endurance limit (weakest) specimens appear to be the triaxially-loaded AISI 304 weld specimens which have an endurance limit near 10,000 psi. Little temperature-dependence of the impact-fatigue properties was observed. For ease in interpretation all stress values in the text are expressed in units of psi. Conversion to other stress units are

$$10^3 \text{ psi} = 0.703 \text{ kg/mm}^2 = 6.90 \times 10^6 \text{ N/m}^2$$

Rubin, R. J., **Comment on "Conformation of adsorbed polymeric chain. II,"** *J. Chem. Phys.* **51,** *No. 10, 4681 (Nov. 15, 1969).*

Key words: Adsorption; polymer chain; random walk; restricted random walk.

There is an error in the paper "Conformation of Adsorbed Polymeric Chain. II" by K. Motomura and R. Matuura, J. Chem. Phys. **50,** 1281 (1969). The effect of this error on the authors' conclusions is indicated.

Rubin, R. J., **Transmission properties of an isotopically disordered one-dimensional harmonic crystal. II. Solution of a functional equation,** *J. Math. Phys.* **11,** *No. 6, 1857–1867 (June 1970).*

Key words: Disordered crystal; energy current; functional equation; transmission coefficient.

The amplitude of a wave of frequency ω which is transmitted by a disordered array of N isotopic defects in a 1-dimensional harmonic crystal is investigated in the limit $N \to \infty$. In particular, the ratio $T_N(\omega)$ of the amplitude of the Nth defect to the amplitude of the first defect is represented as $\exp[-N\hat{\alpha}_N(\omega, Q, \{a_n\})]$, where $\{a_n\}$, $n=2, \ldots, N$, is the sequence of nearest-neighbor spacings and $Q=(M-m)/m$. It is known from earlier work that $\hat{\alpha}_N(\omega, Q, \{a_n\})$ is the logarithm of the Nth root of the magnitude of a continuant determinant of order N. The value of the continuant is expressed formally as a product of N factors $\hat{g}_n$ which are recursively related. In the present case, the $\hat{g}_n$ happen to lie on a circle K_0 in the complex $\hat{g}$ plane. Assuming that the spacings between defects are independent identically distributed random variables with the mean value c^{-1} and going to the limit $N \to \infty$, a functional equation for the limiting distribution function of the $\hat{g}_n$ on K_0 is derived. The limiting value $\alpha(\omega, Q, c) = \lim \hat{\alpha}_N(\omega, Q, \{\alpha_n\})$, as $N \to \infty$, can be determined from the limiting distribution function of the $\hat{g}_n$. We determine the solution of the functional equation in three different ways for three different cases: (a) In the case of the special frequency of Matsuda, $\omega = 2^{-1/2}$ and $Q=1$, we obtain exact values of the integral of the $\hat{g}$ distribution function which are in excellent agreement with Monte Carlo estimates; (b) in the physically interesting case where the mean spacing between defects is small compared to the incident wavelength, i.e., $c^{-1}\omega \ll 1$, we obtain the solution of the functional equation correct to first order in $c^{-1}\omega$ and we calculate the lowest-order nonzero value of $\alpha(\omega, Q, c)$; (c) for the general case of moderate values of ω, Q, and c, we develop a numerical method for solving the functional equation and present the results of the numerical calculations in several representative cases. These numerical results are in good agreement with Monte Carlo estimates. One of the principal results, obtained by solving the functional equation, is that $\alpha(\omega, Q, c) > 0$ for $\omega \ll c < 1$ and $\omega(|Q| + c^{-1}) \ll 1$ with $Q \neq 0$.

Rubin, R. J., Greer, W. L., **Abnormal lattice thermal conductivity of a one-dimensional, harmonic, isotopically disordered crystal,** *J. Math. Phys.* **12,** *No. 8, 1686–1701 (Aug. 1971).*

Key words: Harmonic crystal; isotope defect scattering; thermal conductivity; transmission coefficient.

Energy transport is investigated in a model system for which exact analytic results can be obtained. The system is an infinite, one-dimensional harmonic crystal which is perfect everywhere except in a finite segment which contains N isotopic defects. Initially, the momenta and displacements of all atoms to the left of the defect region are canonically distributed at a temperature T, and the right half of the crystal is at a lower temperature. This initial nonequilibrium state evolves according to the equations of motion, and ultimately a steady state is established in the vicinity of the region containing the defects. The thermal conductivity is calculated from exact expressions for the steady state energy flux and thermal gradient. For a crystal in which the N isotopic defects are distributed at random but in which the overall defect concentration is fixed, we demonstrate that the thermal conductivity approaches infinity at least as fast as $N^{1/2}$. A Monte Carlo evaluation of the thermal conductivity for a given defect-to-host mass ratio and concentration is carried out for a series of random configurations of N defects for N in the range, $25 \leq N \leq 600$. The thermal conductivity is proportional

to $N^{1/2}$ within the statistical uncertainty except for slight deviations at the smallest values of N.

Rukwied, A., Ruff, A., W., Willard, W. A., **Study of the cellular solidification structure in a continuously cast high purity copper,** *Metallurgical Trans.* **2,** *2105–2114 (August 1971).*

Key words: Cavities; cellular solidification; constitutional supercooling, copper (99.999%); dislocation arrangements; distribution of impurities; precipitate particles; thermomechanical treatment.

The aim of this paper is to characterize the principal microstructural features of continuously cast high purity copper (99.999 pct Cu), particularly those which might influence high temperature creep. This material contains a cellular solidification structure resulting from impurity segregation due to constitutional supercooling of the melt during solidification. This structure could not be eliminated from the solid copper by thermomechanical treatment. The grown-in structure was studied using optical and electron metallography as well as etch-pitting techniques. In the as-cast material a loose network of dislocation tangles was observed, and in certain locations, preferential etching attack. In addition, small voids were found within the dislocation tangles. Thermomechanical treatment eliminated the dislocation tangles almost entirely, but left locations susceptible to preferential etching attack. At those locations impurities were probably concentrated into zones of a size of a few 1000 Å. From solubility and concentration considerations, small precipitates (less than 80 Å in size) or clusters of carbon are suspected.

Rupp, N. W., Bowen, R. L., Paffenbarger, G. C., **Bonding cold-curing denture base acrylic resin to acrylic resin teeth,** *J. Am. Dental Assoc.* **83,** *601–606 (Sept. 1971).*

Key words: Acrylic teeth; adhesion; autoadhesion; bonding cold-curing methyl methacrylate; dentures; tensile strength.

Bonding of cold-curing acrylic resin to acrylic resin teeth increases tooth retention and strengthens denture bases because the plastic teeth become an integral part of the denture base. Bonding was effected in this manner; the necks of the teeth were coated with a solution of equal parts by volume of methylene chloride and cold-curing methyl methacrylate monomer. This treatment combines a solvent attack on the teeth with polymerization bonding and develops tensile strengths of more than 80% of those of the acrylic resin denture base materials. The bonding was verified in experimental dentures made of a compression molded and a pour type poly(methyl methacrylate). The resin teeth became integral parts of the denture as evidenced by their retention in the base. On application of stresses, the fracture lines went through the teeth rather than through the tooth-denture base interfaces as before. The technique adds neither time nor equipment to currently used laboratory procedures.

Ryan, J. V., Editor, **The flammable fabrics program 1970,** *Nat. Bur. Stand. (U.S.), Tech. Note 596, 68 pages (Sept. 1971) 65 cents, SD Catalog No. C13.46:596.*

Key words: Annual report to Congress; blankets; carpets and rugs; children's sleepwear; cooperation; flammability; flammability reduction; mattresses; research; small carpets and rugs; standards; test development.

This Annual Report to the Congress, required by the Flammable Fabrics Act, covers calendar year 1970. Specific flammability standards outputs were standards for carpets and rugs and for small carpets and rugs, a proposed standard for children's sleepwear, and notices of possible need and institution of proceedings for standards for certain items of children's apparel, all blankets, and all mattresses. Research included studies, in-house and by contract, on subjects such as full scale carpet burn experiments and heat transfer from burning fabrics. Studies of the feasibility of reducing flammability included pyrolysis of textile materials and chemical aspects of fire retardancy. Test development was completely related to the standards outputs, and training ranged from the preparation of bibliographies through Congressional and public presentations to full time Research Associateship participation in the program. Cooperation was carried out with HEW, the public, industry, and voluntary standards groups.

Saylor, C. P., **Return of the prodigal,** *Capital Chem.* **21,** *No. 6, 95–99 (Sept. 1971).*

Key words: Cathedral; deformation; lead; roof; Washington Cathedral; "1921".

The Washington Cathedral, built in the English style, was given a lead roof. Under the hot Washington sun, it crept. This caused it to leak. E. W. Washburn, Chief Chemist of NBS, diagnosed the difficulty and suggested correction. The events recounted in this article took place shortly after 1921.

Sengers, J. M. H. L., Straub, J., Vicentini-Missoni, M., **Coexistence curves of CO_2, N_2O, and $CClF_3$ in the critical region,** *J. Chem. Phys.* **54,** *No. 12, 5034–5050 (June 15, 1971).*

Key words: Coexistence curve; critical region; rectilinear diameter; CO_2, N_2O, $CClF_3$; refractive index.

The coexistence curves of CO_2, N_2O and $CClF_3$ are analyzed in the critical region. The curves were obtained by refractive index measurements which are virtually free of gravity effects and contain much detail near T_c. After proper weight assignment, it is established that the top of the coexistence curve is asymptotically symmetrically $\rho^{\pm} = \rho_c \pm Bt^{\beta}$; that the exponent B is independent of the range, varies little from substance to substance and is insensitive to impurities; and that the data are in agreement with the law of the rectilinear diameter. "Best" values for β, B and for the slope of the diameter are presented. An analysis of earlier coexistence curves for CO_2 and N_2O, including a weight assignment, is presented; there is agreement between the older and newer data.

Shoup, R. R., VanderHart, D. L., **Effect of CH scalar coupling on ^{13}C transverse relaxation times,** *J. Am. Chem. Soc.* **93,** *2053–2054 (1971).*

Key words: ^{13}C; Fourier transform; nmr; relaxation; scalar coupling; sensitivity.

Experimental ^{13}C NMR relaxation rates are reported for 60% enriched $^{13}CH_3I$, $^{13}CH_3COOCD_3$, and $^{13}CS_2$. Except for CS_2 transverse relaxation rates, R_{2C}'s, are found to be substantially higher than the corresponding logitudinal relaxation rates. This effect is shown, on the basis of the variation of R_{2C} with Carr-Purcell pulse repetition rate, to arise from scalar coupling of ^{13}C with relaxing protons. Implications for ^{13}C spectroscopy, particularly Fourier transform techniques, are discussed.

Smith, J. C., Kermish, G. A., Fenstermaker, C. A., **Separation of filler particles from the matrix in a particulate-loaded composite subjected to tensile stress,** *Proc. 162nd Meeting American Chemical Society, Organic Coatings and Plastics Chemistry, Washington, D.C., Sept. 13–15, 1971, 31, No. 2, 149–155 (Sept. 1971).*

Key words: Composite materials; coupling agents; epoxy polymer; parting agents; poisson's ratio; release agents; stress-strain curve; volume dilation.

Simultaneous measurements of tensile stress, longitudinal strain, and transverse strain were obtained on particulate-filled composites. The matrix was a flexible epoxy polymer. Small glass spheres were used as filler in various volume ratios up to .35. The spheres were pretreated as follows: clean, coated with a parting agent, coated with either of two silane coupling agents. The volume expansion behavior of composites containing parting agent treated spheres could readily be distinguished from that of composites containing clean glass spheres, but differences caused by coating the spheres with coupling agents could not be distinguished. Stress-strain behaviors for the various composite systems also showed differences. These differences in both kinds of data are taken as indicative of matrix-filler separation and subsequent vacuole formation.

Stull, D. R., Prophet, H., **JANAF thermochemical tables Second Edition,** *Nat. Stand. Ref. Data Ser., Nat. Bur. Stand. (U.S.), 37, 1141 pages (June 1971) $9.75, SD Catalog No. C13.48:37.*

Key words: Evaluated data; thermal functions; thermodynamic properties of materials; thermodynamics.

This monograph is the second edition of the JANAF Thermochemical Tables. It contains thermodynamic properties for some 1099 chemical species. The following properties are tabulated as functions of temperatures: C_p°, S°, $(F^\circ - H_{298}^\circ)/T$, $H^\circ - H_{298}^\circ$, ΔH_f° and Log Kp.

Tech. I. L., Ward, J. F., **Accurate wavelength measurement of the $1s2p\ ^3p^0$–$2p^2\ ^3P$ transition in ^{4}He I,** *Phys. Rev. Letters* **27,** *No. 7, 367–370 (Aug. 16, 1971).*

Key words: Atomic energy levels; atomic theory; autoionization; helium; wavelength measurement.

A precise spectroscopic measurement of the $1s2p\ ^3P^0$–$^2p^2\ ^3P$ transition near 320 A in ^{4}He I is reported. The energy of the non-autoionizing $2p^2\ ^3P$ term as derived from this measurement is compared with theory. The experimental and theoretical values for the wavenumber of the transition agree within 1 cm^{-1} which is the experimental uncertainty of our measurement.

Treat, C. F., **A history of the metric system controversy in the United States,** *Nat. Bur. Stand. (U.S.), Spec. Publ. 345–10, 312 pages (August 1971) $2.25, SD Catalog No. C13.10:345–10.*

Key words: Metric system; weights and measures.

A review of the debate between 1790 and 1968 on the question of whether or not the United States should adopt the metric system of weights and measures. Legislative activities with respect to weights and measures and campaigns for and against adoption of the metric system are reviewed. Significant investigations of the question by both public and private bodies are highlighted. An extensive bibliography is included.

Winnewisser, G., Maki, A. G., Johnson, D. R., **Rotational constants for HCN and DCN,** *J. Mol. Spectry.* **39,** *No. 1, 149–158 (1971).*

Key words: Bond distances; hydrogen cyanide; infrared; microwave; molecular structure; rotational constants; spectra.

Microwave measurements of rotational transitions within vibrationally excited states of several isotopic species of HCN have given improved values for the pertinent B_v constants. These new data have been combined with infrared measurements given in the literature (including D_v terms) to arrive at a set of rovibrational constants (α and γ constants) which is consistent with all available data. Bond distances resulting from several different B_e approximations are intercompared to assess the variability of the r_e values and the importance of the γ terms. The latest r_0 and r_s bond distances are also given.

Winogradoff, N. N., Osinsky, V. I., **Density-of-states tails associated with the ⟨100⟩ conduction band minima in heavily doped *n*-type GaAs,** *Solid State Commun.* **8,** *No. 23, 2001–2003 (Dec. 1, 1970).*

Key words: Activation analysis; component identification; result computation; spectral resolution.

Methods of result computation with activation analysis gamma-ray spectra are reviewed, emphasizing recent developments. For NaI(Tl) detector spectra, the multiple linear regression technique is reported. For Ge(Li) detector, methods of peak location, net peak area computation, and complex peak resolution are indicated. Each technique is discussed for applicability and difficulties in utilization. General features of result computation and of various numerical analytic techniques are discussed.

Yule, H. P., **Computer data reduction in activation analysis,** *Proc. NATO Advanced Study Institute on Activation Analysis in Geochemistry and Cosmochemistry, Kjeller, Norway, Sept. 7–12, 1970, pp. 145–166 (1971).*

Key words: Band tailing; gallium arsenide; indirect valleys; *n*-type gallium arsenide; photoluminescence; temperature dependence.

In contrast with the photoluminescence of lightly doped *n*-type GaAs, a *reduction* in the temperature of heavily doped material produced an intensification and a *broadening* of the spectrum on the high-energy side of the band gap. This effect is attributed to the presence of "density-of-states" tails associated with the indirect ⟨100⟩ minima in the conduction band of the heavily doped material.

Ballantyne, J. P., Yakowitz, H., Munro, E., Nixon, W. C., Analysis of a variable geometry cylindrical detector for the scanning electron microscope, Proc. 25th Anniversary Meeting of the Electron-microscopy and Analysis Institute Physics Group Conference, Cambridge, England, June 29–July 1, 1971, pp. 194–197 (1971).

Beers, J. S., Testing of cover glasses for hemacytometer chambers, Nat. Bur. Stand. (U.S.), Tech. Note 579, 7 pages (Sept. 1971) 20 cents, SD Catalog No. C13.46:579.

Bullis, W. M., Methods of measurement for semiconductor materials, process control, and devices. Quarterly Report January 1 to March 31, 1971, Nat. Bur. Stand. (U.S.), Tech. Note 598, 54 pages (October 1971) 55 cents, SD Catalog No. C13.46:598.

Carpenter, R. J., Forman, R. A., Zeeman modulator for nuclear quadrupole resonance spectroscopy, J. Phys. E: Sci. Instr. **3,** 922–924 (November 1970).

Clark, G., Standards Coordinator, Bit sequencing of the code for information interchange in serial-by-bit data transmission, Nat. Bur. Stand. (U.S.), Fed. Info. Process. Stand. Publ. (FIPS Pub.) 16, 4 pages (1971) 10 cents, SD Catalog No. C13.52:16.

Clark, G., Standards Coordinator, Character structure and character parity sense for parallel-by-bit data communication in the code for information interchange, Nat. Bur. Stand. (U.S.), Fed. Info. Process. Stand. Publ. (FIPS Pub.) 18, 4 pages (1971) 10 cents, SD Catalog No. C13.52:18.

Clark, G., Standards Coordinator, Character structure and character parity sense for serial-by-bit data communication in the Code for information interchange, Nat. Bur. Stand. (U.S.), Fed. Info. Process. Stand. Publ. (FIPS Pub.) 17, 4 pages (1971) 10 cents, SD Catalog No. C13.52:17.

French, J. L., Discussion of "Are individual current-meter ratings necessary", J. Hydraulics Div. Proc. Am. Soc. Civil Engrs. HY **1,** 507–511 (Jan. 1969).

French, J. L., Nonenlarged box culvert inlets, J. Hydraulics Div. Proc. Am. Soc. Civil Engrs. HY **6,** 2115–2137 (Nov. 1969).

Gebbie, K. B., Thomas, R. N., The temperature control bracket, Astrophys. J. **168,** No. 3, 461–479 (Sept. 15, 1971).

Gravatt, C. C., The application of light scattering, Appl. Spectry. **25,** No. 5, 509–516 (Sept.–Oct. 1971).

Grimes, D. N., Linear microdensitometry, J. Opt. Soc. Am. **61,** No. 9, 1263 (Sept. 1971).

Grundl, J. A., Fission-neutron spectra: macroscopic and integral results, Proc. Neutron Standards and Flux Normalization, Symp. Argonne National Laboratory, Argonne, Ill., Oct. 21–23, 1970. Sponsored by the European American Nuclear Data Committee, pp. 417–451 (Aug. 1971).

Hall, J. T., Dixon, R. G., Getting it all together the cybernetic way, Management Rev. pp. 16–22 (American Management Association, Inc., New York, N.Y., July 1971).

Hellwig, H., Barnes, J. A., Glaze, D. J., Frequency biases in a beam tube caused by Ramsey excitation phase differences, Proc. 25th Annual Symp. on Frequency Control, Atlantic City, N.J., April 26–28, 1971, pp. 309–312. (Electronic Industries Association, Washington, D.C., April 1971.)

Kulin, G., Discussion of the paper "Triangular broad-crested weir," by C. D. Smith and W. S. Liang, Proc. American Society Civil Engineers, Irrigation Drainage Div. **96,** IR4, 494–497 (Dec. 1970).

Little, J. L., Standards Coordinator, Rectangular Holes in Twelve-Row Punched Cards, Nat. Bur. Stand. (U.S.), Fed. Info. Process. Stand. Publ. (FIPS Pub.) 13, 4 pages (1971) 10 cents, SD Catalog No. C13.52:13.

Little, J. L., Standards Coordinator, Subsets of the Standard Code for Information Interchange, Nat. Bur. Stand. (U.S.), Fed. Info. Process. Stand. Publ. (FIPS Pub.) 15, 10 pages (1971) 25 cents, SD Catalog No. C13.52:15.

Phucas, C. B., Technical Standards Coordinator, Paper Ice Bag Sizes, Nat. Bur. Stand. (U.S.), Prod. Stand. 44–71, 12 pages (Sept. 1971) 15 cents, SD Catalog No. C13.20/2:44–71.

Phucas, C. B., Technical Standards Coordinator, Portable Picnic Coolers, Nat. Bur. Stand. (U.S.), Prod. Stand. 49–71, 9 pages (October 1971) 15 cents, SD Catalog No. C13.20/2:49–71.

Other NBS Publications

J. Res. Nat. Bur. Stand. (U.S.), 75C (Engineering and Instrumentation), Nos. 3 & 4 (July–December 1971), SD Catalog No. C13.22/sec.C:75/3&4. $1.25.

Thermal voltage converters and comparator for very accurate AC voltage measurements. E. S. Williams.

Formulation and experimental verification of an axisymmetric finite-element structural analysis. R. A. Mitchell, R. M. Woolley, and C. R. Fisher.

A Burnett apparatus for the accurate determination of gas compressibility factors and second virial coefficients, and an evaluation of its capability based on some results for argon and carbon dioxide. M. Waxman and J. R. Hastings.

An extension to the sliding short method of connector and adaptor evaluation. G. F. Engen.

Accurate microwave high power measurements using a cascaded coupler method. K. E. Bramall.

J. Res. Nat. Bur. Stand. (U.S.), 75B (Mathematical Sciences), No. 3 & 4 (July–December 1971) SD Catalog No. C13.22/sec. B:75/3&4. $1.25.

Some elementary formulas in "matrix calculus" and their applications. J. T. Fong.

Linear transformations on matrices. M. Marcus.

Eigenvalues of sums of hermitian matrices. III. R. C. Thompson and L. Freede Garbanti.

A new type of boundary value coupling for second order Sturm-Liouville systems. J. Geist.

An ergodic source which is not a function of any finite Markov process. R. D. Traub.

On entire functions of exponential type. S. M. Shah and W. C. Sisarcick.

A table of integrals of the error function. II. Additions and corrections. M. Geller and E. W. Ng.

A note on the time dependence of the effective axis and angle of a rotation. H. Gelman.

A numerical solution of integral equation of the first kind applied to slit correction in small-angle x-ray scattering. J. Mazur.

**Publications for which a price is indicated are available by purchase from the Superintendent of Documents, U.S. Government Printing Office, Washington, D.C. 20402 (foreign postage, one-fourth additional). The NBS non-periodical series are also available from the National Technical Information Service (NTIS), Springfield, Va. 22151, which was formerly the Clearinghouse. Reprints from outside journals and the NBS Journal of Research may often be obtained directly from the authors.*

U. S. GOVERNMENT PRINTING OFFICE : 1972 OL - 453-425

UNITED STATES
GOVERNMENT PRINTING OFFICE
PUBLIC DOCUMENTS DEPARTMENT
WASHINGTON, D.C. 20402

OFFICIAL BUSINESS

PENALTY FOR PRIVATE USE, $300

POSTAGE AND FEES PAID
U.S. GOVERNMENT PRINTING OFFICE

JOURNAL OF RESEARCH of the National Bureau of Standards
A. Physics and Chemistry

Vol. 76A, No. 2 March–April 1972

Contents

		Page
	Guidelines for the reporting of numerical data and experimental procedures. David Garvin.	67
	A study of equilibrium in argon arcs. J. B. Shumaker and C. H. Popenoe.	71
	Rates of reaction of atomic oxygen III. Spiropentane, cyclopentane, cyclohexane, and cycloheptane. Robert E. Huie and John T. Herron.	77
	Densities of compressed liquid methane, and the equation of state. Robert D. Goodwin and Rolf Prydz.	81
	Spin-relaxation effects on the EPR spectrum of gaseous hydrogen atoms. Robert L. Brown.	103
	Photoionization of C_4H_8 isomers. Unimolecular and bimolecular reactions of the $C_4H_8^+$ ions. L. W. Sieck, S. G. Lias, L. Hellner and P. Ausloos.	115
	Theoretical investigation of the odd configurations of Ni II. Y. Shadmi and E. Caspi.	125
	The characterization of linear polyethylene SRM 1475.	
I.	Introduction. C. A. J. Hoeve, Herman L. Wagner, and Peter Verdier.	137
II.	Determination of total methyl content by infrared spectrophotometry. James E. Brown.	141
III.	Density determination. James E. Brown.	143
IV.	Melt flow rate. John R. Maurey.	145
V.	Solution viscosity measurements. Richard G. Christensen.	147
VI.	Preparation of calibrating fractions. Richard G. Christensen.	149
VII.	Differential refractive index of polyethylene solutions. Herman L. Wagner.	151
VIII.	Light scattering studies on polyethylenes in 1-chloronaphthalene. Lois J. Frolen, Gaylon S. Ross, Andrew M. Wims, and Peter Verdier.	156
IX.	Number average molecular weight of fractions by membrane osmometry. James E. Brown and Peter H. Verdier.	161
X.	Gel permeation chromatography. Gaylon Ross and Lois Frolen.	163
	Publications of the National Bureau of Standards	171

Library of Congress Catalog Card Number: 62–37059

For sale by the Superintendent of Documents, U.S. Government Printing Office, Washington, D.C. 20402. (Order by SD Catalog No. C 13.22/sec.A:76/2). Single copy price varies. This issue $1.50. Subscription price: $9.50 a year; $2.25 additional for foreign mailing.

UNITED STATES GOVERNMENT PRINTING OFFICE, WASHINGTON : 1972